ANNALES
UNIVERSITATIS SCIENTIARUM BUDAPESTINENSIS DE ROLANDO EÖTVÖS NOMINATAE

SECTIO GEOLOGICA

TOMUS XVIII.
1976

BUDAPEST
1976

ANNALES
UNIVERSITATIS SCIENTIARUM BUDAPESTINENSIS DE ROLANDO EÖTVÖS NOMINATAE

SECTIO GEOLOGICA

TOMUS XIII.
1976

REDIGUNT
B. GÉCZY
J. KISS
L. STEGENA

BUDAPEST
1976

ANNALES

UNIVERSITATIS SCIENTIARUM BUDAPESTINENSIS DE ROLANDO EÖTVÖS NOMINATAE

SECTIO BIOLOGICA
incepit anno MCMLVII

SECTIO CHIMICA
incepit anno MCMLIX

SECTIO GEOLOGICA
incepit anno MCMLVII

SECTIO GEOGRAPHICA
incepit anno MCMLXV

SECTIO HISTORICA
incepit anno MCMLVII

SECTIO IURIDICA
incepit anno MCMLIX

SECTIO LINGUISTICA
incepit anno MCMLXIX

SECTIO MATHEMATICA
incepit anno MCMLVIII

SECTIO PAEDAGOGICA ET PSYCHOLOGICA
incepit anno MCMLXX

SECTIO PHILOLOGICA
incepit anno MCMLVII

SECTIO PHILOSOPHICA ET SOCIOLOGICA
incepit anno MCMLXII

ELECTRON MICROPROBE ANALYSES OF KARSTIC AND LATERITIC BAUXITES

by

J. HIDASI and P. MENSÁROS

Department of Applied and Engineering Geology, Eötvös University, Budapest

Received: 15 March 1974

SUMMARY AND CONCLUSIONS

On the basis of the studies made on the available sections, the main difference between the karstic and lateritic bauxites – owing to the deposition and accumulation localities and circumstances – is the presence of globular elements in the former, and occurence of fluidal texture and veins in the latter type. The position and form may suggest different material-movements in the same time. The difference arises from the direction of these movements.

The formation of the globular elements, which are dominant in the karstic bauxites, can be due mainly to the parallelly directed massive movement of this colloidal material. The globular elements show – even in thin-section studies – significant differences, which are represented also in the element distribution. These differences enable to separate the pisoid generations, and the genetic bases of these generations are the changed chemical circumstances of the certain intervals. These differences, namely, are sufficiently great to suggest the distant formation of the pisoids and ooids. Their can be explained by redeposition. It is proved also by the standpoints founded for the classification of the pisoids and ooids in our previous studies, and by Fig. 14 to 21., obtained during the electron microprobe analyses. The Mn-rich particle containing Ni, Co and Ti, resembles in its element composition the frequently occuring Mn crust of the bauxite footwalls. On the basis of the analysis, this grain seems to be related to this crust beneath the bauxite bodies.

The underlying rock of the bauxite is Dachsteinkalk, the overlying rock is the Upper Cretaceous spotted marl. The Mn-rich grain came from the middle portion of the bauxite body. Consequently this grain derived from the Mn-crusted footwall of a previously formed then eroded bauxite body, and proves unequivocally the allochtonous character of this bauxite.

The veins recognized in lateritic bauxites show epigenetic processes (pyritization, pyrite decomposition).

In the lateritic bauxites the fluidal textural elements, veins are characteristic. These are directed vertically, in which the solutions also moved in vertical direction. The solutions mobilized the Fe, and in the course of the downward motion this Fe precipitates by the changed chemical circumstances, and infills the veins.

In the distribution of the studied main elements the most striking differences were shown by the Fe. In the case of the karstic bauxites of Hungary the Fe distribution is rather regular – as suggested by the macroscopically visible red colour. In lateritic bauxites the Fe concentration varies within wide extremes. Locally the total abcence of Fe occurs (on the white- or yellow-coloured points of the bauxite). Similar essential differences do not appear in the Al, Si and Ti distribution. The reversed enrichments of the Al and Fe is characteristic in both cases.

In the textural studies the electron microprobe analyses were essentially useful to trace textural elements, wich are inseparable in thin-sections or spectroscopic examinations. The electron microprobe analysis naturally is insufficient for mineral determination,

because its results are element compositions. The most favourable way, in the case of the textural analysis of bauxites, is the accompained use of both thin-section and electron microprobe studies.

Preparation of samples and short description of the method

Electron microprobe analysis requires suitably prepared samples. Owing to the low hardness, loose and heterogenic texture, high porosity and hydrous minerals, the Hungarian bauxites are not convenient for thin-section or surface-section preparation.

The samples were prepared for electron microprobe analysis in the Laboratory for Geochemical Research of the Hungarian Academy of Sciences. After mounting in Araldit-H and Palatal-4 plastics the dry coarse-grinding was made on SiC abbrasive cloth (320, 600 mesh). In every cases the grinding was carried out manually The final surfacial polishing was made on cloth, with Al_2O_3-water pulp. In this way score-free, but slightly uneven surfaces were obtained. The removing of the grinding materials, remained in the small surfacial hollows, required a some minute ultrasonic cleaning. The surface sections, prepared in this way need conducting. The conducting material is a copper layer (about 100 Å), coated in vaacum concentrator. The conductivity between this conducting layer and the sample holder was furnished by Dotit suspended silver painting.

The analyses were carried out in the Laboratory for Geochemical Researches of the Hungarian Academy of Sciences, under the direction of Dr. G y. P a n t ó. The surface of the preparation is scanned by electronic pencil in vacuum. The samples can be studied with the following electron pictures occured on the cathode-ray tubes (only the pictures used in this present studies are listed here):

1. *Back-scattered electron picture.* The picture is built by the greater energy reflected electrons. The fields of the greater mean atomic weights (stronger electron reflection capacity) are brighter on the pictures. The following two types exsist:

a) composition picture. The position of the two detector heads is to add the reflected electrons, and the topographic effect decreases in this way

b) topographic picture. It is a picture built up by the difference of the two detector heads' signals, bringing mainly the "relief" of the surface.

2. *Scanning picture.* The electron radiation induces characteristic X-ray radiation in the material. This element-specific X-ray radiation is detected by two variable induce detectors. These can be stepped to the characteristic wave-length of the element to be studied, and can be recognized on the cathode-luminescent screen.

a) element-distribution radiograph. The frequency and intensity of the scintillating points on the screen show the position and concentration of the represented element.

b) line profiles. The scanning takes place along predetermined lines and results in curves.

Textural studies

The graphs presented in the first part were made from Hungarian karstic bauxite of Halimba. Fig. 1. shows the composition picture of a detail from an oolite. From left to right the matrix, the crust and the core are visible. The matrix is a field of low atomic weight. Within the crust the crustal limits are well visible. The core is a bright, light field, suggesting great atomic weight. Within the core and the crust there are well isolated detrital grains, which were more sharply and distinctly shaped on the screen.

Figs. 2., 3. and 4. show respectively Al, Fe and $Ti_{K\alpha}$X-ray scanning pictures of this composition picture. The three different fields (matrix, crust, core) can be separated also on the basis of these pictures. The enrichment of Al is opposited by that of Fe. It can be proved, that this is an ooid with a core rich in iron and poor in aluminium. The matrix is Al-rich Fe-poor. The crustal part do not show in the element concentration of the X-ray scanning picture the distinct "striate" structure, visible on the composition picture. Si shows a constant, Ti a punctual distribution, and do not follow the Fe enrichment. Two groups are separable:

1. Grains smaller than 10 μm. These are most probably of autigene origin (Bárdossy and Pantó 1971).
2. Aggregations greater than 10 μm. These are well identifiable to the pronounced, bright granules mentioned at the composition picture. These are poor in Al, Fe and Si, but their Ti-content is high. As of other elements, significant enrichment cannot be recognized. Most probably these are some TiO_2 modifications (anatase or rutile). As it is visible on the composition picture, these are not crystallized forms, showing the non-autigene, but rather the detrital origin in this way. (The basis is the work of Bárdossy and Pantó 1971.) The lack of required roundness can be due to the small (about 10 to 20 μm) size of the particles.

Figs. 5. and 6. show the line distribution of the Mn and Ni. The Mn enriches in the crust and in the core, but do not follow certainly the rhythmic alteration of the crustal parts. The Ni-content increases in the direction of the core, attaining here decreases, then decreases again. Figs. 7. and 8. (composition picture and $Al_{K\alpha}$X-ray scanning picture, respectively) show an interesting phenomenon. In the textural studies it was severally recognized the deformation of the ooids, which resulted from external, mainly mechanical effects; thus fragmented, cracked or scoured specimens occured. A rare example of these deformed ooids can be seen here. Since the number of the crustal limits is constant, the crustal layers probably were condensed and depressed by the own weight of the oolite, in its plastic state.

PLATE I.

Fig. 1. Ooid. Halimba III. bauxite body.
Composition picture. Picture-width: 0,1 mm

Fig. 2. $Al_{K\alpha}$X-ray scanning picture

Fig. 3. $Fe_{K\alpha}$X-ray scanning picture

Fig. 4. $Ti_{K\alpha}$X-ray scanning picture

Fig. 5. $Mn_{K\alpha}$ line profile

Fig. 6. $Ni_{K\alpha}$ line profile

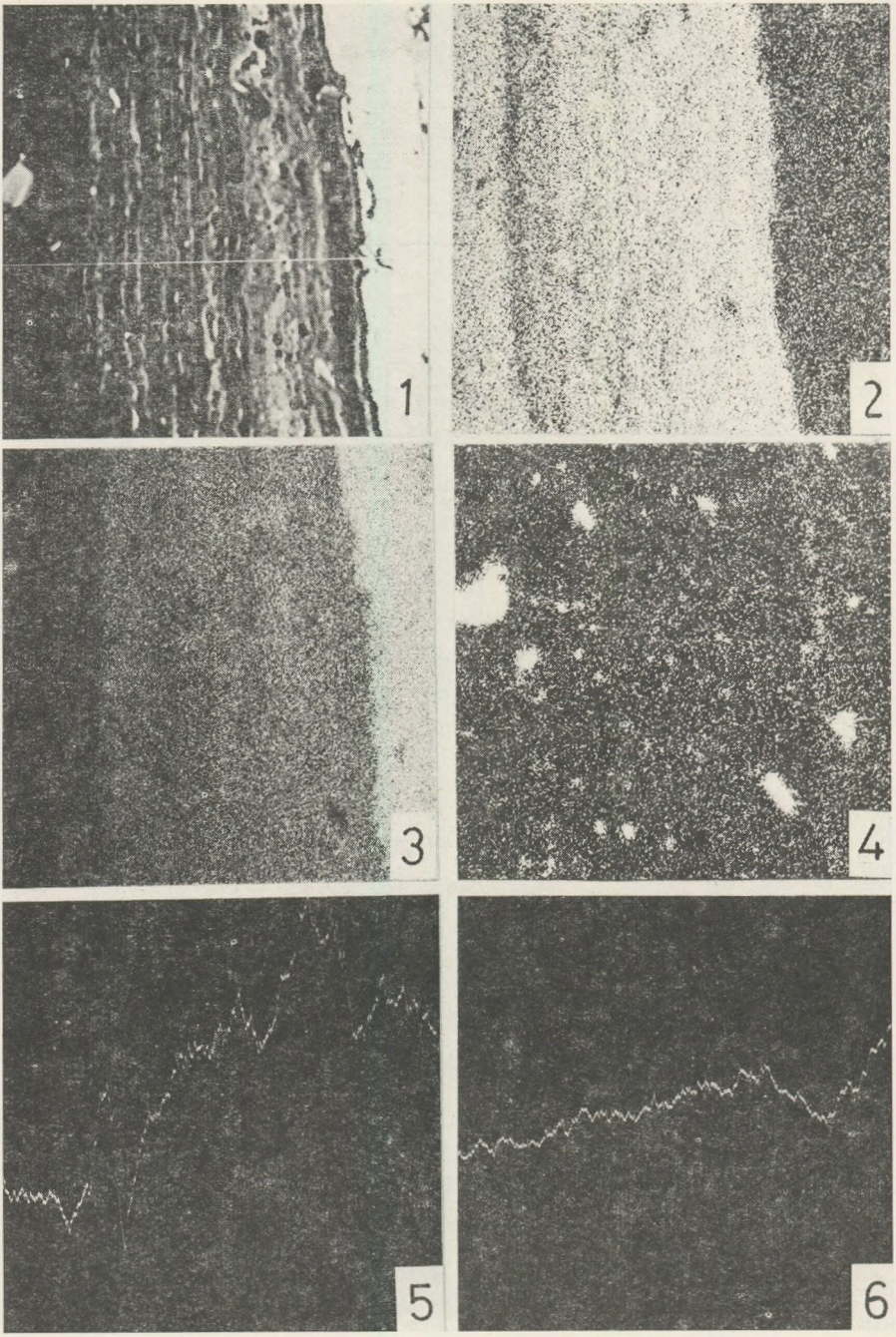
1
2
3
4
5
6

PLATE II.

Fig. 7. Deformed ooid. Halimba III. bauxite body.
Composition picture. Picture-width: 0,2 mm

Fig. 8. Al_{K_α}X-ray scanning picture

Fig. 9. Ooid bauxite detritus, Halimba III. bauxite body.
Composition picture. Picturewidth: 0,1 mm

Fig. 10. Al_{K_α}X-ray scanning picture

Fig. 11. Fe_{K_α}X-ray scanning picture

Fig. 12. Detrital grains, Halimba III. bauxite body.
Topographic picture. Picture-width: 0,2 mm


7

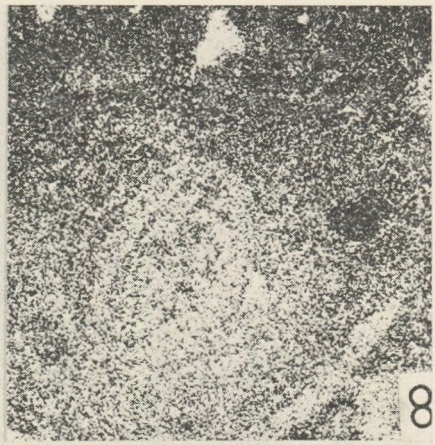
8

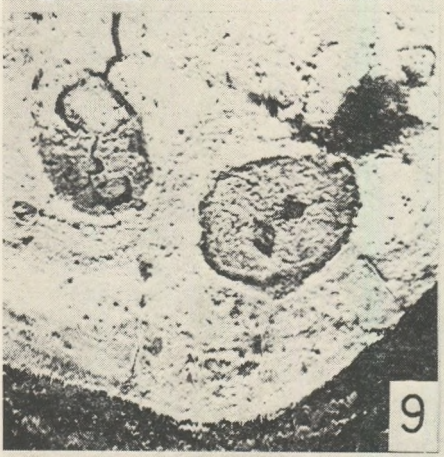
9

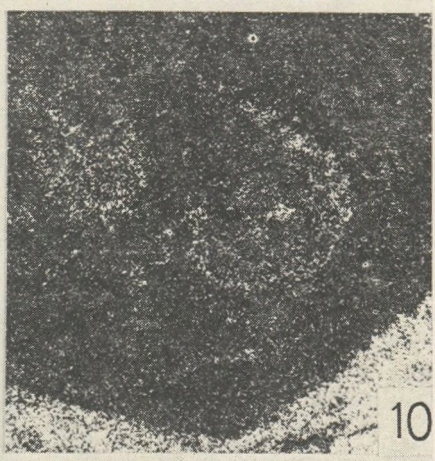
10

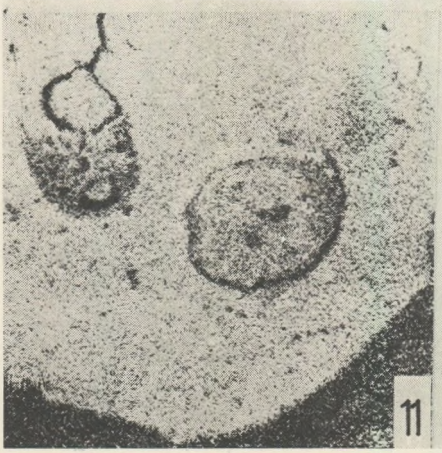
11

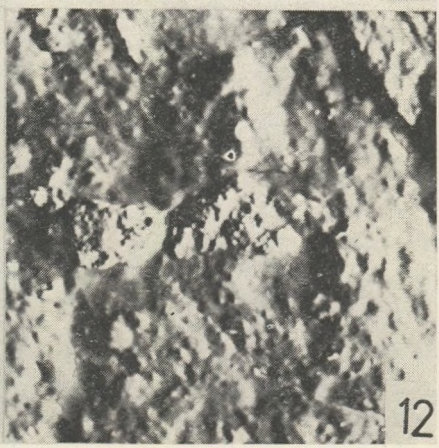
12

Fig. 9. (composition picture) and Figs 10. and 11. (Al and $Fe_{K\alpha}$ X-ray scanning pictures) show a differently deformed detrital bauxite particle. This was scoured during some movement. One of the two ooids (the lower on the figures) is of double-cored. The texture is simple; it is ranged into the ooid-group with continuous transition from the core to the crustal limit.

The next series was made from two crystal grains. On Fig. 12. (topographic picture) the well emerged, i.e. harder, rounded grains are well visible. The back-scattered electron picture (Fig. 13.) shows, that the two grains bear different element composition, and it was proved also by the X-ray scanning picture (the composition picture shown on Fig. 14. is the enlarged variety of Fig. 12.). On Fig. 15. ($Al_{K\alpha}$X-ray scanning picture) the matrix shows a nearly uniform distribution. In the grain of grater mean atomic weight the Al concentration is lower than in the other, close to that. On the $Fe_{K\alpha}$X-ray scanning picture (Fig. 16.) the Fe shows a less uniform enrichment as compared to the Al. The two mineral grains essentially different, because the former, Al-poor grain is rich in Fe, while the latter contains less Fe than the matrix. On the $Mn_{K\alpha}$X-ray scanning picture (Fig. 17.) it is visible, that the enrichment confines to the Fe-poor grain. As compared to the matrix, the Fe-rich grain also contains Mn, but the difference of the two grains is essential. On the basis of Fig. 18 and 19. scanning pictures, the Co- and Ni-content is also high.

Ti-graphs were also made (Fig. 20.) Similarly as on Fig. 4., the Ti occurs also in the aggregates smaller than 10 μm. In comparison with the mean distribution, the Fe-rich grain shows a somewhat higher concentration. The above mentioned facts suggest, that in the two close grains enrich the geochemically related elements, but the concentrations show considerable differences. Because it is unlikely that the circumstances of the formation or the subsequent dissolution were different, these grains possibly formed in distant places, and secondary transportation came them close to each other.

On Fig. 21. the $Si_{K\alpha}$X-ray scanning picture of this same setting is shown. The Si enriches in larger aggregations, suggesting the presence of clay minerals.

The following graph-set is made on grey pyritic bauxite sample. Owing to their large size, the pisoids of this bauxite are unconvenient for the electron microprobe analysis. Besides of the size-problems, the hardness-differences of the textural elements also encumbered the preparation of suitable sections. Hence only pisoidic portion was examinable. It is visible on the composition picture (Fig. 22.), that the pisoid is not a sphaeroidal structure. It has a much greater atomic weight as compared to the matrix. In the matrix scattered small grains can be detected, with great electron reflection. On the boundary of the matrix and the globular grain there is a crust, which has a reflection identical to that of the matrix. On the $Fe_{K\alpha}$X-ray scanning picture (Fig. 23.) appears markedly the nodular Fe-enrichment of the matrix, outside of

the irregular outer crust. These small aggregations would be pyrite-marcasite grains. The Al attains its maximum in the pisoids (Fig. 24.). After a minimum in the outer crust, the Al-content increases again in the matrix. The Ca (Fig. 25.) enriches exclusively in the outer crust and in the matrix. The Ca of the matrix is represented as calcite or dolomite.

The composition picture of Fig. 26. shows a sample from the uppermost degraded zone of the Malomvölgy XII. bauxite body. The three well separable reflection fields can be traced on the X-ray scanning pictures too (Figs 27., 28., 29.). The matrix equally contains Al, Si and Fe. The dark field shows great Al content and complete Fe and Si abscence alike. This macroscopically white aggregate is gibbsite. On the basis of the element composition the matrix is of kaolinitic, and the Fe-rich part is macroscopically violet-coloured. On the other hand the Fe-free aggragate is white. This colour change, which is parallel to the Fe-content, can be due to the differences of the hematite-content. On the basis of trace element analyses, the Mn-content and the related changes in violet colour is opposed.

The sample is derived from a portion penetrated by macroscopically yellowish, 2 to 5 m long vertical veins, beneath the upper Fe crust of the Malomvölgy XII. bauxite body (Fig. 30., composition picure). On the $_{K\alpha}$X-ray scanning picture (Fig. 31.) visible is that the Fe is not represented, consequently these are desironized veins.

The next graph-set was made on this same section. On the composition picture of the globular grain (Fig. 32.) it is a great atomic weight field, as can be identified with the $Fe_{K\alpha}$X-ray scanning picture (Fig. 33.). Also parallel is the Ti distribution (Fig. 34.), which occurs, similarly as in the earlier samples, in the aggregates of about 10 μm size. The Al, as compared to the Fe, enriches in the matrix (Fig. 35.).

In the following part there are presented some samples from the lateritic bauxite of Goa (India), which were available by G y. K o m l ó s s y (ALUTERV). Here also the distribution of the main bauxitic elements (Al, Fe, Si, Ca, Ti) were studied.

The lateritic bauxite bodies are densely penetrated by fissures. These fissures – according to the climate of the given area – are infiltrated by solutions in great quantity. From these Fe-containing solutions goethite and hematite precipitate, infilling slowly the fissures. Some graphs of this "drainage-system"-like texture are figured here (Figs 36. to 45.). This series shows the veins in cross-section. On the composition pictures the high reflection fields represent the Fe-rich infilling of the vein, and within them – where the infilling was incomplete – there are Al-rich fields with low reflection. The X-ray scanning pictures show the Fe (Figs. 38., 40., 45), the Al (Figs. 37., 41., 44.) and the Si (Fig. 42.) distribution.

On the composition picture presented on Fig. 46. a longitudinal section of a vein is shown, with the $_{K\alpha}$X-ray scanning pictures of Fe (Fig. 47.), Al. (Fig. 48.) and Si (Sig. 49.). The Fe and Al enrichments here are in contrast too. On the basis of mineralogic studies the vein-

PLATE III.

Fig. 13. Detrital grains, Halimba III. bauxite body.
Composition picture. Picture width: 0,2 mm

Fig. 14. Detrital grains, Halimba III. bauxite body.
Composition picture. Picture-width: 0,1 mm

Fig. 15. Al_{K_α}X-ray scanning picture

Fig. 16. Fe_{K_α}X-ray scanning picture

Fig. 17. Mn_{K_α}X-ray scanning picture

Fig. 18. Co_{K_α}X-ray scanning picture

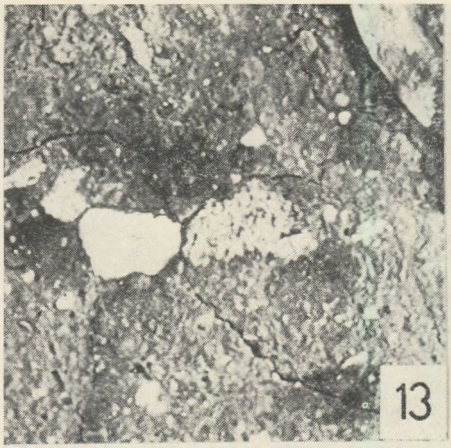
13

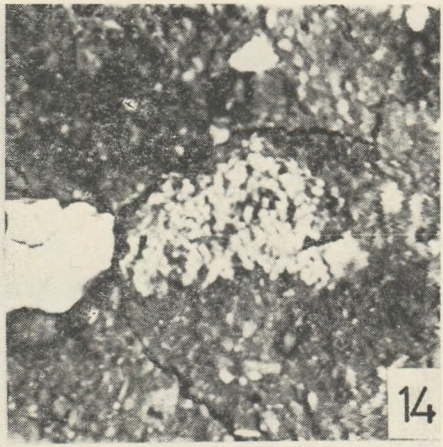
14

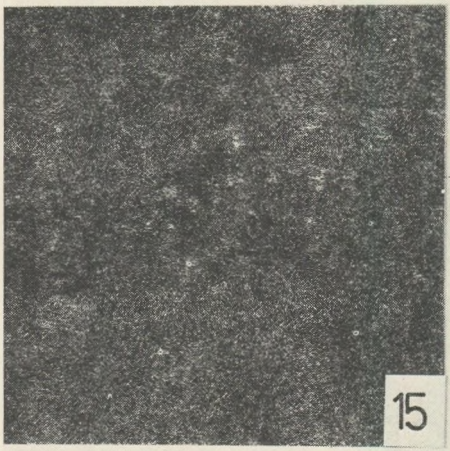
15

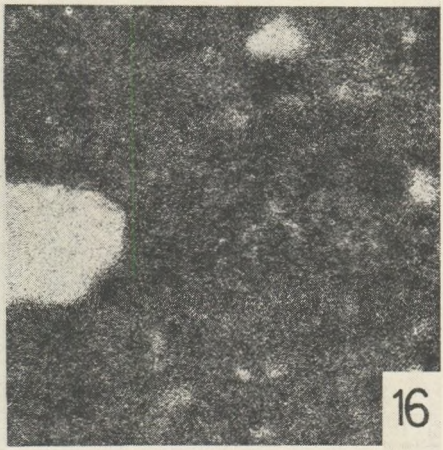
16

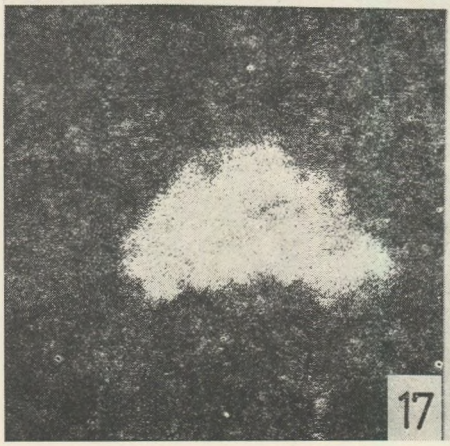
17

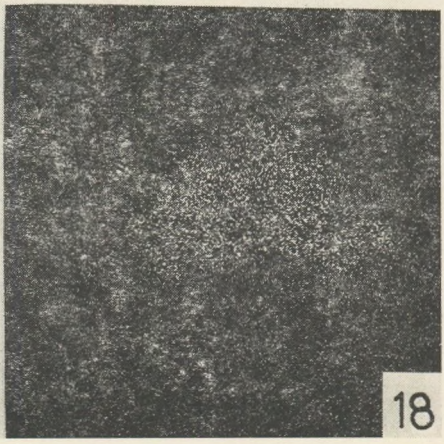
18

PLATE IV.

Fig. 19. Ni_{K_α}X-ray scanning picture

Fig. 20. Ti_{K_α}X-ray scanning picture

Fig. 21. Si_{K_α}X-ray scanning picture

Fig. 22. Pisoid from pyritic bauxite, Halimba III. bauxite body. Composition picture. Picture width: 0,2 mm

Fig. 23. Fe_{K_α}X-ray scanning picture

Fig. 24. Al_{K_α}X-ray scanning picture

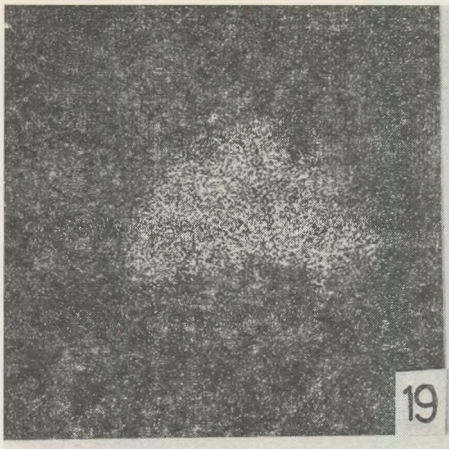
19

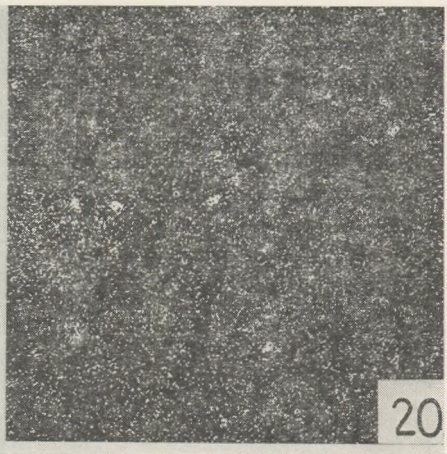
20

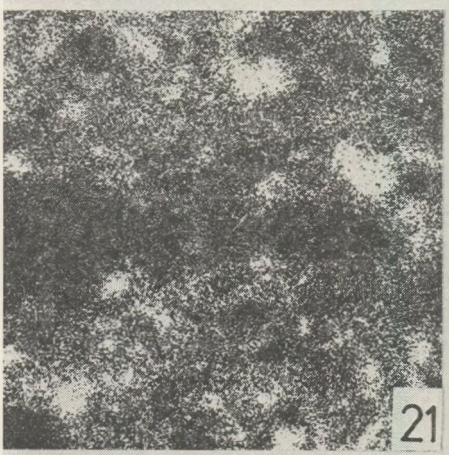
21

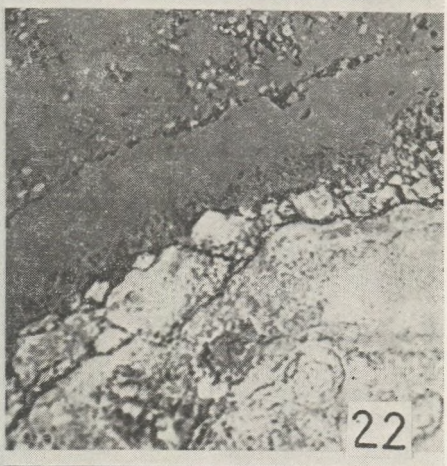
22

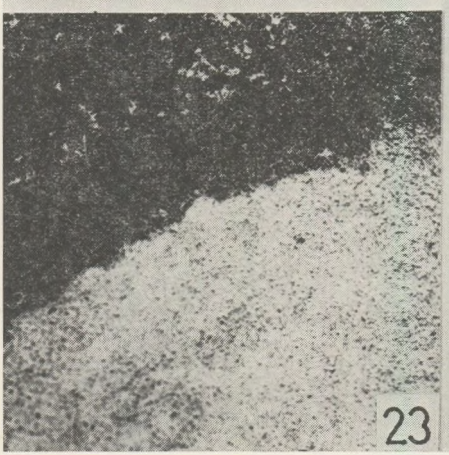
23

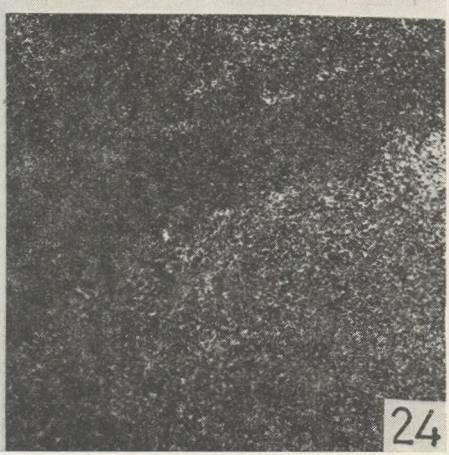
24

PLATE V.

Fig. 25. Ca_{K_α}X-ray scanning picture

Fig. 26. Degraded bauxite, Halimba Malomvölgy XII. bauxite body.
Composition picture. Picture-width: 0,2 mm

Fig. 27. Al_{K_α}X-ray scanning picture

Fig. 28. Si_{K_α}X-ray scanning picture

Fig. 29. Fe_{K_α}X-ray scanning picture

Fig. 30. Desironized vein in bauxite,
Halimba Malomvölgy XII. bauxite body.
Composition picture. Picture-width: 0,2 mm


25

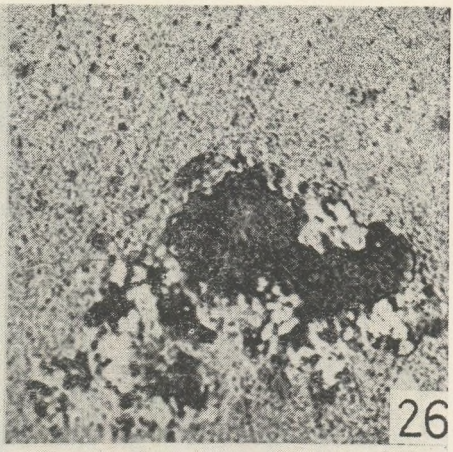
26

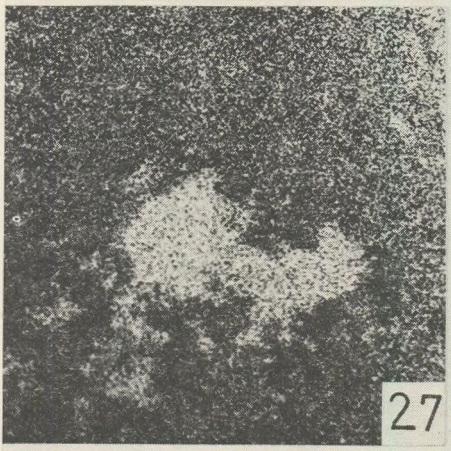
27

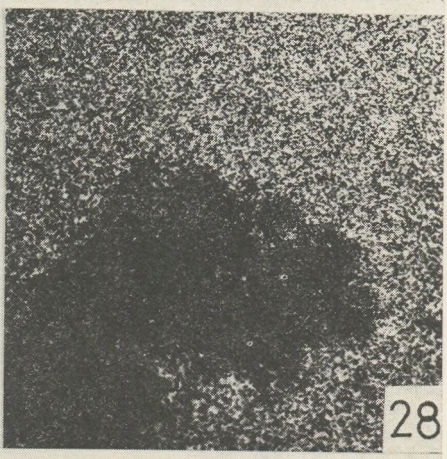
28

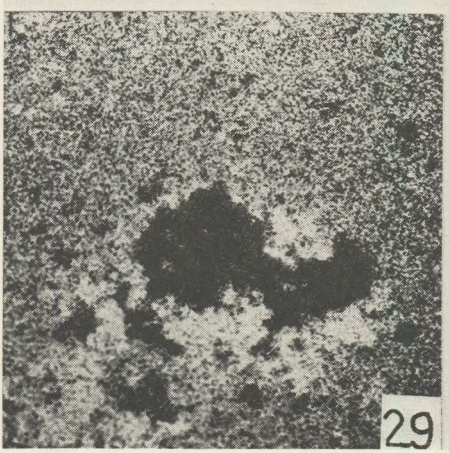
29

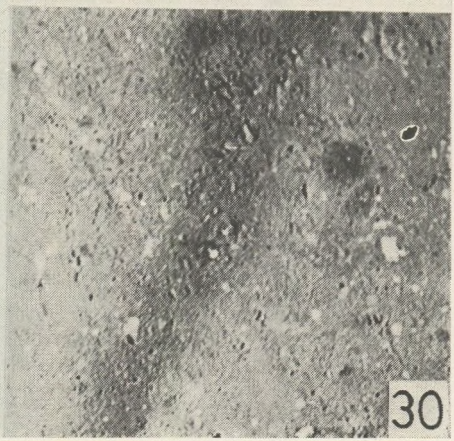
30

PLATE VI.

Fig. 31. $Fe_{K\alpha}$X-ray scanning picture

Fig. 32. Globular grain in bauxite, Halimba Malomvölgy XII. bauxite body.
Composition picture. Picture-width: 0,2 mm

Fig. 33. $Fe_{K\alpha}$X-ray scanning picture

Fig. 34. $Ti_{K\alpha}$X-ray scanning picture

Fig. 35. $Al_{K\alpha}$X-ray scanning picture

Fig. 36. Fe-rich vein-infilling, Goa, Shakti.
Composition picture. Picture-width: 0,2 mm

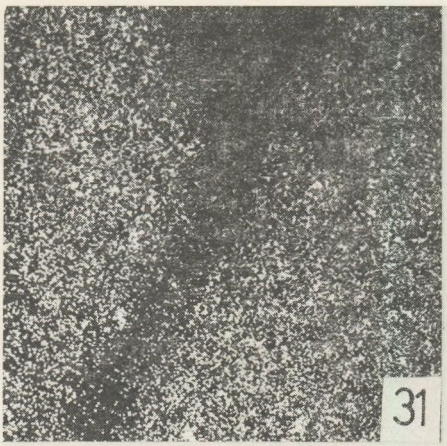
31

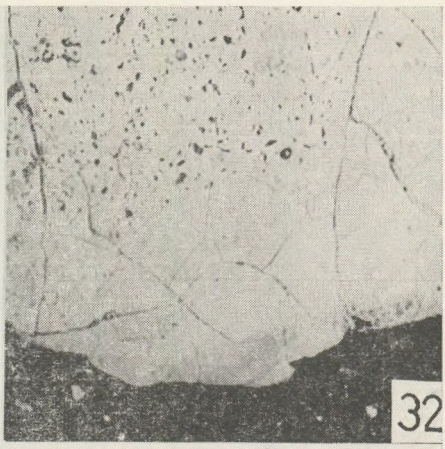
32

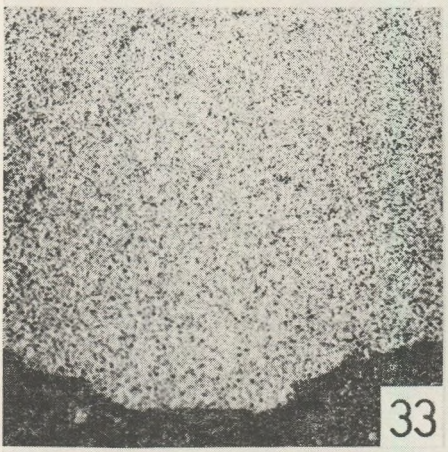
33

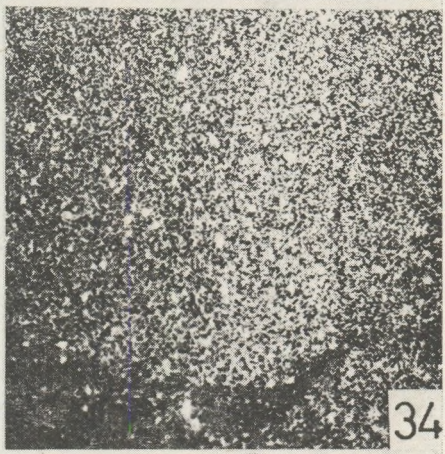
34

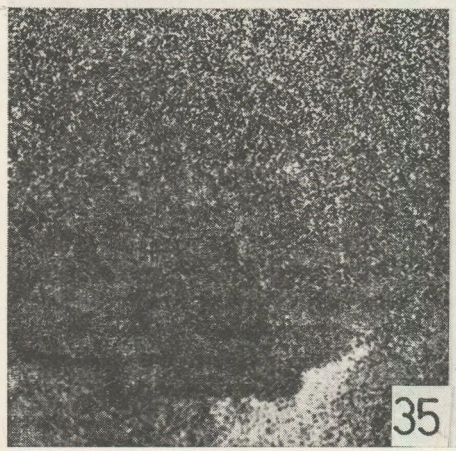
35

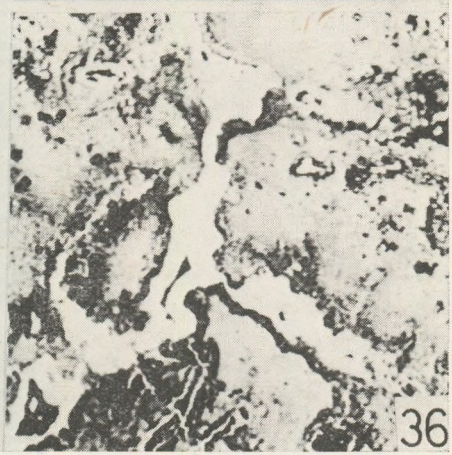
36

PLATE VII.

Fig. 37. Al_{K_z}X-ray scanning picture

Fig. 38. Fe_{K_z}X-ray scanning picture

Fig. 39. Fe-rich vein-infilling, Goa, Shakti. Composition picture. Picture-width: 0,2 mm

Fig. 40. Fe_{K_z}X-ray scanning picture

Fig. 41. Al_{K_z}X-ray scanning picture

Fig. 42. Si_{K_z}X-ray scanning picture

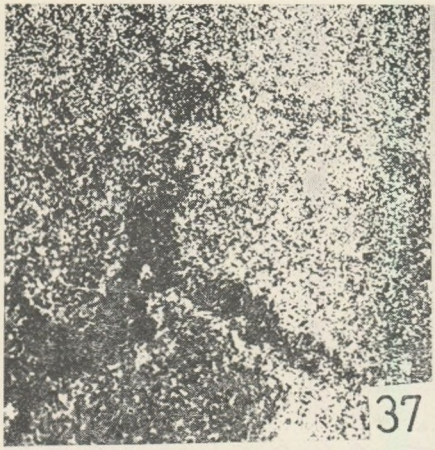
37

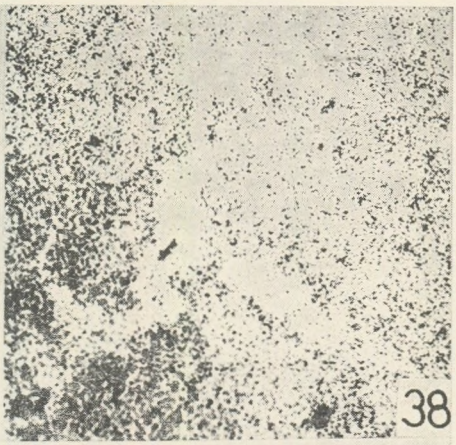
38

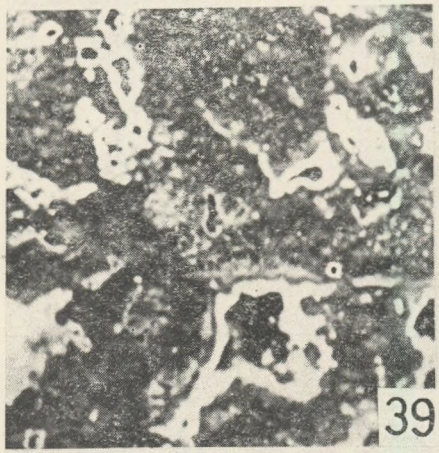
39

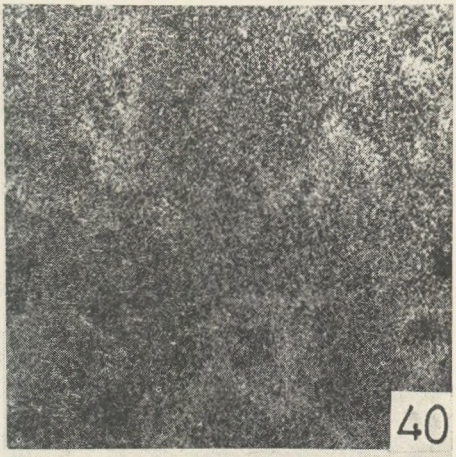
40

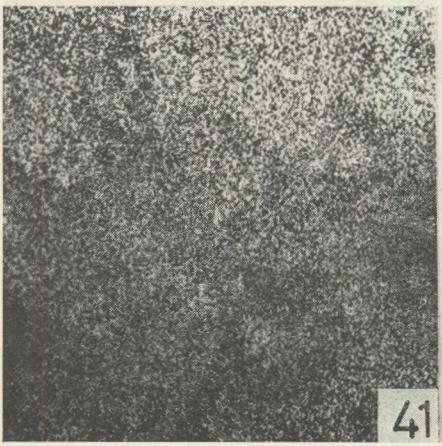
41

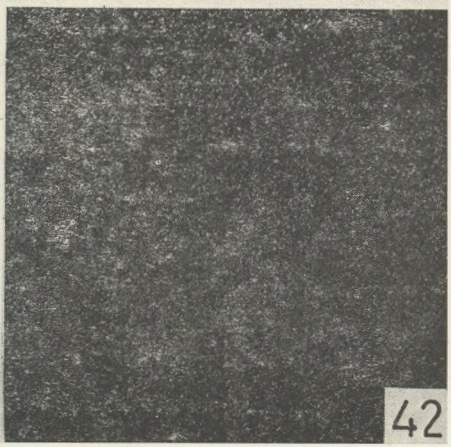
42

PLATE VIII.

Fig. 43. Fluidal vein-infilling, Goa, Shakti.
Composition picture. Picture-width: 0,2 mm

Fig. 44. $Al_{K\alpha}$X-ray scanning picture

Fig. 45. $Fe_{K\alpha}$X-ray scanning picture

Fig. 46. Longitudinal vein section, Goa, Junas.
Composition picture. Picture-width: 0,2 mm

Fig. 47. $Fe_{K\alpha}$X-ray scanning picture

Fig. 48. $Al_{K\alpha}$X-ray scanning picture


43


44

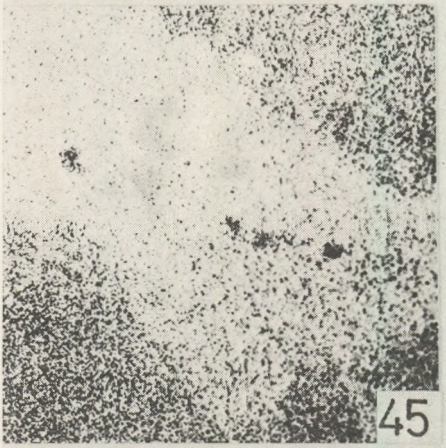
45


46


47

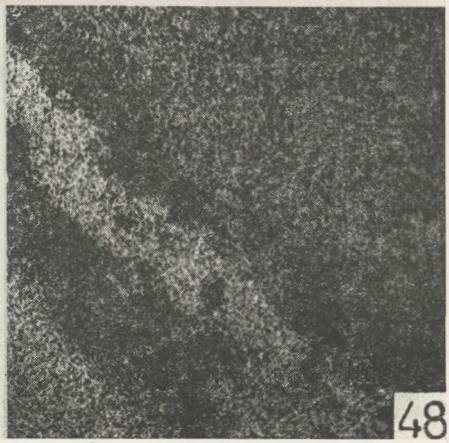
48

PLATE IX.

Fig. 49. $Si_{K\alpha}$X-ray scanning picture

Fig. 50. Detrital grain, Goa, Junas.
Composition picture. Picture-width: 0,15 mm

Fig. 51. $Ti_{K\alpha}$X-ray scanning picture

Fig. 52. $Fe_{K\alpha}$X-ray scanning picture

Fig. 53. $Al_{K\alpha}$X-ray scanning picture

Fig. 54. Detrital grains, Goa, Junas.
Composition picture. Picture-width: 0,075 mm

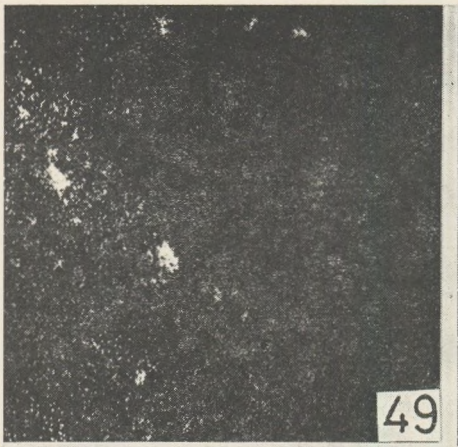
49

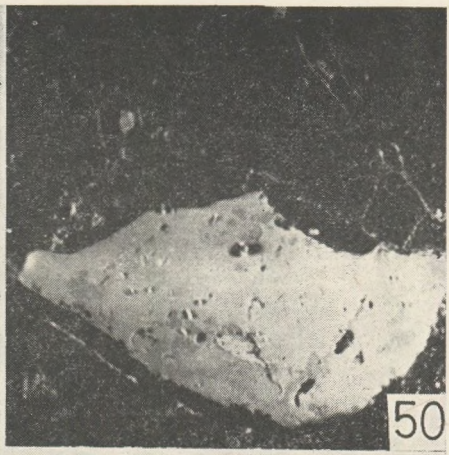
50

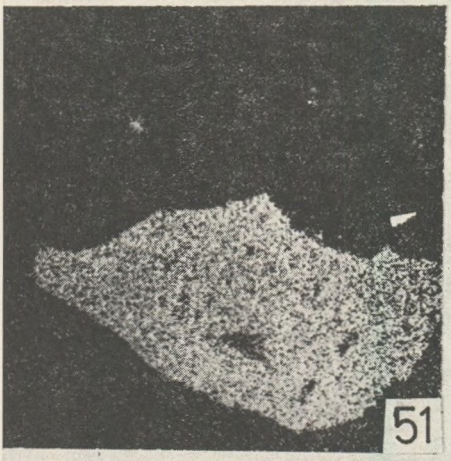
51

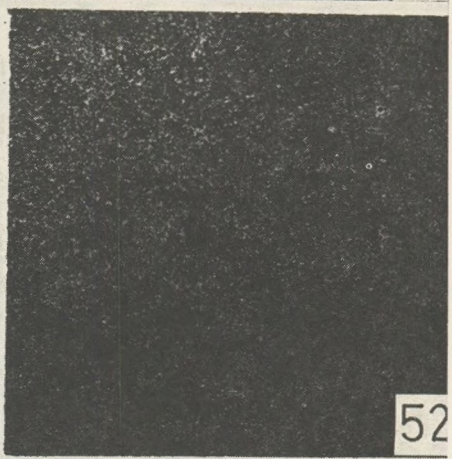
52

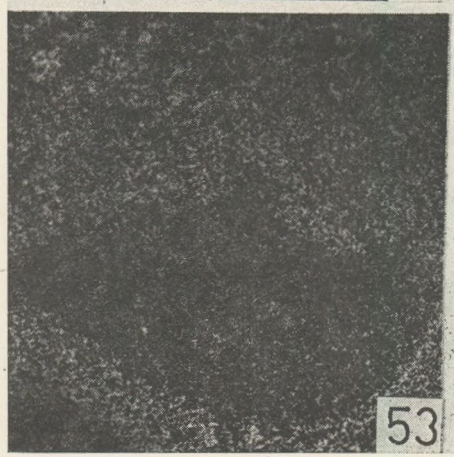
53

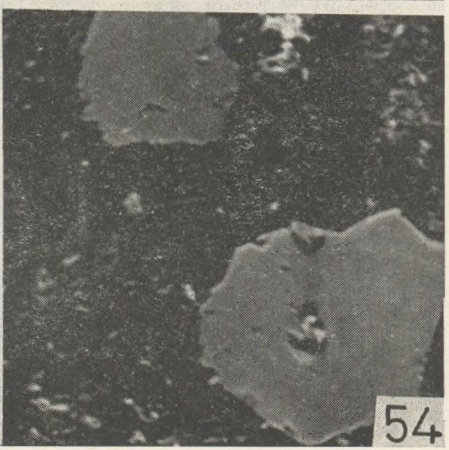
54

PLATE X.

Fig. 55. Mg_{K_α}X-ray scanning picture

Fig. 56. Si_{K_α}X-ray scanning picture

Fig. 57. Al_{K_α}X-ray scanning picture

Fig. 58. Fe_{K_α}X-ray scanning picture

Fig. 59. Detrital grains, Goa, Shakti.
Composition picture. Picture-width: 0,2 mm

Fig. 60. Ti_{K_α}X-ray scanning picture

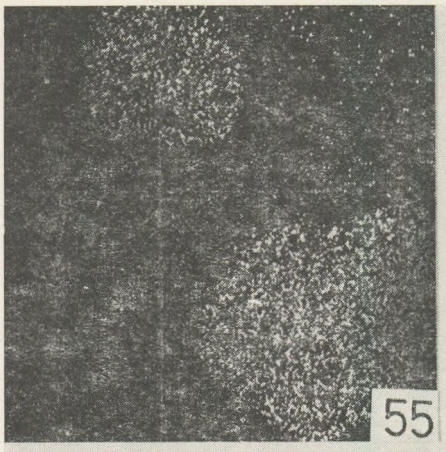
55

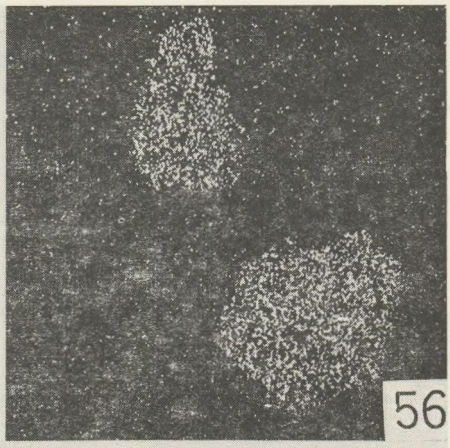
56

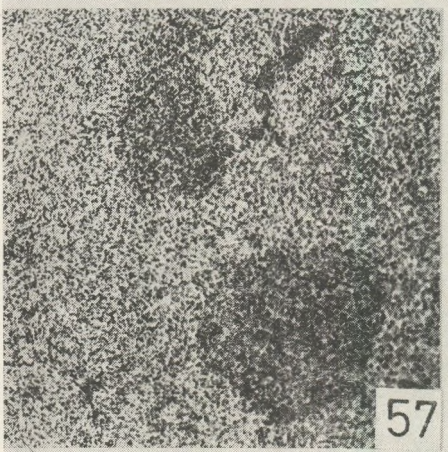
57

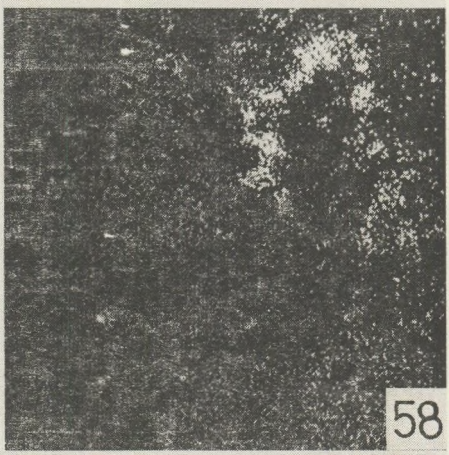
58

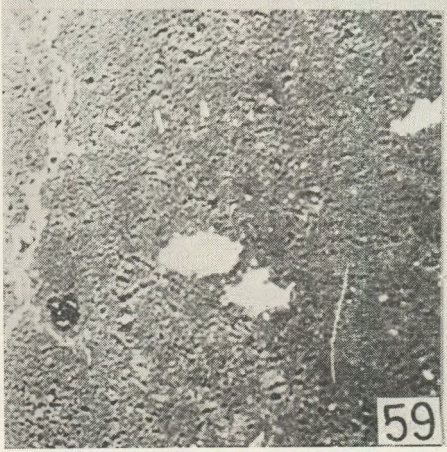
59

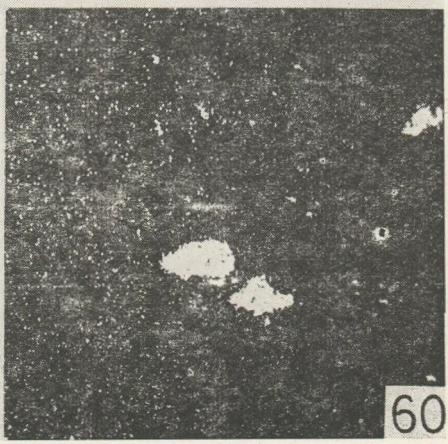
60

infilling within the Fe crust is gibbsite. The Si enriches in the matrix. The Si is connected rather to Al-rich parts then to the Fe-rich fields.

On the basis of corresponding Ti (Fig. 51.), Fe (Fig. 52) and Al (Fig. 53.) $_{K\alpha}$X-ray scanning pictures of composition picture figured on Fig. 50., a high Ti-content mineral grain can be recognized. It is neither an ilmenite, so characteristic in bauxites by the poor Fe-content, nor ulvite (Fe_2TiO_4) and pseudobrookite. The lack of Si excludes the presence of any silicate. Hence this mineral grain may be a TiO_2 modification (anatase or rutile).

Finally two mineral grains are presented on the Fig. 54. composition picture. These bear a lower reflection as compared to the TiO_2 modification mentioned above. On the basis of Fig. 55. $Mg_{K\alpha}$X-ray scanning picture, Mg-content appears, but enrichment exclusively occurs in Si (Fig. 56.). The Fe-content is greater than that of the matrix. Na, K and Ca-content cannot be detected. Considering the element composition and the form, these grains can be determined as Ca-less amphiboles.

REFERENCES

Balkay, B. and Bárdossy, Gy. (1967): Lateritesedési részfolyamat vizsgálata Guinea-i lateriteken. (Étude des processus élémentaires de la latérisation sur latérites guinéennes.) Földt. Közl. XCVII. 1. pp. 91–101.

Bárdossy, Gy. (1961): A magyar bauxit geokémiai vizsgálata. (Geochemical research of Hungarian bauxites). MÁFI kiadványa.

Bárdossy, Gy. and Pantó, Gy. (1970): A bauxitok vizsgálata elektronmikroszondával. (Research of bauxites by electron microprobe.) BKL Bányászat, 103, 2. pp. 825–837.

Bárdossy, Gy. and Pantó, Gy. (1972): On the pyrite types in bauxites. Acta Geol. tom. 16. pp. 3–11.

Dudich, E. Jun. and Komlóssy, Gy. (1969): Ősföldrajzi-szerkezeti szempontok a magyar bauxit korkérdéséhez. (Considérations paléogeographiques et tectoniques sur la probleme de l'age des bauxites en Hongrie.) Földt. Közl. XCIC. 2. pp. 155–165.

Komlóssy, Gy. (1966): A bauxit piritesedés kérdése. (On the problem of the pyritisation of bauxite.) Földt. Közl. XCVI. 2. pp. 220–226.

Pantó, Gy. (1969): Elektronmikroszonda működése és földtani vonatkozásai. (Working of the electron microprobe and its geological application.) MTA X. Oszt. Közl. 3. pp. 263–281.

UNTERSUCHUNGEN ÜBER DEN ZUSAMMENHANG ZWISCHEN MORPHOLOGIE UND STRUKTUR BEI DEN CÖLESTIN-KRISTALLEN DES TRANSSYLVANISCHEN BECKENS (RUMÄNIEN)

von

J. IMREH

Mineralogisches Institut, Univ. Bólyai-Babes, Cluj.

Eingegangen am 15.9. 1973

RÉSUMÉ

Dans le premier chapitre l'auteur présente la morphologie des cristaux, fondée sur l'étude de 874 cristaux recueillis de 5 occurence. On été établie 48 combinaisons différentes des 17 formes déterminées. On constatait la domination des cristaux formées des 5 formes.

On a présenté les valeurs P et les valeurs D, T, S rélatives à la grandeur des formes: D désigne la dominance, T la grandeur de transition et S la grandeur subordonnée des formes.

L'importance des zones a été établie au moyen des valeurs D_z et des valeurs g du P. Niggli. L'order d'importance des zones est présenté dans le tableau 5.

Les habitus des cristaux sont présentés dans la dernière partie du premier chapitre.

Le second chapitre traite la structure de la célestine, la succession des plans réticulaires, la période d'identité, le principe de la construction etc. pour les formes étudiées par l'auteur.

Dans le troisième chapitre est présenté la liaison entre la morphologie et la structure réticulaire.

Se fondant sur l'étude des cristaux recueillis l'auteur est arrivé à la conclusion, que l'hypothèse du P. Niggli, en ce qui concerne l'importance des suites réticulaires avec les distances minimes entre les particules constitutifs, est inapplicable à la célestine.

Dans l'étude de la corrélation l'auteur se fond sur le principe de la construction des plans réticulaires et sur la période d'identité entre les plans réticulaires. Tant que la période d'identité entre les plans réticulaires et leur densité réticulaire est plus grande, tant s'augmente aussi l'importance des formes dans la morphologie des cristaux.

En prenant en considération ces critériums, on a établi l'importance suivante des formes principaux: {011}, {001}, {210}, {101}, {100}, {102}, {111}, {110} et {211}.

Einleitung

Im Studium der Beziehung zwischen Morphologie und Struktur gibt es zwei wichtige Seiten, die äussere Form und die Gitterstruktur.

Die erste Seite des Problems wurde in den früheren Arbeiten über Cölestin des Siebenbürger Beckens vernachlässigt. Die Forscher, die sich mit den Cölestin-Kristallen beschäftigten (Benkő (1885); Koch (1888, 1889); Szádeczky (1889); Stoicovici und Gliszcinszki (1936); Zimányi (1888); Szádeczky (1923); haben im allgemeinen wenige Kristalle untersucht. Selbst in den Fällen, wo die Zahl der untersuchten Kristalle etwas grösser war, wurden die statistischen Daten der Formen nicht zusammengestellt. Wir besitzen nicht einmal Daten bezüglich der Persistenzwerte der Formen.

Die älteren Forscher (Koch, Benkő, Zimányi) haben sich das Problem der statistischen Daten überhaupt nicht gestellt, solche Forschungen wurden zu ihrer Zeit nicht gemacht.

Die neueren Forschungen haben diese so wichtige Seite der Morphologie der Kristalle auch nicht betont. Die statistischen Daten der Formen erlauben eine genaue Beshreibung der Morphologie und durch diese, eine vollständigere Kenntnis einer Seite unserer Beziehung. In dieser Hinsicht müssen wir aber erwähnen, dass nicht einmal die modernen Untersuchungen die Erfordernisse einer umfassenderen Kenntnis der Kristallformen erfüllten.

Es gab drei statistische Hauptwerte: P (Persistenzwert) und g (Besetzungszahl) von P. Niggli (1941) in die kristallographischen Untersuchungen eingeführt, bzw. der Wert G (Grössenzahl) von V. M. Goldschmidt (1923).

Der P-Wert charakterisiert die Persistenz in Kombinationen, g die Wichitgkeit der Zonen und G die Grösse der Formen.

Von der Formel $\sum_{1}^{z} (n\,H)_z$, mit welcher man die g-Werte berechnet, kommt man zur Schlussfolgerung, dass sie auf der Persistenz der Formen basieren.

Die Persistenz gibt uns ein getreues Bild, was die Häufigkeit der Formen betrifft, aber vom Gesichtspunkt des Habitus oder der Bedeutung der Zonen ist es nicht gleichgültig, ob eine Form in dominanter, oder untergeordneter Grösse auftritt, selbst im Falle einer Form mit maximaler Persistenz.

Goldschmidts G-Wert scheint auf den ersten Blick das Problem der Grössenverhältnisse der Formen zu lösen. Diesen Wert berechnet man mit der Formel:

$$G = g\,\frac{100}{3n},$$

wo $g = 3i + 2k + l$. Mit i bezeichnet man die dominierenden Flächen, mit k die Übergangsflächen, mit l die kleinen Flächen. Goldschmidt's G-Wert ist unbestreitbar ein Schritt vorwärts im Studium der Morphologie der Kristalle. Er hat aber den Nachteil, dass die drei Kategorien von Formen (dominante, übergangs- und untergeordnete) durch einen einzigen Wert gekennzeichnet sind, was eine Trennung der Grösse nach und eine genauere Charakterisierung der Formen nicht ermöglicht. G-Werte sagen zum Beispiel nicht, auf wieviel Kristallen eine Form in dominanter oder unregeordneter Grösse auftritt. Dieses ist auch die Ursache, dass G-Werte nicht mehr verwendet werden.

Niggli hat diese Unzulänglichkeiten festgestellt und eine neue Einteilung aufgestellt, indem er die Formen auf Grund der Persistenz in

fünf Kategorien gruppierte (Leitformen, Nebenleitformen usw.). Diese Aufteilung Niggli's hat wiederum den Nachteil, dass sich auch sie auf den Persistenzwerten aufbaut, die Grösse der Formen wurde auch in diesem Fall nicht berücksichtigt.

Unserer Ansicht nach ist Goldschmidt's Idee gut, aber nicht in ihrer ursprünglicher Form. Für die Charakterisierung der Grössenbeziehungen der Formen haben wir drei neue kristallographische Werte eingeführt: D, T und S, welche mit folgenden Formeln berechnet wurden:

$$D = d\frac{100}{n} \qquad T = t\frac{100}{n} \qquad S = s\frac{100}{n},$$

D = Dominationswert; T = Übergangswert (Transitionswert); S = Unterordnungswert (Subordinationswert); d, t, s = Anzahl der Kristalle, auf denen die betreffende Form in dominierender, mitlerer, oder in untergeordneter Grösse erscheint; n = Anzahl der Kristalle, bei denen (abgesehen von der Grösse: ob dominierende, mittlere oder untergeordnete) die betreffende Form gefunden wurde. Die Art und Weise, wie die Werte aus den obigen Formen bestimmt werden, und die Vorteile dieser Werte, wurden ausführlich in früheren Arbeiten dargestellt (I m r e h 1964).

Mit Hilfe dieser Werte kann die Morphologie der untersuchten Kristalle vollständig charakterisiert werden und damit wurde die erste Seite der Beziehung auf eine feste Grundlage gestellt.

Was die zweite Seite der Beziehung die Innenstruktur-betrifft, diese ist bekannt und wir werden in einem gesonderten Kapitel ausführlich darauf zurükkommen.

Im weiteren werden wir zuerst die Morphologie der studierten Cölestin-Kristalle behandeln, dann gehen wir zum Verhältnis zwischen Morphologie und innerer Struktur über.

I. Das morphologische Studium der Cölestin-Kristalle

Weil wir die Cölestin-Kristalle des Siebenbürgischen Beckens vom statistischen Gesichtspunkt aus ungenügend kennen, beruht unsere Arbeit auf dem von uns an 5 Orten gesammelten Material (Cluj, Baci, Copaceni, Cheia, Sandulesti (I m r e h, 1957). Dieses Material lieferte uns 874 für Kristallographische Untersuchungen geeignete Kristalle. Auf diesen Kristallen haben wir folgende Formen bestimmt:

a {100}	I {016}	j {0.1.14}	m 110	y {122}	x {135}
c {001}	Y {017}	d {102}	n 120	ϑ {124}	T {5.2.12}
o {011}	ϱ {018}	l {104}	z 111	f {113}	

Diese Formen sind in den an der Tabelle 1. gezeigten Kombinationen erschienen.

Tabelle 1.

	a	c	m	o	l	d	x	y	z	n	I	Y	ϱ	f	T	j	ϑ	Anzahl der Krist.
1	–	c	m	o	l	d	–	–	–	–	–	–	–	–	–	–	–	270
2	–	c	m	o	l	d	–	y	–	–	–	–	–	–	–	–	–	56
3	–	c	m	o	l	d	x	y	–	–		–	–	–	–	–	–	3
4	–	c	m	o	–	d	–	–	–	–	–	–	–	–	–	–	–	46
5	–	c	–	o	l	d	–	–	–	–	–	–	–	–	–	–	–	17
6	–	c	–	o	l	d	–	–	z	–	–	–	–	–	–	–	–	14
7	–	c	m	o	l	d	–	–	z	–	–	–	–	–	–	j	–	1
8	–	c	–	o	l	–	–	–	–	–	–	–	–	–	–	–	–	7
9	–	c	m	o	l	d	–	–	z	–	–	–	–	–	–	–	–	5
10	–	c	–	o	–	d	–	–	–	–	–	–	–	–	–	–	–	8
11	–	c	m	o	–	d	–	–	–	–	I	–		–	–	–	–	15
12	–	–	m	o	–	d	–	–	–	n	–	–	–	f	–	–	–	21
13	a	c	m	o	–	d	–	–	–	–	–	–	–	–	–	–	–	79
14	–	c	m	o	l	d	–	y	–	n	–	–	–	–	–	–		1
15	–	c	m	o	l	d	–	–	–	n	–	–	–	–	–	–		1
16	–	c	m	o	l	d	–	–	–	n	–	–	–	–	–	–	–	30
17	–	c	m	o	l	d	–	y	–	n	–	Y	ϱ	–	–	–		1
18	–	c	m	o	l	d	–	y	–	n	–	–	–	–	–	–	–	35
19	–	c	m	o	l	d	–	–	–	n	–	Y	ϱ	–	–	–		3
20	–	c	m	o	–	d	–	–	–	–	–	–	–	–	–	–		11
21	–	c	m	o	l	d	–	y	–	–	–	–	–	–	–			1
22	–	c	m	o	l	–	–	y	–	–	–	–	–	–	–	–	–	9
23	a	c	m	o	l	d	–	–	–	–	–	–	–	–	–	–	–	14
24	–	–	m	o	–	d	–	–	–	–	–	–	–	–	–	–	–	19
25	a	c	m	o	l	–	–	–	–	–	–	–	–	–	–	–	–	5
26	a	–	m	o	l	–	–	–	–	n	–	–	–	–	–	–	–	3
27	–	–	m	o	l	d	–	–	–	–	–	–	–	–	–	–	–	3
28	–	c	m	o	–	d	–	y	–	–	–	–	–	–	–	–	–	38
29	–	–	m	o	–	d	–	y	–	–	–	–	–	–	–	–	–	5
30	–	c	–	o	–	d	–	y	–	–	–	–	–	–	–	–	–	3
31	–	c	m	o	–	d	–	–	–	n	–	–	–	–	–	–	–	6
32	–	c	m	o	–	d	–	y	z	n	–	–	–	–	–	–	–	2
33	a	c	m	o	l	d	–	y	–	–	–	–	–	–	–	–	–	1
34	–	c	m	o	l	d	–	–	–	–	–	–	–	–	T	–	–	9
35	–	c	m	o	l	d	–	y	z	–	–	–	–	–	–	–		1
36	–	c	m	o	l	d	–	y	–	–	–	–	–	–	T	–	–	1
37	–	c	m	o	l	–	–	–	–	–	–	–	–	–	–	–	–	13
38	–	c	m	o	l	d	–	–	z	n	–	–	–	–	–	–	–	4
39	–	–	m	o	l	–	–	–	–	–	–	–	–	–	–	–	–	2
40	–	–	m	o	l	d	–	y	z	n	–	–	–	–	–	–	–	2
41	–	–	m	o	l	d	–	–	z	n	–	–	–	–	–	–	–	1
42	–	–	m	o	l	d	–	–	z	–	–	–	–	–	–	–	–	1
43	–	–	m	o	l		–	–	z	n	–	–	–	–	–	–	–	1
44	–	c	m	o	l	d	–	y	z	n	–	–	–	–	–	–	–	2
45	–	c	–	o	l	d	–	y	–	–	–	–	–	–	–	–	–	1
46	–	–	m	o	–	–	–	–	–	–	–	–	–	–	–	–	–	1
47	–	–	m	o	l	d	–	–	–	n	–	–	–	–	–	–	–	1
48	–	–	m	o	l	–	–	y	z	n	–	–	–	–	–	–	–	1

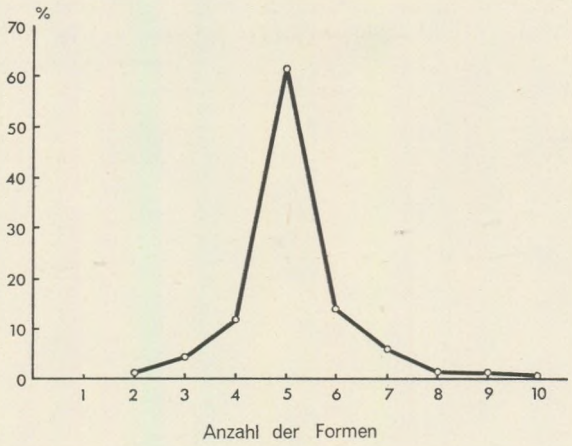

Abb. 1.

Aus dieser Tabelle bzw Tabelle 2. geht die Dominierung der aus 5 Formen gebildeten Kristalle hervor, eine Regelmässigkeit, die auch von andern Forscher bei der Cölestin-Kristallen gefunden wurde. Sowie wie uns von dieser Kombinationen entfernen, fällt die Zahl der Kristalle. Abbildung 1 bringt graphisch die Werte aus Tabelle 2.

Tabelle 2.

Anzahl der Formen	Anzahl der Kristallen	%
2	1	0,11
3	36	4,11
4	108	12,44
5	539	61,65
6	131	14,98
7	52	5,94
8	3	0,33
9	3	0,33
10	1	0,11

Die Persistenzwerte der Formen sind in der Tabelle 3 enthalten.

Auf Grund der Persistenzwerte können die Formen in 3 Kategorien eingeteilt werden. Die erste Gruppe enthält Formen mit hoher und höchster Persistenz ($P = 70{,}93 - 100$), in der zweiter Gruppen sind die Formen mit Werten zwischen 11,67 und 18,65 zusammengefasst, während zur dritten Gruppe Formen mit minimaler Persistenz gehören

($P = 0{,}11-4$). Aus diesem Gesichtpunkt sind die Formen der ersten Gruppe am bedeutendsten: {011}, {102}, {110}, {001} und {104}. Die hohe Persistenz dieser Formen erklärt das Vorherrschen der aus fünf Formen gebildeten Kristalle.

Tabelle 3.

	Symbol	Index	Persistenzwert
1	a	(100)	11,67
2	c	(001)	93,02
3	o	(011)	100,00
4	d	(102)	95,20
5	l	(104)	70,93
6	m	(110)	94,28
7	z	(111)	4,00
8	j	(0.1.14)	0,11
9	n	(120)	13,15
10	y	(122)	18,65
11	x	(135)	0,34
12		(124)	2,06
13	I	(016)	1,72
14	f	(113)	1,72
15	Y	(017)	0,47
16	ϱ	(018)	0,47
17	T	(5.2.12)	1,14

Tabelle 4.

	Symbol	Index	Dominierende		Mittlere		Untergeordnete		n
			d	D	t	T	s	S	
1	a	(100)	19	18,64	41	40,19	42	41,17	102
2	c	(001)	271	33,33	145	17,83	397	48,84	813
3	o	(011)	583	66,70	242	27,69	49	5,61	874
4	I	(016)	–	–	5	33,33	10	66,66	15
5	Y	(017)	–	–	–	–	4	100,00	4
6	ϱ	(018)	–	–	–		4	100,00	4
7	j	(0.1.14)	–	–	–	–	1	100,00	1
8	d	(102)	193	23,20	392	47,12	247	29,68	832
9	l	(104)	84	13,54	142	22,91	394	63,55	620
10	m	(110)	224	27,18	313	37,99	287	34,83	824
11	n	(120)	4	3,48	10	8,69	101	87,83	115
12	z	(111)	1	2,86	3	8,57	31	88,57	35
13	y	(122)	9	5,52	16	9,82	138	84,66	163
14	f	(113)	–	–		–	15	100,00	15
15	x	(135)	–	–	–	–	3	100,00	3
16	δ	(124)	–	–	–	–	18	100,00	18
17	T	(5.2.12)	–	–	–	–	10	100,00	10

Die Grössenverhältnisse der Formen sind in der Tabelle 4 wiedergegeben. Aus dieser Tabelle entnehmen wir, dass es 9 Formen gibt, die auch in dominierender Grösse auftreten: {001}, {011}, {110}, {102}, {100}, {104}, {122}, {120}, und {111}. Auf dem ersten Blick stellt man einen Parallelismus zwischen Persistenz- und Dominationswerten fest. Die Formen mit Persistenzwerten der ersten Gruppe haben auch relativ grössere Dominationswerte, ausgenommen {100}. Betrachten wir aber den allgemeinen Charakter der Formen, so ändert sich das Bild. Eine einzige Form hat dominanten allgemeinen Charakter {011}, weil $D = 66{,}70$ alle anderen Werte übersteigt ($T = 27{,}69$; $S = 5{,}61$). Die Formen {102} und {110} haben im allgemeinen Übergangscharakter ($T = 47{,}12$; $T = 37{,}99$), während die Formen {001} und {104} durchwegs einen untergeordneten Charakter aufweisen, ($S = 48{,}84$; $S = 63{,}55$) *obwohl sie hohe Persistenzwerte haben.* Trotzdem verleiht ihnen die Tatsache, dass diese Formen auch in dominierender Grösse autreten können, eine bestimmte Bedeutung, selbsverständlich im Verhältnis zu ihren D-Werten.

Die bedeutenderen Zonen

Die bedeutenderen Zonen der von uns untersuchten Kristalle sind:

[100] mit den Formen {001}, {011}, {016}, {017}, {018}, {0.1.14}
[211] mit den Formen {120}, {011}, {111}, {102}, {113}, {124}, {135}, {5.2.12}
[111] mit den Formen {110}, {011},
[011] „ „ „ {122}, {100}, {011}, {111},
[110] „ „ „ {001}, {110}, {113}, {111},
[010] „ „ „ {001}, {102}, {104}, {100},
[221] „ „ „ {110}, {102}, {122},
[001] „ „ „ {100}, {110}, {120},
[210] „ „ „ {001}, {120}, {122}, {124},
[441] „ „ „ {110}, {104}, {124}, {5.2.12},
[201] „ „ „ {122}, {102}.

Um die Bedeutung der Zonen zu bestimmen, haben wir in der kristallographischer Untersuchung die Werte D_z eingeführt (10), welche die Summe der Werte D aus der entschprecheden Zone darstellen. Die Werte D_z erhalten wir selbstverständlich nur aus Zonen, wo sich weingstens zwei Formen mit D-Werten befinden.

Die Bedeutung und der Nutzen der D_z-Werte im Vergleich mit andern zur Bestimmung der Wichtigkeit der Zonen, wurde in früheren Arbeiten (I m r e h, 1957) behandelt.

In Tabelle 5 bringen wir die D_z-Werte. Ebenfalls in diese Tabelle haben wir die Werte g aufgenommen, welche W. S c h i l l y (1933) für die Cölestin-Kristalle der Welt berechnet hat.

Tabelle 5.

Wichtigkeits-ordnung	Symbol d. Zonen		D_z-Wert	Wichtigkeits-ordnung	Symbol d. Zonen		g-Wert
	neu	alt			neu	alt	
1	[100]	[100]	100,03	1	010	010	691
2	[111]	[211]	96,24	2	100	100	609
3	[122]	[111]	93,88	3	011	011	518
4	[011]	[011]	93,73	4	120	110	470
5	[010]	[010]	88,71	5	111	211	463
6	[120]	[110]	63,37	6	001	001	421
7	[121]	[221]	55,90	7	122	111	385
8	[001]	[001]	49,30	8	121	221	371
9	[110]	[210]	42,33	9	101	201	281
10	[241]	[441]	40,72	12	241	441	223
11	[101]	[201]	28,72	14	101	201	205

Aus der Tabelle geht hervor, dass zwischen den Werten D_z und g für die ersten 8 Zonen keine grösseren Unterschiede bestehen, ausgenommen die Zonen [010] und [111], wo die Differenz 4 und 3 Einheiten in der Wichtigkeitsordnung beträgt.

Wichtiger ist die Tatsache, dass zwischen den Hauptzonen [100] und [011] die Differenz der D_z- und g-Werte nur eine Einheit beträgt. Weiter ist die Feststellung wichtig, dass die Zone [001] sowohl auf Grund der D_z-Werte, als auch der g-Werte eine geringe Bedeutung hat, nämlich der Ordnung 8 bzw 6. Auf dieses Verhalten der Zone [001] werden wir noch zurückkommen.

Der Habitus der Kristalle

Die von uns untersuchten Kristalle zeigten folgende Habitus-Typen:

1. Prismatische Kristalle, in der Achse a verlängert, mit dem Symbol:

$$A_a\,[100]$$

Im Symbol (C h u d o b a, 1930) ist A = axial; a = verlängert in der Achse a; [100] = dominierende Zone.

2. Tafelartige Kristalle nach {001} und in Richtung der Achse b-verlängert, mit dem Symbol:

$$P^b_{(001)}\,[010],\ [100]\quad (P = \text{Planar}).$$

3. Tafelige Kristalle nach {001}, in Richtung der a-Achse verlängert, mit dem Symbol:

$$P^a_{(001)}\,[100],\ [010].$$

4. Tafelige Kristalle nach {011}, in Richtung der Achse a verlängert, mit dem Symbol:

$$P^a_{(011)}\,[100],\ [110].$$

5. Isometrische Kristalle entstanden durch die Dominanz in Gleichgewicht der Formen {011} und {102}. Symbol:

$$I_{(011),\,(102)}\,[100],\ [010].$$

6. Isometrische Kristalle mit den dominanten Formen }110} und {011}. Symbol:

$$I_{(110),\,(011)}\,[100],\ [001].$$

Von diesen sechs Habitus-Typen sind die ersten drei am häufigsten.

II. Gitterstruktur des Cölestins

Die Struktur des Cölestins wurde von J a m e s und W o o d (1925) bestimmt. Die Raumgrupe ist D_{2h}^{16}, (Pnma). Die Dimensionen der Elementarzelle sind: $a_0 = 8{,}36$ Å; $b_0 = 5{,}36$ Å; $c_0 = 6{,}84$ Å. Das aus den strukturellen Daten hervorgehende Achsialverhältnis ist: 1,558:1:1,280. Wir bemerken also, dass das Achsialverhältnis für a_0 doppelt so groß ist, wie der vorher aus der äusseren Form der Kristalle bestimmte Wert. Aus diesem Grund geben wir im folgenden für die kristallographischen Symbole zwei Bezeichnungen, die neue und in geraden Klammern die alte.

Da in der elementaren Zelle 4 Moleküle enthalten sind, wurden 4 Stellungen für Sr und 4 für S festgestellt. Die von James und Wood für die Sr und S festgestellten Koordinaten erschweren beträchtlich die kristallographischen Berechnungen. Sie können aber vereinfacht werden, indem man 5/16, 1/4, 1/3 als Ausgangswerte nimmt und dann folgende Koordinaten erhält:

$$\mathrm{Sr}\,[[000]];\ \left[\left[\tfrac{1}{2}\ 0\ \tfrac{1}{6}\right]\right];\quad \left[\left[\tfrac{1}{8}\ \tfrac{1}{2}\ \tfrac{1}{2}\right]\right];\quad \left[\left[\tfrac{5}{8}\ \tfrac{1}{2}\ \tfrac{2}{3}\right]\right]$$

$$\mathrm{SO_4}\left[\left[\tfrac{1}{4}\ \tfrac{1}{2}\ 0\right]\right];\quad \left[\left[\tfrac{3}{8}\ 0\ \tfrac{2}{3}\right]\right];\quad \left[\left[\tfrac{7}{8}\ 0\ \tfrac{1}{2}\right]\right];\quad \left[\left[\tfrac{3}{4}\ \tfrac{1}{2}\ \tfrac{1}{6}\right]\right]$$

Der Sauerstoff setzt sich um den Schwefel nach einem Koordinations-Tetraeder, so dass das Zentrum der Gruppe SO_4 der Stellung des Schwefels entspricht.

Diese Koordinaten sind der Ausgangspunkt für alle Berechnungen die Struktur des Cölestins betreffend. Mit ihrer Hilfe kann man die Aufeinanderfolge und den Abstand zwischen den Gitterebenen einer Folge von Ebenen Zwischen $h_0k_0l_0$ und $h_1k_1l_1$, die Besetzung der Ebenen mit Partikeln, die Identitätsperiode, die Entfernung zwischen den Teilchen in Richtung jedweder Gittergerade, usw. verfolgen.

Die Gitterebenen

Da wir die Position der Gruppe SO_4 und Sr kennen, können wir die Aufeneinanderfolge der Serien irgendeines Gitter ebene berechnen. Die Arbeitsformel ist:

$$d_{1-8} = hx + ky + lz\,,$$

wo x, y und z die Koordinaten von Sr bzw. der Guppe SO_4 sind. Indem wir die Werte von x, y, z einsetzen, erhalten wir:

Sr	SO_4
$d_1 = h\,0 + k\,0 + l\,0$	$d_5 = h\frac{1}{4} + k\frac{1}{2}$
$d_2 = h\frac{1}{2} + l\frac{1}{6}$	$d_6 = h\frac{3}{8} + l\frac{2}{3}$
$d_3 = h\frac{1}{8} + k\frac{1}{2} + l\frac{1}{2}$	$d_7 = h\frac{7}{8} + l\frac{1}{2}$
$d_4 = h\frac{5}{8} + k\frac{1}{2} + l\frac{2}{3}$	$d_8 = h\frac{3}{4} + k\frac{1}{2} + l\frac{1}{6}$

Ersetzen wir die Indizes in diesen Formeln, so erhalten wir alle Kennzeichen der Gitterbenen.

Anschliessend bringen wir die Daten der Serien der Gitterebenen

⟨001⟩

$SrSO_4$	$SrSO_4$	$SrSO_4$	$SrSO_4$
0	$\frac{1}{6}$	$\frac{3}{6}$	$\frac{4}{6}$
(1)	(2)		(1)

$I_{001} = 44{,}81\,(\text{Å})^2$; $d_{001} = 6{,}84$ Å; $d_{001\,\min} = \frac{1}{6}d = 1{,}14$ Å; $q_1 = 1$; $q_2 = 1$

Der Wert d wurde mit folgender Formel berechnet:

$$d_{hkl} = \frac{V_{(abc)}}{1}\,,$$

wobei V das Volumen des elementaren Parallelepipeds ist und I die Inhalt des Elementarparallelogramms darstellt. Den Wert von I berechnen wir mit der Formel:

$$I_{hkl} = \sqrt{h^2\,b^2\,c^2 + k^2\,a^2\,c^2 + l^2\,a^2\,b^2}\,,$$

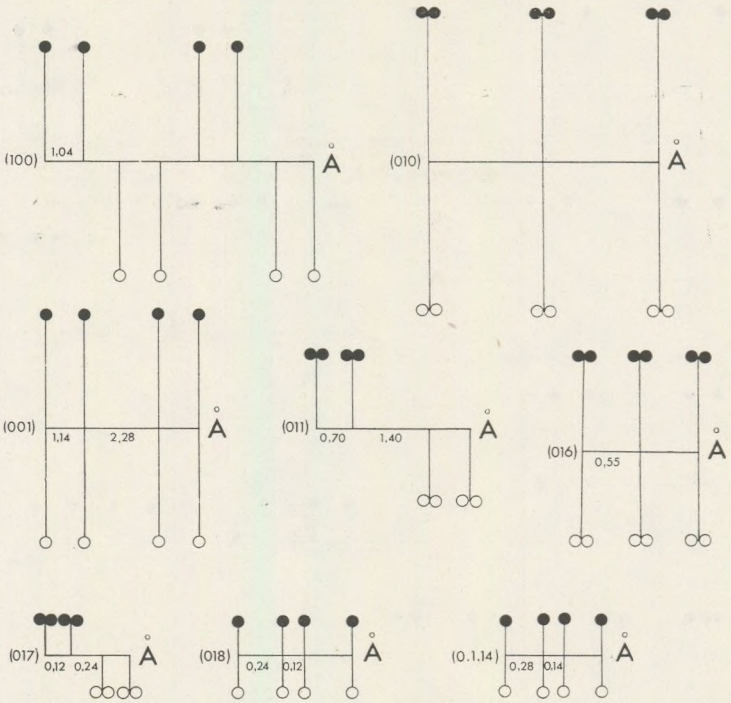

Abb. 2.

Stellen wir die Aufeinandefolge der Gitterebenen graphisch dar (nach N i g g l i), so erhalten wir die Abbildungen 2 und 3. Auf der Abszissen-Achse haben wir die Abstände zwischen den Gitterebenen dargestellt, auf der Ordinaten-Achse Sr mit ausgefüllten Kreisen und SO_4 mit Kreisen am Ende von Linien, deren Länge proportional mit dem Wert L ist.
Der Wert L wurde mit folgender Formel berechnet:

$$L = \frac{q_1 A_1 + q_2 A_2}{I_{hkl}},$$

wo q die Zahl der Partikel darstellt, welche in einem elementaren Parallelogramm enthalten sind, während A_1 bzw A_2 das Atomgewicht des Sr und der SO_4 Gruppe bedeten.

Aus der graphischen Darstellungen geht hervor, dass die Ebenen der Serie {001⟩ doppelt belastete ungemischte Ebenen sind.

⟨100⟩

Sr	Sr	SO_4	SO_4	Sr	Sr	SO_4	SO_4
0	$\frac{3}{24}$	$\frac{6}{24}$	$\frac{9}{24}$	$\frac{12}{24}$	$\frac{15}{24}$	$\frac{18}{24}$	$\frac{21}{24}$
(1)	(1)	(1)	(1)	(1)	(1)	(1)	(1)

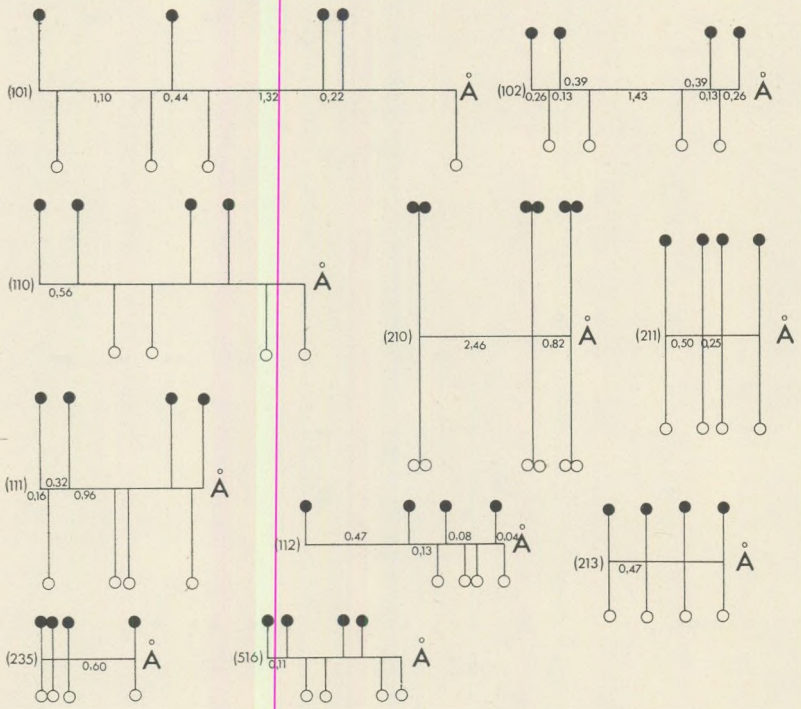

Abb. 3.

$I_{100} = 36{,}66\,(\text{Å})^2$; $d_{100} = 8{,}36$ Å; $d_{010}\,\min = 1{,}04$ Å; $q = 1$.

Einfach belastete, einfache Ebene.

$\langle 010 \rangle$

$$\begin{array}{ccccc} 2SrSO_4 & & 2SrSO_4 & & 2SrSO_4 \\ 0 & & \frac{1}{2} & & \frac{2}{2} \\ & (1) & & (1) & \end{array}$$

$I_{100} = 57{,}18\,(\text{Å})^2$; $d_{010} = 5{,}36$ Å; $d_{010}\,\min = 2{,}68$ Å; $q_1 = 2$; $q_2 = 2$

Vierfach belastete gemischte Ebene.

$\langle 011 \rangle$

$$\begin{array}{ccccccc} 2Sr & & 2Sr & & 2SO_4 & & 2SO_4 \\ 0 & & \frac{1}{6} & & \frac{3}{6} & & \frac{4}{6} \\ & (1) & & (2) & & (1) & \end{array}$$

$I_{011} = 72{,}65\ (\text{A})^2$; $d_{011} = 4{,}22$ Å; $d_{011}\ \min = 0{,}70$ Å; $q = 2$

Doppelt belastete einfache Ebene.

⟨016⟩

$2SrSO_4$	$2SrSO_4$	$2SrSO_4$
0	$\frac{3}{6}$	$\frac{6}{6}$
	(1) (1)	

$I_{016} = 274{,}8\ (\text{Å})$; $d_{016} = 1{,}11$ Å; $d_{016}\ \min = 0{,}55$ Å; $q = 2$; $q_2 = 2$

Vierfach belastete gemischte Ebene.

⟨017⟩

2Sr	2Sr	$2SO_4$	$2SO_4$	2Sr
0	$\frac{1}{6}$	$\frac{3}{6}$	$\frac{4}{6}$	$\frac{6}{6}$
	(1) (2)	(1)	(2)	

$I_{017} = 318{,}8\ (\text{Å})^2$; $d_{017} = 0{,}96$ Å; $d_{017}\ \min = 0{,}16$ Å; $q = 2$

Doppelt belastete einfache Ebene.

⟨018⟩

$SrSO_4$	$SrSO_4$	$SrSO_4$	$SrSO_4$	$SrSO_4$
0	$\frac{2}{6}$	$\frac{3}{6}$	$\frac{5}{6}$	$\frac{6}{6}$
	(2) (1)	(2)	(1)	

$I_{018} = 363{,}0\ (\text{Å})^2$; $d_{018} = 0{,}84$ Å; $d_{018}\ \min = 0{,}14$ Å; $q_1 = 1$ $q_2 = 1$

Doppelt belastete gemischte Ebebene.

⟨0.1.14⟩

$SrSO_4$	$SrSO_4$	$SrSO_4$	$SrSO_4$	$SrSO_4$
0	$\frac{2}{6}$	$\frac{3}{6}$	$\frac{5}{6}$	$\frac{6}{6}$
	(2) (1)	(2)	(1)	

$I_{0.1.14} = 629{,}7\ (\text{Å})^2$; $d_{0.1.14} = 0{,}48$ Å; $d_{0.1.14}\ \min = 0{,}08$ Å; $q_1 = 1$; $q_2 = 1$

Doppelt belastete gemischte Ebene.

⟨101⟩ (102)

Sr	SO_4	SO_4	Sr	SO_4	Sr	Sr	SO_4
0	$\frac{1}{24}$	$\frac{6}{24}$	$\frac{7}{24}$	$\frac{9}{24}$	$\frac{15}{24}$	$\frac{16}{24}$	$\frac{22}{24}$
	(1)	(5)	(1)	(2)	(6)	(1)	(6)

$I_{101} = 57{,}90$ (Å)^2; $d_{101} = 5{,}29$ Å; d_{101} min $= 0{,}22$ Å; $q = 1$

Einfach belastete einfache Ebene.

⟨102⟩ (104)

Sr	SO_4	Sr	SO_4	SO_4	Sr	SO_4	Sr
0	$\frac{2}{24}$	$\frac{3}{24}$	$\frac{6}{24}$	$\frac{17}{24}$	$\frac{20}{24}$	$\frac{21}{24}$	$\frac{23}{24}$
	(2)	(1)	(3)	(11)	(3)	(1)	(2)

$I_{102} = 96{,}83$ (Å)^2; $d_{102} = 3{,}16$ Å; d_{102} min $= 0{,}13$ Å; $q = 1$

Einfach belastete einfache Ebene.

⟨110⟩ (120)

Sr	Sr	SO_4	SO_4	Sr	Sr	SO_4	SO_4
0	$\frac{3}{24}$	$\frac{6}{24}$	$\frac{9}{24}$	$\frac{12}{24}$	$\frac{15}{24}$	$\frac{18}{24}$	$\frac{21}{24}$
	(1)	(1)	(1)	(1)	(1)	(1)	(1)

$I_{110} = 67{,}93$ (Å)^2; $d_{110} = 4{,}51$ Å; d_{110} min $= 0{,}57$ Å; $q = 1$

Einfach belastete einfache Ebene.

⟨210⟩ (110)

	$2SrSO_4$	$2SrSO_4$	$2SrSO_4$
0		$\frac{18}{24}$	$\frac{24}{24}$
		(3)	(1)

$I_{210} = 92{,}99$ (Å)^2; $d_{210} = 3{,}29$ Å; d_{210} min $= 0{,}82$ Å; $q_1 = 2$; $q_2 = 2$

Vierfach belastete gemischte Ebene.

⟨111⟩ (122)

Sr	SO_4	Sr	SO_4	SO_4	Sr	SO_4	Sr
0	$\frac{1}{24}$	$\frac{3}{24}$	$\frac{9}{24}$	$\frac{10}{24}$	$\frac{16}{24}$	$\frac{18}{24}$	$\frac{19}{24}$
	(1)	(2)	(6)	(1)	(6)	(2)	(1)

$I_{111} = 81{,}38\ (\text{Å})^2$; $d_{111} = 3{,}77$ Å; $d_{111}\ \min = 0{,}16$ Å; $q = 1$

Einfach belastete einfache Ebene.

⟨211⟩ (111)

$SrSO_4$	$SrSO_4$	$SrSO_4$	$SrSO_4$
0	$\frac{4}{24}$	$\frac{6}{24}$	$\frac{10}{24}$
	(2)	(1)	(2)

$I_{211} = 103{,}22\ (\text{Å})^2$; $d_{211} = 2{,}97$ Å; $d_{211}\ \min = 0{,}25$ Å; $q_1 = 1$; $q_2 = 1$

Doppelt belastete gemischte Ebene.

⟨112⟩ (124)

Sr	Sr	SO_4	Sr	SO_4	SO_4	Sr	SO_4
0	$\frac{11}{24}$	$\frac{14}{24}$	$\frac{15}{24}$	$\frac{17}{24}$	$\frac{18}{24}$	$\frac{20}{24}$	$\frac{21}{24}$
(11)	(3)	(1)	(2)	(1)	(2)	(1)	

$I_{122} = 287{,}1\ (\text{Å})^2$; $d_{112} = 1{,}04$ Å; $d_{112}\ \min = 0.043$ Å; $q = 1$

Einfach belastete einfache Ebene.

⟨213⟩ (113)

$SrSO_4$	$SrSO_4$	$SrSO_4$	$SrSO_4$
0	$\frac{6}{24}$	$\frac{12}{24}$	$\frac{18}{24}$
	(1)	(1)	(1)

$I_{213} = 163{,}5\ (\text{Å})^2$; $d_{213} = 1{,}87$ Å; $d_{213}\ \min = 0{,}47$ Å; $q_1 = 1$; $q_2 = 1$

Doppelt belastete gemischte Ebene.

⟨235⟩ (135)

$SrSO_4$	$SrSO_4$	$SrSO_4$	$SrSO_4$
0	$\frac{2}{24}$	$\frac{6}{24}$	$\frac{20}{24}$
	(1)	(2)	(7)

$I_{235} = 291{,}6\ (\text{Å})^2$; $d_{235} = 1{,}05$ Å; $d_{235}\ \min = 0{,}088$ Å; $q_1 = 1$; $q_2 = 1$

Doppelt belastete gemischte Ebene.

⟨516⟩ (5.2.12)

Sr	Sr	SO_4	SO_4	Sr	Sr	SO_4	SO_4
0	3/24	6/24	9/24	12/24	15/24	18/24	21/24
	(1)	(1)	(1)	(1)	(1)	(1)	(1)

$I_{516} = 330{,}5$ (Å)^2; $d_{516} = 0{,}92$ Å; d_{516} min $= 0{,}11$ Å; $q = 1$

Einfach belastete einfache Ebene.

Wenn wir die graphischen Darstellungen der Abbildungen 2 und 3 zentralisieren, so stellen wir fest (Abb. 4) das es Gitterebenen gibt, deren Bauprinzipien identisch oder sehr ähnlich ausfallen. Zum Beispiel (110) und (100), oder (210) und (010).

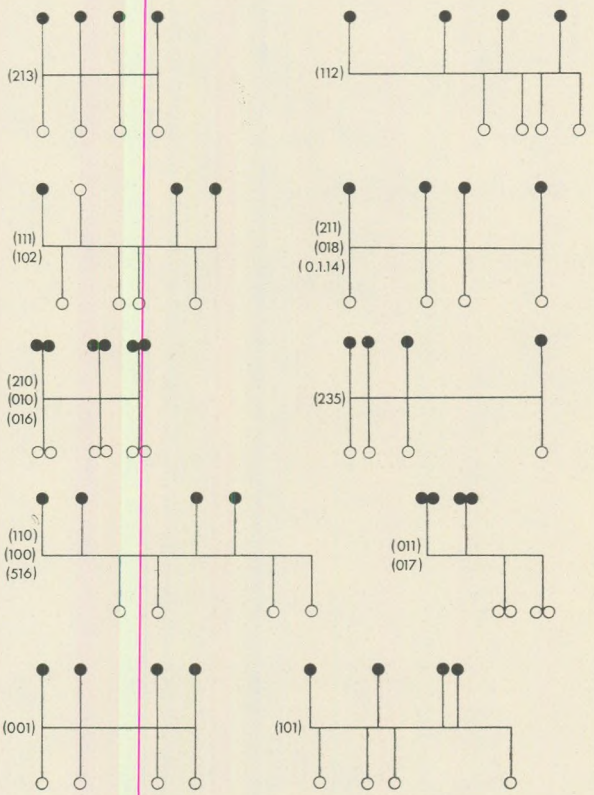

Abb. 4.

Auf Grund dieser Ähnlichkeiten bei den von uns untersuchten Cölestin- Kristalle des Siebenbürger Beckens können zehn Haupttypen aufgestellt werden, von denen vier Typen einfach belastete einfache Ebenen sind, ein Typus doppelt belastete einfache Ebene, vier Typen doppelt belastete gemischte Ebene und ein Typus einfach belastete gemischte Ebene darstellen.

In Zusammenhang mit den Abbildungen 2 und 3 müssen wir erwähnen, dass sie nicht einem absoluten Masstab ausgeführt sind, sondern nach einem relativen, weil einige Gitterebenen sich auf sehr kleinen Abständen wiederholen (zB. 0,04 Å), andere auf recht grossen Abständen (zB 2,46 Å), was die Beibehaltung eines durch gechenden Masstabs bei allen Abbildungen nicht ermöglicht. Aus diesen Grund haben wir zwischen den Gitterebenen derselben Serie ihre Abstände in Ziffern angegeben. Dasselbe kann man über die L-Werte sagen, die durch parallele Linien zu der Ordinatenasche dargestellt sind.

Die Darstellungen aus Abb. 4 sind schematisch und repräsentieren das Bauprinzip der Gitterebenen.

Gittergeraden

Die Abstände zwischen den Partikeln (Massenteilchen) in irgendwelcher Richtung des Kristallgitters haben wir mit folgender Formel berechnet:

$$T = \sqrt{u^2 a^2 + v^2 b^2 + w^2 c^2} ,$$

wo a, b, c die Kanten der Elementarzelle sind.

Bei den Hauptzonen der von uns untersuchten Kristalle erhielten wir die Werte der Tabelle 6.

Tabelle 6.

	Symbol d. Zonen		Parameter auf d. betr. Gittergeraden in Å
	neu	alt	
1	[010]	[010]	5,36
2	[001]	[001]	6,84
3	[100]	[100]	8,36
4	[011]	[011]	8,69
5	[110]	[210]	9,93
6	[101]	[201]	10,81
7	[111]	[211]	12,06
8	[120]	[110]	13,60
9	[121]	[221]	15,22
10	[122]	[111]	19,28
11	[241]	[441]	28,03

struktur muss auf die äussere Form gefolgert werden die der Ausdruck des inneren Aufbaus ist.

Unsere Untersuchungen an den Cölestin-Kristallen des Siebenbürgischen Beckens bestätigten gewissermassen die Richtigkeit von Niggli's Feststellung, dass die Belastung der Gitterebenen nicht der ausschlaggebende Faktor bei der Bildung des Habitus der Kristalle sein kann. Aus diesem Gesichtspunkt müssen wir die Bemerkung machen, dass *die Belastung der Gitterebene als solche* keinen ausschlaggebenden Faktor darstellt.

Trotz aller aufgezeigten Schwächen ist Niggl'is Idee im Vergleich zu anderen besser. Indem man das Prinzip Niggl'is auf den *Identitätsabstand zwischen den Gitterebenen* anwendet und das Bauprinzip der Gitterebenen in Betracht zieht, erhält man wirklichkeitsgetreuere Resultate.

Nehmen wir an, dass ein kleiner Abstand zwischen den Massenteilchen entlang einer beliebigen Richtung eine grosse Wachstumgeschwindigkeit voraussetzt (Niggli), dann sichern die grossen Abständen zwischen den Gitterebenen eine kleine Wachstumgeschwindigkeit in senkrechter Richtung auf diese Ebenen voraus. Je grösser der Identitätsabstand in einer beleibiger Richtung ist, deste grösser sind die der senkrechten Ebenen auf diese Richtung.

Aus Tabelle 7. geht hervor, das der grösste Identitätsabstand (5,29 Å) zwischen der Ebenen der Serie (101) besteht, also in senkrechter Richtung auf diese Ebene. Es folgen (011), (100), (111), (001), (210), (102), (211), (010), und (110), also genau (ausgenommen (010) dieselben Formen, welche beim Cölestin des Siebenbürgischen Beckens auch in dominierender Grösse auftreten können.

Tabelle 7.

	Index		Ident. Abstand (Å)
	neu	alt	
1	(101)	(102)	5,29
2	(011)	(011)	4,22
3	(100)	(100)	4,18
4	(111)	(122)	3,77
5	(001)	(001)	3,42
6	(210)	(110)	3,29
7	(102)	(104)	3,16
8	(211)	(111)	2,97
9	(010)	(010)	2,68
10	(110)	(120)	2,25
11	(235)	(135)	1,05
12	(112)	(124)	1,04
13	(017)	(017)	0,96
14	(016)	(016)	0,55
15	(0.1.14)	(0.1.14)	0,48
16	(213)	(113)	0,47
17	(516)	(5.2.12)	0,46
18	(018)	(018)	0,42

Beziehung Morphologie-Struktur zu lösen. Parallel mit den Hauptentwicklungsrichtungen erscheinen Flächen mit einem langsamen Wachstum und grosser Persistenz, also dominante Flächen. Die von uns bestimmten Dominationswerte (D) widerspiegeln genau diese Lage. Daher die Schlussfolgerung, dass diese Richtungen grosse Wachstumsgeschwindigkeit darstellen. Aus geometrischen Erwägungen geht hervor, dass senkrecht zu Richtungen mit grosser Wachstumgeschwindigkeit Flächen untergeordneter Grösse erscheinen, während parallel zu ihren grosse, dominante Flächen auftreten.

Niggli's Hypothese hat den grossen Nachtteil, dass sie aus der äusseren Form abgeleitet wurde. N i g g l i ist also genau umgekehrt vorgegangen, aus der äusseren Form hat er die Hauptgittergeraden gefolgert, anstatt die äussere Form aus der Gitterstruktur abzuleiten. Der zweite Satz des ersten Zitates zeigt klar diesen umgekehrten Vorgang.

Wenn Niggl'is Verfahren (Bedeutung der Gitterreihen mit kleinen Parametern) beim Quarz einige Ergebnisse gezeigt hat, so kann es beim Cölestin nicht in seiner ursprünglichen Form angewendet werden. Wir müssen erwähnen, dass die Hypothese nicht einmal beim Quarz allgemein gültig ist.

Die von uns untersuchten Cölestin-Kristalle zeigten verschiedenen Habitustypen. Es gibt tafelige Kristalle nach [001] und verlängert nach der Ache b. In diesem Fall bestätigt sich Niggli's Theorie, weil [010] die entwickelste Zone ist, während der Parameter in der Richtung der Gittergerade [010] der kleinste ist (5,36 Å).

Ein anderer Habitus – häufiger als der erste – ist der in Richtung der Achse a verlängerte und mit einer betonten Entwicklung der Zone [100]. Die Achse der Zone [100] hat den Parameter (8,36 Å) grösser als [010]. In diesem Fall könnte man aus der äusseren Form den Schluss ziehen, dass die Richtung [100] die wichtigste ist, was im Wiederspruch mit Niggli's Hypothese ist.

Wenn wir in Betracht ziehen, dass die Zone [001] bei den von uns untersuchten Cölestin-Kristallen eine Bedeutung der Ordnung 8 hat, ist es umso klarer, dass Niggli's Hypothese nicht verallgemeinert werden kann. Der Abstand zwischen den Teilchen längs der Achse [001] beträgt 6,84 Å!

Die Nichtanwendbarkeit der Theorie Niggli's für die Cölestin wird auch durch die g-Werte illustriert. Der g-Wert charakterisiert die Bedeutung der Zonen. Aus Tab. 5 geht hervor, dass die Zone [001] auf Grund der g-Werte eine Bedeutung der Ordnung 6 hat, obwohl die Zonen-Achse [001] einen Parameter aufweist der sie auf den zweiten Platz laut Niggli's Theorie setzt. Anders ausgedrückt wurde Niggli's Hypothese bezüglich der Gitterreihen durch die von ihm eingeführten g-Werte in Abrede gestellt. In diesem Fall die g-Werte wurden aus der Form der Kristalle abgeleitet, die Parameter der Gittergerade wurden aus den strukturellen Daten berechnet. Die zwei Seiten des Problems sind also in Ordnung, die Schlussfolgerungen schliessen sich aber gegenseitig aus. Es ist klar, dass die Methode umgekehrt werden muss, aus der Gitter-

struktur muss auf die äussere Form gefolgert werden die der Ausdruck des inneren Aufbaus ist.

Unsere Untersuchungen an den Cölestin-Kristallen des Siebenbürgischen Beckens bestätigten gewissermassen die Richtigkeit von Niggli's Feststellung, dass die Belastung der Gitterebenen nicht der ausschlaggebende Faktor bei der Bildung des Habitus der Kristalle sein kann. Aus diesem Gesichtspunkt müssen wir die Bemerkung machen, dass *die Belastung der Gitterebene als solche* keinen ausschlaggebenden Faktor darstellt.

Trotz aller aufgezeigten Schwächen ist Niggl'is Idee im Vergleich zu anderen besser. Indem man das Prinzip Niggl'is auf den *Identitätsabstand zwischen den Gitterebenen* anwendet und das Bauprinzip der Gitterebenen in Betracht zieht, erhält man wirklichkeitsgetreuere Resultate.

Nehmen wir an, dass ein kleiner Abstand zwischen den Massenteilchen entlang einer beliebigen Richtung eine grosse Wachstumgeschwindigkeit voraussetzt (Niggli), dann sichern die grossen Abständen zwischen den Gitterebenen eine kleine Wachstumgeschwindigkeit in senkrechter Richtung auf diese Ebenen voraus. Je grösser der Identitätsabstand in einer beleibiger Richtung ist, deste grösser sind die der senkrechten Ebenen auf diese Richtung.

Aus Tabelle 7. geht hervor, das der grösste Identitätsabstand (5,29 Å) zwischen der Ebenen der Serie (101) besteht, also in senkrechter Richtung auf diese Ebene. Es folgen (011), (100), (111), (001), (210), (102), (211), (010), und (110), also genau (ausgenommen (010) dieselben Formen, welche beim Cölestin des Siebenbürgischen Beckens auch in dominierender Grösse auftreten können.

Tabelle 7.

	Index		Ident. Abstand (Å)
	neu	alt	
1	(101)	(102)	5,29
2	(011)	(011)	4,22
3	(100)	(100)	4,18
4	(111)	(122)	3,77
5	(001)	(001)	3,42
6	(210)	(110)	3,29
7	(102)	(104)	3,16
8	(211)	(111)	2,97
9	(010)	(010)	2,68
10	(110)	(120)	2,25
11	(235)	(135)	1,05
12	(112)	(124)	1,04
13	(017)	(017)	0,96
14	(016)	(016)	0,55
15	(0.1.14)	(0.1.14)	0,48
16	(213)	(113)	0,47
17	(516)	(5.2.12)	0,46
18	(018)	(018)	0,42

Auf Grund der *D*-Werte (siehe Tabelle 4) ist die Reihenfolge der Bedeutung der Formen: (011), (001), (210), (101), (100), (102), (111), (110) und (211).

Zwischen der Bedeutungsordnung auf Grund des Identitätsabstand (strukturelle Seite) und der auf Grund der D-Werte bestimmten (morphologische Seite) gibt es Unterschiede. Bei der Form (011) beträgt diese Differenz eine Einheit, bei (001) drei, bei (210) drei, bei (101) drei, bei (100) zwei, bei (102) eine, bei (111) drei, bei (110) zwei, bei (211) eine Einheit. Wir stellen fest, dass die Differenzen höchstens drei Einheiten betragen.

Die Identitätsperiode ist aber nur einer der strukturellen Faktoren. Ein anderer sehr wichtiger Faktor ist das Bauprinzip der Gitterebenen. Wenn wir auch diesen Faktor in Betracht ziehen, lässt sich die Differenz zwischen der zwei Bedeutungsordnungen leicht erklären.

Obwohl zwischen den Ebenen (101) die grösste Identitätsperiode ist, hat sie in der Morphologie eine Bedeutung vierter Ordnung, weil die Serie aus *einfach belasteten Ebenen besteht.*

Die Form (011) hat eine Bedeutung erster Ordnung in der Morphologie, weil diese Serie eine grosse Identitätsperiode hat und aus *doppelt belasteten* Ebenen besteht.

Genauso erklärt sich die Differenz bei der Form (001). Auf Grund der Identitätsperiode belegt sie den fünften Platz, aber weil sie doppelt belastete Ebeben hat, muss ihre Bedeutung grösser sein. In der Morphologie hat sie tatsächlich eine Bedeutung zweiter Ordnung!

Auch die Differenz von drei Einheiten bei der Form (210) lässt sich erklären. Obwohl zwischen der Serie der Gitterebenen (210) die Identitätsperiode kleiner ist, *ist ihre Belastung vierfach* und das verleiht ihr in der Morphologie eine Wichtigkeit dritter Ordnung.

Die Differenzen von drei Einheiten bei der Form (111) erklären sich ebenfalls durch die Tatsache, dass die Serie aus einfach belasteten Ebenen besteht.

Die übrigen Differenzen betragen 1 bis 2 Einheiten.

Abbildung 4 ist die graphische Darstellung von Gitterebenen nach Gruppen identischer oder ähnlicher Bauprinzipien.

Ein Studium dieser Abbildung führt zu interessanten Feststellungen, wenn wir die verschiedenen Gitterebenen im Rahmen der gleichen Gruppe vergleichen.

Die Ebenen (210), (010), und (016) haben dasselbe Bauprinzip. In der Morphologie hat (210) eine Bedeutung dritter Ordnung, während (010) und (016) eine fast vernachlässigbare Bedeutung haben. Die kleinen Werte der Identitätsperiode für diese zwei letzten Formen erklären die grosse Differenz zu (210).

Die Ebenen (110) und (100) gehören zur selben Gruppe, die höhere Identitätsperiode der Serie (100) gibt ihr aber eine höhere Bedeutung, als (110).

Die Ebenen (011) und (017) haben dasselbe Bauprinzip, aber die sehr kleine Identitätsperiode (0,96 Å) von (017) verhindert ein betonteres Verhalten der Form in der Morphologie.

Lehrreich ist auch ein Vergleich der Formen (016), (017) und (018). Diese Formen erscheinen in derselben Zone und sind auf dem Kristall benachbart. Sie zeigen drei Typen von Gitterebenen. Auf dem Kristall erscheinen die zwei letzten ausnahmhlos als Flächen untergeordneter Grösse, während die erste in einigen Fällen auch als Übergangsgrösse auftreten kann.

Auf Grund der Identitätsperiode wäre die Bedeutungsordnung: (017), (016) und (018). Ziehen wir aber den Bau der Gitterebrenen in Betracht, so lässt sich die Tatsache, dass (016) auch als Übergangsgrösse auftritt, erklären: die Ebenen (016) sind *vierfach belastet!*

Der kleinen Dimensionen der Formen (017) und (018) wegen konnten wir keine Ordnung der morphologischen Bedeutung zwischen ihnen aufstellen, aber wenn wir auch den Bau der Gitterebenen in Betracht ziehen, können wir behaupten, dass die doppelt belasteten (017) Ebenen eine grössere Bedeutung haben, als (018), deren Ebenen einfach belastete sind. Die reelle Bedeutungsordnung dieser drei Formen ist: (016), (017) und (018).

Zusammenfassend können wir sagen, dass Niggli's Prinzip anwendbar ist, aber nicht auf die Zonenachsen, sondern auf die Identitätsperiode angewendet (senkrechte Richtungen auf die Gitterebenen) und nicht ausschliesslich, sondern verbunden mit dem Bauprinzip der untersuchten Gitterebenen. Wenn man nur mit der Identitätsperiode, oder nur mit dem Bauprin ip der Gitterebenen arbeitet, erhält man keine realen Resultate.

Zum Schluss müssen wir erwähnen, dass im ersten Kapitel dieser Arbeit für die Bezeichnung der Formen und Zonen alte Symbole verwendet wurden, welche aus dem morphologischen Achsenverhältnis $a : b : c = 0{,}781 : 1 : 1{,}28$ abgeleitet wurden.

In den Kapiteln II und III verwendeten wir die neuen Symbole, abgeleitet aus der strukturellen Achsenverhältnissen. Um die zwei Notierungen vergleichen zu können, wurde im ersten Teil des II Kapitels sowohl die alte, wie auch die neue Notierung verwendet (die alte in geraden Klamern, oder in den Tabellen wurde darauf hingewiesen, welche die alte Notierung ist).

LITERATUR

Benkő, G. (1885): Ein neues Vorkommen von Cölestin und Baryt in Siebenbürgen, Orv. Term. Tud. Ért. 10.

Chudoba, K. (1930): Zur morphologischen Typisierung der verschiedenen Kristalltrachten, C. Bl. Min. Abt. A.

Goldschmidt, V. M. (1923): Beitr. Krist. 2, 29.

Imreh, J. (1964): Noi valori cristalografice pentru caracterizarea habitusului si importantei zonelor. Stud. Cerc. Geol. 1, 9.

Imreh, J. (1957): Noua ocurenta cu celestina de la Cluj si Dumbrava, Bul. Univ. Babes-Bolyai, ser. St. Nat. II, 1 – 2.
Imreh, J. (1957): Noi cristale de celestina de la Baci, Stud. Cerc. Geol. Geogr. 8, 3 – 4.
Imreh, J. (1957): A cölesztin újabb előfordulása Koppándon, Földt. Közl. 87, 1.
Imreh, J. (1957): Cristale de celestina de la Sandulesti, Stud. Cerc. Geol. Geogr. 8, 1 – 2.
James, R. W. and Wood, W. A. (1925): The Crystal Structure of Baryte, Celestine and Anglesite, Proc. Roy. Soc. A.
Koch, A. (1888): Ein neues Cölestin- und Baryt Vorkommen in der nähe von Torda in Siebenbürgen, TMPM 9.
Koch, A. (1889): Ergänzende Beobachtung über des Cölestin- und Baryt-Vorkommen bei Torda in Siebenbürgen, TMPM, 10.
Niggli, P. (1926a): Baugesetze kristalliner Materie, Z. Krist. 63.
Niggli, P. (1926b): Beziehungen zwischen Struktur und äussere Morphologie am Quarz, Z. Krist. 63.
Niggli, P. (1941): Lehrbuch der Mineralogie und Kristallchemie.
Schilly, W. (1933): Zusammenhänge zwischen Morphologie, Struktur und Genesis bei Cölestin, N. Jb. Miner. Beil. Bd. 67.
Stoicovici, E. et Gliszczinski, S. (1936): Mineraux de genèse hydrotermale à Cluj, Compt. Rend. Ac. Sc. Roum. 1, 4.
Szádeczky, K. Gy. (1889): Beiträge zur Mineralienkenntniss Siebenbürgens, Orv. Term. Tud. Ért. 14.
Szádeczky, K E. (1923): Új cölesztin előfordulás Szindről. Föld. Közl. 53.
Zimányi K. (1888): Die kristallographischen Verhältnisse des Barytes und Cölestins von Dobogó-Berge, Mat. Term. Tud. Ért. 6.

FACIES STUDIES ON THE PLIOCENE AT BUDAPEST

by

I. ORSOVAI

Department of Applied and Engineering Geology, Eötvös University, Budapest
Received: 15 March 1974

ZUSAMMENFASSUNG

Das Pliocän im Karpaten-Becken ist ein selbständiger Sedimentzyklus, der sich im allgemeinen mit Erosions-Diskordans auf die älteren Formationen ablagert.

Gleichzeitig mit der weiteren Erhöhung und der Abrasion der Karpaten und des Mittelgebirges, sank der Beckenboden mit veränderlicher Geschwindigkeit, als dessen Ergebnis folgten die Transgressiens und die Auffüllungsperioden mehrmals innerhalb der Pliocänära nacheinander.

Auf dem Gebiet von Budapest befänden sich im Pliocän bis ans Ende Beckenrand-Facies, aber je Zeitalter und je Platz in sehr mannigfaltiger Ausbildung.

Introduction

The Pliocene rocks of Budapest have been studied in several works so far, and a comprehensive paper (F ö l d v á r i 1931) supplied the distribution of some facies-types with paleogeographic and tectonic evaluation. The common failure of the previous investigations was the lack of the over-all evaluation of the different facies features, as well as the lack of the ostracode studies.

Owing to the considerable facies sensity of the ostracodes, these studies enlarged significantly the informations for the geological evaluation. The shore-line reconstructions given by F ö l d v á r i were confirmed by the recent lithological and paleontological studies, but the previously outlined development was slightly modified.

The present paper deals with the paleogeographical reconstruction based on the studies carried out in the years of 1970 – 72.

Lower Pannonian

Within the studied area rocks of Lower Pannonian age are exclusively known around the villages Diósd and Nagytétény. At Diósd the Sarmatian limestone is unconformably overlain by sand and clay of 1 to 5 m thickness, and these are followed by a 22 to 34 m thick quartz-sand, which suitable as moulding sand after preparatory processes. The cross-bedding, as well as the overlying coarse gravel of this quartz-sand suggests nearshore deposition. Presumably equivalent in age and facies is the

light-grey quartz-sand overlying the Sarmatian limestone in the Gubacs brickyard, though the hanging wall is here the Upper Pannonian clay. Because of water-protective causes the quartz-sand is unexcavated in the clay pit; it is known only from boreholes. This quartz-sand is unfossiliferous, both its grain-size composition and roundness are equivalent to those of the sand at Diósd.

In the Lower Pannonian pelitic rocks bordering the Tétény Plateau a striking tendency to transgression can be recognized.

The Sarmatian coarse limestone is immediately overlain by greenish-grey calcareous clay. Together with the autochtonous, characteristic Lower Pannonian ostracodes [*Hungarocypris sieberi* (M é h.), Pl. I., fig. 3., *Amplocypris minuta* Z a l., *Candona (Camtocyprina) granulosa* Z a l.], occur in large numbers derived Sarmatian foraminifers [*Rotalia beccarii* (L i n n é), *Elphidium crispum* (L i n n é), Pl. II., fig. 3.] and otolithi (Pl. II., fig. 1.). Streams carriing detritus did not exist in the vicinity, the fine-grained material of limited quantity was floated from a distance. The influx of the $Ca(HCO_3)_2$ solution from the coarse limestone surroundings could have bear a significance. From 68% $CaCO_3$-content of the limestone originates in 23 percent from the fossils and in 45 percent from the submicroscopic micrite. In the overlying rock the derived Sarmatian faunal elements are subordinated. The 74% $CaCO_3$-content consits of molluscan detritus (49%) and micrite (25%). The majority of the Pannonian ostracode fauna [*Pontocypris redunca* Z a l., *Hungarocypris pannonica* (M é h.), Pl. I., fig. 2., *Hungarocypris trapezoidea* (M é h.), Pl. I., fig. 1., *Candona fossulata* P o k o r n ý, Pl. I., fig. 8.] fragmented before the burial, but the specimens embedded unbroken remained intact later. The uppermost rock-type is a fine-grained clay, with 31% $CaCO_3$-content, which originates in 4% from the fossils, and in 27% from the micrite. Sarmatian faunal elements are completely absent. On the cleavage planes of the rock it is recognizable, that the Pannonian ostracode remains embedded unbroken, and fragmented later by the considerable compaction of the sediments.

The fauna reconstructed from some entire specimens and determinable fragments cannot be identified with any other Hungarian association known so far.

One species of the genus *Hemicytheria* (Pl. I., fig. 7.) resembles the *Hemicytheria pokornýi* S o k a č species, but it is presumably a new subspecies. Owning to the scarcity and the poor preservation of the specimens, a precise description of the available forms cannot be given.

The above mentioned phenomena can be interpreted as the results of slow deepening of water and negative shore-line displacement.

The upper part of the Lower Pannonian is not represented in the area of South Buda.

In the Budapest district, on the left side of the Danube, the only Lower Pannonian rock – apart from the afore mentioned uncertain grey sand of Gubacs – is known from the old Eugel-well (L ő r e n t h e y 1902). On the basis of its faunal association it can be identified with the

Tinnye locality of similar age. According to F ö l d v á r i, it is hard to say whether this occurence is a bay sediment, or an erosional remnant of the pre-Upper Pannonian land (L ő r e n t h e y 1902). On the basis of the similarity with the lagunal facies of Tinnye, it is probably a bay sediment.

Upper Pannonian

In the clay-pits of Kőbánya the Upper Pannonian Congeria ungula caprae horizon lies disconformably (with 10 – 20° angular unconformity) upon the Sarmatian coarse limestone. Characteristic rock-types are:

1. Grey, soft clay, commonly with carbonized plant remains. On the cleavage planes the monoctyledonous features are recognizable (Pl. II., fig. 2.). The ostracodes are frequent (Pl. I., figs. 4 – 6.) and subordinately a few bivalves are also present. On the basis of the washing concentrate two types of this argillaceous facies can be separated: the first with its 5% ostracode, 60% muskovite and 35% carbonized plant remains (Pl. II, fig. 4.) shows near-shore, the second with the 10% ostracode, 20% muskovite and 70% carbonized plant remains (Pl. II., fig. 5.) suggests an off-shore sedimentary environment.

According to these present studies the treshold value of the presence of ostracodes can be dated as the maximal 10% quantity of the 0,1 mm grain-size fraction.

2. Within the clay, sharply bordered sand layers intercalate, which lack ostracodes, but yield bivalves in great profusion (Pl. I., figs. 9 – 10.). These intercalations can be interpreted as temporary sand transportations of a river, which disturbed the fine-grained near-shore clay deposition, and caused the mass extinction of the rare bivalves. Because of the scatterly occurence of the localities, it is doubtful, whether this phenomenon can be due to detrital transportation of the river, or to epeirogenetic oscillation. An additional evidence for the near-shore deposition of the brickyard clays is the relative frequency of the vertebrate fossils: *Mastodon longirostris* K a u p. mandible, *Axis* sp. antler. The lack of the entire skeletons suggest a slights redeposition of these bones.

The rocks of the Congeria balatonica horizon resemble lithologically and sedimentologically those of the Congeria ungula caprae horizon, but the corresponding facies show southward tendency in surfacial occurence.

The characteristic marginal sediment of the Upper Pannonian (F ö l d v á r i 1931) is the 0,5 to 2,0 m thick limonitic sand. It can be found, with considerable local interruptions, from the village of Érd to Veresegyháza. Its occurence certainly shows the ancient coastal line.

The transgression upon the Miocene rocks took place on the left side of the Danube, in the Congeria ungula caprae, while on the right side in the Congeria balatonica times, respectively.

The overlying deposits of the Congeria balatonica horizon are the characteristic fluvial cross-bedded sand with mollusc-detritus of the Unio wetzleri horizon.

PLATE I.

Fig. 1. Hungarocypris trapezoidea (M é h.) Nagytétény, 30X

Fig. 2. Hungarocypris pannonica (M é h.) Nagytétény, 30X

Fig. 3. Hungarocypris sieberi (M é h.); valve shape changes during the ontogenesis: *a)* neanic, *b)* juvenile, *c)* adult specimen Nagytétény, 30X

Fig. 4. Paracypria (Pontonella) acuminata Z a l. Kerámia brickyard. 30X

Fig. 5. Paracypria (Pontonella) paracuminata K r s t i č Kerámia brickyard, 30X

Fig. 6. Caspiolla lobata (Z a l.) Gubacs brickyard, 40X

Fig. 7. Hemicytheria pokornyi S o k a č Nagytétény, 30X

Fig. 8. Candona fossulata P o k o r n y Nagytétény, 40X

Fig. 9. Congeria ungula caprae M ü n s t. Gubacs brickyard, nat. size. The matrix is coarse sand and gravel, cemented with iron sulfide

Fig. 10. Dreisseniomya schöckingeri F u c h s and *Limnocardium penslii* F u c h s shell fragments and quartzite pebble in medium-grained, iron sulfide cemented matrix. Gubacs brickyard, nat. size.

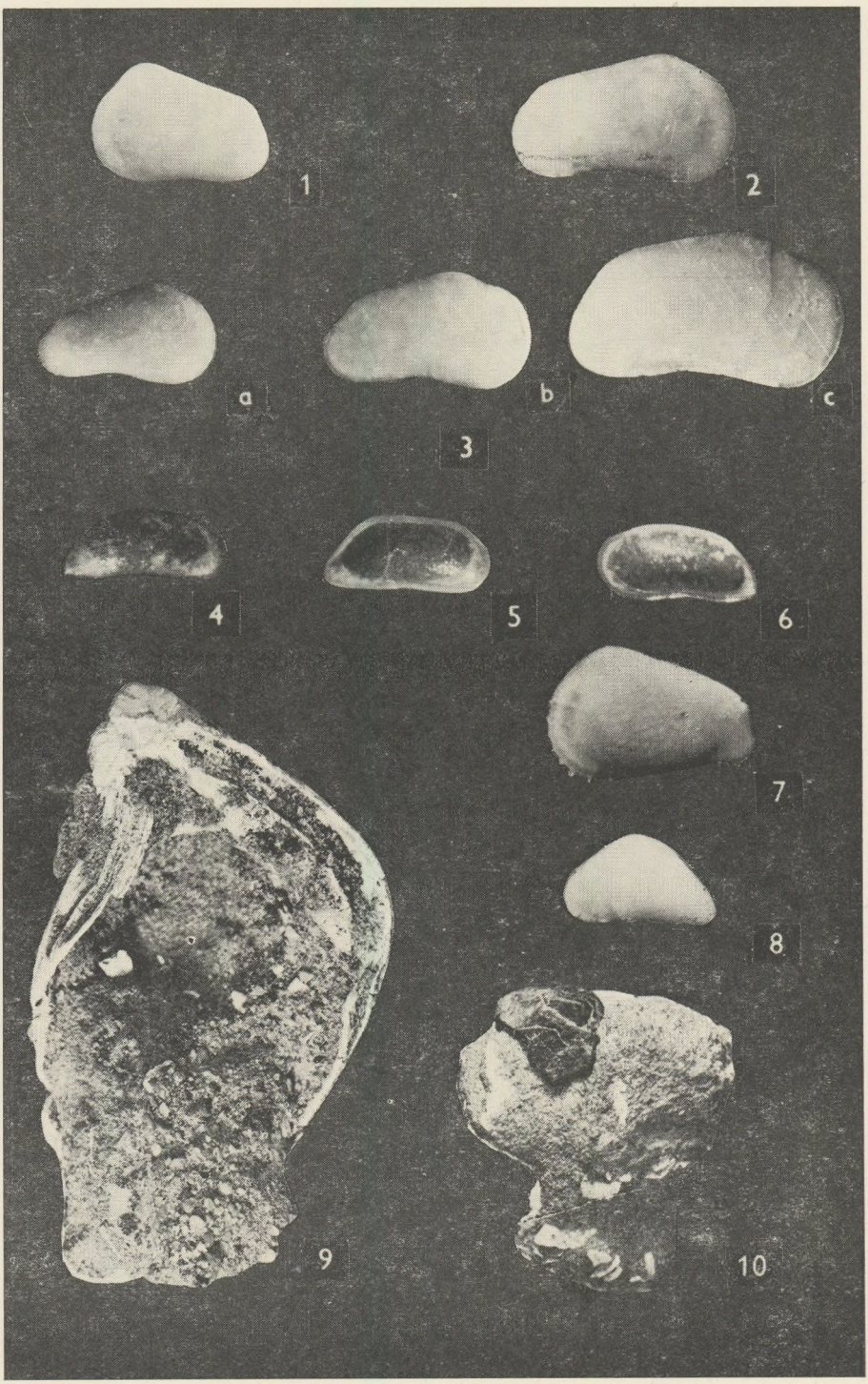
1
2
a
b
c
3
4
5
6
7
8
9
10

PLATE II.

Fig. 1. Otolithi Nagytétény, 40X

Fig. 2. Stem and leaf imprints of monocotyledonous plants. Gubacs brickyard, nat. size.

Fig. 3. Derived Sarmatian foraminifers in the Lower Pannonian clay. Nagytétény, 20X

Fig. 4. Medium-rich washing concentrate. Gubacs brickyard, 5X

Fig. 5. Faunal rich washing concentrate. Gubacs brickyard, 5X

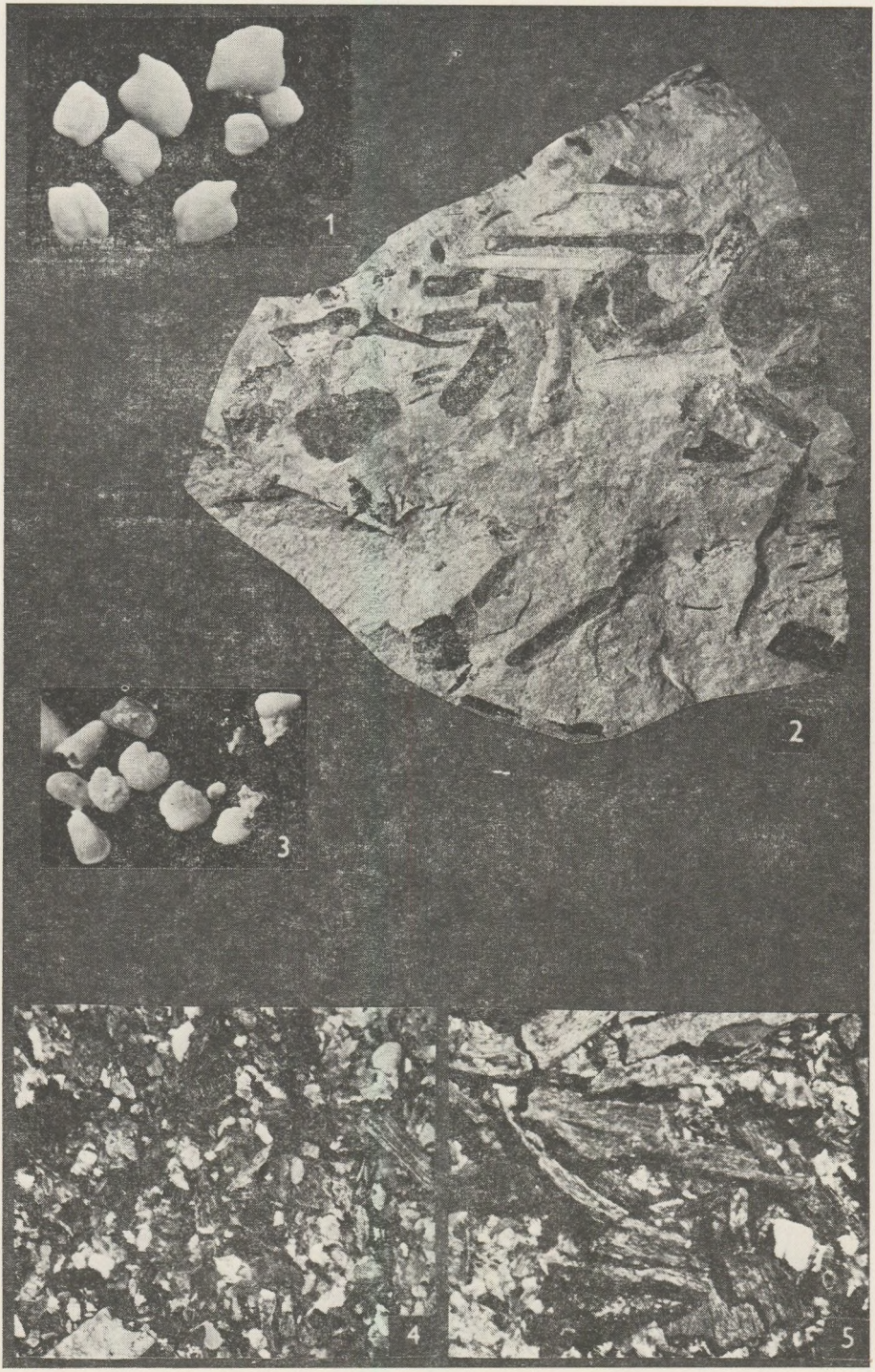
1
2
3
4
5

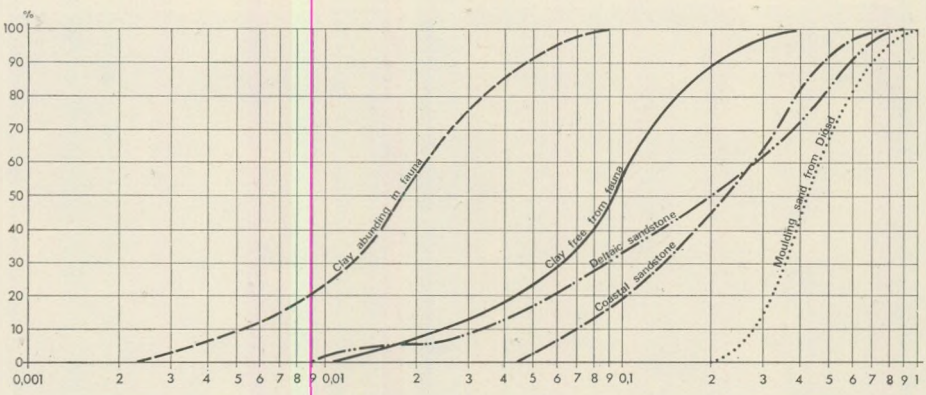

Fig. 1. Typical grain-size characteristics of some distinctive clastic rocks

In the old, small localities existed on the Szabadsághegy-hill of Buda the faunal sands and sandstones of the Congeria balatonica horizon were excavated. This faunal portion is unknown here at the present. On the basis of the stratigraphic position and the grain-size composition these are characteristic deltaic sediments.

"Levantine" (Upper Pliocene)

On the studied area – apart from smaller, local terrestrial sedimentation – only the fresh-water and lacustrine limestone deposition was significant both on the sides of Buda and Pest (N o s z k y 1925). It can be found in larger or smaller erosional remnants around Csillebérc, Szabadsághegy-hill and Rákoskert.

Development and tectonics

The studied area is one of the best known Pliocene region of Hungary, however several uncertainties exist in the point of view of geological interpretation. Owing to the generally loose, lesser petrified character of the Pliocene rocks, the origination is hard to determine after an occasional denudation and redeposition. The greatest obscurity of a model for the development derives from the interpretation of a hiatus, i.e. gap in the sequence can be due to an interruption of the sedimentation, or a subsequent erosion.

It seems to be evident, that at the Miocene/Pliocene boundary a terrestrial, erosional period have been existed.

The special sand of Diósd and the clay excavations of Nagytétény as well, suggest a general transgressive character for the Lower Pannonian in the area of South Buda. On the left side of the Danube the Lower Pannonian is known from scattered spots, which are presumably of lagunal origin.

The 10 – 20° unconformity at the Sarmatian/Pannonian boundary which can be recognized in Diósd, Gubacs and Kőbánya as well, is the result of the Attic orogenic phase.

The center of the Upper Pannonian sedimentation situated on the left side of the Danube, where the transgression started as early as Congeria ungula caprae times. On the contrary, the transgression reached the South Buda region in Congeria balatonica times. The sedimentation cycle generally ends with the fluvial deposits of the Unio wetzleri horizon.

In several places a 5 to 8° angular disconformity can be recognized between the Pannonian and Pleistocene-Holocene sediments. In absence of any other evidence, it can be connected to the Rhodanic or Valachian orogenic phases.

Secular movements have been acted in the geologically recent past too, i.e. the dip of the Pleistocene and Holocene strata is 1 to 3° in SE direction.

REFERENCES

Bartha, F. (1959): Finomrétegtani vizsgálatok a Balatonkörnyéki felsőpannon képződményeken. M. Áll. Földt. Int. Évkönyve, 48. kötet. Függelék: Zalányi, B.: Tihanyi felső pannon Ostracodák pp. 195 – 216. (Feinstratigraphische Untersuchungen am Oberpannon der Balatongegend. Jahrbuch der Ungarischen Geologischen Anstalt Vol. 48. Anhang: Zalányi, B.: Oberpannonische Ostracoden aus Tihany).

Dennis, B. (1963): Size in relation to salinity in fossil and recent eurihaline Ostracods Jour. Mar. Biol. Ass. U. K. 43.

Földvári, A. (1931): Pannon mozgások a Budai-hegységben és a felsőpannon tó partvonala Budapest környékén. Földt. Közl. pp. 51 – 63. (Pontische Bewegungen im Budaer-Gebirge und Strandlinie des oberpontischen Sees bei Budapest. Geologische Mittelungen B. LXI.)

Krstič, N. (1960): Beitrag zur Kenntniss der pannonischen Ostracoden in der Umgebung von Beograd Ann. Geol. de la Penin. Balk. XXVII.

Lőrenthey, I. (1902): Die pannonische Fauna von Budapest Palaeontographica 48. Stuttgart.

Lőrenthey, I. (1906): Budapest pannoniai és levantai korú rétegei és ezek faunája Math. és Term. Tud. Ért. XXIV. 4. pp. 298 – 324. (Pannonische und levantische Sedimenten des Budapest und ihren Fauna.)

Lőrenthey, I. (1912): Újabb adatok Budapest harmadidőszaki üledékeinek geológiájához Math. és Term. Tud. Ért. XXX. 2; pp. 263 – 323. (Neuere Daten zur Geologie des terzier Sedimenten Umgebung von Budapest.)

Méhes, Gy. (1907 – 1908): Adatok Magyarország pliocén Ostracodáinak ismeretéhez Földt. Közl. (Daten zur Kenntniss der Pliozen Ostracoden in Ungarn Geologische Mittelungen Bd. XXXVII – XXXVIII.)

Noszky, J. (1925): A levantei forrásmeszek a pesti oldalon. Földt. Közl. pp. 238 – 239. (Über die levantinischen Quellenkalke auf der Pester Seite. Geologische Mitteilungen Bd. XLV.)

Papp, A. (1959): A Bécsi-medence pannóniai képződményeinek biosztratigráfiai tagolása Földt. Közl. pp. 16 – 22. (Die biostratigraphische Gliederung des Pannon im Wiener Becken Geologische Mitteilungen Bd. LXXXIX.)

Pokorný, V. (1952): Skorepatcit. zv. „basalniho horizontu subglobozovych Wrstev" (Pliocen) v Hodonine Sbor. Ustr. Usta. Geol. XIX. Praha.

Puri, H. S.: Ecologic distribution of recent Ostracoda. Reprinted from the „Procedings of Symposium on Crustacea"

Sohn, I. G. (1958): Chemical constituents of Ostracodes; Some applications to paleontology and paleoecology Journ. of Pal. 32. 4.

Stevanović, P. M. (1959): A szűkebb értelemben vett pontusi emelet kifejlődései és tagolása É-Jugoszláviában, tekintettel a szomszédos országok pontusi képződményeire. Földt. Közl. pp. 3 – 9. [Pont (i. eng. S.) im nördlichen Jugoslavien seinen Fazies und Horizonte, mit einem Rückblick auf die Verhältnisse in den Nachbarländern Geologische Mitteilungen Bd. LXXXIX.]

Strausz, L. (1941) A dunántúli pannon szintezése Földt. Közl. pp. 220 – 235. (Horizontierung des Transdanubischen Pannon.)

Strausz, L. (1942): Magyarországi pannonikum párhuzamosítása délkelet-európai üledékekkel. Földt. Közl. pp. 233 – 236. (Versuch einer Parallelisierung des Pannons).

Széles, M. (1960): Az Ostracodák morfológiai és ökológiai kapcsolatai. Földt. Közl. pp. 132 – 136. (Zusammenhänge zwischen der ökologie der Ostracoden und der Morphologie ihrer Schalen Geologische mitteilungen Bd. CX.)

Zalányi, B. (1944): Magyarországi neogén Ostracodák Geol. Hung. Ser. Pal. 21. (Neogen Ostracoden in IUngarn.)

Zalányi, B. (1929): Morpho-systematische Studien über fossile Muschelkrebse. Geol. Hung. Ser. Pal. 5.

ЗЕМНЫЕ ПРИЛИВЫ И ТОНКИЕ ЗАКОНОМЕРНОСТИ ВРАЩЕНИЯ ЗЕМЛИ

by

B. BODRI

Department of Geophysics, Eötvös University, Budapest

Received: 15 March 1974

SUMMARY

The connection between earth tides and fine effects of the rotation of the Earth is studied. There were computed the dependence of the values of Love numbers on the frequency of forced nutation and also the amplitudes of the forced nutations. There has been found the frequency of free oscillation of the Earth corresponding to the Chandler period of the movement of the pole. All computations were made for an earth model with a liquid core and the theory took into account the effect of external and internal core on both the tidal coefficients and the rotation of the Earth. The results suggest that the dynamic effect of the liquid core on the tidal coefficients as well as on the amplitude of nearly diurnal nutation is quite negligible and it can not be found out neither from astronomical nor from tidal observations as it was considered before.

За последнее время изучение тонких закономерностей вращения Земли все больше и больше привлекает внимание астрономов и геофизиков. Открытие нутационных движений оси фигуры Земли относительно оси вращения заставляет для их интерпретации обращаться к геофизике, поскольку геофизические теории, основывающиеся на различных гипотезах о внутреннем строении Земли, могут предсказать те или иные закономерности в ее вращении.

С точки зрения кинематики общее движение Земли может быть разложено на поступательное движение и вращение бесчисленными способами. Обе эти компоненты довольно сложны. Орбитальное движение центра масс Земли под действием силы тяготения Солнца постоянно возмущается тяготением со стороны других планет солнечной системы. Вращение же относительно центра масс возмущается притяжением Солнца и Луны. Оно еще болше осложняется из-за несовпадения оси вращения с главной осью инерции и наличия неоднородностей в структуре Земли, а также вследствие постоянно происходящих перемещений масс как внутри Земли, так и на ее поверхности, вызываемых различными геофизическими процессами. Таким образом, в результате взаимного действия чрезвычайно сложно меняющихся внешних сил вращение Земли в каждый данный момент представляет собой вращение вокруг некоторой оси, прохойящей через центр масс, но непрерывно меняющей свое положение и в теле Земли, и в пространстве.

Земля в целом очень близка по своим свойствам к абсолютно твердому телу, поэтому разумно ожидать, что влияние на вращение различных геофизических факторов будет иметь вид различных поправок к теоретическим законам вращения, выведенным для абсолютно твердой Земли. Определение этих поправок требует и некоторой геофизической гипотезы, и сравнения законов теоретического движения с астрономическими и геофизическими наблюдениями.

В данной работе нас интересовали поправки к теоретическим законам вращения, вызванные действием лунно-солнечного гравитационного потенциала, так называемая вынужденная нутация. Причем задача рассматривалась для модели Земли с жидким ядром. Еще Молоденский (1961) показал, как можно вывести прецессионно-нутационное движение земной оси в пространстве из разложения приливной силы. Он же обратил внимание на то, что наличие у Земли жидкого ядра, возможно, оказывает влияние на оба вышеупомянутые явления. Если бы жидкое ядро вызывало возмущающие эффекты, то это должно было бы сказаться и на суточных (тессеральных) земных приливах, и на соответствующих членах вынужденной нутации и вообще на любом явлении, связанном со смещением оси вращения Земли. Если бы возмущающие эффекты были достаточно сильны, то следовало бы пересмотреть также теорию свободной нутации (движение полюса, обнаружимое по изменению широты, которое имеет период около 450 суток).

В 1961 году Молоденский предложил красивую теорию нутации вращающегося жидкого тела эллипсоидальной формы, заключенного в тревдую оболочку. Теория учитывала также и упругость оболочки Земли. Совместно с Крамер (1961) им были сделаны расчеты зависимости чисел Лява от частоты возмущающей силы, а также амплитуд различных членов вынужденной нутации. Кроме того, была вычислена частота свободных колебаний, соответствующая чандлеровскому периоду движения полюса. Расчеты были сделаны для нескольких моделей Земли.

В данной работе были проделаны расчеты, аналогичные расчетам Молоденского и Крамер (1961), однако при расчетах использовалась более подробная модель Земли, кроме того, был исправлен ряд неточностей, допущенных в статье Молоденского. Теория Молоденского, излагаемая ниже, дается уже с учетом сделанных исправлений.

Исходными уравнениями у Молоденского являются уравнения движения деформированного тела при существовании объемных сил с потенциалом U:

$$\varrho \frac{D\dot{\vec{r}}}{Dt} = \varrho \operatorname{grad} U + \frac{\partial \vec{X}}{\partial x} + \frac{\partial \vec{Y}}{\partial y} + \frac{\partial \vec{Z}}{\partial z}, \tag{1}$$

где

$\vec{r}$ – радиус-вектор текущей точки с координатами (x, y, z)
ϱ – плотность,

$\vec{X}, \vec{Y}, \vec{Z}$ – векторы давления, действующие на элементы плоскости YZ, XZ и XY соответственно, $\frac{D}{Dt}$ – полная производная по времени,

$$\frac{D}{Dt} = \frac{\partial}{\partial t} + \dot{x}\frac{\partial}{\partial x} + \dot{y}\frac{\partial}{\partial y} + \dot{z}\frac{\partial}{\partial z},$$

причем точка над символом означает частную производную по времени.

В системе координат, вращающейся с угловой скоростью $\vec{\omega}$, левая часть уравнения (I) имеет вид:

$$\frac{D\vec{r}}{Dt} = \frac{\tilde{D}\dot{\vec{r}}}{Dt} = 2[\vec{\omega}\,\dot{\vec{r}}] + [\dot{\vec{\omega}}\,\vec{r}] + (\vec{\omega}\,\vec{r})\vec{\omega} - \vec{\omega}^2\vec{r}. \tag{2}$$

Здесь волнистая черта означает, что производная по времени берется в подвижной системе координат. Для малых смещений, очевидно, $\frac{\tilde{D}}{Dt} = \frac{\partial}{\partial t}$.

Общий потенциал U в данной задаче состоит из следующих членов:

1. Гравитационный потенциал всех масс Земли

$$W_0 = f\frac{M}{r}, \tag{3}$$

где f – гравитационная константа,
M – масса Земли.

2. Потенциал центробежной силы

$$\varphi_0 = \frac{1}{2}\omega^2(x^2 + y^2) = \frac{1}{2}\omega^2 l^2 \tag{4}$$

3. Внешний лунно-солнечный потенциал

$$V_e = \frac{1}{3}\varkappa\frac{g}{a}p_2^m(\cos\Theta)\cos(\sigma t - m\lambda), \tag{5}$$

где

σ – частота приливообразующей силы,
P_2^m – присоединенный полином Лежандра,
Θ – полярный угол,

λ — долгота,
g — ускорение силы тяжести,
a — средний радиус Земли,
$\varkappa = 1.836 \cdot 10^{-7}$ безразмерная константа, определяемая отношением масс Лины и Земли и среднего расстояния Земля-Луна к радиусу Земли.

К этому потенциалу следует добавить потенциал V_i, возникающий вследствие деформации Земли, а также тессеральный потенциал φ, вызванный нутацией оси вращения. Вектор угловой скорости $\vec{\omega}$ (p, q, r), возникающий вследствие возмущающего потенциала V_e имеет вид:

$$\vec{\omega} = \omega\left(\varepsilon \cos\sigma t\, \vec{i} + \varepsilon \sin\sigma t\, \vec{j} + \vec{k}\right),$$

то есть

$$p = \omega\varepsilon\cos\sigma t$$

$$q = \omega\varepsilon\sin\sigma t$$

$$r = \omega,$$

где

ε — малая величина, вызванная эффектом резонанса, зависит только от σ. ε определяет нутацию системы координат в пространстве (заметим, что система координат связана с оболочкой, а не со всем телом Земли).

Таким образом, к полному потенциалу добавится еще некоторый дополнительный потенциал φ, вызванный нутацией оси вращения по отношению к Земле. Этот потенциал равен:

$$\varphi = -\omega^2 \varepsilon\, zl \cos(\sigma t - \lambda). \tag{7}$$

Учитывая конкретный вид $\vec{\omega}$ (6), а также выражение (7), формулу (2) мы можем записать в следующем виде:

$$\frac{D\dot{x}}{Dt} = \ddot{u} - 2\omega\dot{v} - \frac{\partial}{\partial x}\left(\varphi_0 + \frac{\sigma+\omega}{\omega}\varphi\right)$$

$$\frac{D\dot{y}}{Dt} = \ddot{v} - 2\omega\dot{u} - \frac{\partial}{\partial y}\left(\varphi_0 + \frac{\sigma+\omega}{\omega}\varphi\right)$$

$$\frac{D\dot{z}}{Dt} = \ddot{w} + \frac{2\sigma}{\omega}\,\frac{\partial\varphi}{\partial z} - \frac{\partial}{\partial z}\left(\varphi_0 + \frac{\sigma+\omega}{\omega}\varphi\right), \tag{8}$$

где

u, v, w — смещения в подвижной системе координат.

Для определения начальных напряжений необходимо использовать гипотезу Герглотца о том, что когда Земля находится только под влиянием невозмущенного потенциала $W = W_0 + \varphi_0$, то в каждый

данный момент осуществляется состояние гидростатического равновесия, описываемое уравнением Пуассона

$$\varrho_0 \operatorname{grad} W = \operatorname{grad} P, \tag{9}$$

где

P – гидростатическое девление,
ϱ_0 – невозмущенное значение плотности.

Преобразуем с помощью (9) правую часть уравнения (1) и учтем (8), тогда уравнения упругости можно получить в следующем виде:

$$\ddot{u} - 2\omega\dot{v} = -\frac{\partial \Psi}{\partial x} + \left(\frac{\lambda\varrho'}{\varrho^2 W'} - 1\right)\delta\frac{\partial W}{\partial x} + \frac{\mu}{\varrho}\left(\Delta u + \frac{\partial \delta}{\partial x}\right) +$$

$$+ \frac{\mu'}{W'\varrho}\left[u' W' + \frac{\partial u}{\partial x}\frac{\partial W}{\partial x} + \frac{\partial v}{\partial x}\frac{\partial W}{\partial y} + \frac{\partial \omega}{\partial x}\frac{\partial W}{\partial z}\right];$$

$$\ddot{v} + 2\omega\dot{u} = \ldots \tag{10}$$

$$\ddot{w} + \frac{2\sigma}{\omega}\frac{\partial \varphi}{\partial z} = \ldots,$$

где

λ, μ постоянные Ламэ,
Ψ – новый потенциал вида

$$-\Psi = V_e + \frac{\sigma + \omega}{\omega}\varphi + V_i + \eta + \frac{\lambda\delta}{\varrho},$$

в котором V_i, как уже было отмечено, добавочный потенциал, вызванный деформацией Земли,

$$\eta = \frac{\partial W}{\partial x}u + \frac{\partial W}{\partial y}v + \frac{\partial W}{\partial z}w,$$

$$\delta = \frac{\partial u}{\partial x} + \frac{\partial v}{\partial y} + \frac{\partial w}{\partial z}.$$

Штрих означает производную по внешней нормали к поверхности уровня потенциала.

Вместе с уравнениями (10) нужно также рассматривать уравнение неразрывности, поскольку оно определяет полное изменение плотности в фиксированной точке пространства:

$$\dot{\varrho} + \frac{\partial}{\partial x}(\varrho u) + \frac{\partial}{\partial y}(\varrho v) + \frac{\partial}{\partial z}(\varrho w) = 0, \tag{11}$$

отсюда

$$-\dot{\varrho} = \varrho\delta + \frac{\varrho'}{W'}\eta, \tag{12}$$

где

$$\Delta V_i = 4\pi f\left(\varrho\delta + \frac{\varrho'}{W'}\eta\right),$$

Δ — оператор Лапласа. Система уравнений (10)—(12) достаточна для определения всех неизвесных функций.

Во внешнем ядре при $\mu = 0$ получаем уравнения гидродинамики. Если принять, что плотность зависит только от гидростатического давления, то можно записать:

$$\lambda\varrho' = \varrho^2 W'.$$

Тогда вместо (10) получаем систему:

$$\begin{aligned} \ddot{u} - 2\omega\dot{v} &= -\frac{\partial\Psi}{\partial x} \\ \ddot{v} + 2\omega\dot{u} &= -\frac{\partial\Psi}{\partial y} \\ \ddot{w} + \frac{2\sigma}{\omega}\frac{\partial\varphi}{\partial z} &= -\frac{\partial\Psi}{\partial z}, \end{aligned} \tag{13}$$

а уравнение (12) в этом случае эквивалентно следующему:

$$-\frac{W'}{4\pi f\varrho'}\Delta V_i = \Psi + V_e + \frac{\sigma+\omega}{\omega}\varphi + V_i = \frac{P}{\varrho}. \tag{14}$$

Смещения в ядре, которые мы рассматриваем, являются в случае, если движение установилось, гармоническими колебаниями с частотой σ. Положив

$$\ddot{u} = -\sigma^2 u, \quad \ddot{v} = -\sigma^2 v, \quad \ddot{w} = -\sigma^2 \omega, \tag{15}$$

мы после ряда преобразований можем свести систему (13)—(14) к системе двух уравнений в частных производных второго порядка с неизвестными функциями V_i и Ψ :

$$-\frac{W'}{4\pi f\varrho}\Delta V_i = \Psi + V_e + \frac{\sigma+\omega}{\omega}\varphi + V_i = \frac{1}{\omega^2}F(\Psi) - \frac{2}{\sigma\omega}\frac{\partial\varphi}{\partial z}\frac{\partial W}{\partial z};$$

$$F(\Psi) = \frac{\omega^2}{4\omega^2-\sigma^2}\left[\frac{\varrho W'}{\varrho'}\left(\Delta\Psi - \frac{4\omega^2}{\sigma^2}\frac{\partial^2\Psi}{\partial z^2}\right) + \Psi' W' - \right.$$

$$\left. - \frac{4\omega^2}{\sigma^2}\frac{\partial\Psi}{\partial z}\frac{\partial W}{\partial z} - \frac{2\omega m}{\sigma l}\Psi\frac{\partial W}{\partial l}\right]. \tag{16}$$

Наиболее трудным является решение уравнений (10)–(12) для оболочки. Молоденский в своих расчетах использовал ршение для сферической оболочки при $\sigma = \omega = 0$. Для чисел Лява ошибки порядка сжатия эквипотенциальных поверхностей ($e = \omega^2 a/g$) неизбежны, а нутация, по-видимому, слабо зависит от упругости оболочки. Более точное решение невозможно из-за ошибок порядка выше сжатия в функциях ϱ, μ, λ.

Решение системы дифференциальных уравнений (10)–(12) для сферически-симметричной Земли и статического прилива можно получить численным интегрированием. Эти уравнения приводятся методом Лява к системе 6 линейных однородных уравнений первого порядка относительно функций H, T, R, L, M, N:

$$R = \left(\frac{V_i}{V_e + \dfrac{\sigma+\omega}{\omega}\varphi} \right) \frac{r^2}{a} g$$

$$H = \frac{\eta}{V_e + \dfrac{\sigma+\omega}{\omega}\varphi} \frac{g}{W'} \frac{r^2}{a}$$

$$L = (R' - 4\pi f \varrho H) r^2 \qquad (17)$$

$$M = \left(T' + H - \frac{2T}{r} \right) r^2 \mu$$

$$N = (\lambda + 2\mu) H' + \lambda \left(\frac{2H}{r} - \frac{6T}{r^2} \right).$$

Здесь, например,

$$u = H \frac{x}{r} \left(\frac{V_e}{r^2} \right) + T \frac{\partial}{\partial x} \left(\frac{V_e}{r^2} \right)$$

и так далее. Все функции, кроме T, которая входит множителем в компоненты тангенциального смещения, сохраняют непрерывность на границе скачков плотности и упругих параметров.

Общее решение системы (17) имеет вид:

$$\Phi_k(r) = \sum_{i=1}^{6} C_i y_{ik}(r)$$

$k = 1, 2, \ldots, 6$, где

Φ_k – одна из функций H, T, R, L, M, N, а y_{ik} – частные решения системы (17). Например, y_{1k} является частным решением, соответствующим условиям $C_1 = 1$, $C_2 = C_3 = \ldots = C_6 = 0 \cdot C_i$ – константы, которые определяются из граничных условий.

Основное затруднение при решении системы (16) для жидкого ядра состоит в том, что суточные частоты вынужденных колебаний близки к соответствующим частотам собственных колебаний Земли, и поэтому в расчетах необходимо учесть сжатие земного ядра, поскольку собственные колебания заметно зависят от сжатия.

Решение системы (16), следуя Молоденскому, ищем в виде:

$$V+\Psi=\alpha\Phi+\omega^2(V_1+\Psi_1)$$
$$\Psi=(2\omega+\sigma)\sigma\beta lz\cos(\sigma t-\lambda)-\omega^2\Psi_1, \tag{18}$$

где

$$\Phi=-\frac{W'}{4\pi f\varrho'}\Delta\Phi,$$

$$V=V_e+\frac{\sigma+\omega}{\omega}\Phi+V_i. \tag{19}$$

Следует заметить, что когда вынуждающая частота σ приближется к частоте собственных колебаний, параметр β возрстает, вследствие чего возрастает и Ψ, так что в этом диапазоне частот прилив может отличаться от статического. Параметр α, функции $\Phi, V_1\ \Psi_1$ с изменением σ, по-видимому, меняются мало.

Подставив (18) в систему (16) и отбросив члены порядка сжатия, если в них не входит β, для определения функций V_1 и Ψ_1 мы получим 2 уравнения:

$$V_1+\Psi_1=-\frac{W'}{4\pi f\varrho'}\Delta V_1$$

$$F(\Psi_1)=\alpha\Phi-\beta\left(l\frac{\partial W}{\partial z}-z\frac{\partial W}{\partial l}\right)\cos(\sigma t-\lambda)+\nu l\frac{\partial W}{\partial z}\cos(\sigma t-\lambda),$$

где (20)

$$\nu=2\left(\frac{\sigma+\omega}{\omega}\beta-\frac{\omega}{\sigma}\varepsilon\right).$$

Решение уравнения (19) ищем в виде:

$$\Phi=K\frac{lz}{r^2}\cos(\sigma t-\lambda) \tag{21}$$

Подставляя выражение (21) в (19), для функции K получим простое уравнение второго порядка:

$$K''+\frac{2}{r}K'+\left(\frac{4\pi f\varrho'}{W'}-\frac{6}{r^2}\right)K=0. \tag{22}$$

Второй член второго уравнения системы (20) тоже, очевидно, удовлетворяет уравнению (19), если функция K в нем выбрана следующим образом:

$$l\frac{\partial W}{\partial z}-z\frac{\partial W}{\partial l}=K_1\frac{lz}{r^2}. \qquad (23),$$

Функция K_1 ограничена при $r=0$ и удовлетворяет уравнению то есть на границе ядро-мантия при $r=b$

$$K_1(b)=-[w^2 lz]_b=[e^2 W_0'\tau]_b. \qquad (24)$$

Решение уравнения (20) ищем в виде ряда

$$\Psi_1=\cos(\sigma t-\lambda)\sum_{n=2}^{\infty}\chi_n r^n P_n(\cos\Theta), \qquad (25)$$

где неизвестные функции χ_n зависят только от r. Используя рекуррентные соотношения между полиномами Лежандра, можно получить аналогичные рекуррентные соотношения для χ_n. Подставляя их в (20) и приравнивая множители при P_n, получаем бесконечную систему дифференциальных уравнений второго порядка для функций χ_n. В дальнейшем мы будем использовать только уравнение для χ_2. Оно имеет следующий вид:

$$\left[\frac{3}{W'}\varrho r^6\eta_2+\frac{\beta}{W'}\varrho r^4 K_1-\frac{1}{4\pi f}\left(\frac{\alpha K-\beta K_1}{r^2}\right)' r^6\right]'=$$

$$=\frac{2(\omega+\sigma)(2\omega-\sigma)}{\sigma^2}\varrho(\chi_2 r^5)'+5v\varrho r^4. \qquad (26)$$

Обозначив

$$\eta_2=\frac{W'}{3r}\left[v-\frac{K_1}{W' r}\beta-\left(1-\frac{12}{7}\frac{\omega^2}{\sigma^2}\right)\chi_2' r+\right.$$

$$\left.+\frac{80}{63}\frac{\omega^2}{\sigma^2}(\chi_4 r^9)'\, r^{-6}+\frac{2(\omega+\sigma)(2\omega-\sigma)}{\sigma^2}\chi_2\right] \qquad (27)$$

и интегрируя уравнение (26) в пределах от b до c (c – граница внешнее-внутренее ядро), получаем

$$\left[\frac{3}{W'}\varrho r^6\eta_2+\frac{\beta}{W'}\varrho r^4 K_1-\frac{1}{4\pi f}\left(\frac{\alpha K-\beta K_2}{r^2}\right)' r^6\right]_c^b=5v\int_c^b\varrho r^4\,dr. \qquad (28)$$

При интегрировании было введено условие

$$\int_c^b\varrho(\chi_2 r^5)'\,dr=0.$$

Рассмотрим граничные условия. На поверхности Земли отсутствуют нормальные и тангенциальные напряжения, таким образом,

$$C_N = C_M = 0 .$$

Из условия непрерывности производной потенциала для приливов второго порядка получаем

$$C_L = 5 - C_R .$$

Остальные 3 числа Лява должны быть получены из условий на границе ядро-мантия.

Так как ядро жидкое, то тангенциальная компонента смещения, пропорциональная T, может быть разрывной, остальные 5 функций должны быть непрерывны.

Условия на границе ядро-мантия могут быть получены следующим образом.

I. В ядре $\mu = 0$, то есть из (17) имеем

$$M(b) = 0 ,$$

где

b, как уже отмечалось, радиус внешего ядра. Физически это означает, что на границе ядро-мантия отсутствуют тангенциальные напряжения.

2. Функция R — непрерывна.

Так как

$$V = \alpha_1 K_1 + \alpha_2 K_2 - (2\omega + \sigma)\beta\sigma r^2 ,$$

$$\alpha K = \alpha_1 K_1 + \alpha_2 K_2$$

то

$$R(b) = \left[\frac{\alpha_1}{\varkappa} K_1 + \frac{\alpha_2}{\varkappa} K_2 - (2\omega + \sigma)\sigma \frac{\beta}{\varkappa} r^2 \right]_b . \tag{30}$$

3. Функция L — непрерывна.

Используя уравнение для R' из системы (17) и исключая R' с помощью (30), получаем

$$\frac{1}{b^2} L(b) + 4\pi f \varrho_b H(b) = \left[\frac{\alpha_1}{\varkappa} K_1' + \frac{\alpha_2}{\varkappa} K_2' - 2(2\omega + \sigma)\sigma r \frac{\beta}{\varkappa} \right]_b . \tag{31}$$

Используя условия (29)—(31), мы можем определить константы C_i как функции параметров α_2, β и $(2\omega + \sigma)\sigma$. Ппичем, как известно, $C_H = h$, $C_T = l$, $C_R = 1 + k$, где h, l и k — соответствующие числа Лява.

Условие непрерывности функции H дает нам важное уравнение, связывающее параметры β и ε. Подставляя во второе уравнение системы (17) внешний потенциал (5) и учитывая вид функции η_2 имеем

$$\frac{3\eta_2}{W'} r^2 = H\varkappa .$$

Подставляя это выражение в (28) и учитывая формулу (30) и последнее уравнение системы (17), получаем

$$\left[L r^2 - 2 R r^3 - \frac{\beta}{\varkappa} r^4 \left(K_1' - \frac{2K_1}{r} + \frac{4\pi f \varrho}{W'} K_1\right)\right]_c^b = -20\pi f \frac{v}{\varkappa} \int_c^b \varrho r^4 dr .$$

Параметр ε, определяющий нутацию системы координат в пространстве, можно получить из закона сохранения момента количества движения

$$\vec{M} + [\vec{\omega}\, \vec{M}] = \vec{L}, \tag{33}$$

где

$\vec{M}$ – кинетический момент,

$\vec{L}$ – момент внешних сил в подвижной системе координат. При составлении уравнения (33) не был учтен момент сил взаимодействия между мантией и ядром. Подставив в (33) конкретный вид $\vec{\omega}$, при малых значениях ε получим следующие проекции кинетического момента на подвижные оси:

$$\begin{aligned} M_x &= \omega(A\varepsilon \cos\sigma t - I_{xz}) + \Delta M_x \\ M_y &= \omega(A\varepsilon \sin\sigma t - I_{yz}) + \Delta M_y \\ M_z &= \omega C + \Delta M_z , \end{aligned} \tag{34}$$

где A, B, C – главные моменты инерции,
I_{xz}, I_{yz} – центробежные моменты инерции, члены ΔM_x, ΔM_y, ΔM_z определяются движением жидкого ядра. Нам нужно вычислить выда

$$\Delta M_y = \sigma \Delta M_x$$

$$\Delta M_x = \frac{2\omega}{\sigma^2(2\omega+\sigma)} \int \varrho\, y \frac{\partial \Psi}{\partial z} d\tau + \frac{2}{\omega\sigma} \int \varrho\, y \frac{\partial \Psi}{\partial z} d\tau +$$

$$+ \frac{1}{\sigma(2\omega+\sigma)} \int \varrho \left(y \frac{\partial \Psi}{\partial z} - z \frac{\partial \Psi}{\partial y}\right) d\tau .$$

В водя конкретный вид смещений и интегрируя по объему τ, мы получим:

$$\begin{aligned} \frac{1}{\omega} \Delta M_y &= \left[(\beta - \varepsilon) A_1 + \frac{\sigma v}{2\omega} (C_1 - A_1)\right] \sin\sigma t \\ \frac{1}{\omega} \Delta M_x &= \left[(\beta - \varepsilon) A_1 + \frac{\sigma v}{2\omega} (C_1 - A_1)\right] \cos\sigma t . \end{aligned} \tag{36}$$

Далее нам нужно получить выражения для центробежных моментов инерции. Молоденский считает при этом, что смещение границ скачка

плотности при деформации земли равносильно добавлению к каждой такой границе простого слоя с плотностью $\varrho\eta/W'$. Таким образом,

$$I_{yz} = -\frac{1}{4\pi f}\int_{\tau} \Delta V yz d\tau + \int_{S} \frac{\varrho\eta}{W'} yz ds . \tag{37}$$

Преобразуя объемный интеграл с помощью формулы Грина и учитывая то, что функция yz гармоническая, получаем

$$I_{yz} = -\frac{1}{4\pi f} \frac{V' - 4\pi f \frac{\varrho\eta}{W'} - \frac{2V}{r}}{yz} \int_{S} y^2 z^2 ds ,$$

причем интегрирование идет только по поверхности Земли. Учитывая граничные условия на поверхности, получаем

$$I_{yz} = \frac{\varkappa}{3} Ma^2 k \sin\sigma t , \tag{38}$$

и внося (38) в (34), получаем следующие выражения для проекций кинетического момента на подвижные оси:

$$M_x = m\cos\sigma t$$

$$M_y = m\sin\sigma t$$

$$\frac{m}{\omega} = (A - A_1)\varepsilon + \beta A_1 + \frac{\sigma v}{2\omega}(C_1 - A_1) - \frac{\varkappa}{3} Ma^2 k . \tag{39}$$

Проекции момента внешних сил на подвижные координатные оси находим из выражения (5)

$$L_x = L\sin\sigma t$$

$$L_y = -L\cos\sigma t$$

$$L = \frac{g}{a}\varkappa(C - A) . \tag{40}$$

Внес (39)–(40) в уравнение моментов, получаем простое уравнение для:

$$\varepsilon - \frac{\sigma+\omega}{\omega}\left[\frac{A - A_1}{C}\varepsilon + \frac{A_1}{C}\beta + \frac{\sigma v}{2\omega}\frac{C_1 - A_1}{C} - \frac{\varkappa}{3}\frac{Ma^2 k}{C}\right] = \varkappa\frac{C - A}{Cq} . \tag{41}$$

В случае абсолютно твердой Земли уравнение (41) примет вид:

$$\varepsilon_0 - \frac{\sigma+\omega}{\omega}\frac{A}{C}\varepsilon_0 = \varrho\frac{C - A}{Cq} . \tag{42}$$

Поскольку в работе рассматривалась модель Земли с твердым внутренним ядром, к условиям (30)–(32) на границе внешнее ядромантия необходимо добавить и условия на границе внешнее-внутреннее ядро. Ввиду недостаточной изученности внутреннего ядра, Молоденский (1961) предлагает для простоты считать его однородным и несжимаемым и использовать хорошо известное аналитическое решение уравнений (17)

$$H = C_1 r + C_2 r^3, \quad T = \frac{1}{2} C_1 r^2 + \frac{5}{6} C_2 r^4, \quad R = C_3 r^4$$

Преобразуя уравнения системы (17), получаем

$$R' = \frac{2}{r} R, \qquad M = \mu r^2 \left(\frac{5}{r} T - \frac{3}{2} H \right),$$

$$N + \varrho (R + W' H) = \mu \left(\frac{13}{2} \frac{H}{r} - 9 \frac{T}{r^2} \right), \tag{43}$$

причем значения ϱ и μ берутся, очевидно, для внутреннего ядра. На границе внутреннего ядра с жидким внешним ядром функции H, L, R, M, N должны быть непрерывны, то есть граничные условия будут аналогичны условиям (30)–(32).

1. Отсутствие тангенциальных напряжений на границе $r = c$ (c – граица внутреннего ядра) дает $M_c = 0$, а с использованием (43) получаем

$$\left(\frac{5}{r} T - \frac{3}{2} H \right)_c = 0.$$

2. Аналогично, из (30) имеем

$$R(c) = \left[\frac{\alpha_1}{\varkappa} K_1 + \frac{\alpha_2}{\varkappa} K_2 - (2\omega + \sigma) \sigma \frac{\beta}{\varkappa} r^2 \right]_c.$$

3. Подобно предыдущему из (31) получаем

Условие непрерывности H (32), связывающее параметры β и ε вследствие, по-видимому, малого сжатия внутреннего ядра, остается прежним.

Наличие внутреннего ядра меняет также и уравнение моментов (41). В формулу (41) вместо C_1 и A_1 войдут моменты инерции слоя жидкости, заключенного между границами внутреннего и внешнего ядра, $C_1 - C_2$ и $A_1 - A_2$, где C_2 и A_2 – моменты инерции внутреннего ядра. Если пренебреч, некоторыми малыми членами, то условие (41) запишется в виде:

$$\varepsilon - \frac{\sigma + \omega}{C\omega} \left[A\varepsilon + (\beta - \varepsilon)(A_1 - A_2) - \frac{\varkappa}{3} m a^2 k \right] = \varkappa \frac{C - A}{Cq}. \tag{44}$$

Комбинируя условия (32) и (44) мы можем получить частоту свободных колебаний, которая определяется из чандлеровского периода движения полюса. Так как при свободных колебаниях, как это следует из (32),

$$\frac{\varepsilon}{\beta} = \frac{\sigma_0 + \omega}{\omega},$$

где σ_0 — частота свободных колебаний, то в пренебрежении некоторыми малыми членами можно получить

$$\frac{\sigma_0}{\omega} = \frac{C - A}{A - A_1}\left(1 - \frac{k}{k_0}\right), \tag{45}$$

где k_0 — значение числа Лява k для жидкой Земли.

В данной работе проведены вычисления по вышприведенному алгоритму для модели Земли Ванга [W a n g, 1972]. Сжатие Земли принято равным 0.003367, на границе внешнего ядра $b = 0.5464$:

$$W' = -1.0995, \qquad \frac{C_1}{C} = 0.0926,$$

$$e = 0{,}002481 .$$

Изменение плотности Земли с глубиной изображено на рис. 1.

Система уравнений (17) для оболочки решалась методом Рунге-Кутта. В качестве начального базиса на поверхности был взят единичный ортонормированный базис. Таким образом были получены 6 линейно независимых частных решений системы (17) $\frac{\partial \Phi_i}{\partial \Phi_j}(r)$. Их значения на границе ядро-мантия представлены в таблице I. эти значения использовались в дальнейшем для решения граничных условий.

Функции K_1 и K_2 были получены численны интегрированием уравнения (22), которое также проводилось методом Рунге-Кутта. В результате были получены следующие значения:

при $r = b = 0.5464$

$$K_1 = 1, \qquad K_2 = 0,$$

$$K_1' = 3{,}2437, \qquad K_2' = 3{,}3497,$$

при $r = c = 0.1901$

$$K_1 = 0{,}2112, \qquad K_2 = -8{,}0713,$$

$$K_1' = 0{,}1162, \qquad K_2' = 126{,}6135,$$

Используя полученные значения функций K и их производных, а также условия на границе ядро-мантия, можно получить значения чисел Лява h, l, k и параметра α_1, как функций β и частот σ и ω.

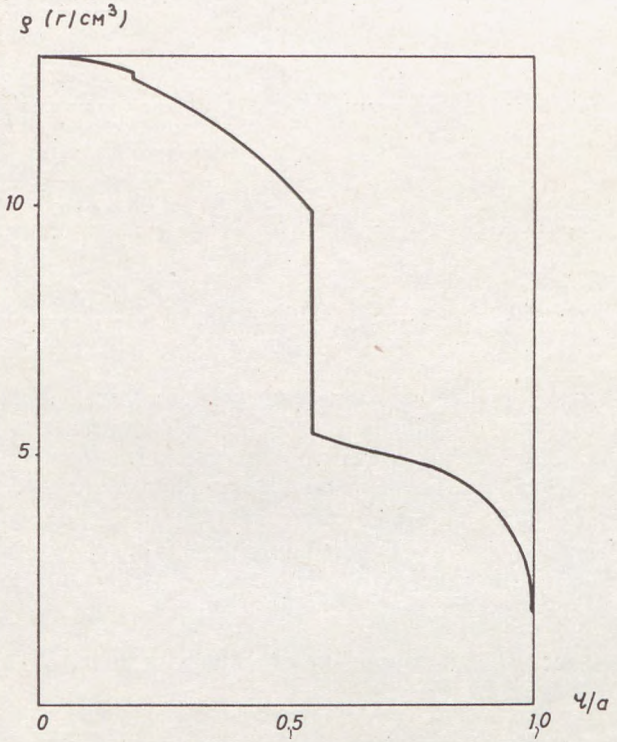

Рис. I. Изменение плотности с глубиной для модели Ванга
Fig. I. Density distribution in the case of Wang's earth model

Таблица I. – Table 1

Частные решения системы дифференциальных уравнений (17) на границе ядро-мантия
Particular solutions of differential equation system (17) at the core-mantle boundary

	$\frac{\partial}{\partial H}$	$\frac{\partial}{\partial T}$	$\frac{\partial}{\partial R}$	$\frac{\partial}{\partial L}$	$\frac{\partial}{\partial M}$	$\frac{\partial}{\partial N}$
H	0,9196	−4,2668	0,4311	−0,1144	4,3060	−0,2321
T	0,3858	1,3332	−0,1678	0,0112	−1,5089	−0,1787
R	−2,3942	−1,5921	2,6385	−1,1274	0 7003	−0,5040
L	3,5488	7,4023	−4,2309	2,0708	−5,6998	−0,8597
M	−0,4499	−3,6176	0,5038	−0,0633	4,0450	0,3249
N	5,3033	48,1721	−7,1684	1,9206	−53,2462	−1,3370

$$\alpha_1 = 0{,}5994\,\varkappa - 0{,}4516\,\alpha_2 + 1{,}3344\times 10^{-3}\,\frac{(2\omega+\sigma)\,\sigma}{\omega^2}\,\beta$$

$$k = 0{,}3017 - 0{,}1199\,\frac{\alpha_2}{\varkappa} + 0{,}2248\times 10^{-3}\,\frac{(2\omega+\sigma)\,\sigma}{\omega^2}\,\frac{\beta}{\varkappa} \qquad (46)$$

$$l = 0{,}0861 - 0{,}0098\,\frac{\alpha_2}{\varkappa} - 0{,}0124\times 10^{-3}\,\frac{(2\omega+\sigma)\,\sigma}{\omega^2}\,\frac{\beta}{\varkappa}$$

$$h = 0{,}6113 - 0{,}1065\,\frac{\alpha_2}{\varkappa} + 0{,}4462\times 10^{-3}\,\frac{(2\omega+\sigma)\,\sigma}{\omega^2}\,\frac{\beta}{\varkappa}.$$

Следует отметить хорошее согласие статических чисел Лява (их значения получаются из (46) при $\sigma = \omega = 0$)с наблюдаемыми. Мельхиор в своей книге (M e l c h i o r 1972) на основании серии наблюдений состоящей из 50 000 дней дает следующие значения статических чисел Лява:

$$k = 0{,}316 \pm 0{,}010$$

$$h = 0{,}637 \pm 0{,}016\,.$$

В таблице 2 представлено изменение статических чисел Лява с глубиной.

Таблица 2. – Table 2

Зависимость статических числех Лява от радиуса для модели Ванга
Dependence of static Love numbers on the radius for Wang's earth model

r	H_0	M_0	T_0	R_0	N_0	L_0
1,00	0,6113	0,0000	0,0861	1,3017	0,0000	1,0949
0,99	0,6120	0,0058	0,0907	1,2775	0,0141	1,0226
0,98	0,6137	0,0101	0,0937	1,2607	0,0242	0,9708
0,97	0,6162	0,0158	0,0975	1,2375	0,0386	0,9000
0,95	0,6201	0,0259	0,1035	1,1952	0,0632	0,7743
0,93	0,6235	0,0350	0,1083	1,1568	0,0838	0,6650
0,90	0,6285	0,0498	0,1152	1,0928	0,1132	0,4986
0,85	0,6341	0,0688	0,1249	0,9915	0,1416	0,2720
0,80	0,6377	0,0783	0,1308	0,9067	0,1486	0,1007
0,75	0,6409	0,0803	0,1351	0,8142	0,1338	−0,0683
0,70	0,6425	0,0738	0,1371	0,7446	0,1046	−0,1848
0,65	0,6424	0,0571	0,1387	0,6766	0,0656	−0,2933
0,60	0,6394	0,0349	0,1404	0,6313	0,0581	−0,3660
0,55	0,6287	0,0000	0,1442	0,5974	0,1655	−0,4289

Отношение k/h с помощью (46) можно выразить следующим образом:

$$k = 0{,}4935\,h - 0{,}0674\,\frac{\alpha_2}{\varkappa} + 0{,}0047\times 10^{-3}\,\frac{(2\omega+\sigma)\,\sigma}{\omega^2}\,\frac{\beta}{\varkappa}.$$

В данном случае интересна слабая зависимость этого отношения от частоты вынуждающей силы, близость его к статическому значению.

Параметр α_2 можно определить из условий на границе ядро внешнее-внутреннее. Для нашей модели Земли мы получили

$$\alpha_2 = 0{,}0059\,\varkappa + 0{,}0132\times 10^{-3}\,\frac{(2\omega+\sigma)\,\sigma}{\omega^2}\,\beta\,.$$

Поскольку параметр $\varkappa$, как уже замечалось выше, имеет порядок $\sim 10^{-7}$, то α_2 имеет, соответственно, порядок $\sim 10^{-10}$. Это указывает на то, что влиянием внутреннего ядра на числа Лява и приливные коэффициенты, по-видимому, можно пренебреч. Следует заметить, что к такому же выводу пришел Молоденский (1961), даже в широких пределах меняя μ ядра (μ от О до ∞).

Далее используя условия (41)–(42), мы можем получить отношение нутаций реальной и абсолютно твердой Земли в функции частоты и резонансного параметра β :

$$\frac{\varepsilon}{\varepsilon_0} = 1 + 0{,}0963\left(\frac{\beta}{\varkappa} - 3{,}248\right)\frac{\sigma+\omega}{\omega}.$$

И наконец, используя граничное условие (32), мы можем значение резонанского параметра в зависимости от частоты приливной силы

$$\frac{\beta}{\varkappa} = \frac{7{,}1345 - 2.6607\,\dfrac{\sigma+\omega}{\sigma}}{0{,}03496 - 9{,}2578\,\dfrac{\sigma+\omega}{\sigma}}. \qquad (47)$$

Частота свободных колебаний получается из (47) следующей

$$\frac{\sigma_0+\omega}{\sigma_0} = 0{,}003776\,,$$

что соответстует периоду „почти суточной" нутации на 5.45 минут короче звездных суток. Период Чандлера расчитывается по формуле (45) . k_0 для нашей модели равно 0.9567, таким образом, чандлеровский период получается равным 442.6 дней, что заметно отличается от периода, полученного Молоденским (433 дня), но близко к периоду, расчитанному Джеффрисом (Jeffreys 1959), (448 – 7 дней), а также к реальному периоду Чандлера, получаемому из наблюденний, который считается равным, примерно, 450 дням. Некоторое отличие

значения, приводимого Молоденским, по-видимому, объясняется несколько завышенным моментом инерции ядра, принятым им в расчетах, так как с уменьшением момента инерции ядра период Чандлера увеличивается.

В таблице 3 представлены значения параметра $\frac{\beta}{\varkappa}$, расчитанные для частот главных приливных волн, динамические значения чисел Лява h, k, δ, γ, а также отношения амплитуд вынужденной нутации Земли с жидким ядром и абсолютно твердой Земли.

Таблица 3. – Table 3.

Значение параметров $\frac{\beta}{\varkappa}$, $\frac{\varepsilon}{\varepsilon_0}$ и динамических чисел Лява для главных приливных волн

The values of parameters $\frac{\beta}{\varkappa}$, $\frac{\varepsilon}{\varepsilon_0}$ and dynamic Love numbers for the main earth tide waves

Волна	$\frac{\sigma+\omega}{\omega}$	$\frac{\beta}{\varkappa}$	$\left(\frac{\varepsilon}{\varepsilon_0}-1\right)\cdot 10^3$	h	k	δ	γ
OO_1	$-\frac{1}{13{,}7}$	−11,69	105	0,6120	0,3020	1,1590	0,6900
φ_1	$-\frac{1}{183}$	−463,67	246	0,6135	0,3028	1,1593	0,6893
K_{565}	$-\frac{1}{6879}$	212,35	−3,0	0,6113	0,3017	1,1588	0,6904
K_1	0	–	0	0,6113	0,3017	1,1588	0,6904
K_{545}	$\frac{1}{6879}$	196,45	2,7	0,6113	0,3017	1,1588	0,6904
P_1	$\frac{1}{183}$	83,30	42,1	0,6117	0,3019	1,1589	0,6902
O_1	$\frac{1}{13.7}$	9,6	44,7	0,6120	0,3020	1,1589	0,6901

Легко видеть, что разность чисел Лява для главных суточных волн K_1 и O_1 весьма невелика

$$\gamma(O_1)-\gamma(K_1) = -0{,}0003$$
$$\delta(O_1)-\delta(K_1) = \quad 0{,}0001,$$

и даже эти разности возникают, скорее, в результате ошибок расчета. Кроме того, ошибка определения чисел Лява из приливных наблюдений составляет, примерно, $\sim 10^{-2} \sim 10^{-3}$, таким образом, полученные разности на один-два порядка меньше достижимой в современных условиях точности. Таким образом, если рассмотренная в данной

работе теория нутации дает достаточное приближение к реальному явлению, то перед исследователями приливов встает важная задача объяснения того, чем вызваны наблюдаемые разности в числах Лява для главных приливных волн. Из наблюдений получаются следующие разности

$$\delta(O_1) - \delta(K_1) = 0{,}001 \div 0{,}040$$

$$\gamma(O_1 - \gamma(K_1) = -0{,}011 \div -0{,}093,$$

и даже если принять, что ошибка в их определении $\sim 10^{-2}$, то тем не менее для некоторых станций наличие таких разностей будет все же бесспорным.

Однако по нашему мнению, эти разности вызваны, скорее, влиянием косвенного эффекта приливов, а не возмущениями Земли. То, что разности, лежащие вне пределов ошибки, наблюдаются, в основном, на станциях, близких к морям и океанам, то, что существует ряд станций, где разности имеют противоположный знак, некоторым образом подтверждает наше предположение.

И наконец, мы можем расчитать поправки к амплитудам вынужденной нутации, получаемым в предположения абсолютной твердости Земли. Слдует срузу заметить, что геофизические следствия проявляют себя в неблюдаемых астрономических величинах довольно незначительно. Вообще, для их обнаружения обычно исключают влияние всех эффектов вращения Земли как абсолютно твердого тела и считают, что отклонения наблюдений от данных этой теории возникают в результате отличия свойств Земли от свойств абсолютно твердого тела и других геофизических причин. Полагают, что тщательный анализ этих отконений позволит получить на основе астрономических наблюдений данные, которые могут служить критерием справедливости тех или иных гипотез о внутреннем строении Земли.

Возьмем постоянную нутации 9".2075 $\pm$ 0".0020 (Ситтер) и используя значения $\frac{\varepsilon}{\varepsilon_0}$ из таблицы 3 расчитаем расхождение между наблюдаемым и теоретическим значением поправки в малой полуси нутационного эллипса. Оно получается равным 0".0016, то есть практически лежит в пределах ошибки определения постоянной нутации. Этот вывод имеет очень большое значение, поскольку амплитуды короткопериодических членов нутации определяются не непосредственно из астрономических наблюдений, точность которых недостаточна для их обнаружения, а из анализа наблюденных амплитуд главных членов прецесси и нутации. Теоретические расчеты, применявшиеся до сих пор для определения амплитуд короткопериодических членов основывались на предположении, что Земля идеально тверда. Предполагалось, что поскольку во внешнем ядре могут происходить некоторые движения, сопровождаемые резонансными явлениями, то в некоторые из теоретических амплитуд нутационных движений не-

бходимо внести соответствующие поправки, вызванные нутационным движением жидкого ядра Земли. Настоящий расчет показывает, что эти поправки лежат в пределах ошибок астрономических наблюдений.

ЛИТЕРАТУРА

Джеффрис, Г. (1960): Земля, ее происхождение, история и строение, ИЛ, Москва

Melchior, P. (1972): Physique et Dynamique planétaires, géodynamique, volume 3, Vander

Молоденский, М. С. (1961): Теория нутации и суточных земных приливов, в книге "Земные приливы и нутация Земли", изд. АН СССР, Москва

Молоденский, М. С. и Крамер, М. В. (1961): Числа Лява для статических земных приливов 2 и 3-го порядков, в книге "Земные приливы и нутация Земли", изд. АН СССР, Москва

Wang, C. (1972): A Simple Earth Model, JGR, vol. 77, No. 23. 4318–4329

AN ITERATIVE SOLUTION OF THE INVERSE GRAVITY PROBLEM FOR CONSTRAINED MODELS

by

A. MESKÓ

Department of Geophysics, Eötvös University, Budapest
Received: 15 March 1975

SUMMARY

An iterative solution of the inverse gravity problem is described in the case where the gravity field is due to the undulation of the interface between two layers with different densities. The method proposed here consists of setting up a starter model computing the gravity field due to the model and modifying the model in an iterative manner until a good approximation between measured and computed gravity fields is obtained. The method resembles to the procedure described by Cordell and Henderson (1968) but the computation of the gravity field is simplified and the corrections to be applied in due course of the iterations are determined more efficiently. As a result the number of iterations, necessary to achieve a given accuracy, are significantly decreased as well as the computer time required by the process.

The accuracy of the approximations used in the computation of the gravity field due to the model are investigated in Part I. and Part II. The iterative process and examples of its applications are described in Part III.

Introduction

The purpose of this paper is to describe an economical algorithm for solving the inverse gravity problem in the simplified but practically useful case when the gravity anomalies are due to a single density contrast. Most methods known form the literature (Cordell and Henderson 1968, M. Al-Chalabi 1971 etc.) set up a geological model, specify some of its parameters and then determine the other parameters by using some sort of iterative or optimization algorithm. The objective is to compute or modify in each step the free or adjustable parameters in such a way that the gravity anomaly, produced by the structural model possessing these parameters be close to the measured gravity anomalies. The fit between the computed and measured data may be considered complete if the differences do not exceed the measurement errors. Some other criterion may also be used to express the goodness of fit between the two sets of data. No author claimed that a unique solution can be reached. An appropriate selection of the adjustable parameters (in most cases the density contrast and the depth of the lower or upper surface of the anomalous bodies), however, could yield geologically feasible solutions. This solution, even if the required goodness of fit has been arrived, still may be incorrect because some additional assumptions

have to be valid e.g. there should be no more than a single density contrast and its maximum depth should be given to a good approximation, regional background and random errors must not exceed an upper limit etc. Feasible models, however, do help the interpretation even if they have obvious limitations and contribute to a better understanding of the prospected area. Therefore it is hoped that the solution of the inverse gravity problem as proposed in the present paper may be of interest.

The iterative solution, described in detail in Part 3. is a modification of the method by Cordell and Henderson (1968). Modifications became necessary because the original version needs too large an amount of computer time. 20 iterations for 20×20 data array run 9,0 minutes on an IBM 360/65 computer (Cordell – Henderson 1968 p. 598). Solutions, obtained by different approaches require also too large computer times.

We have to work on larger data array and the computers available to us are slower than those mentioned in the cited publication. The computation of the gravity field due to the model had to be simplified and the convergence of the iterative process had to be made faster.

Gravity fields due to irregularly shaped bodies are usually obtained by dividing the bodies into rectangular prisms and adding up the effects of these elements (e.g. Nagy 1966). Some authors (e.g. Botezatu et al 1971) suggest the use of cubes. The gravity field of rectangular prisms can be given analytically. Various expressions are known from the literature (Nagy 1966, Goodacre 1973 etc.) none of these is easy to handle. Long and tedious computations are involved the repeated use of which in each iterative step for all observation points requires so much computer time that practically prohibits the use of the exact formula. In its stead we approximate the fields of rectangular prisms by fields of mass points. The masses are equal to the mass of the corresponding prisms and all points lie in a horizontal plane parallel to the reference plane through the center of mass of the whole irregularly shaped body. The accuracy of this approximation has been investigated and results are summarized in Part 1. of this paper. In practical applications we assume that the gravity anomaly is due to the undulations of the depth of an interface between homogeneous layers with different densities such as e.g. the interface between the upper and lower Pannonian sediments or more often the interface of the sediments and the cristallyne basement. It also involves that there are no other inhomogeneities either horizontally or vertically (such as lateral variations in density or other interfaces corresponding to density changes). We also assume that the regional background has been properly removed, random variations have been smoothed.

The deepest point of the interface determines the depth of the horizontal reference plane. This will be considered the lower boundary of the causative body, while the upper boundary is defined by the interface. The gravity effect of horizontal and constant density layers is an additive

constant therefore the whole anomaly is due to the irregular „body" defined above.

The thickness of the body is usually no more than some hundred meters, and the average depth is not less than 1 km. It can be seen that in order to avoid side-effects the thickness have to be very small around the boundary of the investigated area or some additional procedure is necessary to overcome the disturbances of the side effects. We shall assume in the followings that the thickness and the average depth satisfy this requirements and call attention to that limitations the algorithm. All the assumptions should be checked in practical applications.

The undulations of the density contrast surface acts as a peculiar sheet-like body i.e. it is thin and large horizontally.

The gravity field due to a prism is approximated in turn by a mass point concentrated in the neighbourhood of its center.

Gravity anomalies due to various bodies are shown in Part 2. The accuracy of the double approximation is also dealt with in that part of the paper.

PART 1.

Approximation of the gravitational attraction due to a rectangular prism by that of a mass point in its center

The vertical component of the gravitational attraction of a rectangular prism is given by the integral

$$g(x, y, z,) = G \Delta g \int_{x-u_1}^{x-u_2} \int_{y-v_1}^{y-v_2} \int_{z-w_1}^{z-w_2} \frac{w}{[u^2+r^2+w^2]^{3/2}} \, du \, dv \, dw \,, \qquad (1.1)$$

where $g(x,y,z)$ denotes the vertical component of the field at the point x,y,z

G is the gravitational constant

($6.67.10^{-8}$ cgs unit)

$\Delta\varrho$ is the density of the prism and

(u_1,v_1,w_1), $(u_1,v_1\ w_2), \ldots (u_2,v_2,w_2)$

are the coordinates of the corners of the prism and z is positive downwards.

The notations used in (1.1) are shown in *Fig. 1.1.* Various expressions were published for the integrated results (K e l l o g 1929, B o t e-

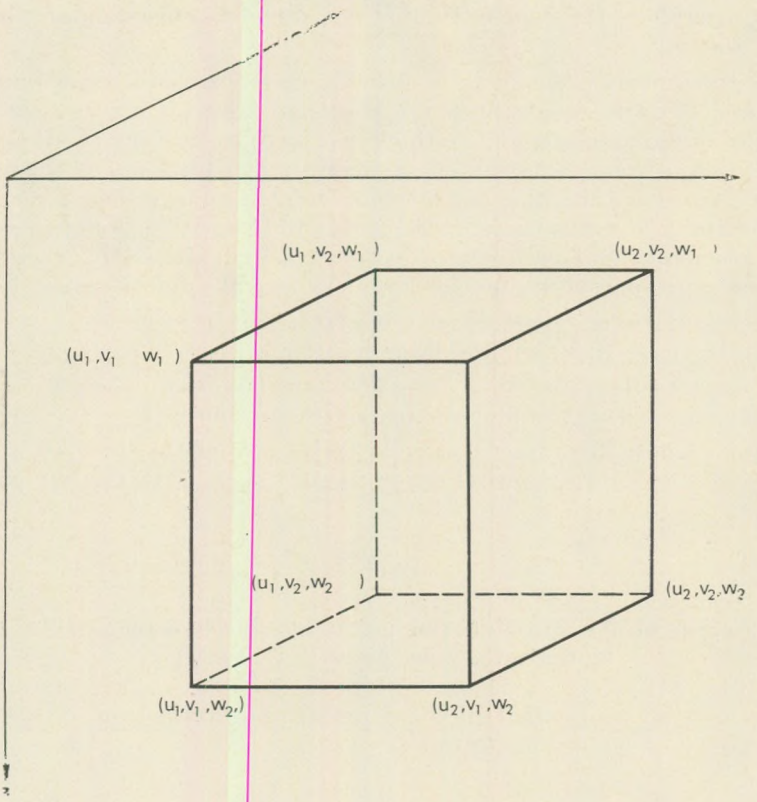

Fig. 1.1 Notations used in the derivation of the gravitational attraction of a rectangular prism

z a t u et. al 1971, N a g y, 1966 etc.) As G o o d a c r e (1973) pointed out a convenient from for $g\ (x,y,z)$ is

$$g(x,y,z) = G\Delta\varrho \left| \left| \left| u \ln(v+r) + v \ln(u+r) - w \operatorname{atan}\left(\frac{uv}{wr}\right) \right|_{x-u_1}^{x-u_2} \right|_{y-v_1}^{y-v_2} \Bigg|_{z-w_1}^{z-w_2}, \quad (1.2)$$

where $r = (u^2+v^2+w^2)^{1/2}$

Equation (1.2) is an abbreviation for an expression consisiting of 8 terms. Before writing down the explicite version of the full expression let us introduce some notations. In practical applications $z = 0$ and the two other coordinates are integer multiples of the grid spacing; the latter be denoted by s, i. e.

$x = ks\ (k = -n, \quad -n+1, \ldots 0, \quad \ldots n-1,\ n)$ and

$y = ls\ (l = -m, \quad -m+1, \ldots 0, \quad m-1,\ m).$

The detailed expression for the z components of the gravity field in the point $(ks,\ ls,\ 0)$ is than

$$g(x, y, z) = G\,\Delta\varrho \sum_{i=1}^{8} t_i; \tag{1.3}$$

$$t_1 = (ks-u_2)\ln[ls-v_2)+r_1]+(ls-v_2)\ln[(ks-u_2)+r_1]+ \\ +w_2\,\mathrm{atan}\frac{(ks-u_2)(ls-v_2)}{-w_2\,r_1}, \tag{1.4a}$$

$$t_2 = -\left[(ks-u_1)\ln[(ls-v_2)+r_2]+(ls-v_2)\ln[(ks-u_1)+r_2]+ \right. \\ \left. +w_2\,\mathrm{atan}\frac{(ks-u_1)(ls-v_2)}{-w_2\,r_2}\right], \tag{1.4b}$$

$$t_3 = (ks-u_2)\ln[(ls-v_1)+r_3]+(ls-v_1)\ln[(ks-u_2)+r_3]+ \\ +w_1\,\mathrm{atan}\frac{(ks-u_2)(ls-v_1)}{-w_1\,r_3}, \tag{1.4c}$$

$$t_4 = -\left[(ks-u_1)\ln[(ls-v_1)+r_4]+(ls-v_1)\ln[(ks-u_1)+r_4]+ \right. \\ \left. +w_1\,\mathrm{atan}\frac{(ks-u_1)(ls-v_1)}{-w_1\,r_4}\right], \tag{1.4d}$$

$$t_5 = (ks-u_1)\ln[(ls-v_2)+r_5]+(ls-v_2)\ln[(ks-u_1)+r_5]+ \\ +w_1\,\mathrm{atan}\frac{(ks-u_1)(ls-v_2)}{-w_1\,r_5}, \tag{1.4e}$$

$$t_6 = -\left[(ks-u_2)\ln[(ls-v_2)+r_6]+(ls-v_2)\ln[(ks-u_2)+r_6]+ \right. \\ \left. +w_1\,\mathrm{atan}\frac{(ks-u_2)(ls-v_2)}{-w_1\,r_6}\right], \tag{1.4f}$$

$$t_7 = (ks-u_1)\ln[(ls-v_1)+r_7]+(ls-v_1)\ln[(kr-u_1)+r_7]+ \\ +w_2\,\mathrm{atan}\frac{(ks-u_1)(ls-v_1)}{-w_2\,r_7}, \tag{1.4g}$$

$$t_8 = -\left[(ks-u_2)\ln[(ls-v_1)+r_8]+(ls-v_1)\ln[(ks-u_2)+r_8]+ \right. \\ \left. +w_2\,\mathrm{atan}\frac{(ks-u_2)(ls-v_1)}{-w_2\,r_8}\right], \tag{1.4h}$$

where

$$r_1^2 = (ks-u_2)^2+(ls-v_2)^2+w_2^2 \tag{1.5a}$$

$$r_2^2 = (ks-u_1)^2+(ls-v_2)^2+w_2^2 \tag{1.5b}$$

$$r_3^2 = (ks-u_2)^2+(ls-v_1)^2+w_1^2 \tag{1.5c}$$

$$r_4^2 = (ks-u_1)^2+(ls-v_1)^2+w_1^2 \tag{1.5d}$$

$$r_5^2 = (ks-u_1)^2+(ls-v_2)^2+w_1^2 \tag{1.5e}$$

$$r_6^2 = (ks-u_2)^2+(ls-v_2)^2+w_1^2 \tag{1.5f}$$

$$r_7^2 = (ks-u_1)^2+(ls-v_1)^2+w_2^2 \tag{1.5g}$$

$$r_8^2 = (ks-u_2)^2+(ls-v_1)^2+w_2^2 \tag{1.5h}$$

Let us consider now the special case when the center of the prism is in the point (0,0,H) and therefore, the corners are given by

$$\left.\begin{aligned} u_1 &= -\frac{s}{2}, & u_2 &= \frac{s}{2} \\ v_1 &= -\frac{s}{2}. & v_2 &= \frac{s}{2} \\ w_1 &= H-\frac{h}{2}, & w_2 &= H+\frac{h}{2} \end{aligned}\right\} \tag{1.6}$$

which involves that the cross section of the prism is a grid square.

If we introduce the following abbreviations

$$\left.\begin{aligned} A_1 &= \left(k-\frac{1}{2}\right)s & A_2 &= \left(k+\frac{1}{2}\right)s \\ B_1 &= \left(l-\frac{1}{2}\right)s & B_2 &= \left(l+\frac{1}{2}\right)s \\ C_1 &= \left(H'+\frac{h'}{2}\right)s & C_2 &= \left(H'-\frac{h'}{2}\right)s \end{aligned}\right\} \tag{1.7}$$

where H' and h' are the depths of the mass center and the height of the prism, respectively, both measured in units of the grid spacing, the expressions (1.4a)–(1.4h) become

$$t_1 = A_1\ln(B_1+r_1)+B_1\ln(A_1+r_1)-C_1\,\mathrm{atan}\,\frac{A_1B_1}{C_1r_1}, \tag{1.8a}$$

$$t_2 = -\left[A_2\ln(B_1+r_2)+B_1\ln(A_2+r_2)-C_1\,\mathrm{atan}\,\frac{A_2B_1}{C_1r_2}\right], \tag{1.8b}$$

$$t_3 = A_1 \ln(B_2 + r_3) + B_2 \ln(A_1 + r_3) - C_2 \operatorname{atan} \frac{A_1 B_2}{C_2 r_3}, \tag{1.8c}$$

$$t_4 = -\left[A_2 \ln(B_2 + r_4) + B_2 \ln(A_2 + r_4) - C_2 \operatorname{atan} \frac{A_2 B_2}{C_2 r_4} \right], \tag{1.8d}$$

$$t_5 = A_2 \ln(B_1 + r_5) + B_1 \ln(A_2 + r_5) - C_2 \operatorname{atan} \frac{A_2 B_1}{C_2 r_5}, \tag{1.8e}$$

$$t_6 = -\left[A_1 \ln(A_1 + r_6) + B_1 \ln(A_1 + r_6) - C_2 \operatorname{atan} \frac{A_1 B_1}{C_2 r_6} \right], \tag{1.8f}$$

$$t_7 = A_2 \ln(B_2 + r_7) + B_2 \ln(A_2 + r_7) - C_1 \operatorname{atan} \frac{A_2 B_2}{C_1 r_7}, \tag{1.8g}$$

$$t_8 = -\left[A_1 \ln(B_2 + r_8) + B_2 \ln(A_1 + r_8) - C_1 \operatorname{atan} \frac{A_1 B_2}{C_1 r_8} \right], \tag{1.8h}$$

where

$$r_1^2 = A_1^2 + B_1^2 + C_1^2, \tag{1.9a}$$

$$r_2^2 = A_2^2 + B_1^2 + C_1^2, \tag{1.9b}$$

$$r_3^2 = A_1^2 + B_2^2 + C_2^2, \tag{1.9c}$$

$$r_4^2 = A_2^2 + B_2^2 + C_2^2, \tag{1.9d}$$

$$r_5^2 = A_2^2 + B_1^2 + C_2^2, \tag{1.9e}$$

$$r_6^2 = A_1^2 + B_1^2 + C_2^2, \tag{1.9f}$$

$$r_7^2 = A_2^2 + B_2^2 + C_1^2, \tag{1.9g}$$

$$r_8^2 = A_1^2 + B_2^2 + C_1^2. \tag{1.9h}$$

The computation of the z components of the gravity field of the rectangular prism having the corners (1.6) in a regular grid with spacing s can be performed according to the following scheme

a) determine the variables A_1, A_2, ... C_2 by equations (1.7)
b) computate the r_i values by equations (1.9)
c) evaluate formulas (1.8) i.e. calculate the t_i values
d) multiply the sum of the t_i–s by $G\varrho\Delta$. These steps are repeated for each (k, l) pairs.

The mass of the prism is

$$m = \Delta \varrho s^2 h$$

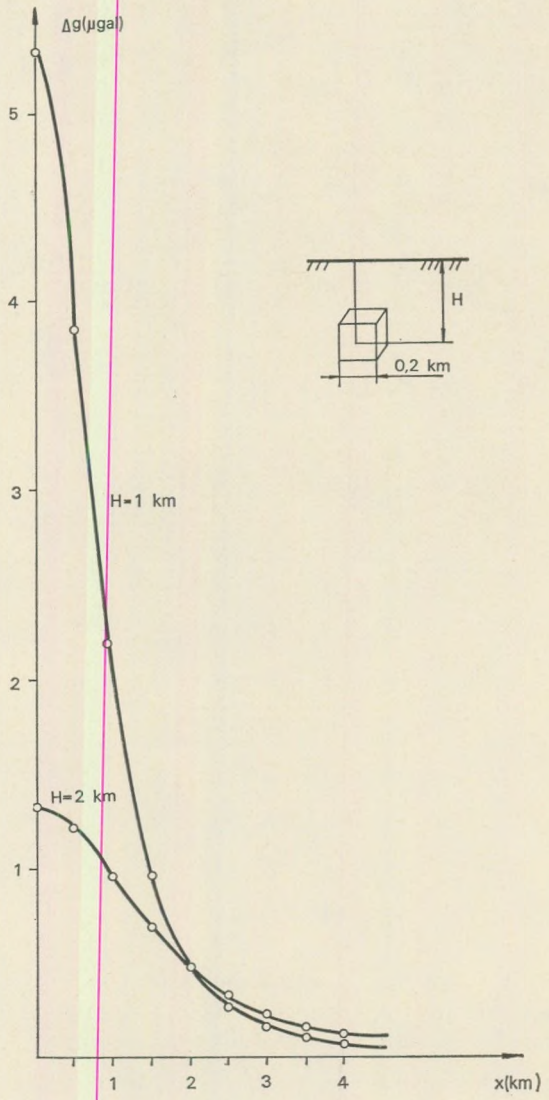

Fig. 2.2 Comparison between the z-components of the gravitational attraction due to cubes with edges of 0.2 km (empty circles) and that of mass points in their centers (continuous curves)

and because the center of mass lies in (O, O, H) the z component of the gravity field due to that mass, concentrated in the center becomes

$$g^*(ks, ls, 0) = G\,\Delta\varrho \frac{s^2\, h\, H}{[(ks)^2 + (ls)^2 + H^2]^{3/2}}$$

$$= G\,\Delta\varrho \frac{h'\, H'}{[k^2 + l^2 + (H')^2]^{3/2}} \qquad (1.10)$$

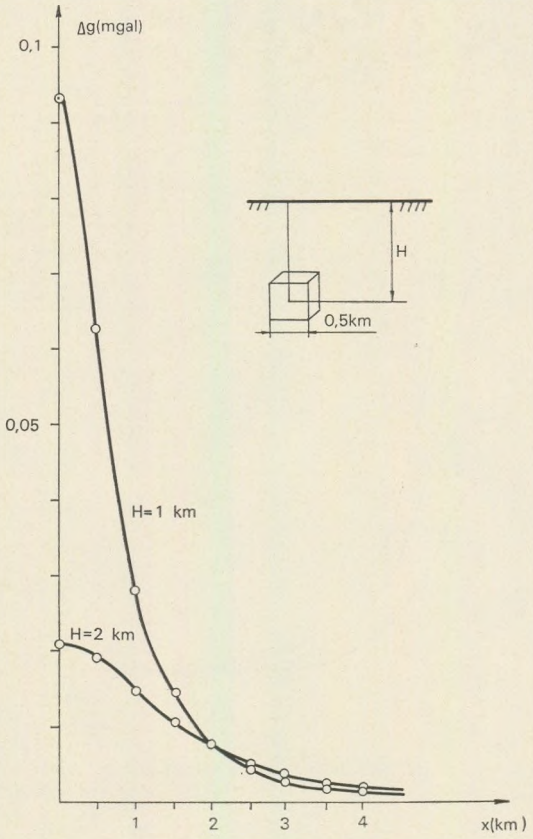

Fig. 1.3 Comparison between the z-components of the gravitational attraction due to cubes with edges of 0.5 km (empty circles) and that of mass points in their centers (continuous curves)

The goodness of fit between the exact field and its approximation (1.10) can be evaluated by direct comparison of the effects due to prisms with realistic parameters.

In those applications which are our main concern in Parts 2. and 3., H varies between 1 km and 2 kms while k is somewhere between 0 and 500 meters.

Figures 1.2 and *1.3* show the $g(ks, 0,0)$ values as empty circles for cubes with edges of 200 and 500 meters, respectively, in each case for two depths (1 km and 2 kms). The approximations obtained from the fields of mass points are drawn by continuous lines.

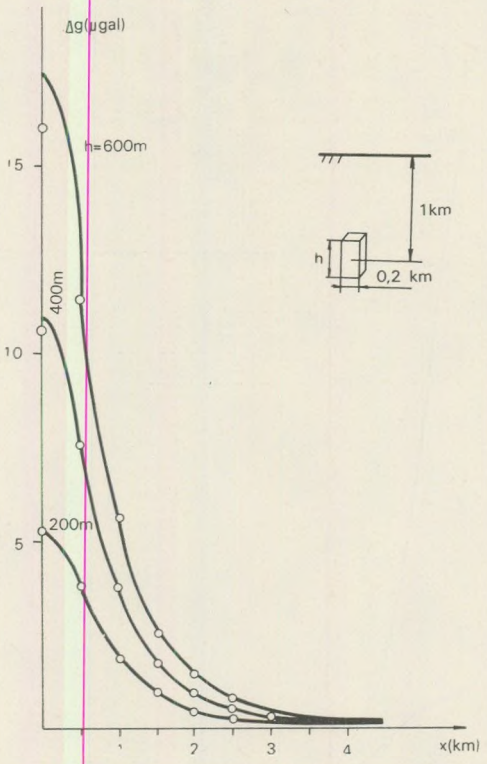

Fig. 1.4 Comparison between the z-components of the gravitational attraction due to rectangular prisms with $0{,}2 \times 0{,}2$ km^2 base and various height and that of mass points in their centers (continuous curves) when the depths of the mass centers are 1 km

Further exaples are shown in *Figs. 1.4* and *1.5*, where rectangular prisms have square cross sections with edges of 200 ms and heights of 200, 400 and 600 ms. The depths of the centers of masses are 1 km in *Fig. 1.4* and 2 kms in *Fig. 1.5*, respectively.

In all cases, shown as *Figs. 1.2* to *1.5*, the two-dimensional functions $g(x,y,0)$ and $g^*(x,y,0)$ are investigated along the x direction, only. This approach is justified if the field possesses circular symmetry. The field

due to a point source is indeed direction independent but the fields due to rectangular prisms are not. The largest deviations from gravity values along the direction of the x coordinate axis can be expected along the direction of the diagonal i.e. along the line $x = y$. The deviation from circular symmetry in the gravitational attraction of the prism can best be estimated by comparing the curves

$$g(x, y = 0, 0) \quad \text{and} \quad g(\sqrt{2}x, \sqrt{2}y, 0).$$

The directivity diminishes as the dimensions of the body decrease and the center of mass gets deeper therefore the worst situation which

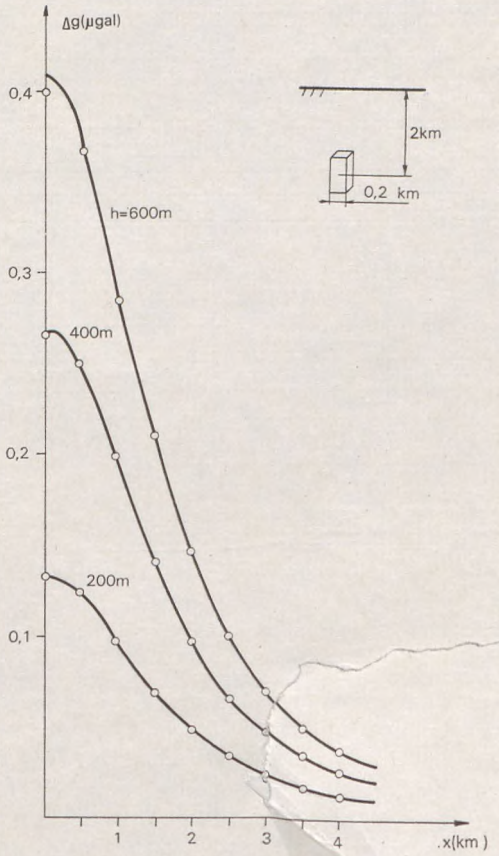

Fig. 1.5 Comparison between the z-components of the gravitational attraction due to rectangular prisms with $0{,}2 \times 0{,}2$ km^2 base and various heights and that of mass points in their centers (continuous curves) when the depths of the mass centers are 2 kms

has to be dealt with is that of the prism with $0,5 \times 0,5$ km^2 base and with center of mass at 1 km. Deviations for some situation are shown in *Fig. 1.7*. Numerical values were computed for various heights of the prisms along the directions $y = 0$ and $y = x$. The deviations, as it can be seen in *Fig. 1.7*, are very small. No values were found above 2 μgal which proves that the one-dimensional approach is justified. As a summary it may be said that the gravity field of an irregularly shaped body can be approximated by a sum of gravity fields due to point masses about the same accuracy as by a sum of gravity fields due to rectangular prism when the prisms are not larger than $500 \times 500 \times 500$ m^3 and the centers of masses lie in 1 km or deeper.

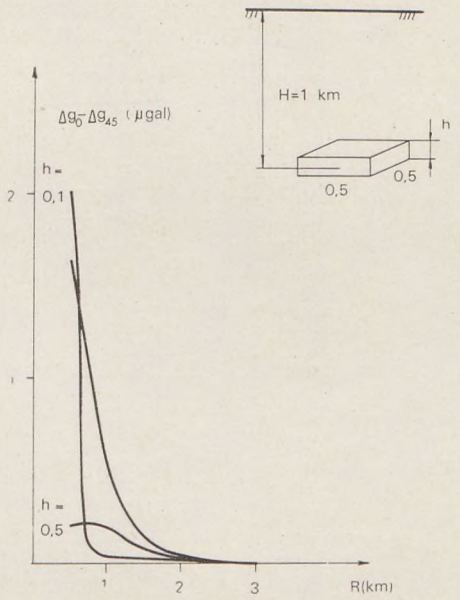

Fig. 1.6 Deviations between the z-components of the gravitational attraction measured along two profiles with directions 0° and 45°. The gravity fields are due to rectangular prisms with mass centers at 1 km and have a $0,5 \times 0,5$ km^2 square base and various thicknesses (denoted by h)

The economical advantage of the first approach is obvious because the computation of the gravity field due to a mass point is at least a hundred times faster. As a matter of fact the building up of the gravity field due to larger geological bodies or complicated surfaces from the field of rectangular prisms is really out of question when considering the limitations of our computational facilities.

Part 2.

Computation of the gravity field due to geological structures

Let us assume that the gravity anomaly field is solely due to the undulations of the interface between two homogeneous layers with different formation densities ϱ_1 and ϱ_2. The deepest point of the interface in the whole area defines the reference plane, the depth of which is denoted by H. (Notations are shown in *Fig. 2.1*). The mean depth of the interface will be denoted by H, the density contrast $\varrho_2 - \varrho_1$ by $\Delta\varrho$.

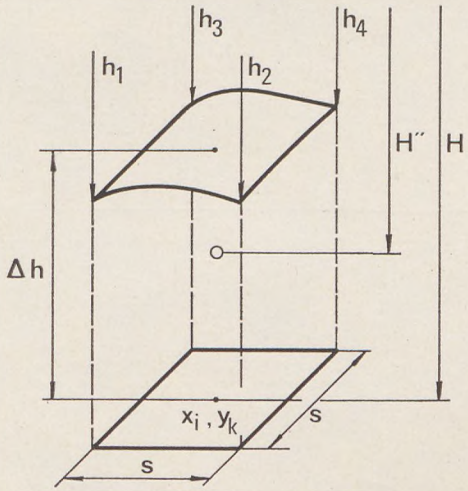

Fig. 2.1 To the computation of the gravity field due to a density interface

It is clear that the gravity anomaly caused by the undulations can be computed as the gravity effect of an irregular body bordered from below by the horizontal reference plane and otherwise by the interface and possesses a density $\Delta\varrho$. It is supposed that the interface reaches or comes close to the reference plane around the boundary of the area. We also assume that the mean depth is 1 km or more and the undulations around the mean depth do not exceed 0.3 km.

When the two latter assumptions are valid the body can be approximated by a bundle of rectangular prisms.

It is convenient to use the same rectangular grid system in the reference plane as the one determined by the observation points on the surface. The prisms therefore possess square bases. Observations are usually made at regular 0.5 km intervals in recent measurements, thus

the square basis are also of dimensions 0.5×0.5 km^2. In *Fig. 2.2* one of the prisms is shown (s stands for the grid interval). The heights of the prisms are estimated by

$$\Delta h_{ik} = H - \frac{h_1 + h_2 + h_3 + h_4}{4} \tag{2.1}$$

Where h_i denotes the depth of the interface in a grid point. (h_1, h_2, h_3 and h_4 are depths in the corners of a grid square). The mass of the prism is approximately

$$m_i = s^2 \Delta h \Delta \varrho \,. \tag{2.2}$$

The mass is then "concentrated" into a point with coordinates (x_i, y_k, H') where (x_i, y_k) is the center of the base and

$$H' = \frac{H + \overline{H}}{2} \,. \tag{2.3}$$

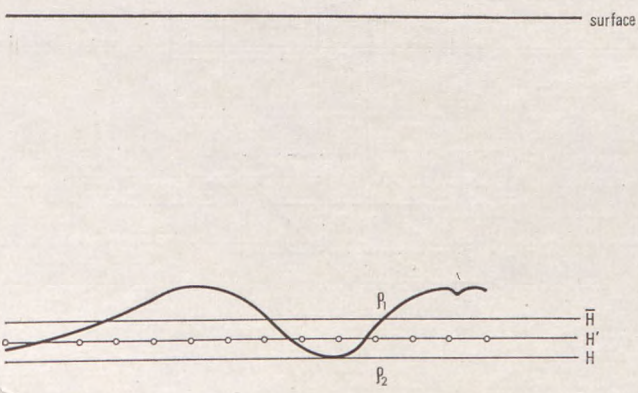

Fig. 2.2 Notations used in formulas (2.1) and (2.3)

The gravity effect of the prism is substituted by the effect of a mass point in (x_i, y_k, H') with mass determined by (2.2) i.e. the z-component of the gravity field in the point (u, v) is approximated by

$$g(u, v) = \frac{G \Delta \varrho \Delta h s^2 H'}{[(u - x_i)^2 + (v - y_k)^2 + (H')^2]^{3/2}} \,. \tag{2.4}$$

If the distances are given in kilometer units, $\Delta \varrho$ in *c.g.s* units and $g_i(u, v)$ in mgals $G = 6.67$.

The gravity field due to the whole body is the sum of the individual fields each given by (2.4). When (u,v) is a point in a square grid $u = ms$; $v = ns$ and the coordinates x_i and y_k are also measured in units of the grid spacing the contributions from the prisms sums up to give

$$g(m,n) = 6{,}67 \sum_i \sum_k \frac{\Delta\varrho\, h_{ik} H''}{[(m-x_i')^2+(n-y_k')^2+(H'')^2]^{3/2}} \tag{2.5}$$

Where

$$H'' = \frac{H}{s},$$

$$x_i' = \frac{x_i}{s},$$

$$y_k' = \frac{y_k}{s},$$

Formula (2.5) can be thought of as a convolution between Δh_{ik} and

$$s(x_i, y_k) = \frac{H''}{[(x_i')^2+(y_k')^2+(H'')^2]^{3/2}} \tag{2.6}$$

$$x_i' = i+\frac{1}{2} \quad (i = -n,\ -n+1,\ \ldots,\ n-1);$$

$$y_k' = k+\frac{1}{2} \quad (k = -n,\ -n+1,\ \ldots,\ n-1).$$

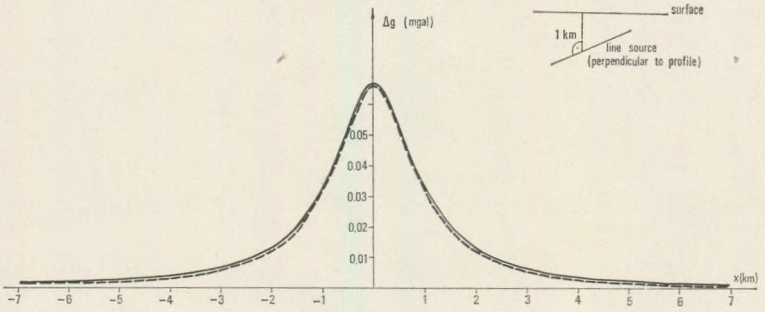

Fig. 2.3 Theoretical values of the gravity field of an infinite horizontal line source as measured along a profile perpendicular to the line (continuous curve) and its approximation obtained by (2.5) $y = 0$ (broken curve)

The accuracy of the proposed procedure has been checked by comparing gravity fields of simple bodies whose fields could have been expressed analytically to the gravity fields computed by (2.5) Some of the results are given in *Fig. 2.3–2.7*. *Fig. 2.3* shows the field of an infinite horizontal line source, buried at a depth of 1 km, along a line perpendicular to the body (continuous curve).

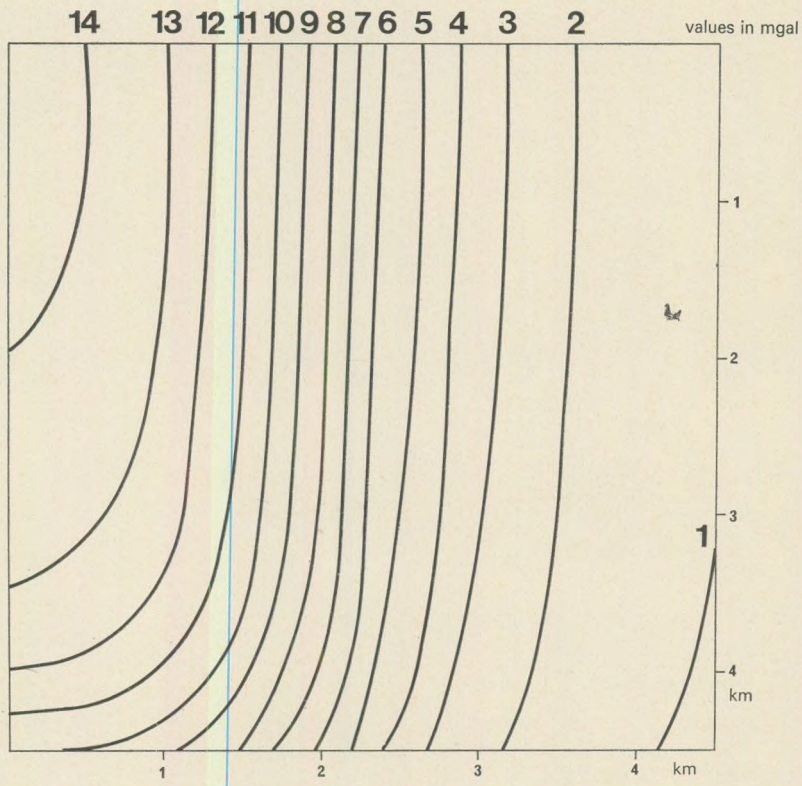

Fig. 2.4 The z-component of the gravity field due to a rectangular prism with dimensions $4\times10\times0{,}5$ km^2 with mass center at the depth of 1 km (exact formula) $\Delta\varrho = 1$ gcm^{-3}

The theoretical values come from the well known formula:

$$\Delta g(x) = 2G\,\lambda\frac{H}{H^2+\lambda^2}, \tag{2.7}$$

Where λ denotes the line density
and H is the depth.

The one dimensional modification of (2.5) gave the values connected by the broken curve in *Fig. 2.3.* The sampling distance was 0.5 km and 41 points were used to compute the convolution.

Fig. 2.4 shows the gravity field due to a rectangular prism whith dimension $4 \times 10 \times 0.5$ km^3, and with mass center at 1 km depth, as computed by the exact formulas (1.6) – (1.9).

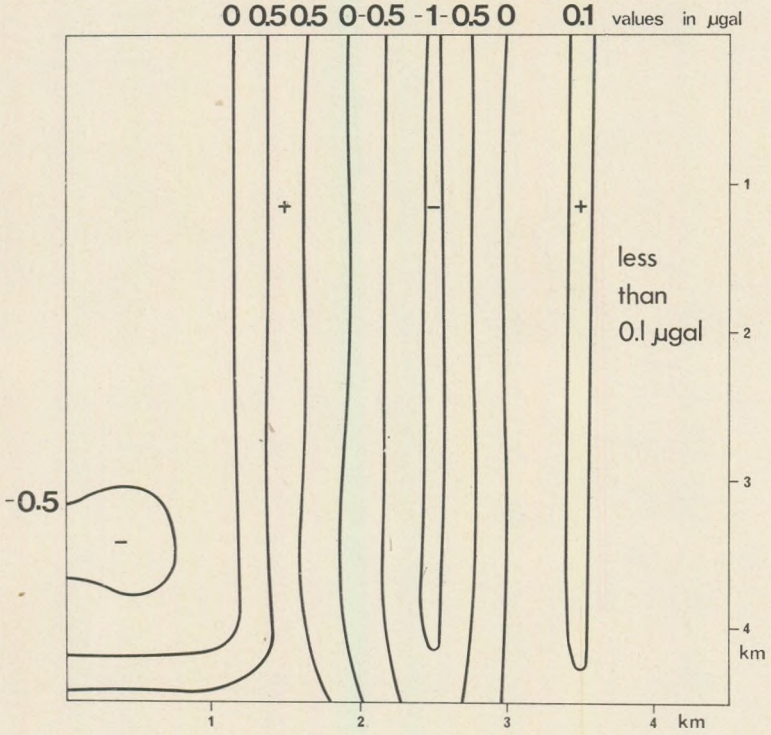

Fig. 2.5 Error field i.e. deviations between the theoretical gravity field shown in Fig. 2.4 and its approximation obtained by (2.5)

The convolution (2.5) gave a field so close to the theoretical one that the map, drawn from the approximate values is apparently identical to the "theoretical map" in *Fig. 2.4.* Therefore the difference field or "error field" has also been computed. Contours of the error field are shown in *Fig. 2.5.* We call the attention to the fact that the errors are given in 1μgal units and the isolines are 0,5μ gals apart. The deviations as indicated by the map can not be detected by the present measuring techniques.

Figs. 2.6 and *2.7* show similar quantities. *Fig. 2.6* is a field due to a $4 \times 4 \times 0.5$ km^3 rectangular prism at 1 km depth as computed according to the exact formulas while *Fig. 2.7* is the „error field" i.e. the difference of the theory and its approximation. The match of the convolution to the exact formula is excellent again. Numerous other models have been computed but the maximum of the deviations never exceeded 0.1 mgal for plausible geological models and $s = 0.5$ km sampling interval.

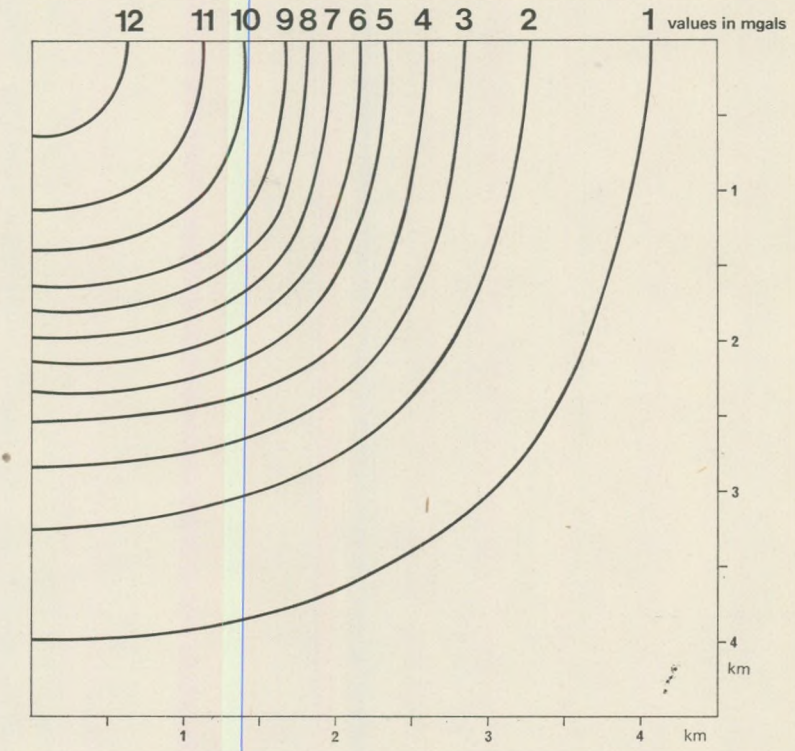

Fig. 2.6 The z-component of the gravity field due to rectangular prism with dimensions $4 \times 4 \times 0{,}5$ km^3 with mass center at the depth of 1 km (exact formula)

The application of equation (2.5) is further illustrated by *Fig. 2.8* and *2.9* where the gravity fields of a cone and a cylinder are shown respectively. On the upper parts of the figures the two dimensional fields are depicted by isolines on the lower part cross sections through the center of the models resp. the gravity fields are shown. The base

circle of the cone resp. the cylinder are drawn by broken lines. No comparison with theoretical values is possible because the gravity fields due to these bodies can not be expressed analitically.

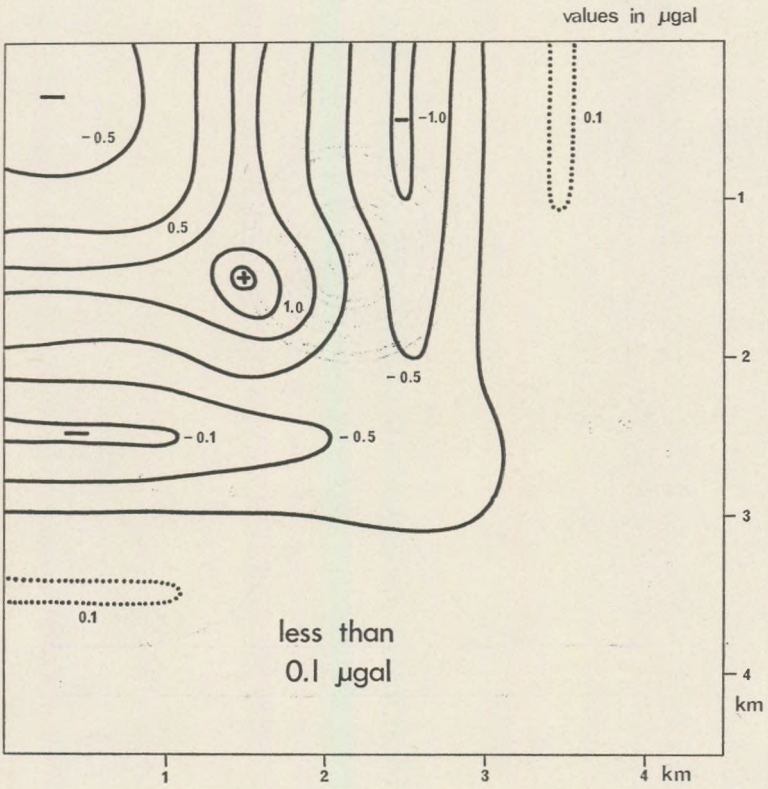

Fig. 2.7 Error field i.e. deviations between the theoretical gravity field shown in Fig. 2.6 and its approximation (the latter obtained by (2.5)).

The computation is rather fast and it does not need elaborate preparations as e.g. the method of T a l w a n i (1968) or storing and searching for the fields of appropriate cubes as the method proposed by B o t e z a t u et al (1973). It may therefore be of interest in itself. The simplified algorithm was developed in order to be able to solve the inverse problem by an iterative procedure in course of which the computation of the gravity fields due to geological models becomes necessary very often. Therefore our main concern had to be the speed and though some improvement of the algorithm can obviously be made (e.g. producing

denser spacing by interpolation, accurate positioning the center of mass for each prism etc.) but only at the cost of computer time. The approximation being satisfactory as it is now, we shall not deal with the improvement of the accuracy of the direct problem in this paper.

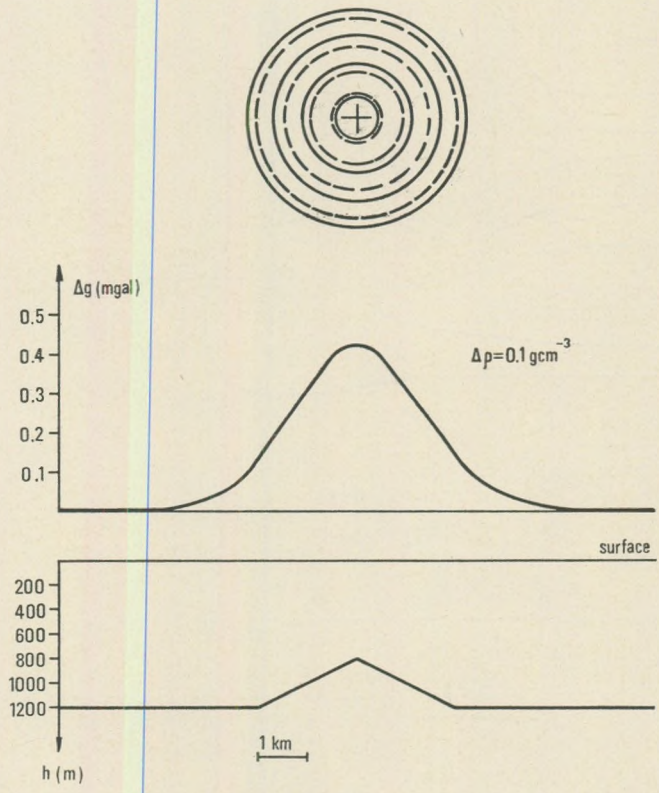

Fig. 2.8 The z-component of the gravity field due to a cone. Two-dimensional representation (upper part) and a profile through the center (lower part)

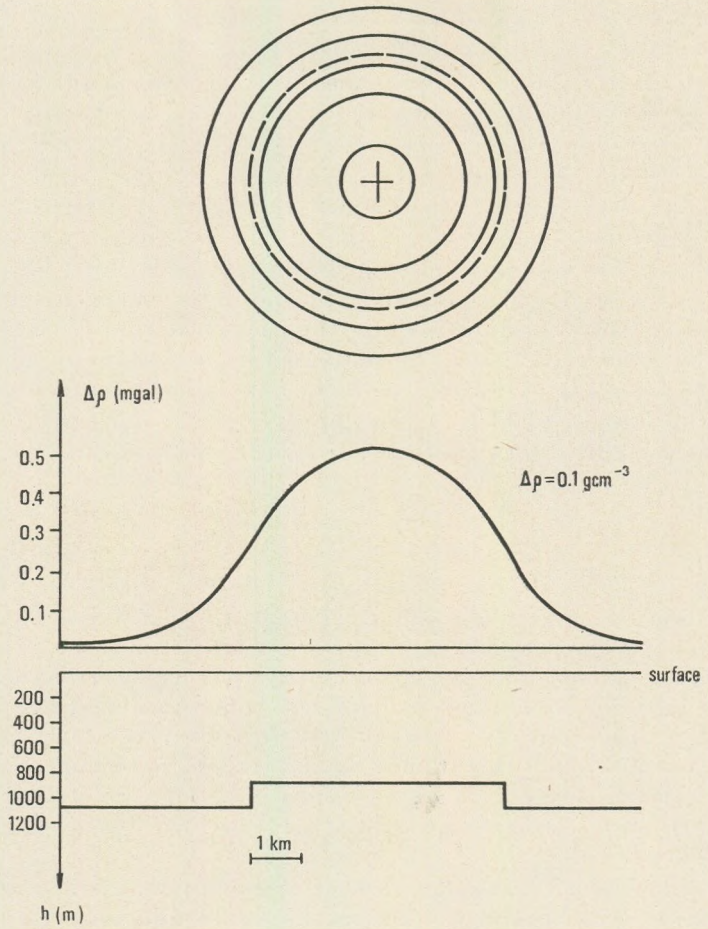

Fig. 2.9 The z-component of the gravity field due to a cylinder. Two-dimensional representation (upper part) and a profile through the center (lower part)

PART 3.

The iterative solution of the inverse problem

The inputs of the iteration are the measured gravity anomaly digitized in a square grid, the depth of the reference plane and the density contrast $\Delta\varrho$. As it has been mentioned in the previous sections it is assumed that the regional and random noise have been removed (or attenuated as much as possible) and therefore the anomaly is supposed to be due to the undulations of the density contrast surface alone.

The lower boundary of the causative body is the reference plane the upper boundary is the undulating interface.

The causative body is approximated by vertical prisms each having a cross section of one grid square and a thickness given by the average of the four vertical distances between the interface and reference plane in the corners of the grid square.

The density of the prisms is equal to the density difference between the two layers i.e. $\Delta\varrho = \varrho_2 - \varrho_1$.

The iterative process consits of setting a starter model for the thicknesses h_{ik}, computing the gravity field due to the model by the method described in Part 2. and modify the thicknesses in a way which diminishes the differences between the measured data (i.e. the input) and the computed data. Let us denote the thicknesses in the j-th iterative step by $h_{ik}^{(j)}$ and the measured and calculated gravity data by $g_{ik}^{(m)}$ and $g_{ik}^{(c)}$, respectively. The caculated data are functions of the thicknesses

$$g_{ik}^{(c)} = f[h_{ik}^{(j)}]. \tag{3.1}$$

The explicit form of the connection is described by (2.5). We have to find the best fit between $g_{ik}^{(m)}$ and $g_{ik}^{(c)}$. The goodness of fit can be expressed by various measures e.g. by the mean square deviation or by the sum of the absolute values of the deviations or by the largest error etc. None of them yields a feasible algorithm for the computation of the unknown parameters. Theoretically (3.1) can be rewritten in the form of simultaneous equations and this would unambigously determine all the h_{ik} values, but the solution of simultaneous equations with some hundred unknows is such a tremendous task that this way obviously should be abandoned.

Some heuristic approach is needed, which allows the fast determination of the h_{ik}-s and is able to improve the values in successive approximations. The chosen measure of the goodness of fit is then used only to check whether the new approximation is better than the previous and when a certain limit is reached it may be used to terminate the process. When $g_{ik}^{(c)}$ is greater than $g_{ik}^{(m)}$ it obviously means that the thicknesses in and around the grid point P_{ik} should be diminished. Though the $g_{ik}^{(c)}$ is a sum of various contributions from all prisms the greatest contribution comes from the prism vertically beneath that grid point. Therefore we modify the thickness of that prism by

$$K(g_{ik}^{(m)} - g_{ik}^{(c)}) = \Delta h_{ik}^{(j)} \tag{3.2}$$

where K is a constant multiplier the choice of whose numerical value will be dealt with later. The starter model may also be constructed by using this consideration. If the gravity field at the grid point P_{ik} would be

solely due to the prism vertically beneath and this is concentrated to a mass point lying in the mean depth H', g_{ik} would be

$$g_{ik} = \frac{G\, h_{ik}\, s^2\, \Delta\varrho}{(H')^2}\,. \tag{3.3}$$

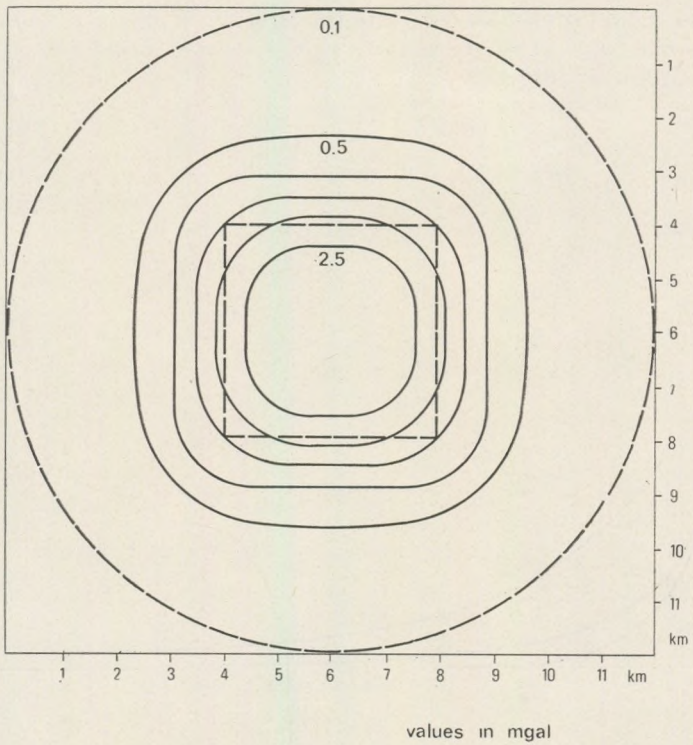

Fig. 3.1 The z-component of the gravity field due to a thin rectangular prism with base of 5×5 km^2 and height 0,1 km. Density contrast is 0.1 cgs unit. Values of the field over an area of 21×21 km^2 were used as input to the iterative process

From that equation follows

$$h_{ik}^{(o)} = \frac{g_{ik}}{f\, \Delta\varrho} \left(\frac{H'}{s}\right)^2 = \frac{g_{ik}}{0{,}667}\, (H'')^2 \tag{3.4}$$

when g_{ik} is measured in mgals and $h_{ik}^{(o)}$ in kilometers. This choice is different from that suggested in the literature e.g. by B o t t (1960) or by

Cordell and Henderson (1968). They used the Bouguer slab formula i.e.

$$h_{ik}^{(o)} = \frac{g_{ik}}{2\pi G \Delta\varrho}. \tag{3.5}$$

It can be shown, however, that the starter models (3.4) and (3.5) are very similar, both giving thicknesses proportional to the gravity data. The starter model is used to compute the first set of $g_{ik}^{(c)}$ data and equation (3.2; gives the first set of corrections to the starter model i.e. in this and in all the following steps

$$h_{ik}^{(j+1)} = h_{ik}^{(j)} + \Delta h_{ik}^{(j)}. \tag{3.6}$$

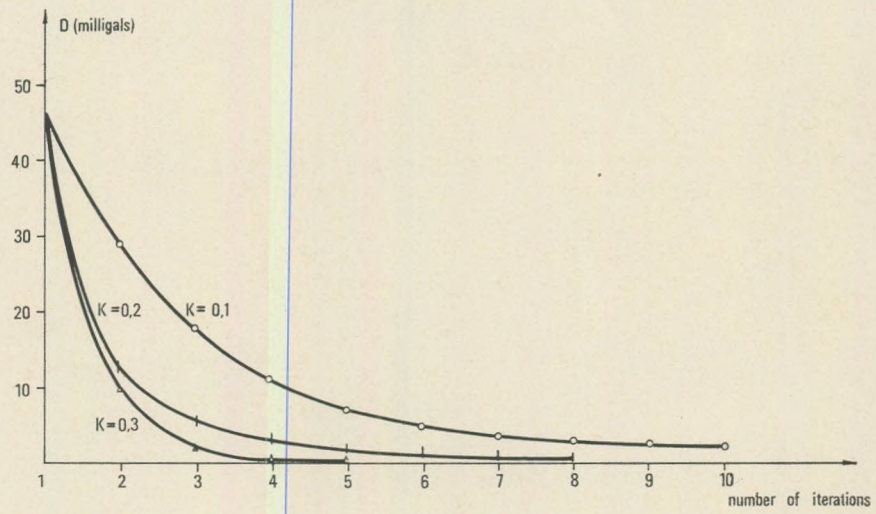

Fig. 3.2 Deviations between exact and computed values, represented by the first absolute moments (formula 3.7) plotted against the number of iterations for three values of the parameter

The gravity field due to the model with the „improved thicknesses" is computed by the approximations described in Part 2. The computed $g_{ik}^{(c)}$ values are input to equation (3.2) yielding new corrections to be applied again in equation (3.6).

The sum of the absolute values of the differences are also computed in each step. The process terminates when

$$D = \sum_{i,\,k} \left| g_{ik}^{(m)} - g_{ik}^{(c)} \right| \leq 0{,}001\, N \quad \text{(mg als)} \tag{3.7}$$

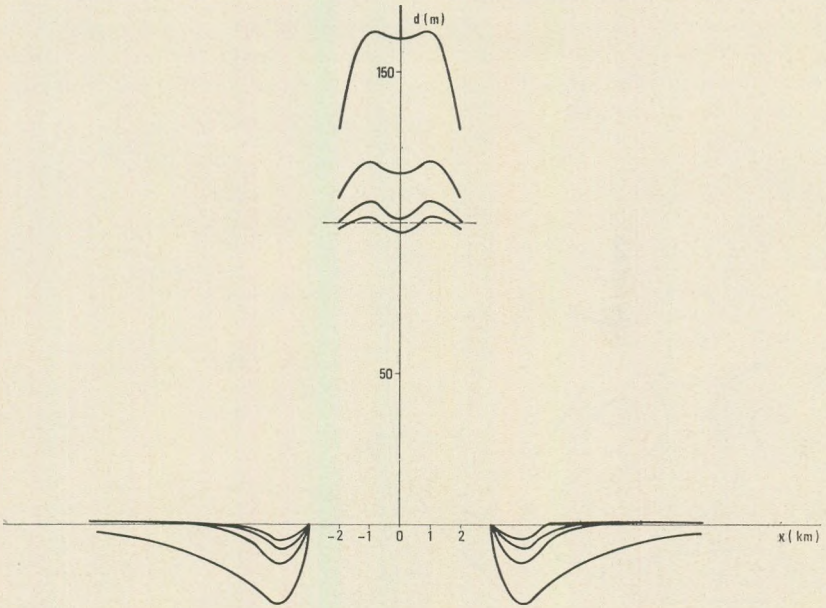

Fig. 3.3 Variation of the calculated cross sections of the structure obtained in iterative steps

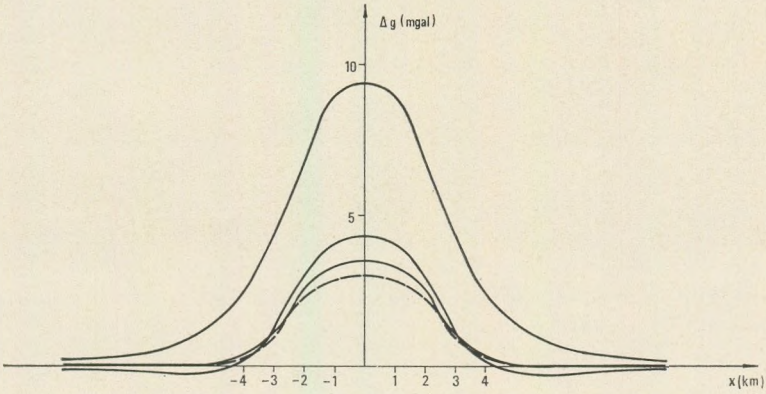

Fig. 3.4 Variation of the calculated gravity field along a profile in the iterative steps

where N is the number of grid points. Equation (3.7) involves that the measured and calculated fields are considered identical when the average difference is less than 0.001 mgal. It is not proved that the iterative process converges but in all cases investigated so far rather fast convergence have been found.

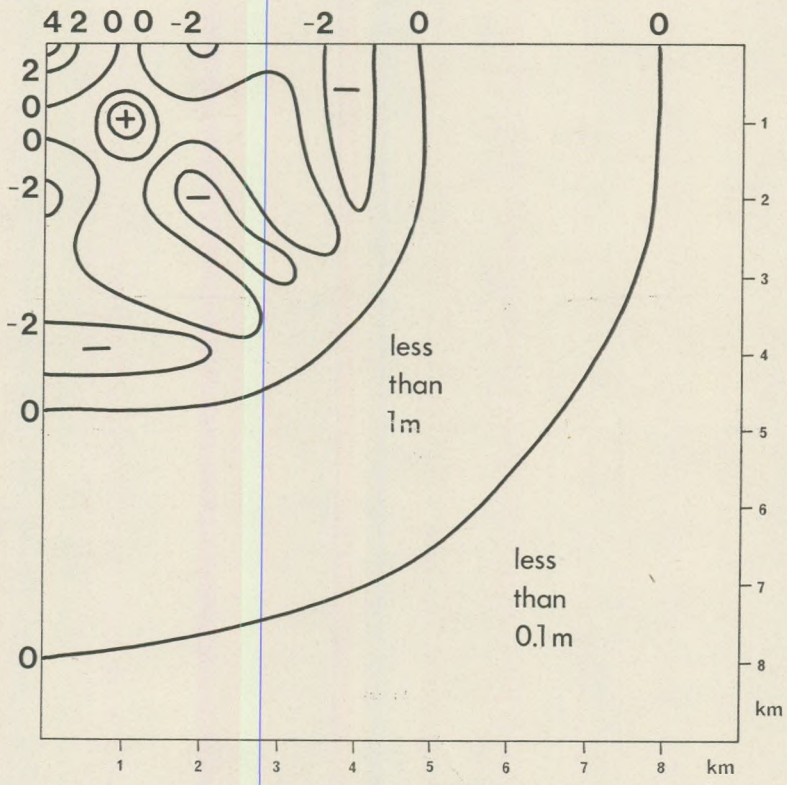

Fig. 3.5 The map of the deviations between the model structure and its last approximation

A method described by Cordell and Henderson (1968. p. 597) uses the following defining relationships between thicknesses in two consecutive iterative steps

$$h_{ik}^{(j+1)} = \frac{g_{ik}^{(m)}}{g_{ik}^{(c)}} h_{ik}^{(j)}. \tag{3.8}$$

(Instead of the denotations of the cited publication we used those defined in this paper for a better comparison.) The convergence of Cordell and Hendersons procedure is slower that the convergence obtained by (3.4) and (3.6) by a factor about 2 depending on the properties of the geological test model.

A further disadvantage of equation (3.8) is that it can not be modified when necessary while equation (3.4) contains a parameter K which may also be used to influence the speed of convergence.

Fig. 3.1. through *3.4* illustrate both the application of the present procedure and the role of the parameter K.

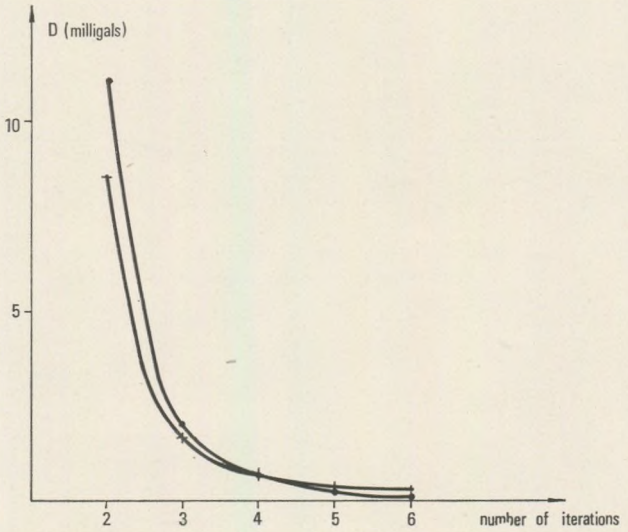

Fig. 3.6 The variation of the D (first absolute moment) if the depth of the reference plane has a 10% error (continuous line) the variation of D for the exact depth is also shown for a comparison (broken line)

The test structure is a thin rectangular prism with a square horizontal cross section. The edges of the prism are 5 km, 5 km and 0.1 km. The depth of the reference plane is 1 km, the density contrast $\Delta\varrho = 0.1$ cgs unit. The gravity field produced by the test model is shown in *Fig. 3.1* over an area of 21×21 km^2. The field was digitized and input to the iterative procedure. It would be cumbersome and superfluous as well to show all intermediate results for various K values and in each iterative steps. *Fig. 3.2* illustrates rather clearly the role of K by showing the D (defined by the left hand side of (3.7)) plotted against the number of iterations. If

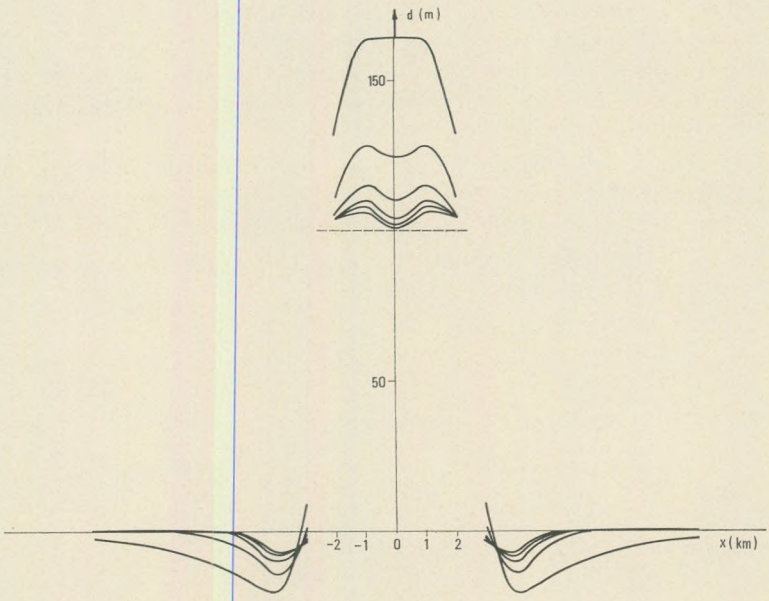

Fig. 3.7 Calculated cross sections of the structure obtained in the iterative steps if the depth of the reference plane has a 10% error

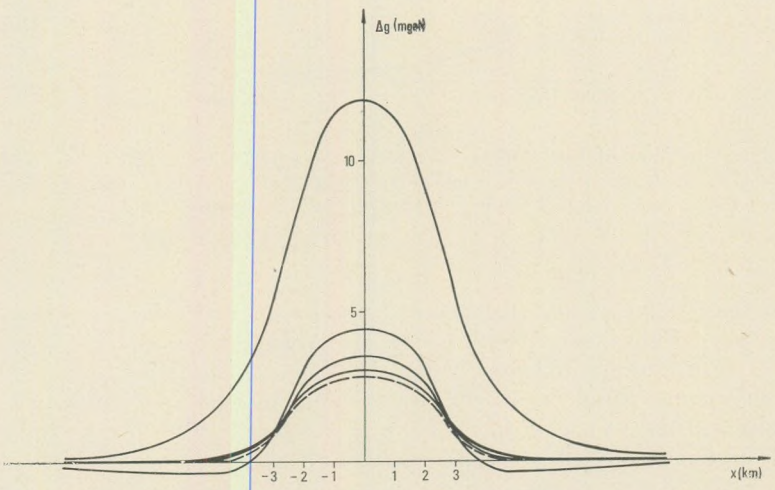

Fig. 3.8 Calculated gravity fields along a profile in the iterative steps if the depth of the reference plane has a 10% error

$K = 0.1$ convergence is slow. With $K = 0.2$ the process become faster but some improvement is desirable. $K = 0.3$ proved to be the proper choice. In order to give an idea of the variations of the computed structure and its calculated gravity field in the consecutive iterations vertical cross sections are shown in *Fig. 3.3.* and *3.4* respectively. The section goes through the center of the structure (and therefore through the center of the gravity field). It is worth to mention that while the computed

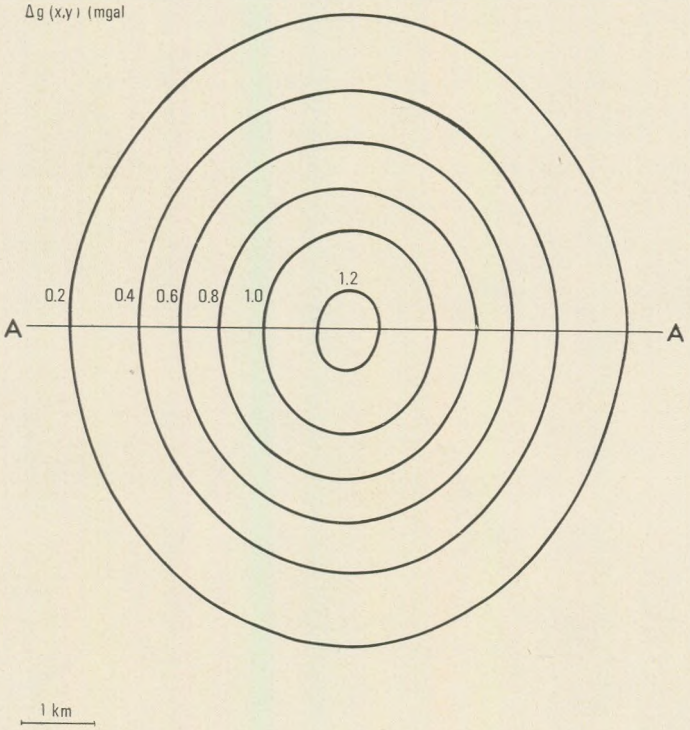

Fig. 3.9 Gravity field due to a realistic geological structure. The place of a profile is indicated by straight line A – A'

gravity field becomes appearently identical with the measured field the computed structure deviates from the model. The errors i.e. the deviations between the model and the computed structures are shown by isolines in *Fig. 3.5.* Similar map for the deviations between „measured" and computed gravity fields is not worth to construct because deviations are smaller than 0.005 milligal everywhere. The errors in the computed struc-

ture are not due to the computational method but may be considered as due to the limited "resolving power" of gravity field measurements. Undulations of order of some meters at about the depth of 1 km can not be detected at the surface.

It may be of interest that a slight change in the depth of the reference plane gives a solution whose field is also very close to the field of the model and the convergence of the iterations remains rather fast. The speed of convergence is illustrated by a plot of D values against the number of iterations shown in *Fig. 3.6*. The similar quantities obtained by the use of the exact depth are also shown for a comparison. It would be difficult to say from the speed of convergence which is the correct depth. Cross sections illustrating the change in the calculated structure and the corresponding gravity fields in the iterative steps are shown in *Fig. 3.7.* and *3.8*, respectively. As it might be expected the structure seems to be thicker than it is in reality because more anomalous mass is necessary to produce the same gravity effect if the depth becomes greater.

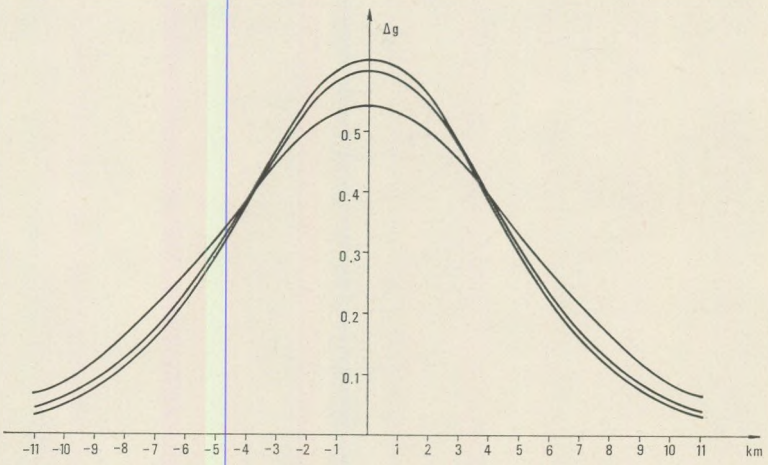

Fig. 3.10 Calculated cross sections of the structure obtained in iterative steps

The gravity field of a realistic structure is shown in *Fig. 3.9*. Results of the iterations are illustrated by data along a profile through the peak of the structure. Some of the calculated cross sections and the calculated gravity values are shown in *Fig. 3.10.* and *3.11.* The exact values are So close to the last iteration that separate lines could not be drawn. The illustrations show that the iterative process converges very rapidly and the obtained values are very close to the model structure.

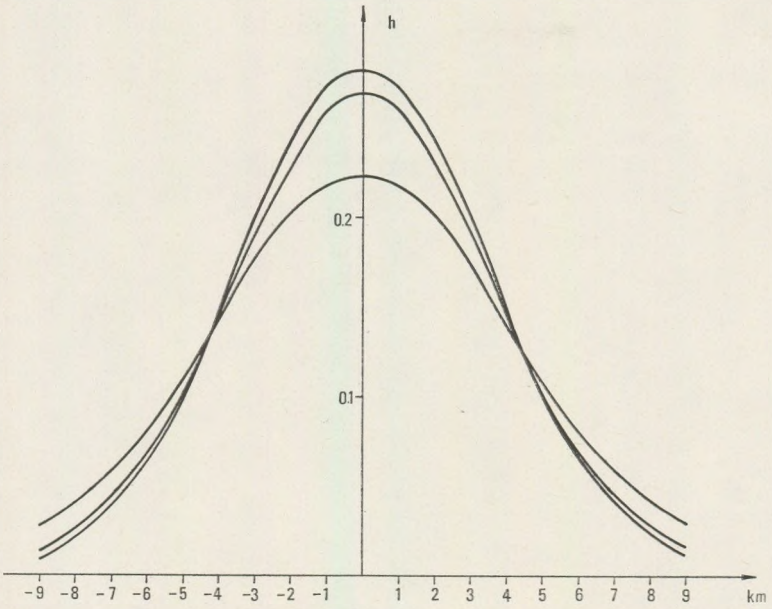

Fig. 3.11 Calculated gravity values along the profile in the iterative steps ($\triangle g$ values should be multiplid by 2)

REFERENCES

Al-Chalabi, M. (1971): Interpretation of gravity anomalies by non-linear optimization. Geophysical Prospecting, Vol. 20. p. 1 – 16.

Botezatu, R., Visarion, M., Scurtu, F. and Cucu, G. (1971): Approximation of the gravitational attraction of geological bodies. Geophys. Prosp. Vol. 19. pp. 218 – 227.

Bott, M. M. P. (1960): The use of rapid digital computing methods for direct gravity interpretation of sedimentary basin. Royal Astronomical Soc. Geophys. Jour. Vol. 4. No 1. p. 63 – 67.

Cordell, L. and R. G. Henderson, (1968): Iterative three-dimensional solution of gravity anomaly data using a digital computer. Geophysics. Vol. 33. No 4. p. 596 – 601.

Goodacre, A. K. (1973): Some comments on the calculation of a homogeneous rectangular prism. Geophys. Prosp. Vol. 21. pp. 66 – 69.

Kellogg, O. D. (1929): Foundations of potential theory Julius Springer, Berlin.

Nagy, D. (1966): The gravitational attraction of a right rectangular prism. Geophysics, Vol. 31. p. 362 – 371.

Talwani, M. and M. Ewing (1960): Rapid computation of gravitational attraction of threedimensional bodies of arbitrary shape. Geophysics, Vol. 25. No 1. p. 203 – 225.

ГЛУБИННЫЕ ИЗМЕНЕНИЯ ТЕМПЕРАТУРЫ В ВЕНГЕРСКОМ БАССЕЙНЕ

Л. ШТЕГЕНА

Университет им. Этвеша Лоранда

РЕЗЮМЕ

Паннонский бассейн является молодым межгорным басейном (интермонтейн – интерарк, ретроарк), покрытым миоценскими и, главным образом, плиоценскими осадочными породами общей толщиной в 3 км. и тонкой сиальной корой. Геотермические температуры чрезвычайно высоки. Средняя геотермическая температура на глубине 1 км. составляет 65 °С, а средний геотермический градиент – 0,055 °С/м. Для бассейнов – интерарк высокий геотермический уровень вообще характерен.

Градиент геотермического глубинного градиента – $\partial^2 T/\partial^2 z = 4 \cdot 10^{-60}$ С/м^2 в среднем. Исходя из этого, среднее производство температуры осадочных пород является $6.7.10^{-3}$ m W m^{-3} (16HGU), со средним значением (6HGU), вычисленным в соответствии с количественной последовательностью на основе радиометрических анализов.

Геотермические температуры отражают локально, по линии разлома то движение воды, направленное к поверхности Земли, которое компакция осадочных пород выжимает из пород. Детальными измерениями температурных потоков можно было определить количество воды, поднятое этими системами сбросов.

Больше 90% мировых участков нефти имеют геотермическую температуру ниже 11 °С, а температура самых горячих нефтяных участков является около 170 °С. Эти факты и кроме этого, так называемый порфириновый термометр способствуют тому, чтобы на основе геотермических температур готовились прогностические карты о нахождениях глубинной нефти.

Нефтяные участки Паннонского бассейна находятся в том геотермическом глубинном интервале, в котором происходит диогенез монтмориллонит – иллита в глинистых породах. Это показывает, что первичная миграция генезиса нефти, при которой дисперсная нефть из глинистой материнской породы переходит в соседние пористые транспортирующие слои, вызывается диагенезом глины.

Панонский бассейн является менее сейсмической областью с поверхностными сотрясениями малой звездной величны. Сейсмическая энергия проявляется, главным образом, там, где горизонтальный геотермический градиент является большим. Это свидетельствует о том, что горизонтальные температурные различия оказывают влияние на сотрясения таким образом, что эти температурные различия показывают механические напряжения.

За прошедшие десятилетия, главным образом при поисках нефти и термальной воды, на территории Венгрии было сделано несколько тысяч глубоких бурений для измерения геотермической температуры. В результате этих измерений стало возможным составление прило-

женных геотермических карт Венгрии для различных глубин (рис. 1, 2, 3, 4, 5, 6).

Сбор данных и их критический анализ были самыми трудными и утомительными моментами этой работы. Геотермические измерения часто имеют свои неизвестные, иногда очень грубые ошибки. При проверке достоверности данных мы разделили страну на 75 частей (это листы карты с масштабом 1 : 100000) и для каждой части изготовили диаграмму глубинной температуры. В результате исследований предшедствующей глубокому бурению термической жизни, метода измере-

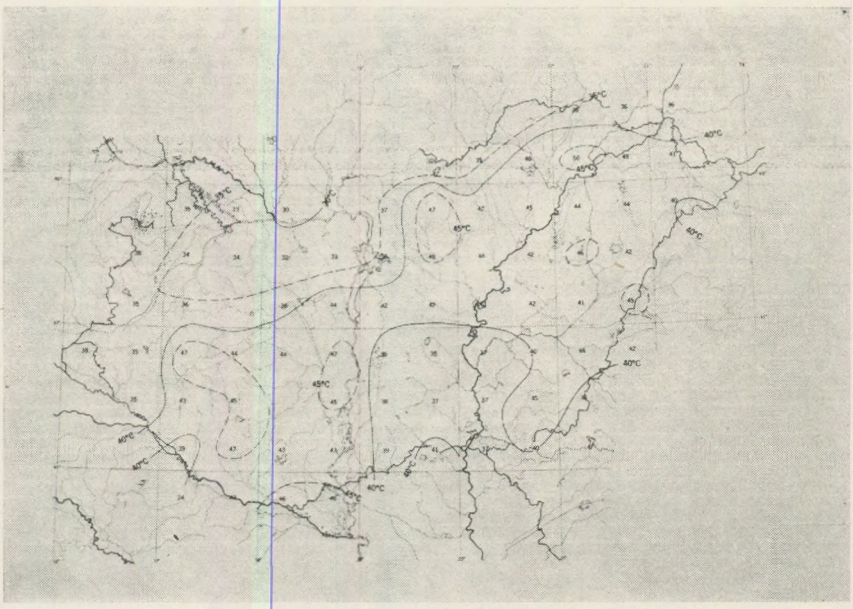

Fig. 1. Mean geothermic temperatures and geoisotherms on the area of Hungary at a depth of 0.5 km

ния, геологических условий, а также в результате согласования данных, относящихся к данной территории, и сопоставления кривых, изображающих глубинную температуру соседних территорий, удалось устранить ошибочные данные. Глубинный пересчет измерительных данных происходил способом, названным методом мастерских кривых. Для всей страны, для ее больших территориальных единиц, а также для тех листов карты 1 : 100000, на которых было очень много данных, таким образом, можно было составить достоверную функцию глубинных температур. В процессе работы заметили, что эти функции

глубинных температур похожи друг на друга, каждая из них может быть получена из другой с хорошим приближением в результате умножения на постоянное число:

$$T'(z) = n\,T(z)$$

n — близкое к единице число (0.6 – 1.5), а измерение температуры производится начиная со средней годовой температуры поверхности

Fig. 2. Mean geothermic temperatures and geoisotherms on the area of Hungary at a depth of 1.0 km

(10 °C; рис. 7). Благодаря этому методу, отдельные геотермические данные можно было пересчитать сравнительно без гипотез на выбранную для изображения геоизотерм глубину – 0.5, 1, 1.5, 2, 2.5, 3 км. Так мы получили среднюю температуру для каждой из 75 территориальных частей на интересующие нас глубины. Изготовление геоизотерм происходит на основе этих температур.

Приложенные карты являются генерализованными видами изготовленных нами более детальных карт. Карты изготовлены с ошибкой °C порядка.

Из карт могут быть сделаны следующие выводы:

Венгерский бассейн является одной из геотермически самых теплых территории Европы (Штегена 1972), как это видно и из находящейся в нашем томе геотермической карты восточной Европы. Действительная средняя геотермическая температура Венгрии на глубине 1 клм. – 65 °C.

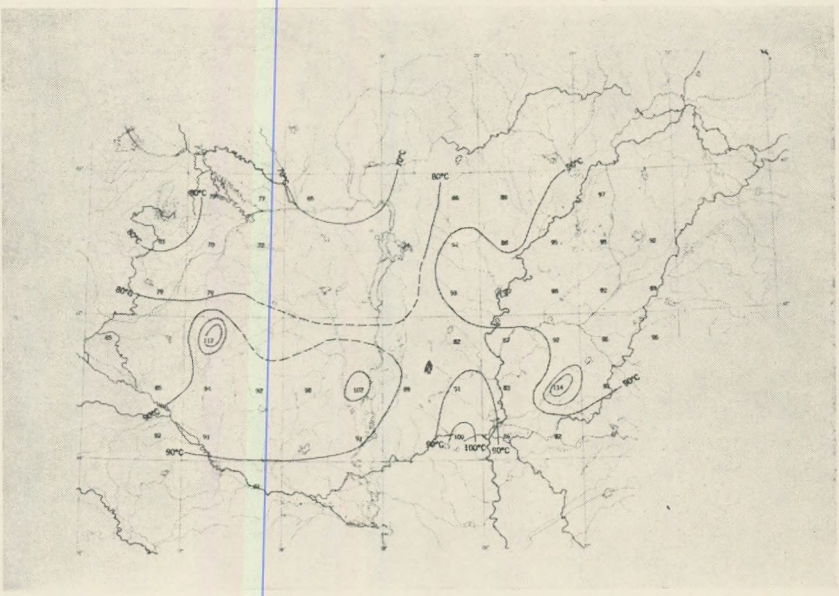

Fig. 3. Mean geothermic temperatures and geoisotherms on the area of Hungary at a depth of 1.5 km

Средние геотермические градиенты показаны в таблице 1:

Таблица 1.

Средние величины геотермических градиентов в Венгрии

Глубинный интервал (м)	°C/м	м/°C	глубинний интервал (м)	°C/м	м/°C
0 – 500	0,056	17,9	0 – 500	0,056	179
500 – 1000	0,054	18,5	0 – 1000	0,055	182
1000 – 1500	0,050	20,0	0 – 1500	0,053	189
1500 – 2000	0,044	22,7	0 – 2000	0,051	196
2000 – 2500	0,038	26,3	0 – 2500	0,048	208
2500 – 3000	0,032	31,3	0 – 3000	0,046	218

Средняя величина геотермического градиента на глубину до 1 км. в осадочных породах – 0.055 °С/м [18м/ °С]. Территориальное измерение геотермических температур отражает в общих чертах распространение мезозойской и палеозойской подстилок мио – плиоценского бассейна; там, где массивная подстилка находится ближе к поверхности, температура является более высокой. Эта корреляция, однако, не очень тесная.

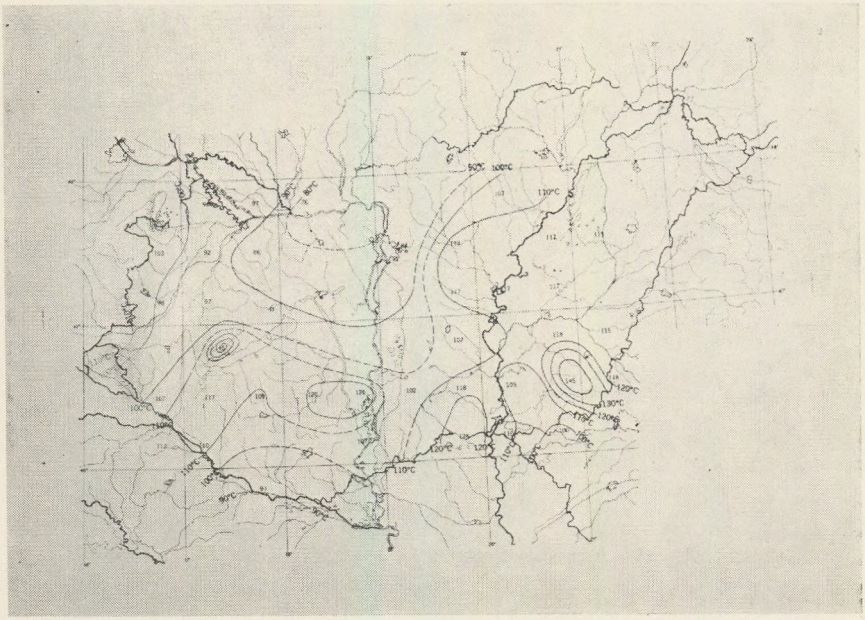

Fig. 4. Mean geothermic temperatures and geoisotherms on the area of Hungary at a depth of 2.0 km

Миграция воды и геотермика осадочных пород Венгерского бассейна

Рисунки 8 и 9 являются образцами двух измерительных территорий, где мигрирующие вверх по линии сбросов термальные воды оказали значительное влияние на геотермические условия.

Общеизвестна функция средней глубинной плотности осадочных пород Венгерского бассейна (Штегена 1970). По ней можно вычислить глубинную функцию средней пористости (рис. 10), предполагая, что плотность недавно отложившихся панонских морских осадочных пород была постоянной. С глубиной пористость пород уменьшается по указанной на рис. 10 мере. На основе этого понижения пористости можно вычислить, что из мио-плиоценских осадочных пород

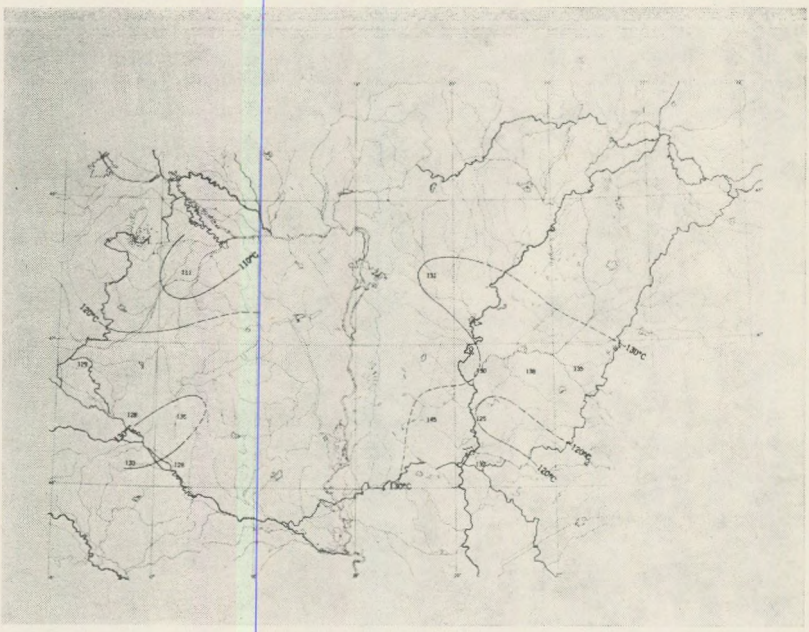

Fig. 5. Mean geothermic temperatures and geoisotherms on the area of Hungary at a depth of 2.5 km

бассейна, обладающих в среднем толщиной в 3 клм., за около 5 миллионов лет в результате компакции пород (и их консолидации) удалилось к поверхности около 15,000 км³ воды.

Это вычисление утверждается и определениями тяжелой воды (рис. 10). Содержание тяжелой воды в водах отдельных слоев глубиной растет в следствие того, что D_2O менее мобильна, чем H_2O. Вязкость D_2O в 1.25 раза больше вязкости H_2O. На основе этого и посредством измерений концентраций D_2O тоже можно определить количество удалившейся из-за концентрации воды. Это определение удовлетворительно совпадает с вычисленным на основе уменьшения пористости количеством воды.

На указанной на рис. 10 территории геотермальной аномалии термальная вода мигрирует вверх на месте пересечения двух линий сбросов. На этой территории проводились измерения релятивных тепловых потоков. Исходя из этих измерений и имея ввиду величину территории аномалии, миграцию воды вверх можно считать удовлетворительной. Ее количество — 0.8. 10^{-3} км в год (Штегена 1972). Сравнивая это количество с количеством всей компакционной воды (15,000 м³) можно установить, что нужно иметь несколько источников термальной воды, подобных системе разлома при Тиссакечке, чтобы за время существования бассейна, что значит несколько миллионов

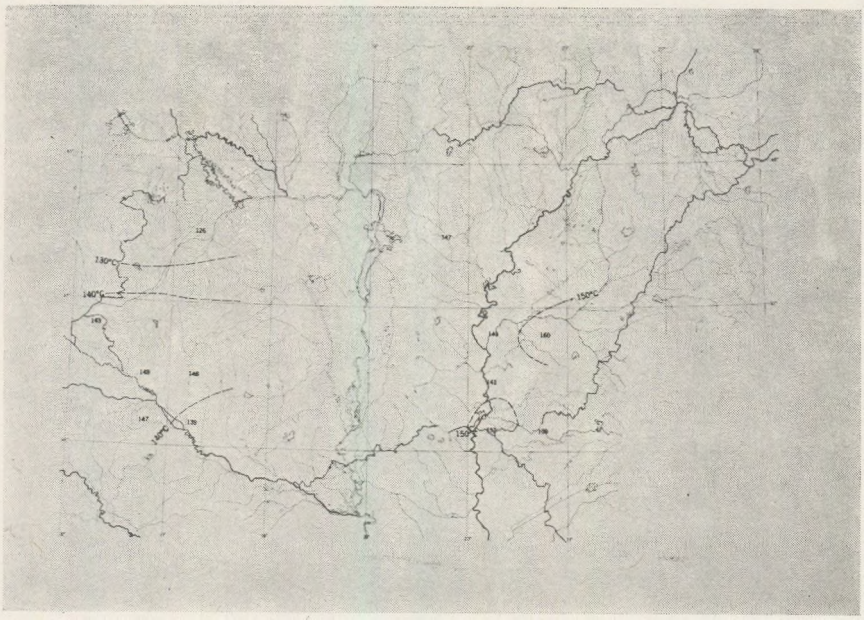

Fig. 6. Mean geothermic temperatures and geoisotherms on the area of Hungary at a depth of 3.0 km

лет, компакционная вода бассейна могла подняться на поверхность. У нас и сейчас имеется несколько таких открытых источников, поднимающих вверх горячую воду слоев (Хевиз, Вегардо; рис. 11).

Генезис нефти и геотермика. Больше 90% мировых участков нефти имеют геотермическую температуру ниже 110 °С. Температура самых горячих нефтяных участков как Васко филд, Калифорния; Паркер, 1954; Пато-2, Венесуэла, Хедберг, 1964; Ставрополь, 1963 является 150—180 °С. Нефть всегда содержит порфириновые комплексы, которые по лабораторным исследованиям распадаются при температуре 250—300 °С (порфириновый термометр).

Эти температуры дают возможность изготовить геотермическим путем прогностические карты о нахождениях глубинной нефти. Глубинное распространение геотермической поверхности с температурой 110 °С означает предел очень благонадежной с точки зрения добычи нефти глубины, а геотерма 170 °С означает предел той глубины, на которой еще считается возможным существование нефти.

Сказанное выше находится в соответствии с тем значительным достижением современной нефтяной генетики, что генезис нефти связан с известными изменениями органических веществ горных пород (метаморфоз, диагенезис, степень обугливания). Диагенез органических веществ является функцией термодинамических условий (р,

Т.). Так как глубинное распространение давления довольно постоянно, геотермические температуры обозначают тот глубинный интервал, где происходит генезис нефти; Этот глубинный интервал Вассоевич (1973) называет основной фазой образования нефти, а Хунт (1973) называет ее Ликвид окно (Liquid window/ – рис. 13). Здесь образуется жидкий углеводород; над этой зоной и под ней образуются углеводородные газы – над ней главным образом метан, а под ней результатом крекирующих процессов можно найти более высокие гомологи.

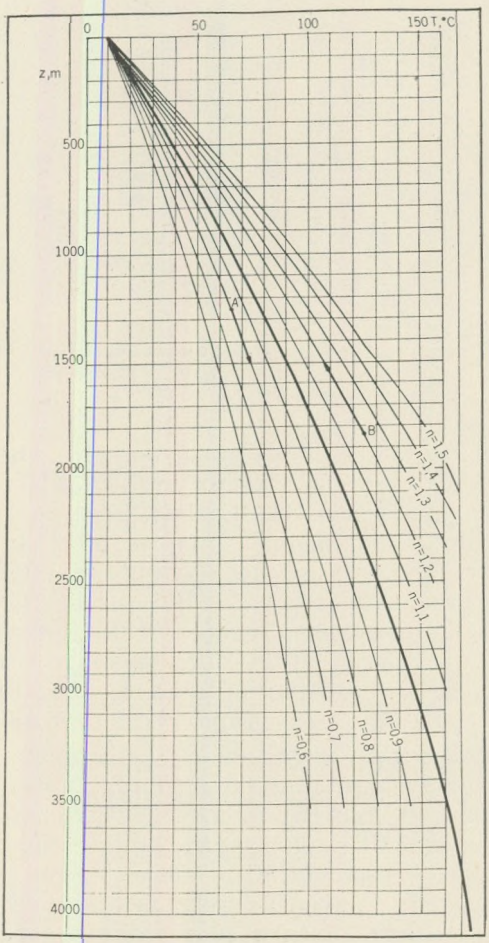

Fig. 7. Mean depth-function (T/z) of geothermic temperatures and master-curves used for the reduction to depth of the observed temperatures ($n = 0.6 - 1.5$)

Нижнюю границу ликвид окно определяет геотермическая температура 75 °С, а верхнюю – 150 °С (Хунт 1973). Рис. 12 показывает глубинное распространение этих изотермальных поверхностей.

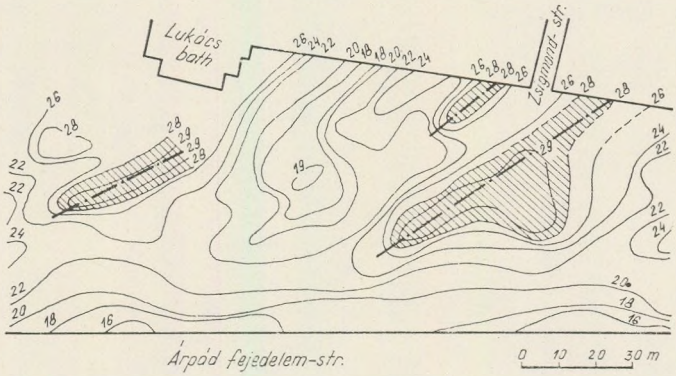

Fig. 8. Geothermic soil-temperatures at a depth of 2 m in the surroundings of Lukácsbath in Budapest. Thermal waters flowing upwards along fault lines are producing geothermic anomalies of 10 – 20 °C

Самые важные физические процессы генезиса нефти следущие: органические вещество песчаных слоев обычно уничтожается, оксидирует, прежде чем попасть в глубину. Органические вещества глинистых пород попадают в глубину и тут при соответственных p, T проходя через диагенез порождают слегка распространенную в глинистых слоях нефть. Эта дисперсная нефть при первичной миграции из глинистой материнской породы попадает в соседние транспортирующие пористые слои (если есть такие) и в них в процессе вторичной миграции переносится на места скопления. Последовашие затем тектонические движения могут снова перемешать материалы нефтяного участка (третья миграция).

Одним из очень спорных вопросов генеза нефти является вопрос о прохождении первой миграции. Рассуждения и опыты Хилл и Леворсена указывают на то, что распространившаяся дисперсным образом нефть только при очень больших водных градиентах может мигрировать из глинистых пород. Опыты Капоюшникова, Двали Жузе, Соколовой–Миронова (1962) показывают, что при высоком давлении газы могут хорошо растворить из глинистых пород жидкие углеводороды; однако первичная миграция, происходящая за счет растворения газами, встречается в общем с известными трудностями (Юркевич 1962). В настоящее время причиной первичной миграции считается диагенез глины. Находящийся в осадочных породах в больших количествах монтмориллонит под действием определенного давления и температуры превращается в иллит. Это

превращение сопровождается удалением воды и ростом объема, так как плотность связанной воды монтмориллонита является около 13 см³ (Немец 1970). В результате этого роста объема получается тот гидравлический градиент, который переводит дисперсную нефть из глинистой материнской породы в ограничивающие ее пористые транспортирующие слои.

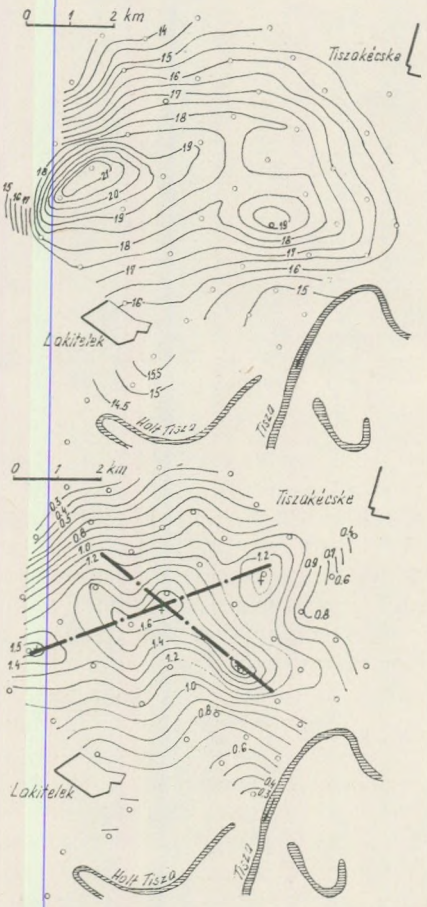

Fig. 9. Above: Geothermic gradients (m/°C) near the river Tisza. Below: Gradients freed from the alternation of clay- and sand- layers (according to Alföldi and Gálfi, 1966). The lower graph indicates the crossing of faults, along which the thermal waters causing the geothermic anomaly are flowing upwards

На рис. 14 изображается расположение участков углеводорода в Венгрии и еще глубинные зоны диагенеза монтмориллонита-иллита в глинистых породах. Последний определяется геодавлением и гео-

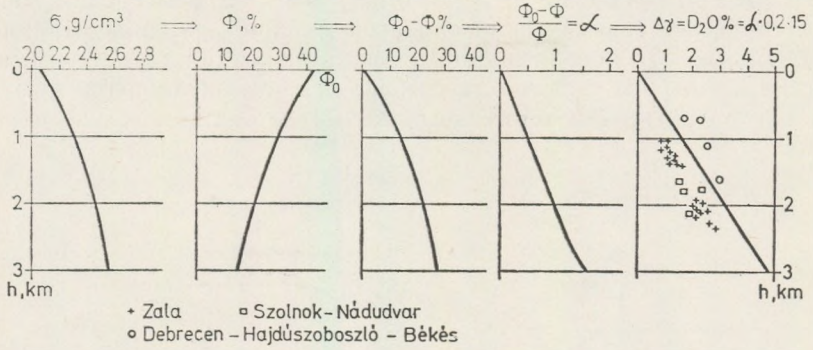

Fig. 10. Average depth-density function of the sediments of the Pannonian basin, the depth-porosity funcion calculated on the basis of the former, and the function $\Phi_0 - \Phi$ being the measure of the water moved away; n indicates the ratio of the water moving away againts the remaining amount. From n and from the viscosity ratio of D_2O/H_2O the enrichment in D_2O of the remaining water at various depth can be computed. Sings denote measured values

температурой (Берст 1969: Джонс 1970); в случае одинаковой плотности пород геотермической температурой считается — 80—100 °С. Из 40 исследованных углеводородных участков около 33 находится в геотермической глубинной зоне диагенеза монтмориллонита-иллита с отклонениями до —200 м. Для каждого из 7 оставшихся вне этой зоны участков углеводорода можно показать, что они сдвинулись с своего начального глубинного положения в результате третей миграции. Рис. 14 утверждает теорию первичной миграции нефти, основывающуюся на происходящий в глинистых породах диагенез.

Fig. 11. Thermal water wells and springs issuing from the fractured basements in Hungary. After Korim, 1972.

Землетрясения и геотермика. Венгерский бассейн является менее сейсмической областью с малой звездной величной и неглубокими сотрясениями коры. Можно предполагать, что эти сотрясения, хотя бы частично, вызываются горизонтальными различиями в температуре, которые возбуждают механические напряжения в коре.

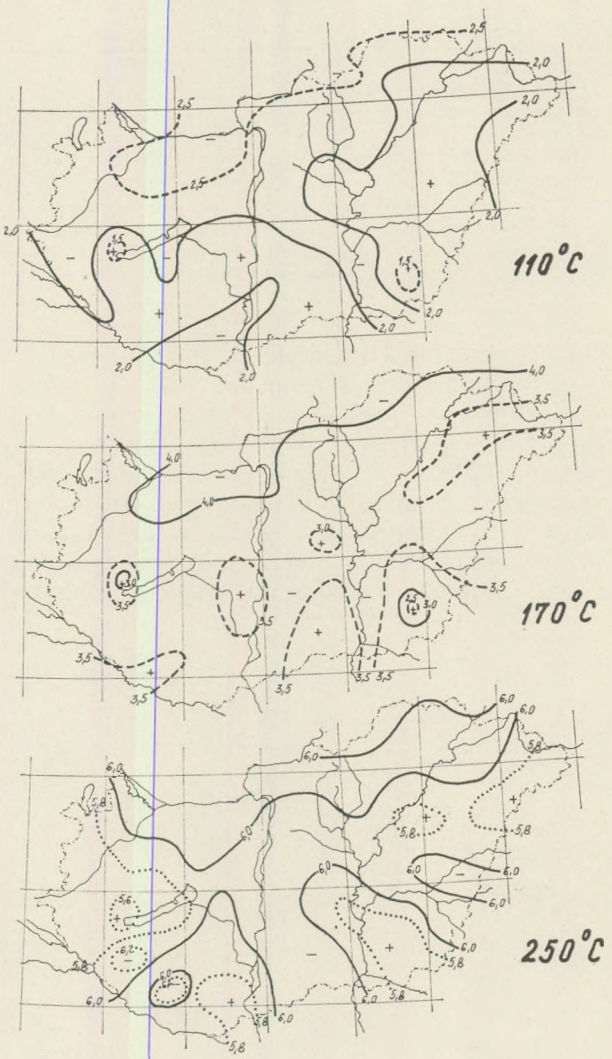

Fig. 12. Depth conturs of isotermic surfaces of 110, 170 and 250 C° temperature in Hungary (in km)

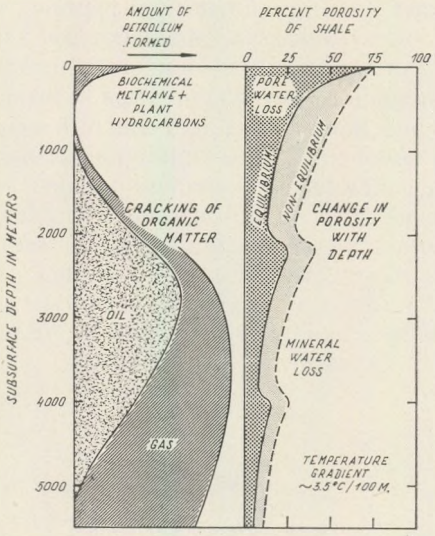

Fig. 13. Petroleum generation and depth zones of compaction according to Hunt (1973)

Рис. 15 является картой горизонтального геотермического градиента, действующего на глубину до 1 км. Он изготовлен на основе геотермической карты рис. 2. Абсолютное значение относящихся к отдельным точкам горизонтальных геотермических градиентов дается находящимися на Север, Юг, Восток и Запад от точки средними величинами температурных различий ближайших точек. Изолинии на рис. 15 изготовлены на основе этих значений (Мартон 1974).

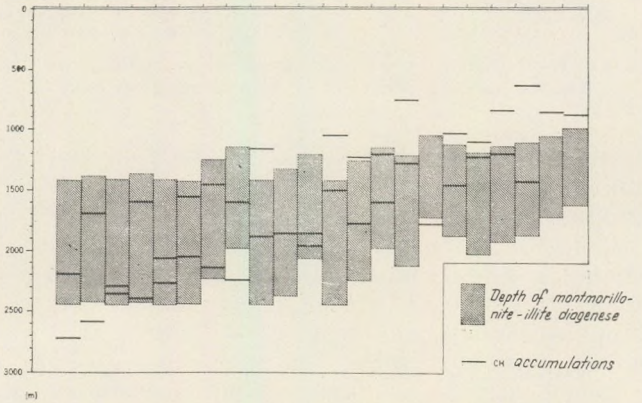

Fig. 14. Arrangement of oil-deposits and of the depth intervals of geotemperatures of 80 – 100 °C which correspond to the montmorillonite-illite clay mineral diagenesis at the Hungarian hydrocarbon beds

Рис. 15 изображает еще на основе проведенных Д. Чоморо м 1974) исследований и сейсмическую энергию, проявившуюся за 100 лет и вычисленную для территории каждого листа карты 1 : 100000 (350 км²). Методом, подобным встречающимся в литературе, Чомор (1974) на основе макросейсмических наблюдений вычислил звездную величину прежних, замеченных без приборов землетрясений. Изображенные на рисунке сейсмические энергии основываются на этом.

Рисунок показывает, что на территории Венгрии землетрясения, в действительности, происходят прежде всего на местах, обладающих большим горизонтальным геотермическим градиентом. Если принять во внимание непоказанные на рис. 15 численные значения сейсмической энергии, проявившейся на территории отдельных листов карты, получается следующая картина:

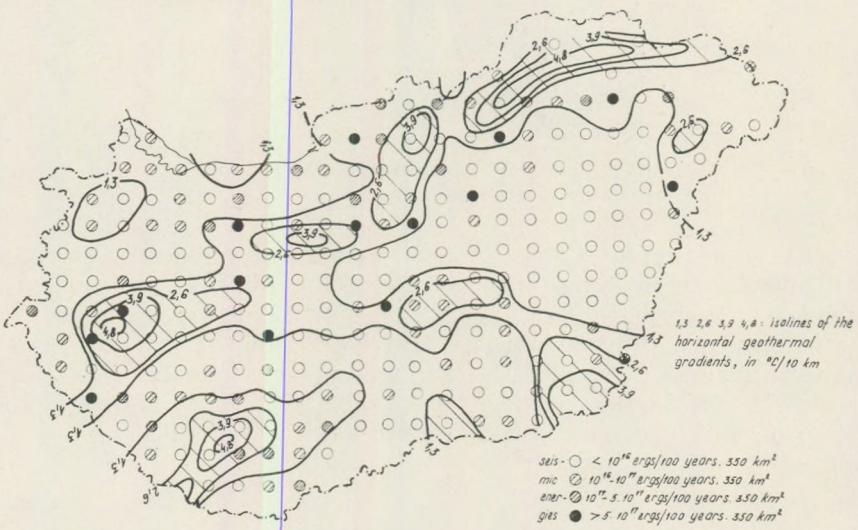

Fig. 15. Isolines of the horizontal geothermic gradient valid for 1 km depth and values of seismic energy released on the territory of Hungary during the past 100 years

Территории с большим, чем 1,3 °С/10 клм. горизонтальным градиентом составляют 45,900 клм² (49,5%); проявившаяся за 100 лет на этой территории сейсмическая энергия — 1,720 · 10^{23} эрг, частота энергии — 3,75 10^{15} эрг) км².

Территории с меньшим, чем 1.3 °С/км. горизонтальным градиентом составляют 47,000 км² (50.5%); проявившаяся за 100 лет на этой территории сейсмическая энергия — 0,098 10^{20} эрг, а частота энергии — 0,21 10^{15} эрг / км².

Более точное вычисление корреляции невозможно из-за неточности геотермических и сейсмических данных. Кроме этого, на статистический характер указанных выше двух частот энергии оказывают большое влияние некоторые более крупные сотрясения. Абстрагиру-

ясь от трех самых сильных сотрясений (Кечкемет, Егер, Дунахарасти), частота сейсмической энергии на территориях с большим горизонтальным геотермическим градиентом является 0,39 · 10^{15} эрг/км^2, а на территориях с меньшим градиентом и в дальнейшем остается 0,21 · 10^{15} эрг/км^2.

Итак, корреляция является довольно успокоительной и кажется, что землетрясения Венгерского бассейна вызваются горизонтальными неоднородносгяни в температуре коры.

REFERENCES

Alföldi, L. and Gálfi, J. (1966): Hydrogeological and geophysical investigations of a geothermal anomaly in Hungary. Bull. IASH., VI. 1.

Burst, Y. F. (1969): Diagenesis of Gulf Coast clayey sediments and its possible relation to petroleum migration. Bull. AAPG. 53. p. 73 – 77.

Csomor, D. (1974): Cand. thesis. Library of MTA, Budapest.

Hedberg, H. D. (1964): Geological Aspects of origin of petroleum. Bull. AAPG 48. 1755 – 1803.

Hunt, J. M. (1973): An Examination of Petroleum Migration Processes. Geochemie (Vorträge zu geochemischen und chemisch- physikalischen Problemen. VII. Int. Konf. des Kohlenwasserstoffbergbaus); Budapest, OGIL, p. 219 – 229.

Korim, K. (1972): Geological Aspects of Thermal Water Occurrences in Hungary. Geothermics, I., 3.

Márton, M. (1974): Dipl. thesis Library of ELTE, Budapest.

Nemetz, E. (1970): Present state of the investigation of clay minerals in the oil geochemistry (in Hungarian). Application of geochemical methods in the oil prospection. Szeged, p. 35 – 41.

Parker, F. S. (1954): Origin, migration and tapping of oil in California. Geology of Southern California: Bull. Oil and as, Div. of Mines, san Francisco, p. 11 – 19.

Sokolova, M. N. and Mironov, S. I. (1962): On the primary migration of hydrocarbons and other oil components under the action of compressed gases in Russian. Geokhim. nefti i neftjannik ' most. Izd. ANSSSR.

Stegena, L. (1957): Praktische geothermische Untersuchungen in Ungarn. Ann. Sci. Budapest. Sec. Geol. I.

Stegena, L. (1970): Compaction, heavy water content and water flow in the sediments of the Hungarian Basin (in Hungarian) MTA X. Oszt. Közl. 3.

Stegena, L. (1973): Clay minerals and migration of natural oil in the Pannonian Basin. – Studies on the material and energy flows of the Earth (Ed. E. Szádeczky-Kardoss) Budapest, p. 258 – 261).

Stegena, L. (1973): Hydrocarbon accumulation and geological watermigration in the sediments of the Hungarian Basin. Studies on the material and energy flows of the Earth (Ed. E. Szádeczky-Karodos) Budapest, p. 262 – 270.

Stegena, L. (1972): Petroleum accumulation and geological water flows in the sediments of the Hungarian Basin (in Hungarian). IIth Symposium on the Material and Energy Flows, Academic Publishers, Budapest, p. 199 – 209.

Stegena, L. (1972): Geothermal map of Eastern Europe. Geothermics, 1.4. p. 140 – 141.

Tkhostov, B. A. (1963): Initial rock pressures in oil and gas deposits. Pergamon Press.

Vassoevich, N. V. et al. (1973): Principal zone of oil formation. Geochem. Cosmochem. 6emex Congr. Int. Paris.

Yones, P. H. (1970): Geothermal resources of the Northern Gulf of Mexico Basin. UN Symp. Pisa.

Yurkevich, I. A. (1962): The study of geochemical facies. G. nefti i neftjanik most. (in Russian) Izd. ANSSR.

INVESTIGATIONS ON THE AREAL DISTRIBUTION OF SURFACE ALBEDO IN HUNGARY

by

Z. DOBOSI

Department of Meteorology, Eötvös University, Budapest
Received: 15 March, 1975

ZUSAMMENFASSUNG

Es wird die Möglichkeit der Berechnung und Benutzung einer durchschnittlichen Albedo erörtert und festgestellt, dass in Ungarn die Albedo keinen Zusammenhang – abgesehen vom Februar – mit der globalen Strahlung zeigt, so dass eine Durchschnittsbildung zugelassen werden kann. Für Februar, die Anbringung einer Korrektion soll gesichert sein.

Unter Benutzung von Messresultaten gewonnen in Ungarn und in anderen Ländern wird die territoriale Verteilung der Albedo der Oberfläche in Ungarn an mehreren Abbildungen dargestellt.

In climatology the albedo (A) is defined as quotient of the global radiation reflected by the surface (R) and of the incoming value (G) as follows:

$$A = \frac{R}{G}.$$

It is our aim to determine the areal distribution of the monthly mean value of the surface albedo. The value of the albedo is one of the important characteristics of the surface from meteorological point of view; its knowledge is needed for the calculation of that part of the irradiated energy of the sun which is actually absorbed by the surface and transformed into heat, respectively into latent heat. The absorptivity of the surface (E) and the albedo are connected with one another by the formula

$$E = 1 - A.$$

1. Computation of monthly averages of albedo

In what follows we show [D o b o s i 1961] that monthly averages of albedo are to be used in our calculations only in case there is no connection between the value of the albedo and that of the intensity of global radiation in the given month, as it will be obvious from the ensuing calculation. At Erdőhát nearly half of the days of January are days with snow cover. Assuming the value 0,18 for the albedo of the uncovered

surface and 0.64 for the mean albedo value of the snow cover we obtain for the January average of the albedo the value : 0.41. The average value of the global radiation at Erdőhát is 3.1 kcal/cm² in this month. The reflected radiation computed using the albedo average is: $0.41 \cdot 3.1 = 1{,}27$ kcal/cm²/month. If we assume the existence of such a connection between snow cover and global radiation that days with snow cover show a clear sky, while those without snow cover are overcast, and if we take into account for the clear days radiation sums as high a value as 190 cal/cm², while for the overcast days we use the value of 20 cal/cm², then we obtain for the monthly sum of the reflected radiation the value: 2,0 kcal/cm². On the other hand, if we assume a reversed connection, i.e. we suppose the days with snow cover to be overcast and those without a snow cover as clear ones, then the monthly reflected radiation will take the value : 0,7 kcal/cm².

Of course we can not suppose in reality the existence of such an extremely strong connection between state of ground and global radiation. Nevertheless it is possible that we can find such climatic regions, where there is some connection between the albedo of the surface and the intensity of the global radiation. The existence of such a connection can be supposed even in summer: it may happen that the wet state of ground – producing a small value of the albedo – is more frequent in case of overcast skies than during clear weather situations.

In case there is a connection between the albedo and the global radiation – as we saw it in our supposed example above – the albedo can not be averaged. In order to state, whether there exists a connection between the two climatic characteristics in our climatic region we computed correlation coefficients for Erdőhát between the albedo calculated from the state of the ground and the radiation sum of the day involved from data of the years 1951 – 1960.

We assumed that the following albedo values correspond to the state of ground values figuring in the calculations:

dry ground	0.18
wet ground	0.12
snow cover	0.64
snow patches	0.41,

The correlation coefficients obtained are:

I	II	III	IV	V	VI
−0.05	−0.24	0.07	0.01	−0.06	0.02
VII	VIII	IX	X	XI	XII
−0,07	0.07	0.09	0.05	−0.02	0.10

The highest random value belonging to the values of the table at the 5% level is $r' = 0{,}11$. We see that only the February value deviates significantly from zero, that of December is approaching only the said value. The February correlation value is supposedly the consequence of the fact that the average date of disappearing of the snow cover is the 24th of February. In that month the altitude of the sun is increasing rapidly, so that the decrease of the surface albedo owing to the disappearence of the snow cover becomes connected with an increase of radiation. In December the frequency of snow cover increases, thus the average albedo of the surface increases too. The absence of the expected negative correlation is probably brought about by the overcast character of the month, and the fact that the altitude of the sun decreases in the first half of December does not change even towards the end of the month significantly. The effect of the albedo change in connection with the beginning and the end of the vegetation period does not present itself in the data, because the albedo of the green vegetation does not deviate in a perceptible manner from that of the uncovered surface.

Thus, in our climate we can use the monthly albedo averages – except for February – for the calculations of monthly sums of the reflected, respectively absorbed radiation. The error made by the use of the average albedo values in February can be corrected by applying a difference-term, which is for Erdőhát given by the formula:

$$\overline{A} - \frac{A_i - G_i}{G_i} = 0{,}01 .$$

Here $\overline{A}$ denotes the average albedo for February, A_i and G_i are the albedo- respectively global radiation – values of the individual days. In what follows we applied this correction to the February albedos, though this correction is rather of a theoretical importance only owing to the accuracy of the albedo measurements.

2. The basic map of vegetation

The albedo is such a characteristic of the surface, which does not depend only on natural conditions. The interference of man modifies the surface through the ways of agricultural use and cultivation.

Our aim is to construct albedo maps reflecting not a momentary state, but the average conditions of a longer period.

We can assume that the surface of Hungary is covered with vegetation during the growth period. From this state there is a deviation only in the winter season, respectively in the case of ploughed surfaces. Since the albedo of forests – especially of those containing pines – significantly deviates from that of the other areas, first of all we need a map showing the measure of afforestation, giving for the single regions the ratio of afforestation as well as its aspects. The average albedos of agricultural

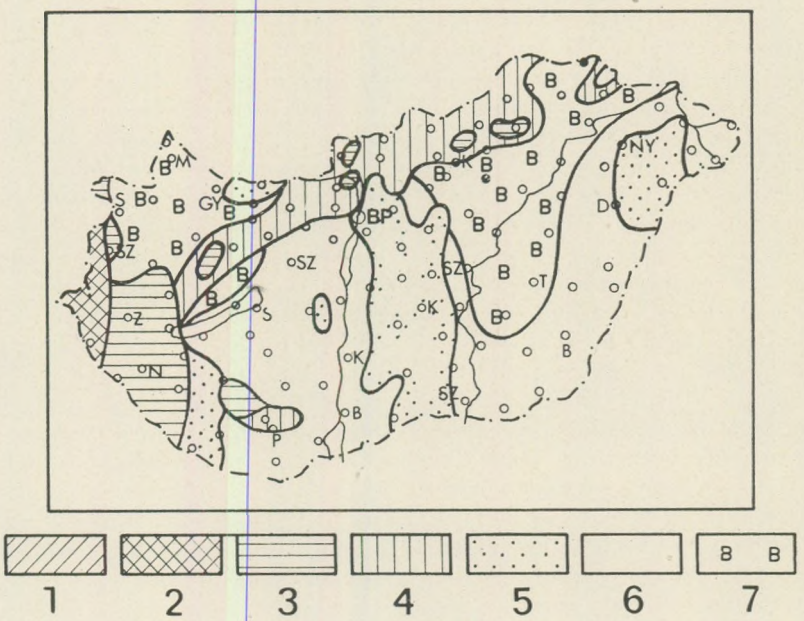

Fig. 1. Distribution of substrata taken into account in albedo determinations. 1. pines, 2. mixed pines, 3. beeches, 4. oaks, 5. agricultural sandy areas, 6. agricultural areas, 7. $3^2/_3$ cornfields
(according to Borhidi)

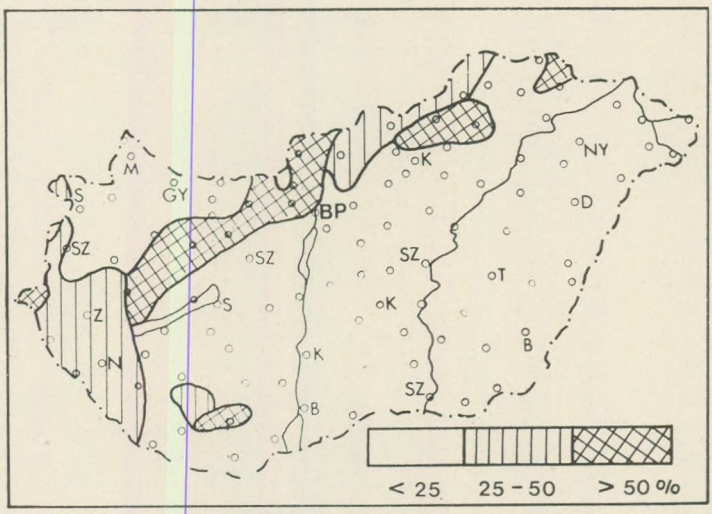

Fig. 2. Amount of afforestation

plant-stocks do not show significant deviations one from another [Weingartner 1968], though there appear differences in the various growth-phases. Thus it is practical tc denote such areas, where the ratio of wheat is greater than the average. It is also necessary to mark the sandy soil owing to the somewhat higher albedo-value of the sand. All these aspects are taken into account in a most satisfactory manner by the vegetation- and afforestation- maps of Borhidi [1967] prepared exclusively for the construction of albedo charts. (Fig. 1. and 2.). We accepted these as a base for our present albedo maps.

The representation of grass-lands on the map in case of the given scale was not possible owing to their small dimension. By the way, the albedo of grass-lands is nearly the same as that of corns and of the most important fodder plants according to the investigations of *Weingartner* [1968]. We had also to disregard displaying saline soil owing to the scale used.

Our aim was that the vegatation map serving for base for albedo distribution display should separate the most important areas, for which albedo values can be determined with a practically constant validity in time.

3. Observation material used for the albedo determinations

Data of the reference literature regarding measurements abroad are rather deviating one from another even in case of an identical plant-stock too. Thus they represent only approximations for us and may be used in cases only where data of our own land are not at our disposal. Here, a progress was achieved by the observations of Weingartner made at Szarvas, who has measured for several years the albedo values of agricultural plants cultivated in our land. He computed not only average albedo values, but he gave data also for the various phases of development of the individual plants.

The albedo-maps [Weingartner 1970] of Weingartner has been prepared on the basis of his own measurements. Since he prepared his maps according to the same principles we applied [Borhidi and Dobosi 1967], using the same vegetation – and afforestation – map for the months during which the surface is overwhelmingly covered by living vegetation (April to October), we accepted his maps, based on albedo observations made in Hungary, instead of our earlier maps based mostly on foreign data. In the interval November to March, when the frequency of snow cover [Péczely 1966], the dry or wet state of the uncovered ground etc., i.e. the general state of ground play an important role, we used for the preparation of our maps [Borhidi and Dobosi 1967] – besides the earlier data – also the paper of Mrs Adámi containing a study of ground state frequencies [Adámi 1970] giving a rather detailed information for the whole area of Hungary.

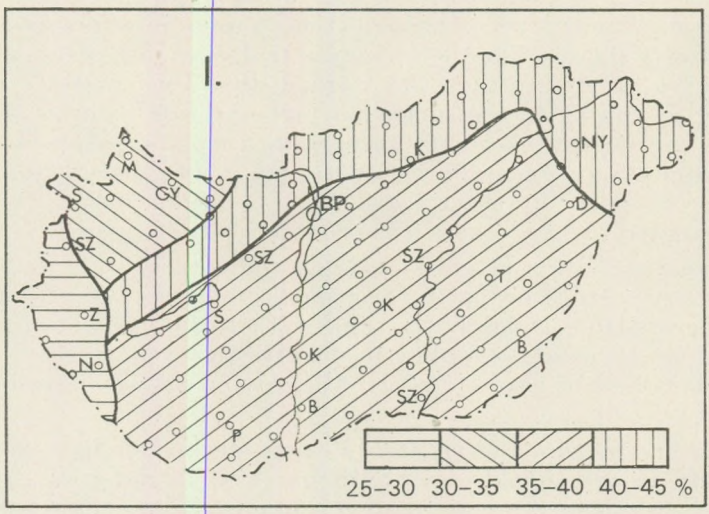

Fig. 3. Areal distribution of the albedo in January

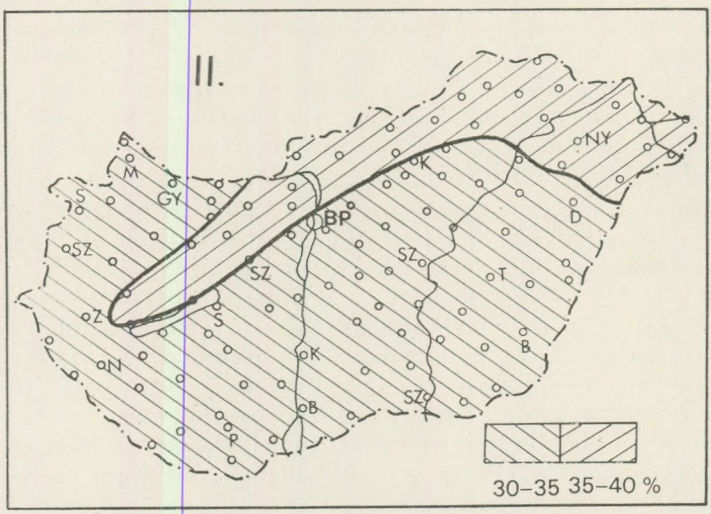

Fig. 4. Areal distribution of the albedo in February

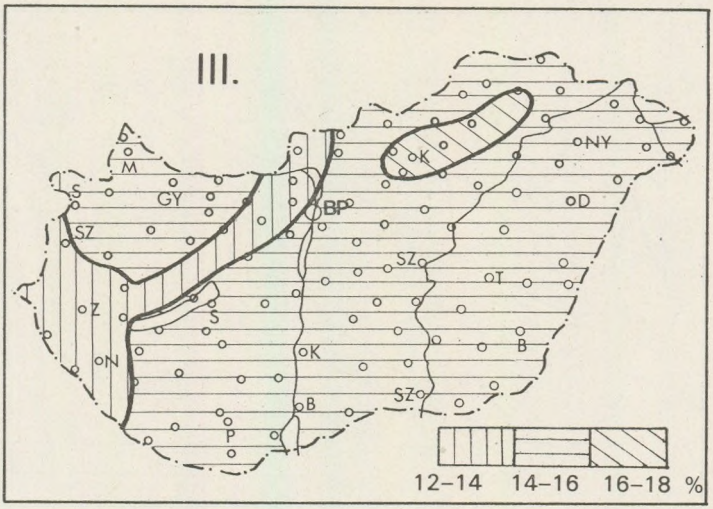

Fig. 5. Areal distribution of the albedo in March

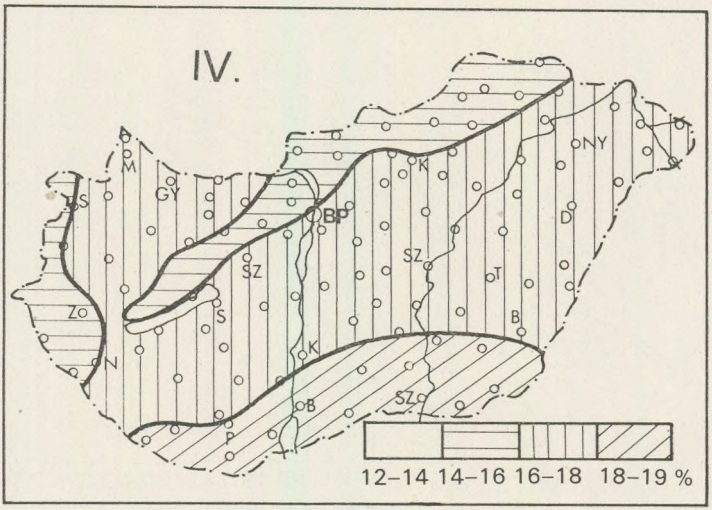

Fig. 6. Areal distribution of the albedo in April (after Weingartner)

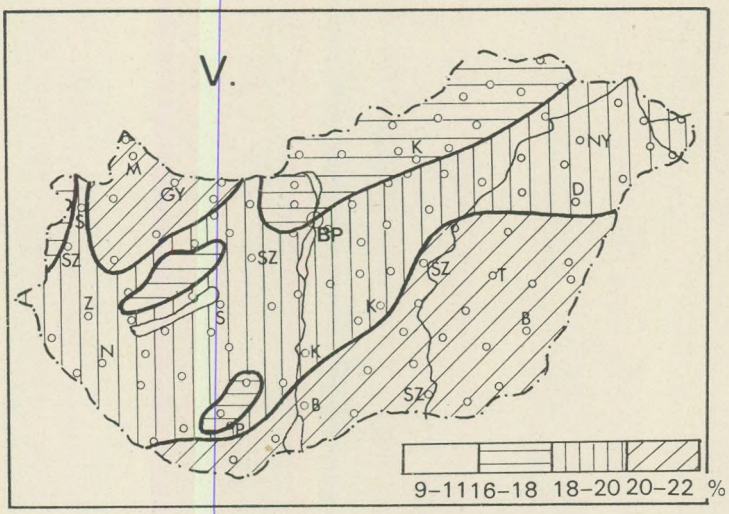

Fig. 7. Areal distribution of the albedo in Mai (after Weingartner)

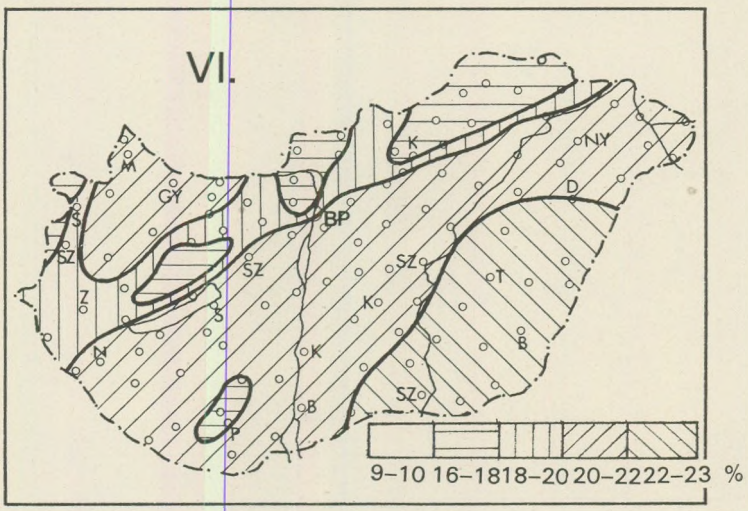

Fig. 8. Areal distribution of the albedo in June (after Weingartner)

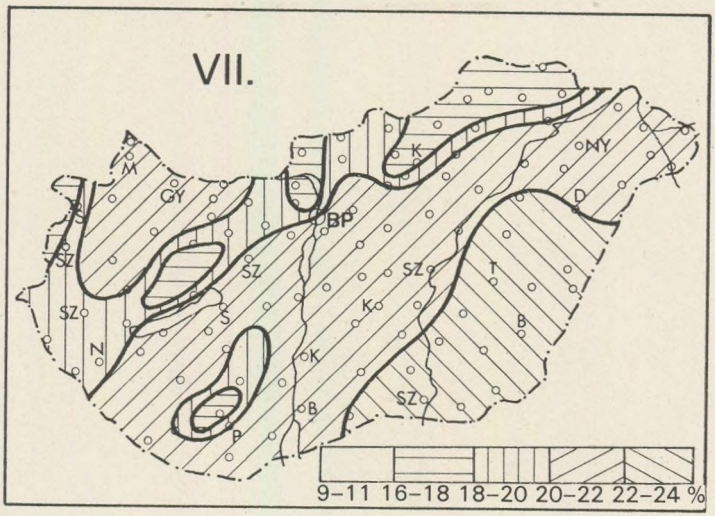

Fig. 9. Areal distribution of the albedo in July (after Weingartner)

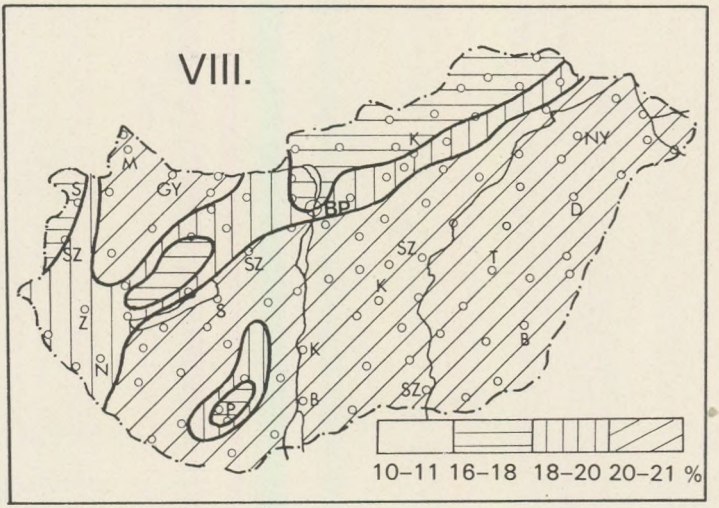

Fig. 10. Areal distribution of the albedo in August (after Weingartner)

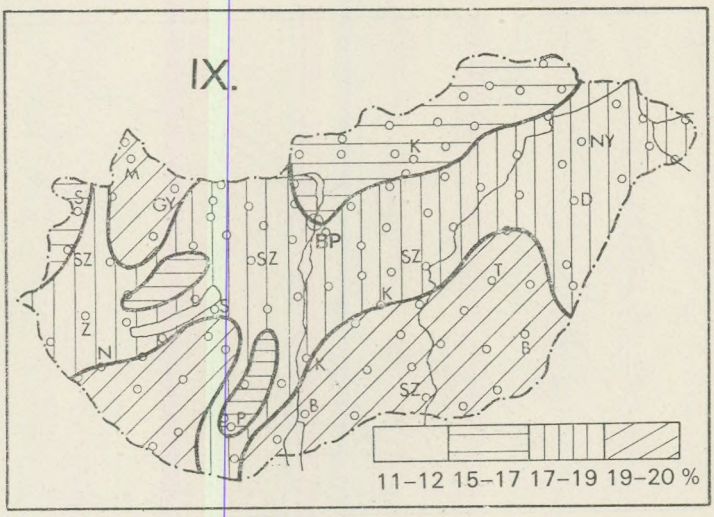

Fig. 11. Areal distribution of the albedo in September (after Weingartner)

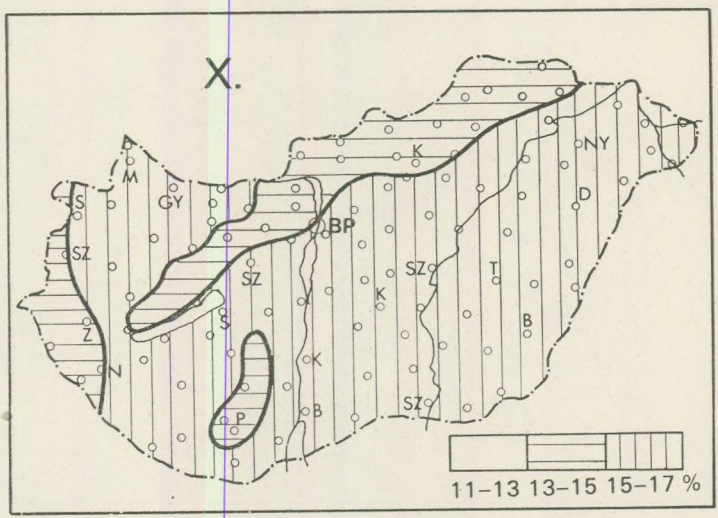

Fig. 12. Areal distribution of the albedo in October (after Weingartner)

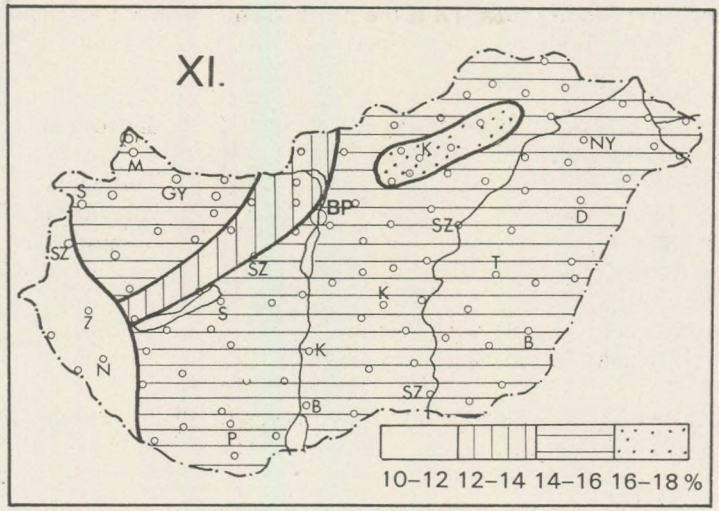

Fig. 13. Areal distribution of the albedo in November

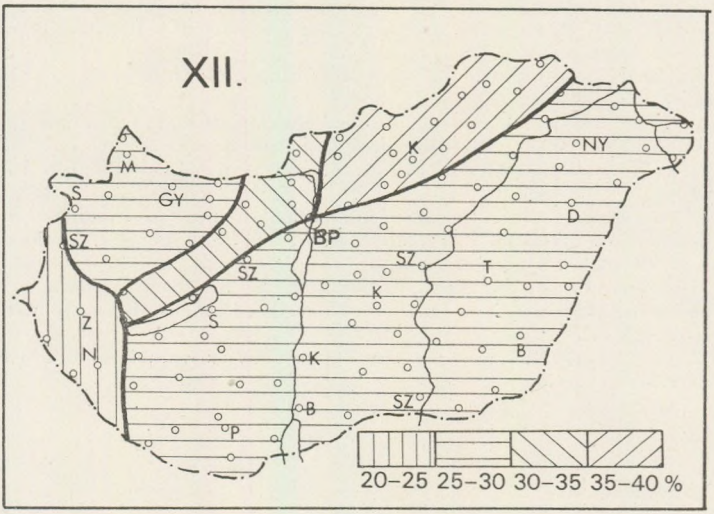

Fig. 14. Areal distribution of the albedo in December

For the preparation of albedo maps of the winter months we used the following albedo data [Zubenok 1949, Davies 1965, Tárkányi 1959, Baroskova et al. 1961, Goll 1964]:

Pine forest	12–2%	Zubenok
Beech-tree, oak without foliage	9%	Dirnhirm
Brown field soil, dry	17%	Dobosi
Brown field soil, wet	12%	Dobosi
Sand (Kecskemét)	18%	Tárkányi
Balaton	10%	Weingartner
Snow cover	60%	
Dry grass	21%	Tárkányi
Winter wheat (5 cm) with wet soil	14%	Dobosi
Winter wheat (5 cm) with dry soil	19%	Dobosi

The albedo maps constructed by averaging the albedo values on the basis of their frequencies are shown on the Figures 3–14.

REFERENCES

Adámi Koflanovics, E. (1970): Frequency distribution of the states of ground in Hungary (Manuscript).

Baroskova – Gajevszkij – Djacsenko – Lugina Pivovarova (1961): Radiacionnüj rezsim territorii SZSZSZR. (In Russian) Leningrád.

Borhidi, A. and Dobosi, Z. (1967): Areal distribution of the surface albedo in Hungary. Időjárás 71. pp.: 150–157. Budapest.

Davies, J. A. (1965): Albedo investigations in Labrador Ungava. Archiv für Met., Geoph. und Bioklim. Band 13.

Dobosi, Z. (1961): Remarks on the climatological use of the albedo. Időjárás 65. pp.: 364–366. Budapest.

Goll, Gy. (1964): The increase of albedo presenting itself on freezing soil. Időjárás 68., p. 112–117.

Péczely, Gy. (1966): Frequencies of snow cover in Hungary. Climate of Hungary. Off. Publ. of the State Meteorological Institute Budapest.

Tárkányi, Zs. (1959): Albedo measurements on the Lake Balaton Időjárás 63., p. 100–102.

Weingartner, F. (1968): The albedo of various surfaces and plant stocks. Reports on the scientific investigations made in 1967. Off. Publ. of the State Meteorological Institute XXXIV. Budapest.

Weingartner, F. (1970): Areal distribution of the albedo in Hungary. Reports on the scientific investigations made in 1968. Off. Publ. of the State Meteorological Service XXXV. Budapest.

Zubenok, L. I. (1949): Izmerenie albedo pokrovov sz szamoleta. Trudü GGO 18/80 (In Russian.) Leningrád.

CYCLOGENESIS AND ENTROPY

by

M. MAKAI – CSÁSZÁR

Department of Meteorology, Eötvös University, Budapest
Received: 15 March, 1974

ZUSAMMENFASSUNG

Zwischen den in Wechselwirkung stehenden Körpern besteht fortwährend eine Tendenz des Ausgleichs. Ein allgemein brauchbares Mass dieses Ausgleichprozesses ist die Entropie. Die Artikel setz es zum Ziel, eine nähere Klärung des energetischen Hintergrundes der Entwicklung der synoptischen „Störungen" unter Betonung des recht engen Zusammenhangs zwischen den atmosphärischen Transformationsprozessen und der Entropieänderungen zu geben.

Mit Hilfe von die Werte der Entropie zeigenden Karten und mit besonderer Betonung der Rolle der orographischen Hindernisse wird auf die Bedeutung der durch die Reibung verursachten Entroipieänderung hingewiesen.

The mechanism of weather processes is determined by the relative position of acting forces and by the variety of interactions. If the system is under simultaneous action of several forces, these tend to reintegrate the system into its equilibrium state. The necessary and sufficient condition of the equilibrium is that we should have uniform temperatur, pressure etc. values within the system. In the course of approaching the equilibrium state various movements appear within the system and the energy needed for these movements will be covered by the respective reserve of potential and internal energy of the system. The amount of energy usable for transformation into kinetic one is given by the amount of the available potential energy.

For the atmosphere the equilibrium state is represented by the barotropic stratification and hydrostatic equilibrium, when the value of available potential energy is zero, while the entropy function set up for the characterisation of the equilibrium state reaches its maximum. The process control function of the entropy function is due to the fact that within a closed system only such processes can be generated, which do not lead to a decrease of the entropy of the system investigated, i.e. the entropy changes during the processes taking place within the body only if we are dealing with an adjustment trend: the smoothing of inhomogeneities is always accompanied by entropy production.

The individual change of the mechanical energy of a volume τ bounded by surface σ is given by the expression

$$\frac{d(K+\Phi)}{dt} = -\int_{\sigma} p V_n \, d\sigma + \int_{\sigma} V_n F \, d\sigma + \int_{\tau} \left(p \frac{d\alpha}{dt} - \delta \right) \varrho \, d\tau , \qquad (1)$$

where K is the kinetical, Φ the potential energy of the system, p is the pressure, $\alpha = 1/\varrho$ the specific volume, V_n the outward normal wind component, F the friction force, $\delta = F$ grad V the so called Stokes-dissipation function, $p \frac{d\alpha}{dt}$ is the work done by the fluid when it is extended (compressed) on to the specific volume α.

The individual change of the internal energy is represented by the formula

$$\frac{dI}{dt} = -\int_{\tau} \left(p \frac{d\alpha}{dt} - \delta \right) \varrho \, d\tau + \int_{\tau} \frac{dq}{dt} \varrho \, d\tau , \qquad (2)$$

where $\frac{dq}{dt}$ represents the heat-income (-expenditure) without the friction heat —, the individual forms of which are: the various radiation components, evaporation, precipitation etc. From (2) it follows that the change of internal energy is depending also on processes within the system this connection being implemented through the expansion work $p \frac{d\alpha}{dt}$ resulting in an increase in case of compression and in decrease during expansion, furthermore owing to the dissipation heat, this being always positive, thus causing an increase of the internal energy.

The change of specific entropy is given by the expression

$$T \, ds = dI + p \, d\alpha . \qquad (3.a)$$

In case of a dry adiabatic change we have

$$T \, ds = c_v \, dT + p \, d\alpha . \qquad (3.b)$$

Thus the individual change of entropy of the system is

$$\frac{dS}{dt} = \int_{\tau} \frac{\frac{dq}{dt} + \delta}{T} \varrho \, d\tau . \qquad (4)$$

Analysis of equations (1), (2) shows that the various forms of the entire energy are continuously transforming one into another. The transformation is accompanied by various weather processes, but as regards a longer time interval no unidirectional progress will be made, the entire energy of the atmosphere remains constant and we have the relation:

$$\frac{dK}{dt} = \frac{d\Phi}{dt} = \frac{dI}{dt} = \frac{dS}{dt} = 0 . \qquad (5)$$

The relations (1), (2) and (4) demonstrate the existence of an energy cycle and if we add the identity (5), we can draw a few very important consequences regarding the characteristics of the circulation prccesses of the atmosphere.

Let us take the equation (1) describing the change of the mechanical energy. If τ denotes the volume of the whole atmosphere and if we take relations (5) as granted, we get

$$\int_{\tau} p \frac{d\alpha}{dt} \varrho \, d\tau = \int_{\tau} \varrho \delta \, d\tau . \tag{6}$$

Since $\delta > 0$, it follows – with a view to a compensation of the dissipation of the kinetic energy – the necessity that the expansion should take place at a pressure higher than average, while the compression occurs at a pressure lower than the average value.

Let us express the value of $p \frac{d\alpha}{dt}$ from (3.b) and apply from (5) the relation $\frac{dI}{dt} = 0$, we get

$$\int_{\tau} T \frac{ds}{dt} \varrho \, d\tau = \int_{\tau} \varrho \delta \, d\tau . \tag{7}$$

From (7) it follows that the increase of entropy is taking place at a temperature higher than the average, while its decrease occurs at a lower temperature. If we substitute the potential temperature into the expression giving entropy, we get the expression

$$\int_{\tau} c_p \frac{T}{\Theta} \frac{d\Theta}{dt} \varrho \, d\tau = \int_{\tau} c_p \left(\frac{p}{p_{00}} \right)^{R/c_p} \frac{d\Theta}{dt} \varrho \, d\tau > 0 \tag{8}$$

meaning that the increase of potential temperature should take place at a pressure higher than the average, while its decrease occurs at a lower than the average pressure level. Referring again to (4) and (5) we obtain

$$\int_{\tau} \frac{1}{T} \frac{dq}{dt} \varrho \, d\tau = - \int_{\tau} \frac{\delta}{T} \varrho \, d\tau . \tag{9}$$

Owing to $\delta > 0$

$$- \int_{\tau} \frac{\delta}{T} \varrho \, d\tau < 0 ,$$

i.e. in view of a compensation of entropy increase setting in spontaneously as a consequence of friction, heat sources of the atmosphere

occur at a temperature higher than average, while sinks are located at places with a temperature lower than the average.

Consequences drawn from (8) respective (9) are essentially the mathematical expressions of the Sandström – Wenger circulation theory, according to which: a stationary circulation can be maintained only in the case, if heat sources are on the average situated at higher pressure than heat sinks.

Further application of the Sandström circulation theory favours a closer knowledge of the atmospheric circulational systems (B j e r k n e s 1902) and what is more, we get an explanation of the circulation mechanisms originating from the interaction of the atmosphere and Earth. The Sandström – Höiland – Hansen circulation theorem states that: if we disregard friction, on the northern hemisphere the streamlines show a turning to the right at the windward side, thus creating an anticylonic circulation. In case of an overflowing of the crest we experience a turning to the left behind the mountain (lee-side), thus a cyclonic curvature appears.

Let us complete this theorem by the equation under (4). If we take friction into account, the friction heat owing to $\delta > 0$ causes an increase of the entropy, thus it seems also energetically justified that cyclones degenerate when approaching orographic obstacles. Although owing to (2) the positive value of the dissipation function results in an increase of the internal energy too, the irreversibility of the process makes its transformation into kinetic energy impossible. This rule involves essentially the idea of the "perpetuum mobile psychikum" the verification of which seems to be possible by the analysis of the equation describing the variation of the available potential energy.

Let τ denote the entire volume of the atmosphere defined by the surface pressure p from below and by the $p = 0$ isobaric surface from above and σ the entire surface of the Earth, then the variation of the available potential energy will be given by the expression

$$\frac{dA}{dt} = \frac{\partial A}{\partial t} = \frac{1}{g} \int_{\sigma} \int_{o}^{p_0} \left[\left(\frac{p^k - p_r^k}{p^k} \right) \left(\frac{dq}{dt} + \delta \right) + \alpha\omega \right] dp\, d\sigma \,, \qquad (10)$$

where p_r is the so called reference-pressure – practically the pressure belonging to the equilibrium state –, $k = \frac{R}{c_p}$, $\omega = \frac{dp}{dt}$, the vertical velocity. The first term of the right side of (10) is a "generation term", while the second one represents the transformation into kinetic energy. The ascent of warm air and the descent of cold one fives a negativ sign to the term $\alpha\omega$, i.e. the available potential energy decreases, the process supports the transformation into kinetic energy.

Let us study the events in connection with the cold air coming up againts the mountains, where it is partly forced to rise, partly it flows

round. In the rising process of the cold air the sign of the term $\alpha\omega$ is positive, thus an increase of the available potential energy is to be expected, while a decrease of the kinetic energy is probable.

The first term of the right side of (10) contains the product of the expression "$\frac{dq}{dt}+\delta$" and of the "efficiency factor" $\frac{p^k-p_r^k}{p^k}=N$. In case the absorbing of heat takes place at a pressure higher than the reference

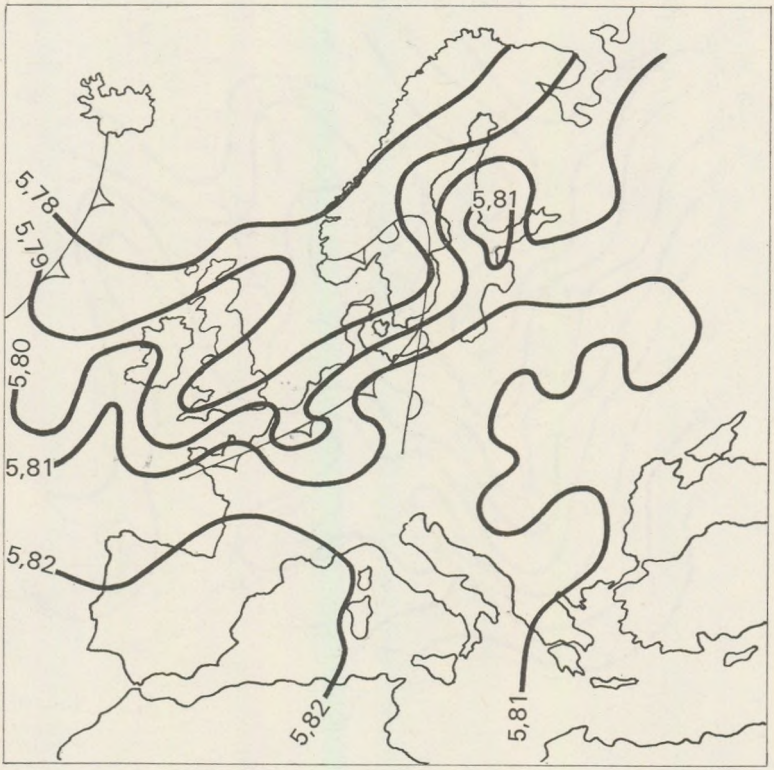

Fig. 1. Average entropy value of the layer between the 1000 and 200 mb surfaces in. units of 10^{10} erg/cm^2 at 12 hours on the 19th October 1970

pressure, and the loss of heat at a value lower than p_r, we can count on an increase of the usable potential energy. Regarding the dissipation heat δ we know that it is always positive, so that in case of $p<p_r$ a decrease of the available potential energy takes place, although the value of the internal energy increases. The actual sum of the internal and potential energy became higher, but the usable part is not defined by this sum alone. Taking into account (4) we see that there was an increase in the

value of the entropy and as a result of diminution of the original temperature differences the system came nearer to the equilibrium state.

The basic effects changing the entropy are coming to the air mass mainly from below. The dissipation-heat brought about by the friction is important obviously in the lower layer of the troposhere and particularly in the vicinity of orographic obstacles, but it is not to be neg-

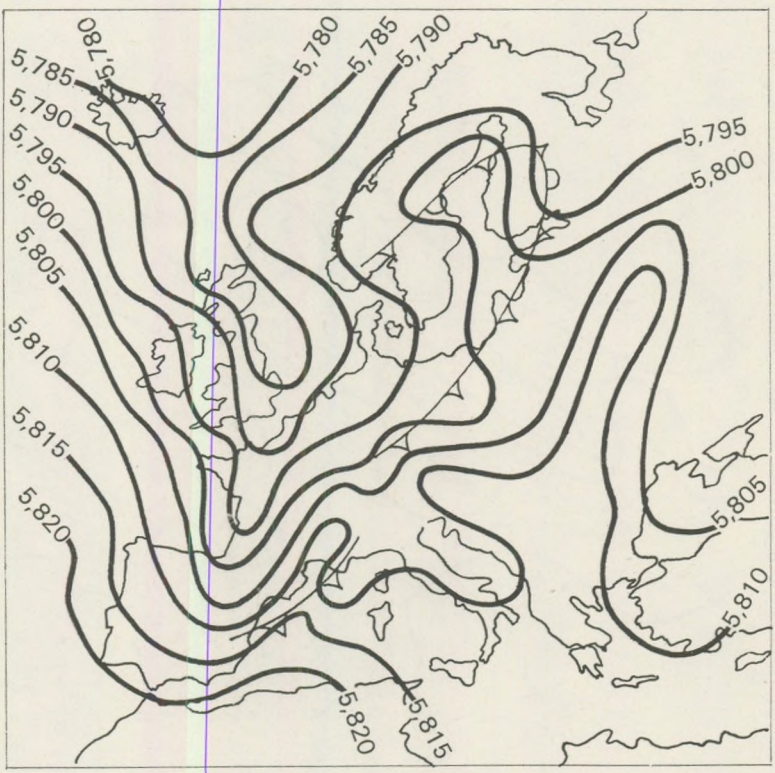

Fig. 2. The same as with Fig. 1. at 00 hour on the 20eth October 1970

lected even in the higher layers of the troposphere, where – owing to $\delta = \alpha p$ grad **V** – its significance increases because of the relatively high wind velocity and of a negative efficiency factor.

Our reasoning gives an energetical explanation for the weakening of cyclones or fronts coming accross the mountains. As regards the further development of the processes under special geographical conditions, we can sometimes witness – with a certain phase lag – the regeneration of cyclones registered earlier in the literature about cyclone-statistics in the form that "cyclones prefer inland seas". It is therefore not without

interest studying the energetical background of this later process. Under such special geographical conditions, where on the lee-side of the mountains, respectively southwards of it an inflow of warm air is to be expected, in the warm air coming up to the mountains we have an increase of temperature owing to the dissipation heat and a steeper slope of the isosteric surfaces, thus an increasing inhomogeneity and so a strengthening of

Fig. 3. Entropy change between 12 hours on the 19th October 1970 and 00 hours on the 20eth October 1970 in units of 10^7 erg/cm^2

the baroclinic zones. Thus, in that process the value of the available potential energy will be increased, at the same time the total entropy of the system diminishes, while the term $\alpha\omega$ obtains a negative sign in the equation (10) describing the variation of the available potential energy, i.e. the transformation into kinetical energy will be favoured.

The quantitative interpretation of the equation describing the change of the usable potential energy becomes even more complicated if we restrict our considerations only to a small partial domain of the at-

mosphere, and we take into account also the energy-flow across the boundaries of the partial domain.

Between the interacting air masses a continuous adjusting tendency is in action and a commonly usable measure of this tendency is represented by the entropy. The maps representing the values of the entropy and its variations in magnitude and sign provide an orientation regard-

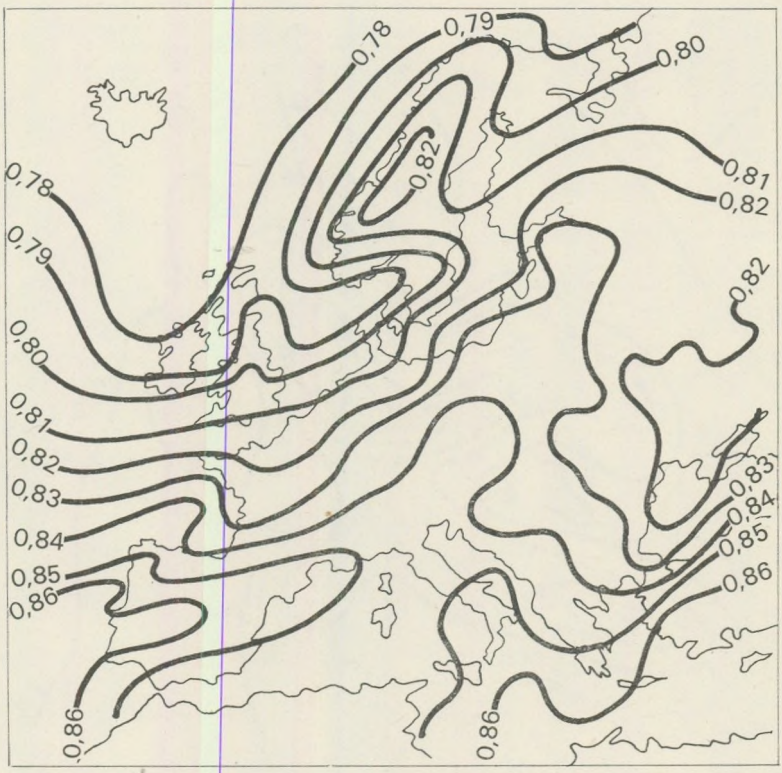

Fig. 4. Average entropy value of the layer between the 1000 and 900 mb surface in units of 10^{10} erg/cm^2 at 12 hours on the 19th October 1970

ing the possible development of the processes. Localities with low entropy values reflect the inhomogeneity and can be found obviously at places being asymmetrical from the point of view of temperature distribution, mainly at the frontal zones, where we have a great number of solenoids.

Maps 1. and 2. represent average entropy values of the layer between the ground and the 200 mb-surface on the 19th October at 12^h and 20^{eth} October 00^h, given in units of 10^{10} erg/cm^2. On both maps thick lines denote the position of fronts near the ground, spikes on the

lines denoting the direction of moving cold fronts, half-circles that of the warm fronts, as it is commonly used. An area characterized by high entropy values is running through Middle-Europe, Poland and the Baltic Sea, as well as over the southeast part of the Atlantic, over Spain and Asia Minor, while in the North-Atlantic area and over Western Europe, as well as across the Balkans and Eastern Europe up to the

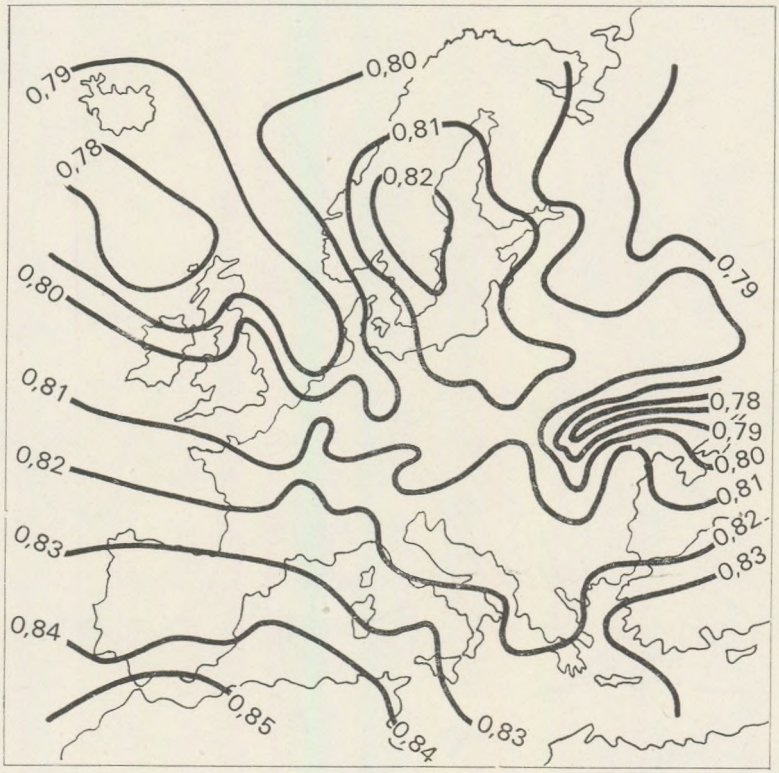

Fig. 5. The same as with Fig. 4. at 00 hours on the 20eth October 1970

70 degrees of Northern latitude we have got low values. After 12 hours, as it can be seen on Fig. 2. a significant change in the entropy-values has taken place: the total entropy of the area has increased. Owing to the occlusion of the cyclone of the North-Sea a significant adjustment occured over the northern territories, the average increase being 14.10^7 erg/cm^2. Because of the eastward shifting of fronts also the places with low entropy values can be found further eastwards and even in the area of the Mediterranean a significant decrease can be experienced, while

over Western Europe an increase has taken place. The amount of change is represented on Fig. 3, broken lines denoting zero value, continuous lines the increase, dotted ones decreasing entropy values. Since on Fig. 3. representing the change we find a more significant increase around the mountains, therefore we constructed maps of entropy of the layer between the 1000 and 900 mb-surfaces for both dates (Figs. 4, 5, and 6).

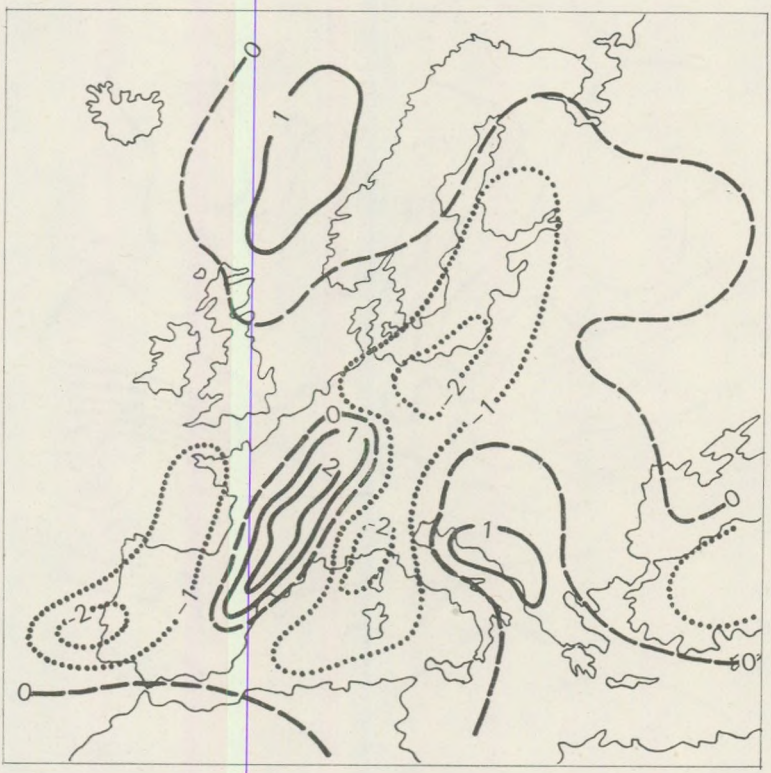

Fig. 6. Entropy change between 12 hours on the 19th of October 1970 and 00 hours on the 20eth of October 1970 concerning the layer between the 1000 mbar and 900/mb surfaces in units of 10^7 erg/cm^2

The distribution of entropy is like that of the layer up to the 200 mb-surface, although effects originating from the interaction of the ground surface and the moving air masses are decidedly predominant here. On the map of the entropy values of the lower layer and on that representing the changes we can clearly see the lagging behind of the lower section of the cold front which can be attributed to the effect of the Alps. This seems to be supported also by the significant entropy-

increase seen on Fig. 6. A considerable entropy decrease can be found over the Mediterranean: this can be explained by the advection of warm air from south and by its meeting the cold air masses going round the Alps from southwest, thus producing a new frontal zone. The effect of friction caused by the mountains can be observed over the Balkans, Carpathians and even over the Scandinavian mountains too.

The areas of entropy decrease denote the places of departing from the equilibrium state, at the same time, however, the usable potential energy increases. An earlier study of us dealt with the clearing of the relation between the efficiency factor and non -adiabatic heating up concerning the same time interval from 19 to 21 October 1970. The results supported energetically the possibility of formation of a Genoa-cyclone as reflected by the data contained in the generation-term of the usable potential energy. The map of distribution of the efficiency factor also proved that especially in the lower layers of the troposphere, on the isentropic surface belonging to $\Theta = 290°$ K the diminution of the efficiency factor caused by the mountains presented itself in the configuration of the isolines in the foreground of the Alps (1973).

The entropy-analysis of the lower layer significantly indicates the action of local effects, although these cyclones do not attain the order of magnitude of the length of great atmospheric waves, i.e. 6000 – 8000 km, but they can even surpasse them as regards activity and effect. Furthermore, entropy analysis proves also that the Mediterranean cyclone can be classified as a synoptic disturbance of a smaller scale (their wave-length amounts to 2000 – 3000 km according to Bjerknes and Holmboe 1944).

During our study we did not differentiate between coolings and heatings of different origin so that the released latent heat can also be of importance and its effect – according (10) – in the eastern basin of the Mediterranean together with positive efficiency factor can result in an increase of the usable potential energy, especially in the middle region of the troposphere. According to the calculation of Radinovič (1960) in the development of the Mediterranean cyclone the released latent heat is of importance first of all in the later phase of development and it does not figure among the primary factors as regards the formation of the cyclone.

The maps shown for the period investigated represent a phase of cyclone development and if completed by the computations regarding the formation of usable potential energy as well as its transformation into kinetic energy, they will furnish in all probability detailed knowledge for clearing up of the energetical background of certain synoptic disturbances. Nevertheless we do not get by this a full explanation of the energy cycle, since besides solving our present problem we have still to clear up all data-to be taken into account- of the possible heat sources and sinks, which after all determine the specific distribution of the temperature.

REFERENCES

Bjerknes, V. (1902): Zirkulation relativ zu der Erde, Öfversigtafk. vetenskaps-akaddmiens förhandlingar 739 – 775

M. Császár, M. (1973): Role of the efficiency factor and non-adiabatic effects in generation of the Mediterranean cyclones. Annales Tom. XVIII (in press).

Godske, C. L., T. Bergeron, J. Bjerknes and R. C. Bundgaard (1957): Dynamic Meteorology and Weather Forecasting, Boston – Washington.

Höiland, E. (1939): On the interpretation and application of the circulation theorems of V. Bjerknes Arch. Math. og Naturv. Vol 42, No. 5, pp. 68.

Radinović, D. (1960): Analysis of the cylogenetic effects in the Western Mediterranean, 6th Intern. Meeting Alpine Meteorol., 1960, Bled, Yugoslavia pp. 33 – 40

VERSUCH EINER DARSTELLUNG DES GROSSRÄUMIGEN BEWÖLKUNGSFELDES DURCH TSCHEBYTSCHEFF'SCHE POLYNOME

von

RÁKÓCZI F.

Institut für Meteorologie, Eötvös Universität, Budapest

Eingegangen: 15 März 1974

SUMMARY

The picture of the large scale cloudiness-field obtained through artificial satellites is described by means of Chebyshev polynomials. The results show that an accuracy desired by the practice can be attained using a few polynomials only.

Die Erscheinung der meteorologischen künstlichen Satelliten und die praktische Anwendung der durch diese erhaltenen Informationen lenkten die Aufmerksamkeit wiederholt und in verstärktem Masse an die Eigenschaften der Wolkenfelder hin. Die von den Televisionsapparaten übermittelten Wolkenbilder, als Zeichen der am meisten grundlegenden meteorologischen Vorgänge können als sichtbare Bilder der sich im Grossraum abspielenden Ereignisse aufgefasst werden. Schon der Besitz der Wolkenbilder selbst representiert eine ernste Stütze sowohl für Theorie als auch für die Praxis. Es ist verständlich, dass man sich bemüht, die Konturen der erhaltenen Bilder so genau wie möglich darzustellen. Solch eine Anforderung trat schon im Laufe der Analyse der an der Erde durchgeführten Beobachtungen auf (Muszaeljan und Csekirga 1964), jedoch nicht selbstbezweckt, sondern dem Wunsch entsprechend, um das Wolkenfeld mit dem mit ihm eng verbundenen vertikalen Strömungsfeld quantitativ vergleichen zu können und so aus den Bedeckungsverhältnissen auf die mit ihnen verbundenen barischen Bildungen Folgerungen zu ziehen

Die quantitative Analyse der durch die Televisionsapparate der künstlichen Satelliten aufgenommenen Bilder ist eine Aufgabe, die keinesfalls von Problemen frei ist. Vielmehr stellt sie eine Arbeit dar, die eine grosse Aufmerksamkeit und gehörige Erfahrenheit beansprucht. Zurzeit ist es üblich, die durch künstliche Satelliten bestimmten Bedeckungsverhältnisse mit fünf Stufen anzugeben: 10 Zehntel = bedeckt, 9 – 7 Zehntel: kompakte Bewölkung, 6 – 4 Zehntel: erhebliche Bewölkung, 3 – 1: geringe Bewölkung, 0 Zehntel: klarer Himmel. Wie wir sehen, wird die Analyse der Bedecktheit in der täglichen Praxis in form von Stufen angegeben. Neben der numerischen Angabe der Gesamtbedeckung enthalten die auf Grund der Wolken-Bilder ausgearbeiteten Neph-Analysen noch weitere Indikatoren, die sich auf die

Wolkenform, auf die eventuell mit diesen zusammenhängenden Strömungen, sowie auf ihren vertikalen Aufbau beziehen.

Unsere Fragestellung war eine Beschreibung der grossräumigen Verteilung der Bedecktheit mittels einer mathematischen Formel. Und zwar, wir zerlegten das Bedeckungsfeld mit Hilfe von orthogonalen Tschebitscheff'schen Polynomen, bestimmten die Koeffizienten dieser Polynome, und untersuchten es, dass die einzelnen Grundpolynome oder Kreutzpolynome einen wie hohen Prozentsatz der Streuung um den Mittelwert darstellen. So konnten wir feststellen, welche sind diejenige Polynome, mit deren Hilfe das Feld mit angegebenen Genauigkeit reproduziert werden könnte.

Vor einer eingehenden Diskussion der Untersuchungsresultate geben wir eine kurze Zusammenfassung der benutzten mathematischen Methode.

Bei der Anwendung der Tschebytscheff'schen Polynome ist der erste Schritt die angebrachte Auswahl der zu benutzenden Netzpunkte. Im Falle einer Untersuchung von meteorologischen Elementen können die Schnittpunkte der Breiten- und Längen-Kreise ein zweckmässiges Netz representieren.

Die Netzpunkte seien durch $x_i (i = 1, 2, \ldots, m)$ und y_i $(j = 1, 2, \ldots, m')$ angegeben. Die in den Netzpunkten abgelesenen Feldwerte werden durch z_{ij} bezeichnet und in Form einer Potenzreihe, wie folgt, dargestellt:

$$z_{ij} = a_{00} + a_{10} x_i + a_{01} y_j + a_{20} x_i^2 + a_{11} x_i y_j + a_{02} y_j^2 \ldots$$

$$= \sum_{n=0}^{m-1} \sum_{k=0}^{m'-1} a_{nk} x_i^n y_j^k . \tag{1}$$

Die höchsten Potenzen der Reihenentwicklung sind $m-1$, bzw. $m'-1$. Die zu Verfügung stehenden Gleichungen der Anzahl a_{nk} werden gleich viele Unbekannten enthalten.

Es sollen nun in (1) die Polynome folgender Form eingeführt werden:

$$f_{ni} = \sum_{r=0}^{n} A_{nr} x_i^r , \qquad g_{kj} = \sum_{j=0}^{k} B_{ks} y_j^s \tag{2}$$

Als Resultat erhalten wir die folgenden Ausdrücke:

$$z_{ij} = b_{00} f_{0i} g_{0j} + b_{10} f_{1i} g_{0i} + b_{01} f_{0i} g_{1j} + b_{20} f_{2i} g_{0j} +$$

$$+ b_{11} f_{1i} g_{1j} + b_{02} f_{0i} g_{2j} + \ldots \tag{3}$$

$$= \sum_{n=0}^{m-1} \sum_{k=0}^{m'-1} b_{nk} f_{ni} g_{kj} ,$$

wobei die Koeffizienten b_{nk} Funktionen der Koeffizienten A_{nk} sind, und wenn wir von der Annahme $A_{00} = B_{00} = 1$ Gebrauch machen, werden wir $f_{01} = g_{01} = 1$ haben; (3) geht dann in den Ausdruck

$$z_{ij} = b_{00} + \sum_{n=1}^{m-1} b_{n0} f_{ni} + \sum_{k=1}^{m'-1} b_{0k} g_{jk} + \sum_{n=1}^{m-1} \sum_{k=1}^{m'-1} b_{nk} f_{ni} g_{kj} \qquad (4)$$

über. So erhalten wir mm' Gleichungen mit mm' Unbekannten; es ist nähmlich die Anzahl der Koeffizienten b_{nk}: $(m-1)\,(m'-1)$, die der

$\lambda = 20° \text{ W} - 10° \text{ E}$ $\varphi = 55° \text{ N} - 35° \text{ N}$

n	k	b_{nk}	U_{nk}	$r = U_{nk}/S$	$PR = 100\, r^2$
1	0	−0,91	−10,74	−0,38	*15*
2	0	0,42	8,54	0,30	*9*
3	0	0,53	2,47	0,09	1
4	0	0,07	2,02	0,07	0
5	0	0,09	1,81	0,06	0
6	0	−0,08	−5,10	−0,18	*3*
0	1	−1,93	−16,13	−0,56	*33*
0	2	0,24	2,32	0,08	0
0	3	0,07	0,60	0,02	0
0	4	0,09	1,94	0,07	0
1	1	0,01	0,12	0,00	0
2	1	0,02	0,69	0,03	0
3	1	−0,68	−5,29	−0,19	*3*
4	1	−0,09	−3,44	−0,12	*2*
5	1	−0,07	−2,07	−0,07	0
6	1	−0,05	−4,60	−0,16	*3*
1	2	0,09	1,72	0,06	0
2	2	−0,10	−3,50	−0,13	*1*
3	2	0,04	0,33	0,01	0
4	2	0,20	9,46	0,34	*11*
5	2	0,06	2,10	0,08	0
6	2	0,02	2,02	0,07	0
1	3	−0,03	−0,54	−0,02	0
2	3	0,16	4,66	0,17	*3*
3	3	0,28	2,19	0,08	0
4	3	0,02	0,64	0,02	0
5	3	−0,14	−3,97	−0,14	*2*
6	3	0,03	2,53	0,09	1
1	4	0,00	0,07	0,00	0
2	4	0,00	−0,33	−0,01	0
3	4	−0,36	−7,27	−0,26	*7*
4	4	−0,06	−6,15	−0,22	*5*
5	4	−0,01	−1,08	−0,04	0
6	4	−0,01	−3,46	−0,12	1

Tab. 1. 3ter Juli 1968

b_{0k}: $(m'-1)$, die der b_{n0}: $(m-1)$; dazu kommt noch ein einziger Koeffizient: b_{00}.

Zur Vereinfachung der Berechnungen machen wir die folgenden Annahmen:

1. Sowohl m, als m' sollen gerade sein.
2. f_{ni} und g_{kj} sind orthogonale Polynome, d. h.

$$\sum_{i=1}^{m} f_{ri} f_{si} = 0\,, \qquad \sum_{j=1}^{m'} g_{rj} g_{sj} = 0\,, \qquad \text{wenn } r \neq s \text{ ist}, \tag{5}$$

$\lambda = 5\,\mathrm{E} - 35\,\mathrm{E}$ $\qquad$ $\varphi = 55\,\mathrm{N} - 35\,\mathrm{N}$

n	k	b_{nk}	U_{nk}	$r = U_{nk}/S$	$PR = 100\,r^2$
1	0	0,57	6,76	0,27	*7*
2	0	0,12	2,44	0,09	1
3	0	−0,23	−1,27	−0,05	1
4	0	−0,12	−3,19	−0,13	*2*
5	0	0,32	6,54	0,27	*7*
6	0	0,04	2,51	0,10	1
0	1	−1,64	−13,74	−0,56	*31*
0	2	−0,44	−4,34	−0,18	*3*
0	3	0,43	3,58	0,15	*2*
0	4	0,22	4,87	0,20	*4*
1	1	−0,30	−4,95	−0,20	*4*
2	1	0,01	0,17	0,00	0
3	1	0,12	0,91	0,04	0
4	1	0,16	6,39	0,26	*7*
5	1	−0,21	−6,11	−0,25	*6*
6	1	−0,01	−1,34	−0,05	1
1	2	0,07	1,36	0,06	1
2	2	0,01	0,20	0,01	0
3	2	0,30	2,73	0,11	1
4	2	−0,10	−4,82	−0,20	*4*
5	2	0,03	1,08	0,04	0
6	2	−0,01	−1,12	−0,05	1
1	3	−0,12	−2,03	−0,08	1
2	3	−0,13	−3,66	−0,15	*2*
3	3	0,10	0,77	0,03	0
4	3	0,00	−0,05	0,00	0
5	3	0,06	1,86	0,08	1
6	3	0,01	0,60	0,02	0
1	4	0,01	0,23	0,01	0
2	4	0,04	3,00	0,12	1
3	4	−0,36	−7,42	−0,30	*9*
4	4	0,02	2,27	0,09	1
5	4	−0,03	−1,90	−0,08	1
6	4	0,00	1,08	0,04	0

Tab. 2. 3ter Juli 1968

wobei

$$r, s = 1, 2, \ldots, m-1, \qquad r, s = 1, 2, \ldots, m'-1 .$$

Dadurch erreichen wir, dass die A_{nr} und B_{ks} Koeffizienten nur von den Koordinaten x und y abhängen und die Polynome voneinander unabhängig sind, und somit voneinander unabhängig berechnet werden können.

3. Die Verteilung des Netzes ist gleichmässig, wobei erreicht wird, dass die Koeffizienten A_{nr} und B_{ks} nur die funktionen von m und m' sind.

$\lambda = 20° \text{ W} - 10° \text{ E}$ $\varphi = 55° \text{ N} - 35° \text{ N}$

n	k	b_{nk}	U_{nk}	$r = U_{nk}/S$	$PR = 100\, r^2$
1	0	0,23	2,71	0,21	*4*
2	0	0,04	0,88	0,07	0
3	0	−0,27	−1,46	−0,11	1
4	0	−0,01	−0,22	−0,02	0
5	0	0,18	3,71	0,28	*8*
6	0	−0,02	−1,32	−0,10	1
0	1	−0,67	−5,62	−0,43	*18*
0	2	−0,19	−1,92	−0,15	*2*
0	3	−0,37	−3,11	−0,24	*6*
0	4	−0,01	−0,27	−0,02	0
1	1	−0,18	−2,99	−0,23	*5*
2	1	0,00	0,00	0,00	0
3	1	0,15	1,16	0,09	1
4	1	0,03	1,25	0,10	1
5	1	−0,05	−1,38	−0,11	1
6	1	−0,02	−2,31	−0,18	*3*
1	2	−0,11	−2,12	−0,16	*3*
2	2	0,05	1,81	0,14	*2*
3	2	−0,04	−0,33	−0,03	0
4	2	0,02	0,93	0,07	0
5	2	−0,07	−2,45	−0,19	*3*
6	2	0,01	1,35	0,10	1
1	3	−0,11	−1,79	−0,14	*2*
2	3	−0,01	−0,35	−0,03	0
3	3	−0,05	−0,39	−0,03	0
4	3	0,04	1,45	0,11	1
5	3	0,07	2,07	0,16	*2*
6	3	0,02	1,91	0,15	*2*
1	4	0,13	5,69	0,43	*19*
2	4	0,00	−0,16	−0,01	0
3	4	0,08	−1,61	−0,12	1
4	4	0,00	0,38	0,03	0
5	4	−0,05	−3,83	−0,29	*8*
6	4	0,01	3,03	0,23	*5*

Tab. 3. 13ter Februar 1974

4. Im Laufe der Berechnungen werden wir orthogonale Tschebytscheff-Polynome anwenden, die der Bedingung

$$\sum_{i=1}^{m} f_{ni} = 0 \quad \text{und} \quad \sum_{j=1}^{m'} g_{kj} = 0 \tag{6}$$

Genüge leisten. Die Werte dieser Funktionen stehen uns in tabellarischer Form zu Verfügung. [2, 3, 4].

$\lambda = 5° \text{ E} - 35° \text{ E}$ $\varphi = 55° \text{ N} - 35° \text{ N}$

n	k	b_{nk}	U_{nk}	$r = U_{nk}/S$	$PR = 100\, r^2$
1	0	0,09	1,01	0,09	1
2	0	0,04	0,78	0,07	1
3	0	0,27	1,46	0,12	2
4	0	−0,03	−0,87	−0,07	1
5	0	−0,02	−0,49	−0,04	0
6	0	0,00	0,21	0,02	0
0	1	−0,71	−5,97	−0,50	25
0	2	−0,33	−3,23	−0,27	8
0	3	−0,50	−4,18	−0,35	12
0	4	0,04	0,86	0,07	1
1	1	0,20	3,41	0,29	8
2	1	0,03	0,79	0,07	1
3	1	−0,32	−2,46	−0,21	4
4	1	−0,04	−1,68	−0,14	2
5	1	0,02	0,66	0,06	0
6	1	0,01	0,57	0,05	0
1	2	−0,08	−1,67	−0,14	2
2	2	−0,06	−2,04	−0,17	3
3	2	−0,24	−2,18	−0,18	4
4	2	0,00	0,00	0,00	0
5	2	−0,01	−0,32	−0,03	0
6	2	0,01	1,13	0,10	1
1	3	0,08	1,26	0,11	1
2	3	−0,07	−2,11	−0 18	3
3	3	0,12	0,90	0,08	1
4	3	0,00	−0,08	−0,01	0
5	3	0,01	0,24	0,02	0
6	3	0,02	1,82	0,15	3
1	4	−0,08	−3,46	−0,29	9
2	4	0,03	2,10	0,18	3
3	4	−0,04	−0,83	−0,07	1
4	4	0,00	0,20	0,02	0
5	4	0,03	1,89	0,16	3
6	4	0,00	−0,63	−0,05	0

Tab. 4. 13ter Februar 1974

Es sollen diejenige b_{nk} – Koeffizienten gesucht werden, für welche die Bedingung

$$\sum_{i=1}^{m}\sum_{j=1}^{m'}\left(z_{ij}-\sum_{n=0}^{m-1}\sum_{k=0}^{m'-1} b_{nk} f_{ni}\, g_{kj}\right)^2 = \min \tag{7}$$

erfüllt wird. Die Formeln zur Berechnung der erwünschten Koeffizienten sind die folgenden:

$$\left.\begin{aligned} b_{00} &= \sum_{i=1}^{m}\sum_{j=1}^{m'} z_{ij} : mm' = \overline{z_{ij}},\\ b_{n0} &= \sum_{i=1}^{m} f_{ni} \sum_{j=1}^{m'} z_{ij} : m' \sum_{i=1}^{m} f_{ni}^2,\\ b_{0k} &= \sum_{i=1}^{m'} g_{kj} \sum_{i=1}^{m} z_{ij} : m \sum_{j=1}^{m'} g_{kj}^2,\\ b_{nk} &= \sum_{i=1}^{m}\sum_{j=1}^{m'} f_{ni}\, g_{kj}\, z_{ij} : \sum_{i=1}^{m} f_{ni}^2 \sum_{j=1}^{m'} g_{kj}^2. \end{aligned}\right\} \tag{8}$$

Wenn wir die Koeffizienten b_{n0}, b_{0k} und b_{nk} – einen nach dem anderen – mit den Ausdrücken

$$\sqrt{m' \sum_{i=1}^{m} f_{ni}^2}, \qquad \sqrt{m \sum_{j=1}^{m'} g_{kj}^2}, \qquad \sqrt{\sum_{i=1}^{m} f_{ni}^2 \sum_{j=1}^{m'} g_{kj}^2}$$

multiplizieren, dann erhalten wir die Antwort auf die Frage, welcher Prozenstsatz der Streuung um den Feldmittelwert durch das betreffende Polynom dargestellt wird. Weiterhin, wenn wir das Quadrat des erhaltenen Resultats (u_{n0}^2, u_{0k}^2, u_{nk}^2) mit der Anzahl der Netzpunkte (mm') dividieren, dann erhalten wir die Information darüber, welcher Prozentsatz der Streuung des Feldes durch die f_n – bzw. g_k – Polynome, oder aber durch die Produkte $f_n g_k$ der Polynome (diese sind die sogenannten Kreutz-Polynome) representiert wird. Standardisierte Grössen erhalten wir durch Division mit der Grösse:

$$s^2 = \sum_{i=1}^{m}\sum_{j=1}^{m'} (z_{ij}-\bar{z})^2 = \sum_{i=1}^{m}\sum_{j=1}^{m'} z_{ij}^2 - mm'\,\bar{z}^2 \tag{9}$$

und die Güte der Approximation des Feldes mittels des gegebenen Polynoms können wir durch die Grösse

$$r_{nk} = u_{nk}^2 : s^2 \tag{10}$$

messen. Die Zahl 100 r_{nk}^2 gibt denjenigen Prozentsatz der ganzen Streuung an, welchen das gegebene Polynom leisten kann. Dies Grösse soll als prozentige Reduktion gelten.

Nach der Beschreibung der mathematischen Grundlagen sollen wir uns nun dem Anwendungsbeispiel zuwenden.

In unseren Beispielen werden wir uns mit den Bewölkungsfeldern beschäftigen, die am 13ten Februar 1968 durch die künstlichen Erdsatelliten „ESSA – 3" und „KOZMOSZ 184 – 144" aufgenommen, bzw. auf Grund der Wolkenbilder der Satelliten „ESSA 5 – 6" und „KOZMOSZ 226" analysiert wurden. Das Untersuchungsgebiet ertstreckt sich zwi-

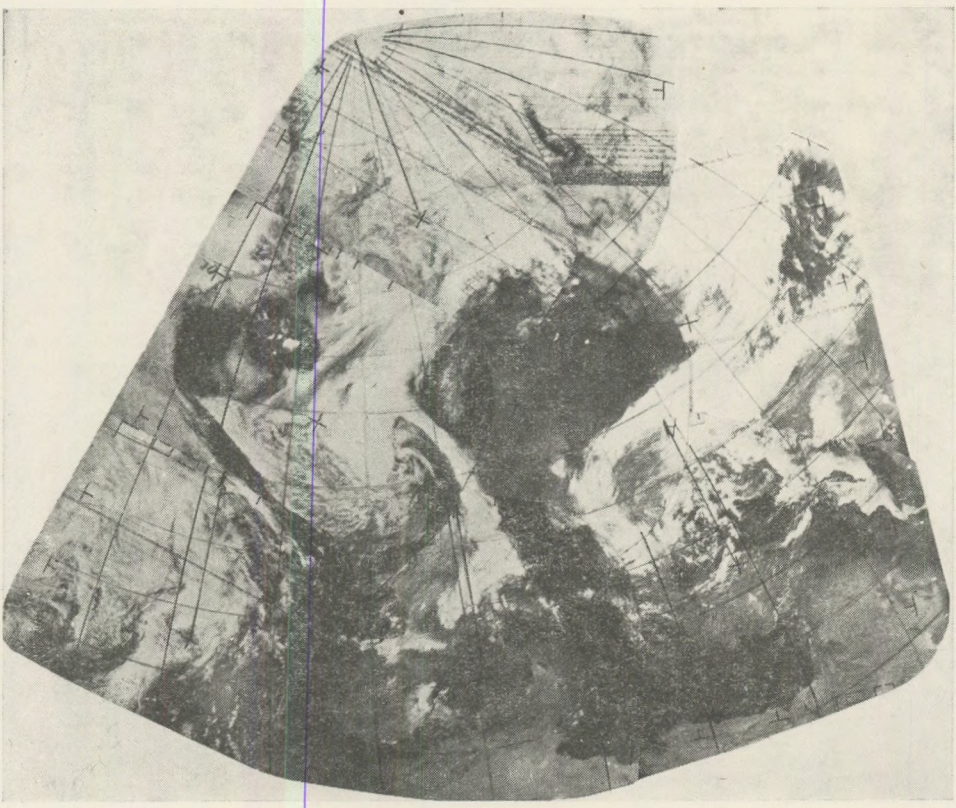

Abb. 1.

schen 55° – 35° nördlicher Breite und zwischen 20° W – 35° E Längengraden. Als Netzpunkte wurden die Schnittpunkte der Breiten- und Längenkreisen, und zwar von 5 zu 5 Graden genommen; da wir aber die Werte $m = 7$ und $m' = 5$ als Rechnungsgrundlage einführten, zerlegten wir das Untersuchungsgebiet in zwei Untergebiete so, dass in der östlichen und westlichen Hälfte des Gebietes eine Überdeckung zustande kommen soll.

Die Analyse der sommerlichen und winterlichen Wolkenbilder wurde in der Hydrometeorologischen Zentrale der Sowjetunion vorgenommen und uns zusammen mit den forzuführenden Neph-Analysen-Karten zu Verfügung gestellt. Am 3ten Juli 1968 wurden die Daten der über uns hinwegziehenden Satelliten auch vom ungarischen Dienst aufgenommen, so dass wir im Stande sind, diese zu zeigen (Abb. 1.) Wir können sehen, dass – entsprechend der sommerlichen Wetterlage – im Untersuchungsgebiet recht komplizierte Bedeckungsverhältnisse herrschten. Ein winterliches Lagebild können wir nicht vorführen, da die enstprechenden Aufnahmen nicht zu Verfügung stehen.

Das Resultat des oben dargestellten mathematischen Verfahrens wurde in tabellarischer Form zusammengestellt. Infolge der schon erwähnten Aufteilung auf zwei Untergebiete erhalten wir insgesamt vier Tabellen. Davon beziehen sich die ersten zwei auf die sommerlichen Wolkenverhältnisse, während die zwei andere das winterliche Bild angeben.

Der Aufbau der Tabelle ist wie folgt: Die erste und zweite Kolonne enthalten die sich auf die entsprechenden Koeffizienten beziehenden n bzw. k Zahlen. In der dritten Kolonne finden wir die Werte der gewünschten b_{nk} Koeffizienten, während in der vierten Kolonne die nicht normalisierten u_{nk}-Werte figurieren und deren normalisierte Werte in der 5ten Kolonne zu finden sind. Die in der 6ten Kolonne angeführten Zahlenwerte geben an, welchen Prozentsatz der Streuung um den Mittelwert des Feldes die in Frage stehenden Polynome representieren, d. h. diese zeigen an, welcher von den Koeffizienten b_{nk} bei der Bechreibung des Feldes durch Tschebitscheff'sche Polynome in Betracht gezogen werden soll, bzw. sich als vorteilhaft dazu darbietet. Gleichzeitig gibt deren Summe an, mit welcher Genauigkeit wir das Feld beschreiben können. Die in der Tabelle unterstrichenen Zahlen geben an, welche Koeffizienten von uns bei der tatsächlichen Berechnung benutzt wurden. So bei der Beschreibung der östlichen Hälfte des sommerlichen Lagebildes benutzten wir die folgenden 14 Koeffizienten b_{00}, b_{01}, b_{10}, b_{40}, b_{50}, b_{02}, b_{03}, b_{04}, b_{11}, b_{41}, b_{51}, b_{42}, b_{23}, b_{34}, und erreichten dabei eine Beschreibung des Feldes mit 88%-iger Genauigkeit.

Bei der Beschreibung der westlichen Hälfte des Feldes benutzten wir bei der Berechnung die Koeffizienten: b_{00}, b_{10}, b_{20}, b_{60}, b_{31} b_{61}, b_{42}, b_{23}, b_{34}, b_{54}, b_{01} und mit diesen 11 Koeffizienten erreichten wir einer Genauigkeit von 92%.

Im Falle des weniger kompliziert erscheinenden winterlichen Bildes hatten wir bei einer 87%-tigen Beschreibung des östlichen Teilgebietes 16 Koeffizienten in Betracht zu ziehen; diese sind, wie folgt: b_{00}, b_{30}, b_{01}, b_{02}, b_{03}, b_{11}, b_{31}, b_{41}, b_{12}, b_{22}, b_{32}, b_{23}, b_{63}, b_{14}, b_{24}, b_{54}. In der Westhälfte bei der Beschreibung von Gebieten über dem Meer konnten wir die Darstellung des Bewölkungsfeldes mit der Benutzung von 17 Koeffizienten mit einer Genauigkeit von 92% durchführen.

φ \ λ	20° W	15°	10°	5°	0°	5°	10°	15°	20°	25°	30°	35° E
55° N	10 10	10 8	10 10	10 9	10 10	0 0	10 9	0 0(-1)	0 1	10 10	10 10	10 8
50°	10 10	10 10	10 9	0 2	0 1	0 0(-1)	10 9	4 4	4 6	10 8	4 5	7 8
45°	10 9	10 10	0 0	0 1	0 0(-1)	10 10	0 0	2 1	4 6	10 10	7 7	7 6
40°	4 5	7 6	0 0(-1)	0 3	0 0(-1)	0 0	0 1	0 1	0 0	0 0	0 3	4 5
35°	7 8	0 0	0 0(-1)	0 3	0 0(-2)	0 0(-2)	0 0	0 1	0 1	0 0	0 1	0 1

Tab. 5. Die beobachteten und berechneten Werte der Bewölkung (3ter Juli 1968)

φ \ λ	20° W	15°	10°	5°	0°	5°	10°	15°	20°	25°	30°	35° E
55° N	7 7	7 7	7 8	7 8	9 9	10 10	10 10	10 9	10 10	7 8	7 7	7 8
50°	7 6	10 9	4 4	7 7	10 10	4 4	7 7	10 10	7 8	7 7	7 6	9 7
45°	4 3	4 5	6 7	6 6	10 10	10 9	10 10	7 7	7 7	7 8	7 8	10 10(13)
40°	7 7	10 10	4 4	9 10	6 7	7 6	7 6	7 8	7 8	7 7	10 9	10 8
35°	7 6	4 5	4 4	6 5	4 4	4 4	4 4	4 4	4 5	7 7	7 7	4 4

Tab. 6. Die beobachteten und berechneten Werte der Bewölkung (13ter Februar 1968)

Die Werte der b_{00}-Koeffizienten sind wie folgt:

Juli 3. 1968		13. Februar 1968.	
Östliche Feldhälfte	Westliche	Östliche Feldhälfte	Westliche
3,52	4,23	7,40	6,83

Und jetzt wollen wir die in der Hydrometeorologischen Zentrale der Sowjetunion dargestellten, sich auf die oben behandelten zwei Wetterlagen beziehenden Neph-Analysen-Karten betrachten. Im Juli 1968 befindet sich im nordöstlichen Teil des untersuchten Gebietes ein Frontal-Wolkensystem; westlich von diesem Frontal-Wolkensystem – sich auf nahezu identisches Breitenintervall ausbreitend – befand sich ein Wolkenmassiv bestehend aus mehreren Schichten Eine ausgedehnte Wolkenzone konnte auch im nordwestlichen Teil des analysierten Gebietes wahrgenommen werden, während an den südlicheren Teilen des Gebietes – entsprechend dem Charakter der Jahreszeit – sehen wir nur geringe Bedeckungswerte.

Auch die Wolkenverhältnisse des untersuchten Wintertages zeigen keine einfache Struktur. Im zentralen Teil des Gebietes, besonders in der nördlichen Hälfte finden wir – der Neph-Analyse entsprechend – eine ausgedehnte, mehrschichtige Bewölkung. An der westlichen Grenze des Gebietes können sogar zwei Wirbelkerne herausanalysiert werden. In Gegensatz zum sommerlichen Bild zeigt sich eine Bewölkung auch in den südlicheren Breiten, besonders aber im südöstlichen Teilgebiet.

Es ist nun unsere Aufgabe nachzusehen, in welchem Masse der 5-Grad-Zerlegung das grossräumige Wolkenfeld representiert, sowie in welchem Masse die Zerlegung mittels Tschebitscheff'scher Polynome die realen Verhältnisse zu widerspiegeln im Stande ist.

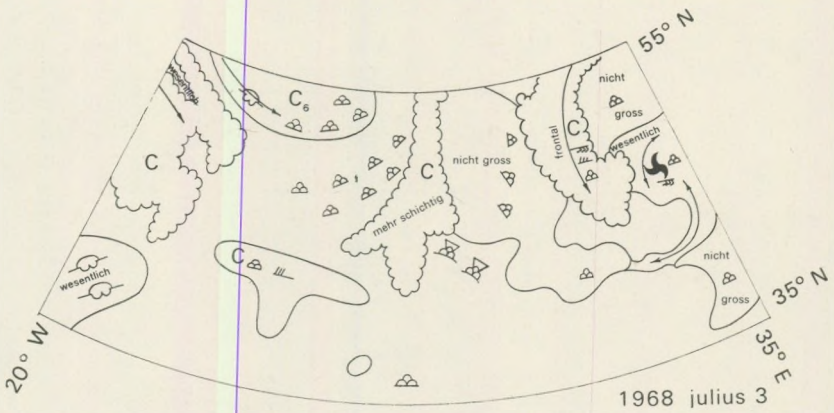

Abb. 2. 3ter Juli 1968

Zur Beantwortung der aufgeworfenen Frage zeigen wir die Verteilung der auf die Netzpunkte berechneten und der tatsächlich beobachteten Bewölkung. Das Bild für den 3ten Juli 1968 spiegelt genau die Struktur des grossräumigen Bewölkungsfeld wieder: an den bedeckten Gebieten finden wir hohe Feldwerte, während in den weniger bedeckten Gebieten kleine Werte anzutreffen sind. In der linken oberen Ecke der Tabellenfelder finden wir die analysierten Werte, während die rechte untere Ecke diejenige Werte enthält, die durch Anwendung der Formel (4) berechnet wurden. Auch die numerischen Werte des tatsächlichen und des berechneten Feldes zeigen gute Übereinstimmung und geben im wesentlichen die besprochenen Genauigkeitsgrenzen an.

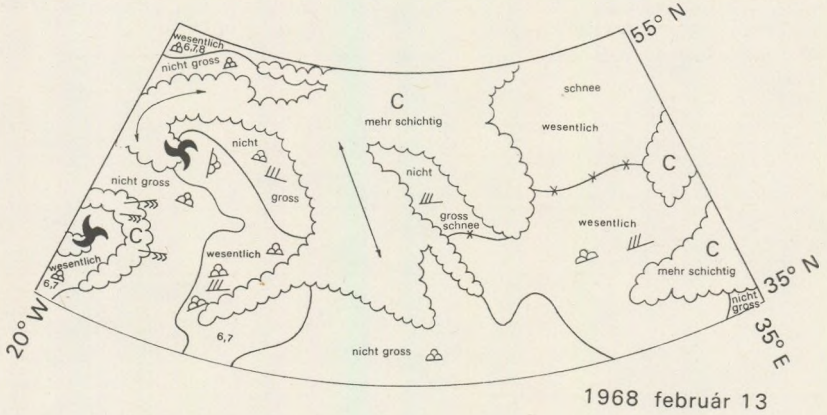

Abb. 3. 13ter Februar 1968

Gleichfalls finden wir eine genügende Beschreibungsart im Falle der winterlichen Bedeckungsverhältnisse am 13ten Februar 1968, hier ist sogar die Übereinstimmung noch grösser zwischen den berechneten und beobachteten Werten.

Aus der Auswertung der gezeigten Beispiele können wir diese Folgerungen ziehen:

1. Das grossräumige Bewölkungsfeld kann mit Hilfe der Tschebytscheff'schen Polynome mit gegebener Genauigkeit dargestellt werden.

2. Es ist zu hoffen, dass durch die Beschreibung mittels Tschebitscheff'scher Polynome von weiteren meteorologischen Feldern, zB. von absoluten und relativen Topographien sowie des Bodendruckes etc., und durch die Betrachtung der Koeffizientenwerte eine Mehrfachregressionsbeziehung zwischen dem Bewölkungsfeld und anderen meteorologischen Feldern gefunden werden könne.

3. Das angezeigte Verfahren kann auf maschinellem Wege und mit der von der Praxis erwünschten Schnelligkeit durchgeführt werden.

4. Die Beschreibung mittels Tschebytscheff'scher Polynome ermöglicht eine recht kompakte Speicherung der an das Wolkenfeld beziehenden Informationen.

5. Bei der Erforschung der analogen Wolkenfelder kann die Zerlegung mittels Tschebytscheff'scher Polynome als geeignetes Hilfsmittel gehandhabt werden.

LITERATUR

Cehak [1962]: Die Verwendung von orthogonalen Polynomen in der Meteorologie. Arch. f. Met. Geoph. u. Biokl. S. A. 12. 40 – 61.

Czelnai, R. and F. Rákóczi [1971]: Expansions of Certain Meteorological Fields in Chebyshev Polynomials. Annales. Sectio Geologica Tomus XV. 17 – 28.

Muszaeljan, S. A. and A. Z. Csekirga [1964]: O csiszlennij interpretacii informacii ob oblacsnoszti posztupajuscsej sz meteorologicseszkih szputnyikov. Trudi G. G. O. vüp. 166. 189 – 202.

Miller, R. G [1966]: Advanced topics of statistical prediction in meteorology. WMO. Techn. Not. No. 71. 115 – 133.

STRUKTUR- UND KOVARIANZ- FUNKTIONEN DES TEMPERATURFELDES DER 850 MBAR- OBERFLÄCHE ÜBER EUROPE

von

F. RÁKÓCZI, A. FARKAS-SZAKÁCS, and K. ORENDI

Institut für Meteorologie, Eötvös Universität, Budapest
Eingegangen: 13. März 1974

SUMMARY

Starting from the temperature field of the AT_{850} mbar surface empirical structure and covariance functions have been determined for the seasons. Using the functions obtained interpolation errors and weights have been computed.

Die Untersuchung der statistischen Struktur von meteorologischen Feldern ist wichtig sowohl aus theoretischen, wie auch aus praktischen Gründen. Im Besitze der, die statistische Struktur darstellenden charakteristischen Funktionen – der Struktur- und Kovarianz-Funktionen – können wir Aussagen machen, die auch für die Praxis unumgänglich notwendig sind. Wir können Fragen beantworten, wie jene einer rationellen Stationsdichte und Beobachtungssystems, wir sind im Stande, Interpolationsfehler anzutreffen, Interpolationsgewichte festzulegen und das Fehlerniveau der Berechnung territorialer Durchschnittswerte zu berechnen.

Zweck der betreffend das einheimische Temperaturbeobachtungsnetz durchgeführten Untersuchungen war es, die rationelle Verteilung der Stationen im Lande zu bestimmen [Czelnai et al. 1963]. In den Studien von Hrida [1968] und Boldürev und Hamarin [1967] wird über die Frage der Homogenität und Isotropie des bodennahen Temperaturfeldes und über die zur Anwendung gelangenden Untersuchungsmethoden berichtet. Karpov und Hamarin [1971] analysieren in ihrer Arbeit die Verhältnisse des europäischen Temperaturfeldes und – unter Berücksichtigung des Anisotropie- und Ahomogenitäts- Effekts – schlagen Separation in vier Gebiete vor. In der Arbeit von Lugina und Malasenko [1972] wird das Anomalienfeld der Temperatur vom Gesichtspunkt der Rationalisierung des Stationsnetzes behandelt. Melesenko und Guseva [1972] untersuchen die statistische Struktur des Feldes der Temperatur und des Taupunkts an der 850 und 700 Mbar – Fläche auf Grund der Daten von 60 Stationen aus drei Jahren. Die Berechnungen wurden unter der Annahme der Homogenität und Isotropie bezüglich des Feldes ausgeführt. Auch die – auf Grund des Temperaturfeldes des 500 Mbar-Niveaus auf

empirischen Weg bestimmte – Struktur- und Korrelations- Funktion wurde bekanntgegeben (C z e l n a i 1966).

In der hier vorgelegten Arbeit werden wir uns mit der statistischen Struktur des Temperaturfeldes des 850 Mbar-Niveaus befassen. Die statistischen Eigenschaften des Feldes werden hier durch die Berechnung von zwei charakteristischen Funktionen, der Struktur- und der Kovarianz-Funktion studiert. Für die Bestimmung der empirischen Funktionen werden wir vom Material der täglichen Topographiekarten – bezogen auf 00 GMT – ausgehen. Die betreffenden Funktionen werden in jahreszeitlicher Zerlegung bestimmt, wobei der Winter durch Januar, der Frühling durch April, der Sommer durch Juli und der Herbst durch Oktober bzw. durch die auf diese Monate beziehenden Kurven representiert wird. Die Anzahl der in Betracht gezogenen Stationen ist 59 und die betreffenden Funktionswerte werden für alle die möglichen 1711 Kombinationen bestimmt. Die benutzten Stationen liegen im Sektor $\varphi = 60° - 40°$ N und $\lambda = 5° - 35°$ E, so dass unsere Werte den europäischen Kontinent betreffen. Die gegebenen Abbildungen stellen die Werte der Funktionen nach einer Glättung auf Grund von Durchschnittswerten bezogen auf Kombinationsentfernungen von $\Delta\varrho = 150$ km dar. Selbsverständlich ist die Anzahl der Fälle in den einzelnen 150 km Entfernungskategorien verschieden. Die absolute Häufigkeit der in Rede stehenden Kombinationen wird in der Abb. 1. dargestellt: wir sehen hier, dass die Zuverlässigkeit der Kurven zwischen 300 und 2400 km genügend ist, da in diesem Gebiet eine Stationskombination-Anzahl von 13 – 183 für die Bestimmung eines Einzelwertes angebracht wird. Natürlich müssen wir bei der Bestimmung der Anzahl der Fälle die obige Zahl der Kombinationen mit der

Abb. 1.

Anzahl der verwendeten Situationen – so zB. für den Fall von Januar mit 93 etc. – multiplizieren.

Die Strukturfunktionen wurden auf Grund der Formel

$$b_T(\varrho) = \overline{[f'(\vec{r}) - f'(r + \delta r)]^2} \tag{1}$$

berechnet, wobei $f' = f - \overline{f}$ (der Strich über den Buchstaben bedeutet Durchschnittsbildung).

Die Bestimmung der Kovarianz-Funktion wird durch die Formel

$$\mathrm{cov}(f_i, f_j) = M[(f_i - \overline{f_i})(f_j - \overline{f_j})] \tag{2}$$

durchgeführt.

Die für die Jahreszeit bezogenen empirischen Funktionen weisen die in der Abb. $2/a-d$ erscheinenden Eigentümlichkeiten auf. Im Falle von gleichen Abständen (an der Abb. $0-2500$ km.) finden wir die höchsten Funktionswerte in Januar, die tiefsten in Juli. Die Werte der zwei Übergangsjahreszeiten befinden sich zwischen den Extremen so, dass die Oktoberwerte ähneln vielmehr dem Winterbild. Aus den Strukturfunktionenwerten is zu ersehen, dass der Baroklinitätsgrad der Atmosphäre an der 850 -mbar-Fläche im Winter grösser, im Sommer kleiner ausfällt. Ein am meisten ausgeglichenes Temperaturfeld ist an der Untergrenze der freien Atmosphäre im Sommer anzutreffen. Entsprechend den isobarischen Temperaturdifferenzen können wir sagen, dass im Durchschnitt die winterlichen thermischen Windkomponenten überwiegen die Sommerwerte, so dass wir mit den höheren Windänderungen mit der Höhe im Winter zu rechnen haben.

Auf Grund der die Zusammenhang der Feldwerte representierenden Kovarianzfunktionenwerte trat im Winter innerhalb der untersuchten Distanzen kein gegenläufiger Zusammenhang auf. Im Frühling, Sommer und Herbst die Funktionen nehmen negative Werte in den Entfernungen von 1800, 1600 bzw. 1950 km an. Der Abschnitt der Kurven bis zu 1200 km kann in den Monaten April und Oktober als quasi-linear angesehen werden. Im Winter, sowie im Sommer tritt auch an die Stelle des anfänglichen linearen Zusammenhangs eine kompliziertere Beziehung. Die Werte der Korrelationsradiussen fallen zwischen 950 (Juli) und 1300 (Januar) km. Das Verhalten der Kovarianzfunktionen entspricht, soweit es um deren Hauptcharakteristiken handelt, den von M a l a s e n k o und G u s e v a [1972] erhaltenen Resultaten, obwohl die von ihnen abgeleiteten Funktionen negative Werte im Falle von etwas grösseren Abständen annehmen.

Die empirischen Strukturfunktionen ermöglichen die Bestimmung der Interpolationsfehler. Die Jahreszeitlichen Werte der Interpolationsfehler wurden von uns für zwei Konfigurationen bestimmt: auf Grund von zwei Stationen für den Mittelpunkt des die Stationen verbindenden Geraden $E(\varrho)_{\max}$, nach Hrida und für den Fall von sechs Stationen

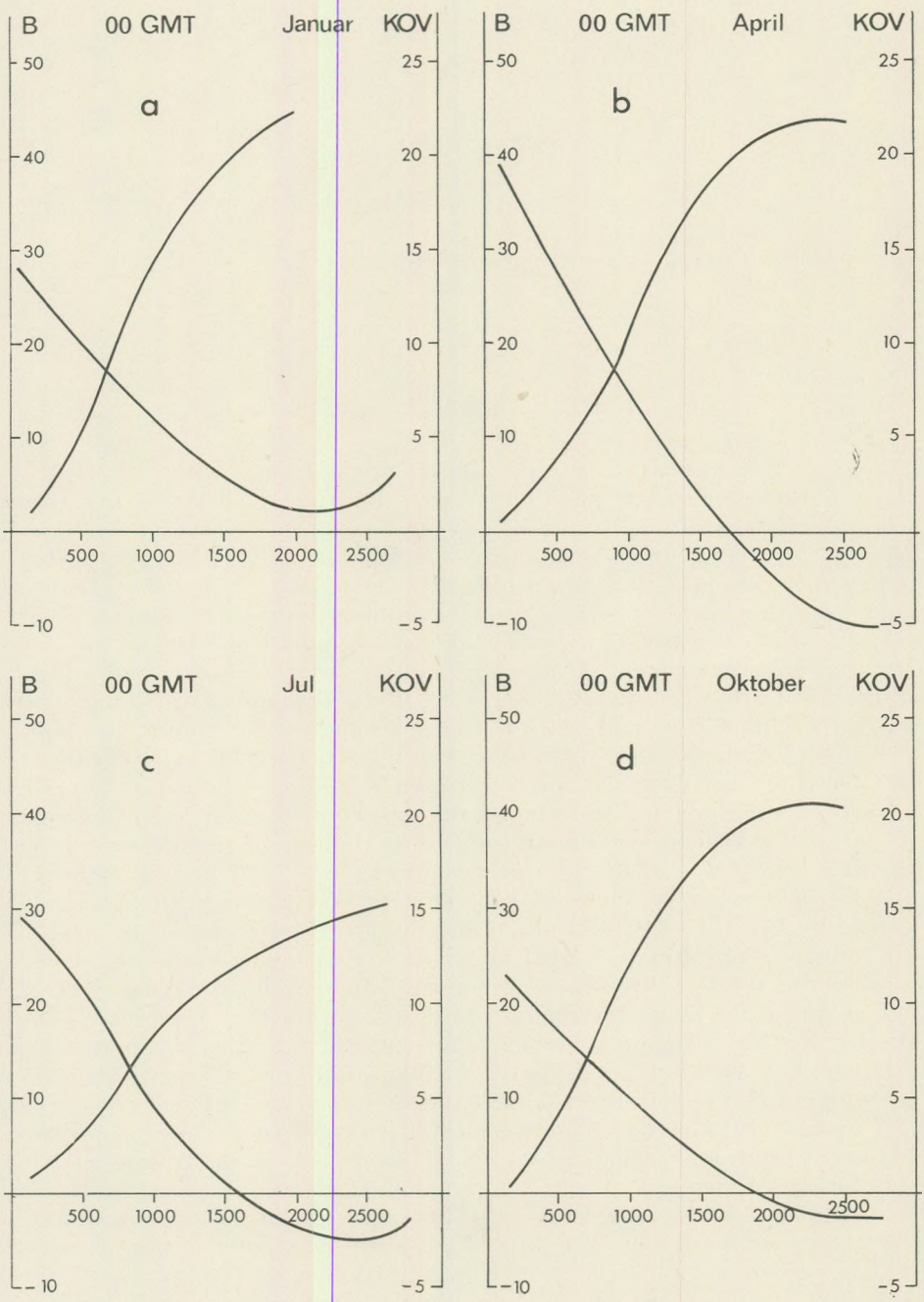
B
00 GMT
Januar
KOV
a
50
40
30
20
10
25
20
15
10
5
500
1000
1500
2000
2500
−10
−5
B
00 GMT
April
KOV
b
50
40
30
20
10
25
20
15
10
5
500
1000
1500
2000
2500
−10
−5
B
00 GMT
Jul
KOV
c
50
40
30
20
10
25
20
15
10
5
500
1000
1500
2000
2500
−10
−5
B
00 GMT
Oktober
KOV
d
50
40
30
20
10
25
20
15
10
5
500
1000
1500
2000
2500
−10
−5

Abb. 2.

für das Dreiecksnetz ($E(\varrho)_{\max}$ nach Guseva. Die Berechnung der Interpolationsfehler wird mit Hilfe folgender Formel ausgeführt:

$$E(\varrho)_{\max[2]} = b\left(\frac{\varrho}{2}\right) - \frac{1}{4}b(\varrho) \tag{3}$$

$$E(\varrho)_{\max[6]} = b\left(\frac{\varrho}{2}\right) - \frac{1}{6}\left[b\left(\frac{\varrho}{2}\right) + b\left(\frac{\sqrt{3}}{2}\varrho\right) + \frac{1}{2}b(\varrho)\right] \tag{4}$$

Die Resultate der Berechnung werden in der Tabelle I. dargestellt.

Tabelle I

Monat	200		500		1000		1500	
	km							
	1	2	1	2	1	2	1	2
Jan.								
April								
Juli								
Okt.								

1 = $E(\varrho)$ [2]; 2 = $E(\varrho)$ [6].

Es ist zu ersehen, dass die Interpolationsfehler vergrössern sich mit der Erhöhung der Distanz in allen Jahreszeiten, die Vergrösserung ist aber nicht linear. Der Wert der auf Grund von sechs Punkten berechneten Interpolationsfehler – besonders im Falle von grösseren Distanzen – ist kleiner, wie diejenige berechnet auf Grund von zwei Punkten. Mit den kleinsten Interpolationsfehlern können wir im Juli, mit den grössten im Januar rechnen. Unsere Resultate bestätigen die bekannte Tatsache, dass in dem in Rede stehenden Gebiet genügend genaue Karten mit Hilfe der bei der zahlenmässigen Vorausberechnung üblichen Netzpunktwerte hergestellt werden können.

Bezüglich der ziemlich verwickelten Frage der Interpolationsgewichte, wir haben mit Berücksichtigung der Strukturfunktionenwerte auf Grund von nur zwei Punkten Interpolationsgewichte errechnet. Die in Frage stehenden Berechnungen wurden für die Monate Januar und Juli ausgeführt. Die Ableitung der bei den Berechnungen gebrauchten Formeln

$$p_1 = \frac{1}{2}\left(1 + \frac{b_{02} - b_{01}}{b_{12}}\right): \qquad p_2 = \frac{1}{2}\left(1 + \frac{b_{01} - b_{02}}{b_{12}}\right) \tag{5}$$

kann in G a n d i n, 1970 nachgesehen werden. Hier b_{01} bedeutet denjenigen Funktionswert, der der Distanz zwischen dem Teilungspunkt und dem Endpunkt angehört und dem Endpunkt näher liegt, während b_{02}

den von dem Endpunkt weiter entfernteren Punkt gehörigen Wert bezeichnet; b_{12} aber den der Distanz der zwei Punkte angehörigen Strukturfunktionswert darstellt.

Wie wir sehen, die optimalen Interpolationsgewichte p_1, p_2 sind normalisierte Werte. Durch Anwendung von (5) bestimmten wir die in Rede stehenden Gewichtswerte für einigen Teilungspunktkombinationen. Die Resultate der Berechnungen sind in der Tabelle II. dargestellt.

Tabelle II

km	200	400	600	800	1000
		. . .			
		Juli			

Der Aufbau der Tabelle soll hier erläutert werden. In der Hauptdiagonale befinden sich die zum Halbierungspunkt der betreffenden Distanz gehörenden Gewichte. In diesem Falle die „optimalen" Gewichte stimmen mit dem Gewicht der linearen Interpolation überein, und ihr Wert ist selbstverständlich: $p_1 = p_2 = \frac{1}{2}$. Rechts von der Hauptdiagonale sind die p_1 – links von ihr die p_2 – Gewichte angebracht, und zwar so, dass zB. für die Abschnitte, die den $200+400 = 600$ km langen Abstand auf 200 und 400 km Distanzen aufteilen, das Gewicht p_1 als zweiter Wert der ersten Zeile angegeben wurde, während der Gewichtswert $p_2 = 0{,}359$ als zweiter Wert der ersten Kolonne figuriert. Ähnlicherweise im Falle des Punktes, der die 800 km Distanz auf die Abschnitte $200+600$ km aufteilt, der zum 200 km Abstand gehörige $p_1 = 0{,}742$ Wert als dritter Wert der ersten Zeile erscheint, der entsprechende $p_2 = 0{,}258$ aber befindet sich in der dritten Zeile der esten Kolonne.

Weiterhin, der Gewichtsfaktor $p_1 = 0{,}613$, der dem 400 km Abschnitt des Teilungspunktes gehört, welchen die 1000 km Distanz auf $400+600$ km – Abschnitte aufteilt, figuriert als dritter Wert der zweiten Zeile der Tabelle, während der Wert $p_2 = 0{,}387$ in der dritten Zeile der zweiten

Kolonne ansässig ist. Alle diese Beispiele beziehen sich auf die Januarwerte.

Der Aufbau der Tabelle II. – Juli ist völlig dem der Januar – Tabelle analog. Es ist zu ersehen, dass die Berücksichtigung der statistischen Struktur des Felds ein wichtiger Faktor im Falle der Berechnung der Interpolationsgewichte ist. Gandin [19] leitete auch eine Formel her, die auch für die Berechnung von Interpolationsgewichten geeignet ist, die sich auf eine verwickeltere Konfiguration beziehen. Die Representation der Auswertung von diesen ist aber ziemlich kompliziert, so dass wir diese hier nicht behandeln werden.

LITERATUR

Czelnai, R., Dési, F. and Rákóczi, F.: 1963, On the determination of the rational density of the temperaturmeasuring network. Időjárás, 67. 129 – 139.

Czelnai, R. (1966): On the Statistical Structure of Meteorological Fields. Gerlands Beiträge zur Geophysik 75. 129 – 153.

Хрига, И: О статистической структуре приземного поля температура воздуха на территории Чехии и Моравии. Időjárás 72. 1968. 210 – 215.

Болдырев В. Г., Хамарин В. И.. К вопросу об однородности и изотропности поля приземной температуры. Труды. Г. М. Ц. 1967. вып. 11. 159 – 168.

Карпов А. В., Хамарин В. И.: О статистических характеристиках поля приземной температуры на территории Европы. Труды Г. М. Ц. 1971. вып. 89. 35 – 49.

Лугина К. М., Малашенко Л. Я.: Пространственная корреляция аномалый температуры воздуха и использование ее при рационализации сети станций. Труды Г. Г. О. 1972 вып. 286. 26 – 39.

Гандин. Л. С.: Задача об оптимальной интерполяции. Труды Г. Г. О. вып. 99. 67 – 76.

BAJOCIAN (MIDDLE JURASSIC) SECTIONS FROM THE NORTHERN BAKONY (HUNGARY)

by

A. GALÁCZ

Department of Paleontology, Eötvös University, Budapest
Received: 15 March, 1974

РЕЗЮМЕ

Речь идет о биостратиграфической интерпртации четырех профилей, относящихся к среднему юрскому периоду, находящихся в серевной части гор Баконь. Наиболее полная байоцская сория была обнаружена в залеже холма Локут. Аммонитовая фауна, состоящая из 16 000 образцов, и являющаяся основой разделения по зонам и субзонам, может быть рассмотрена как первостепенно важная с точки зрения медитерранской средней юры.

В остальных сильно прерывистых профилях было обнаружено намного меньше палеонтологических остатков, однако и они хорошо коррелировались с ранее иследованными и с локутскими образцами

На основании исследования фауны было найдено, что в профилях-байоц гор Баконь рамыми распоостраненными являются зоны Стефаносерас хумприесинум, а зоны нижнего и верхнего байоца часто отсутствуют.

Introduction

The Middle Jurassic of the Transdanubian Central Mountains, including the Bakony, have been reviewed recently in three comprehensive works. In his synthesis prepared for the Mesozoic Conference of Budapest N o s z k y jun. (1961) listed the localities, rock-types and presented the sequence of several occurences in profiles. V a d á s z (1960) in his book "The Geology of Hungary" summarized the available data about the Jurassic of the Transdanubian Central Mountains, and presented some faunal lists. In his account introduced on the Mediterranean Jurassic Colloquium in 1969, F ü l ö p (1971) dealt with the Middle Jurassic too, mainly from the point of view of microfaunistic studies.

On the basis of the above mentioned works and the faunas collected recently from some new localities, it is proved, that among the Middle Jurassic stages the Bajocian is the one represented by ammonite-bearing limestones on larger areas. The Aalenian is known from some localities (e.g. Csernye), and only a single occurence of the Bathonian ammonitic limestone facies (Gyenespuszta, G a l á c z 1970) have been found. In other places the Bathonian is known as radiolarite, containing microfauna exclusively. The Callovian of the Bakony Mountains developed in radiolaritic facies.

The detailed biostratigraphy of the Bajocian of the Bakony Mountains have been concerned in two works. In connection with the treating the Aalenian ammonites of Csernye, Géczy (1967a, b) proved – on the basis of a poor fauna – the presence of the Sonninia sowerbyi Zone. On the other hand, in the lower part of the Middle Jurassic section of Gyenespuszta a well dividable Middle and Upper Bajocian sequence have been known, with rich ammonite fauna (Galácz 1970).

During the years 1969–1973 the staff of the Geological Survey of Hungary collected the faunas of several Middle Jurassic sections in the Bakony Mountains. This extremely rich material, encountered through precise collection work, enables the more detailed cognition of the Bakony Mountains' Bajocian.

This present paper deals with the subdivisioning and parallelization of the Bajocian sections known previously from scattered references of the literature. The paleontological and more detailed stratigraphical results of the fauna consists of more than 17.000 ammonite specimens are the bases of subsequent publications.

The studied sections are situated in the Northern Bakony (Fig. 1.). The Lókút section belongs to the so-called continuous, or basinal sequences, and the others (Somhegy-hill, Közöskút- and Kisnyerges-ravine) into the group of discontinuous, or "sea-mount" sequences.

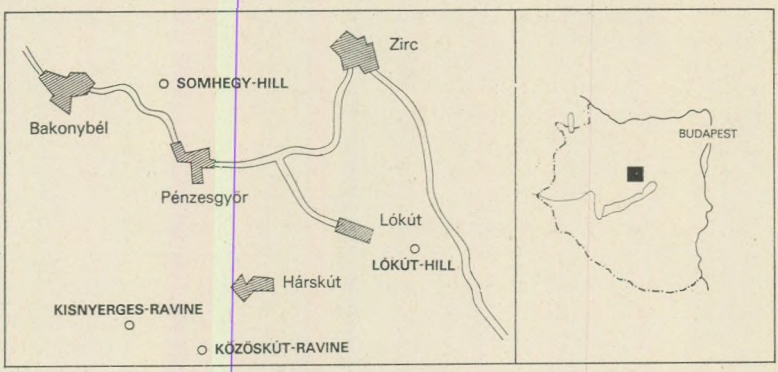

Fig. 1. Sketch-map of the locations of the studied Bajocian sections in the Northern Bakony

Study of the sections

Lókút

The Jurassic sequence of the Lókút-hill is well known from the Hungarian geological literature long before, but only the lower part, containing Liassic faunas have been treated so far.

The first to mention the locality of the Bajocian ammonites was Telegdi-Roth (1934, p. 217). On the basis of some listed ammo-

nites *(Phylloceras nillsoni* H é b., *Cadomites bayleanus* O p p., *Cadomites brodiaei* S o w.) he suggested the presence of the Middle Jurassic Stephanoceras humphriesianum Zone.

K o n d a (1970) reexamined the Middle Jurassic rocks of the area in detail, and on the basis of some newly collected ammonites (graphoceratids and stephanoceratids – determinations by B. G é c z y) he proved the Upper Aalenian and the Lower and Middle Bajocian.

From 1970, under the direction of J. K o n d a, a large-scale, layer by layer collection work started at the SW margin of the Lókút hill, SW of the original locality of K. T e l e g d i-R o t h. The excavated sequence and the extremely rich fauna made the clearing up of the stratigraphical and successional situation possible.

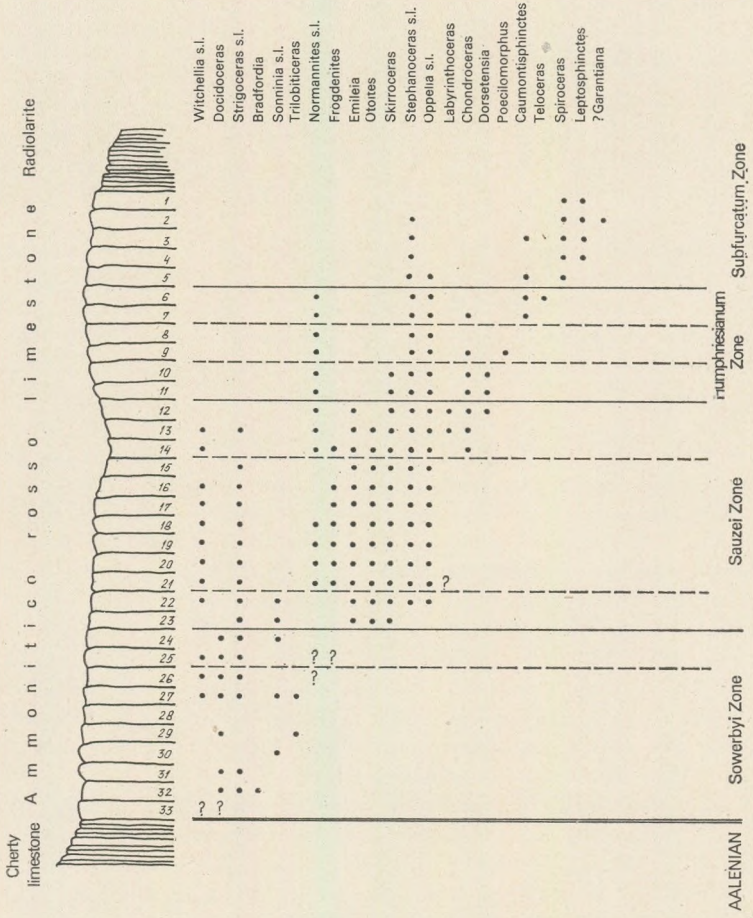

Fig. 2. The Bajocian sequence of the Lókút-hill locality, with the characteristic ammonite genera (in order of their appearance)

Succession

The uppermost part of the Liassic sequence forming the mass of SW portion of the Lókút hill is the so-called cherty, Paleotrix-Radiolaria-bearing limestone, lacking megafossils. It is the overlying rock of the Toarcian manganiferous sequence, therefore it is regarded conditionally as of Aalenian (c.f. Fülöp et al. 1969, p. 59, Fig. 17; Konda 1970 p. 171, Fig. 2). The unfossiliferous cherty beds are overlain by the Bajocian ammonitic limestone in 6 m thickness. This limestone sequence is built up by irregularly alternating more marly and more calcareous beds. In the upper part of the section the lithological characters vary continuously, together with simultaneous faunal impoverishment. Above a few decimetre thick, transitional faunal-free group of layers, follows the Bathonian-Callovian radiolarite.

Fauna and zonation

The collection work from the 33 ammonitic beds yielded an enourmous material. Beside of the 16.465 (!) ammonite specimens, collected from a 19 m^2 surface on average, 10 nautiloids, about 400 belemnite rostra, 212 *Inoceramus* sp. and 31 *Anisocardia* sp. bivalves and 17 echinoid *(Orbignyana* spp.) occured.

The overwhelming majority of the ammonite fauna (about 85%) is constituted by phylloceratids and lytoceratids. In the stratigraphical evaluation, however, only the diagnostic Ammonitina are considered and tabulated (Fig. 2.). Taking the preliminary character of this paper into consideration, the determinations in the text and figures are confined to generic level.

Sonninia sowerbyi Zone. The lower ten beds (Nos. 33–24.) of the section yielded a poor fauna suggesting the presence of the Sowerbyi Zone. Beside of some *Sonninia* and *Witchellia* specimens characteristic elements are the *Strigoceras*, *Bradfordia*, *Docidoceras* and *Trilobiticeras* species. The presence of *Trilobiticeras* was to be expected, because earlier, from the adjacent old section of Telegdi-Roth a specimen of this genus was encountered (Galácz 1971).

In spite of the poor fauna the subdivision within this zone seems to be recognizable. The *Bradfordia* and *Trilobiticeras* specimens, characteristic to the lower, Discites Subzone, can be found in the lower beds (Nos. 33–26), while the upper beds, No. 25. and 24. yielded only some *Strigoceras* and *Sonninia* specimen. These latter two beds presumably represent the Laeviuscula Subzone.

Otoites sauzei Zone. Going upwards in the Bajocian section of Lókút, the first *Otoites* and *Emileia* specimens occur in the Bed No. 23; conclusively the boundary of the Sowerbyi and Sauzei Zones is indicated between the Beds No. 24 and No. 23. The zonal index *Otoites* genus forms a gradually enriching group, but from Bed No. 20 upwards its species and specimen number decreases. The last, fragmentary *Otoites* sp. indet. specimen is yielded from the Bed No. 13.

The representatives of the genus *Emileia* from the Bed No. 23 up to the Bed No. 12 form a consistently very rich group. Additionally common forms are in the middle beds the species of the genus *Frogdenites* and in the upper part of the zone (Beds Nos. 13–12) the *Labyrinthoceras* species.

In the middle portion of the zone appear the stephanoceratids, with the genera *Stephanoceras, Skirroceras* and *Normannites* s. l.

In the lower part some late species of the characteristic Sowerbyi Zone genera *Sonninia* and *Witchellia* are also present. The first *Dorsetensia* species [*D. liostraca* Buckm., *D. deltafalcata* (Quenst.)] appear as early as the uppermost bed of this zone.

On the basis of this faunal sequence it is probable a threefold subzonal subdivision of the Sauzei Zone. Its lower part is characterized by the *Sonninia* and *Witchellia* species, the middle part by the abundant *Otoites, Frogdenites* and the earliest Stephanoceratidae, and the upper part by the *Labyrinthoceras* and the first *Dorsetensia* species.

Stephanoceras humphriesianum Zone. The lower boundary of the zone can be drawn at the base of the Bed No. 11, where the earlier dominant Otoitidae are replaced by the Stephanoceratidae. The great specimen and species number of the genera *Stephanoceras* and *Normannites* are characteristic throughout in the zone; the additional elements are the *Dorsetensia, Chondroceras* and oppeliid species. The upper boundary of the zone is recorded by the abrupt decline of the stephanoceratids between the beds Nos. 5. and 6.

The lower part of the Humphriesianum Zone is marked in the Lókút section by the genus *Dorsetensia*. In the middle part the massive appearance of the various *Stephanoceras* species and the enrichment of the *Chondroceras* is characteristic. It is interesting to note, that the single *Poecilomorphus* specimen came from the Bed No. 9, i.e. from the middle part of the zone. It can be regarded an extremely lucky found, because beside this specimen this bed yielded 1.235 other ammonites.

In the upper part of the Humphriesianum Zone characteristic elements are the *Teloceras* and the earliest representatives of the superfamily Perisphinctaceae. In these same beds are forms which can be regarded as transitions between the genera *Stephanoceras* and *Cadomites*. These forms survive into the Subfurcatum Zone. This is a group untreated so far, and comprises forms which were alternately determined as *Stephanoceras* or as *Cadomites*, but lacking the precise stratigraphical control, their exact systematic arrangement was uncertain. A presumably similar "*Cadomites*" fauna is that mentioned by Arkell (1965, p. 264.) from North Africa.

The Humphriesianum Zone of Lókút shows a threefold character. Similarly three subzones were recognized by Pavia and Sturani (1968) in the section of Digne (SE France). The lower, "Poecilomorphus" Subzone of these authors cannot be identified in the Lókút section, because the single *Poecilomorphus* specimen came from the middle part of the zone. On the other hand the middle, "Stephanoceras" Subzone of

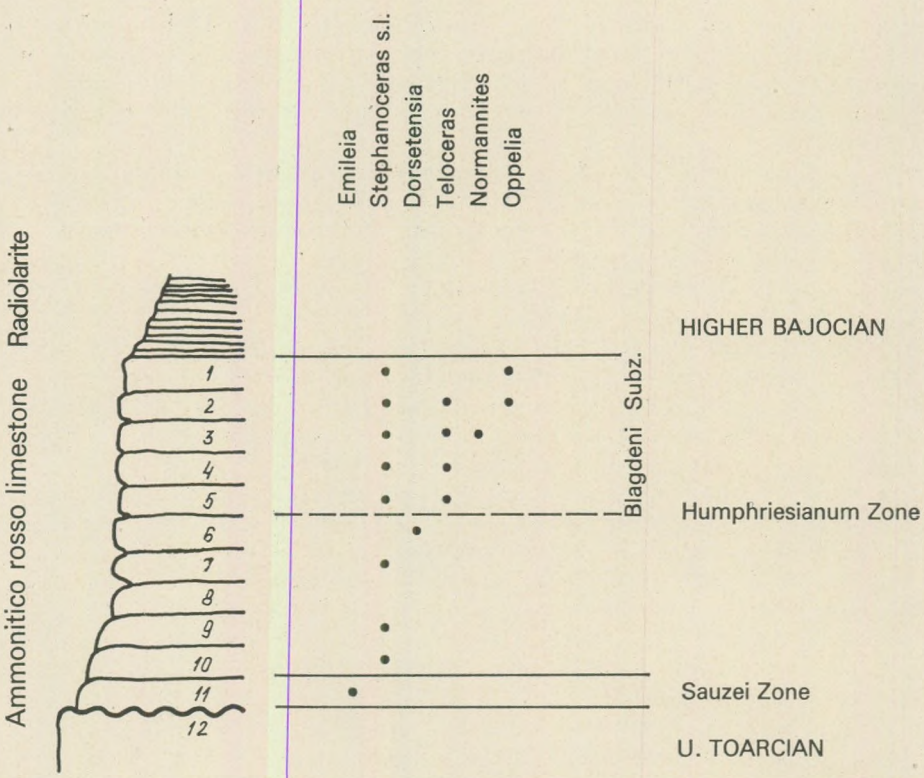

Fig. 3. The Bajocian section of the Közöskút-ravine, with the characteristic ammonite genera (in order of their appearance)

P a v i a and S t u r a n i is recognized at Lókút, on the basis of the rich *Stephanoceras* and *Normannites* fauna. The presence of the upper subzone of the Humphriesianum Zone is evidenced by the subzonal index *Teloceras blagdeni* (S o w.). This subzone comprises the Beds Nos. 7 and 6, where the earliest representatives of the perisphinctids (*Leptosphinctes* spp., *Caumontisphinctes* spp.) appear in relatively great specimen and species number. The beds characterized by similar fauna were placed by P a v i a (1971) into the lower Subfurcatum Zone. It seems more reasonable to drow the boundary of the Humphriesianum and Subfurcatum Zones with the disappearance of the genera *Stephanoceras*, *Normannites* and *Teloceras*, and to regard the earliest appearance of the perisphinctids within the Humphriesianum Zone, because the first representatives of the superfamily Perisphinctidae occur, outside of Europe, as early as in the Sauzei Zone (e.g. I m l a y 1973).

S t r e n o c e r a s s u b f u r c a t u m Z o n e. From the Bed No. 6. upwards – apart from the *Stephanoceras-Cadomites* transitions mentioned above – the number of the stephanoceratids diminishes comp-

letely. In the gradually poorer fauna besides the badly preserved *Leptosphinctes* and *Caumontisphinctes* species a few *Spiroceras* and in Bed No. 2 a single *Garantiana?* sp. indet. occur.

Owing to the poor state of preservation and small specimen number the subzonal-division cannot be traced.

Somhegy-hill

The Middle Jurassic of the Somhegy-hill, situated East of the village Bakonybél, on the northern side of the road to Pénzesgyőr, is well-known from the Hungarian geological literature. The first list of the ammonites collected from this locality was published by P a u l (1862, pp. 228 – 229). His determined species were as follows (with the probable modern names in brackets):

Ammonites ptychoicus Q u e n s t. (=*Ptychophylloceras* sp.)
A. Zignodianus d' O r b. (*Holcophylloceras* sp.)
A. Kudernatschi H a u. (*Phylloceras* sp.)
A. dimorphus d'O r b. [*Dimorphinites dimorphus* (d'O r b.)]
A. biplex S o w. (= ? *Leptosphinctes* sp.)
A. Achilles d'O r b. (= ? *Leptosphinctes* sp.)

As noted by P a u l, the phylloceratids („Heterophyllen") form the majority of the fauna.

In spite of this early contribution to the Middle Jurassic of the Somhegy-hill, this sequence remained unknown for the following geologists. S c h a f a r z i k (1890) studied a profile on the Somhegy-hill, but did not mention the Middle Jurassic rocks. T a e g e r (1912a, b) similarly missed these beds from his treaties.

During his revisions N o s z k y jun. (1943) found the Bajocian beds, and indicated the rich fauna. Beside of the Posidonomyas he mentioned *Phylloceras* spp. and *Sonninia*. From an other, hitherto unknown locality of the Somhegy-hill he recorded *Stephanoceras*, *Phylloceras*, *Sphaeroceras*, *Morphoceras* (=*Dimorphinites?*) and *Perisphinctes* (s. l.) genera, and *Spiroceras bifurcatum* Q u. and *Apsorroceras baculatum* Q u.

Recently K o n d a restudied the Jurassic sequence of the Somhegy-hill (1970, p. 187). In the neighbourhood of the point 649.6 m he excavated the Triassic-Jurassic rocks and recorded some ammonites, by the determinations of B. Géczy. These ammonites (*Stephanoceras* sp., *Nannolytoceras* sp., *Holcophylloceras mediterraneum* (N e u m.) and *Sphaeroceras* sp.) suggested the presence of the Upper Bajocian.

During the Mediterranean Jurassic Colloquium held in 1969 in Budapest, J. W e n d t examined the fauna, and preliminarly, without knowing the succession precisely, recognized as a fissure-infilling association (W e n d t 1971, p. 125).

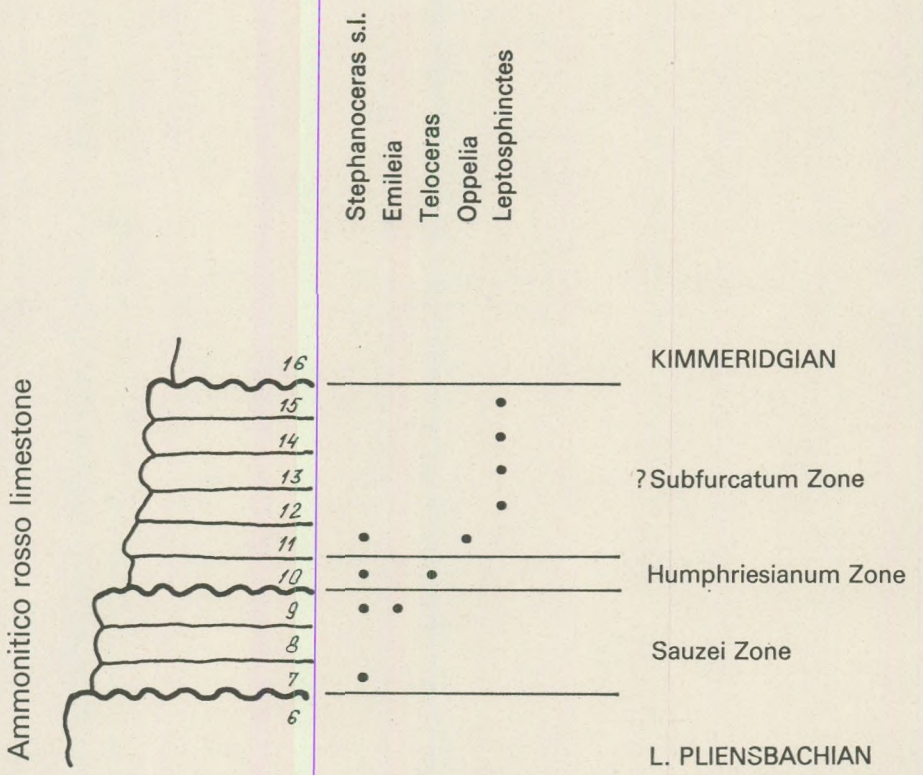

Fig. 4. The Bajocian section of the Kisnyerges-ravine, with the characteristic ammonite genera (in order of their appearance)

Succession

On the basis of the material collected under the direction of J. K o n d a from the excavation near the point 649.6 m on the Somhegy-hill, it was impossible to reconstruct the actual rock-succession. In the meantime the excavation was destructed and the exact location of the smaller faunal collections became unidentifiable.

During the field work for his graduate thesis geologist-student J. S z a b ó collected a large Middle Jurassic gastropod fauna, and by his studies, a part of the old collections can be evaluated.

According to the communications of K o n d a and S z a b ó the Lower Liassic limestone of Dachsteinkalk-type is overlain, on the Somhegy-hill, by the red, nodular, ammonitic Bajocian limestone. Within the Dachsteinkalk-type limestone there is a gradually attenuated fissure of about 60 cm in thickness, filled with reddish, manganiferous limestone, and yielding Bajocian fossils. Upon the red, nodular, ammonitic limestone rests the Kimmeridgian limestone, with *Aspido-*

ceras and other ammonites. This is, therefore, a highly condensed sequence, suggested not only by the stratigraphic record, but by the sedimentologic features, too (uneven, manganese-encrusted hard-ground of the Dachsteinkalk-type limestone, the fissure-infilling etc.).

Fauna and zonation

Within the red, nodular, ammonitic limestone overlying the Dachsteinkalk-type limestone, two Bajocian zones can be recognized (Fig. 5.). The ammonites yielded by the lower 3 beds are as follows:

Phylloceras sp.
Calliphylloceras sp.
Lytoceras sp.
Eurystomiceras polyhelictum (B ö c k h)
Oppelia sp.
Lissoceras semicostulatum B u c k m.
Stephanoceras spp.
Normannites spp.

Beside of the ammonites some *Inoceramus*, brachiopods, belemnites and echinoderms also occur.

This is a faunal association characteristic to the ammonitico rosso limestones, and suggests the middle Humphriesianum Zone. In the relatively rich group of ammonites the phylloceratids are in majority. These 3 beds is followed by a lithologically similar member, consisting of 5 beds, which contains a poorer fauna. The following ammonites were encountered:

Phylloceras sp.
Holcophylloceras mediterraneum (N e u m.)
Lytoceras sp.
Eurystomiceras polyhelictum (B ö c k h)
Dimorphinites dimorphus (d'O r b.)
Parkinsonia spp. indet.

In the lower bed (No. 5) the *Dimorphinites* is characteristic, while very poorly preserved *Parkinsonia* specimens came from this same (No. 5), and from the uppermost (No. 1) bed. On the basis of the presence of *Dimorphinites dimorphus* (d'O r b.) this upper five beds can be ranged into the upper part of the Parkinsoni Zone (c.f. G a l á c z 1970).

Between the lower three and the upper five beds a considerable hiatus can be recognized, which endures from the upper Humphriesianum up to the middle Parkinsoni Zone. The indicating of this missing record is represented in the fissure-infilling within the Dachsteinkalk-type limestone. This infilling yielded a very rich gastropod fauna, and an ammonite-assemblage, indicating the Subfurcatum and Garantiana Zones. The specimens are coated by manganese layers and are of excel-

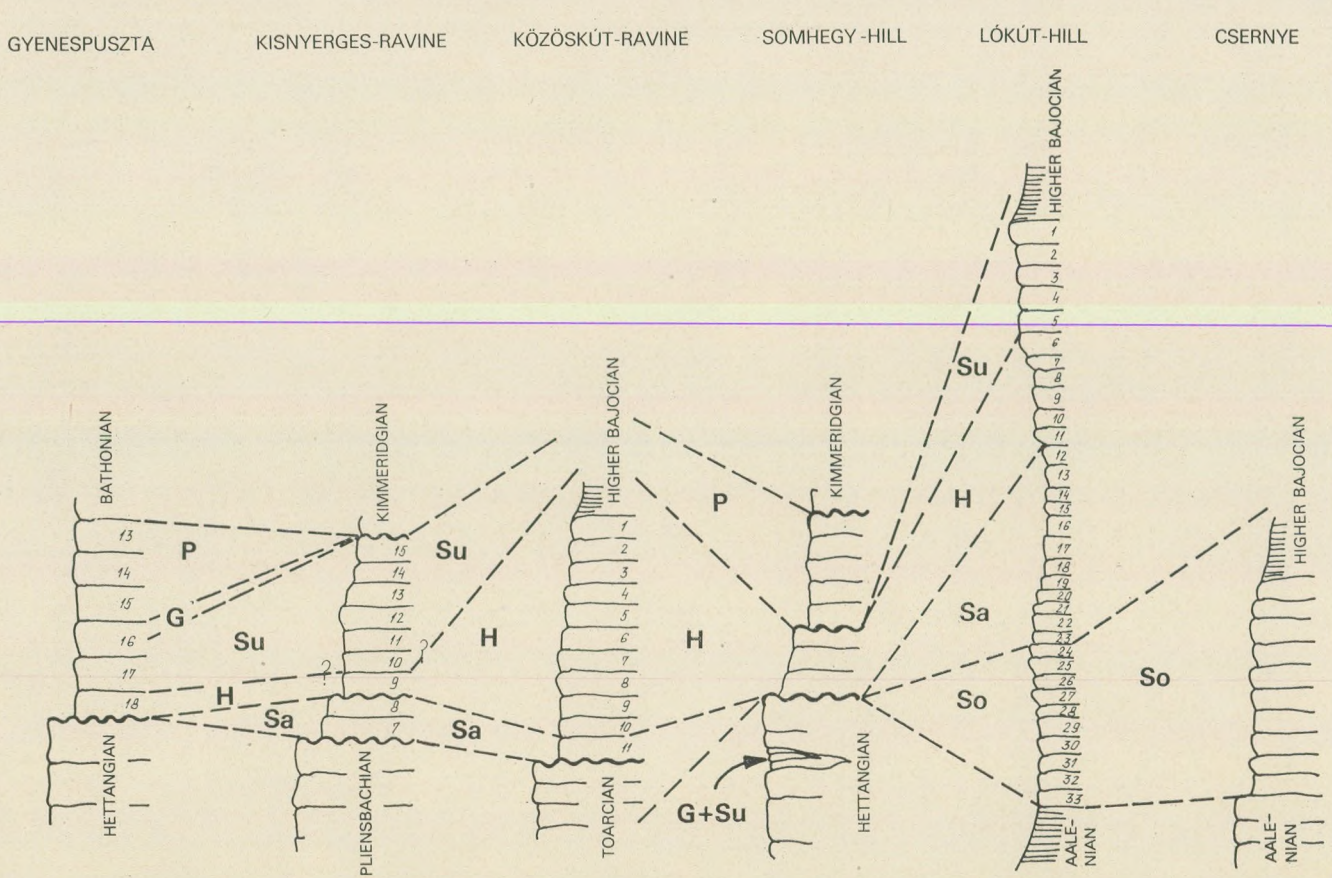

Fig. 5. Stratigraphical correlation of the Bajocian sections of the Northern Bakony (not to scale!)

lent preservation. The preparation from the matrix, however, is difficult, because under thin layer of manganese these specimens are filled with sparry calcite. The determinated forms are as follows:

Phylloceras sp.
Partschiceras sp.
Holcophylloceras sp.
Lytoceras sp.
Eurystomiceras polyhelictum (B ö c k h)
Oecotraustes (O.) genicularis W a a g e n
Sphaeroceras brongniarti (S o w.)
Sphaeroceras spp.
Spiroceras sp.
Garantiana sp. indet.

This fauna indicates the Subfurcatum and Garantiana Zones, but the answer to the question: whether it is a regular succession of the layers of the two zones, or a faunal mixture, needs a further, refined collection. In any case, the recognition of W e n d t (1971, p. 125) is proved: the condensed fauna contained in this "S-fissure" represents in part, or as a whole, the zones missing in the succession of the red nodular limestone. The fauna cannot regarded as a dwarfed fauna. It is constituted partly by specimens cf small-sized species *(Oecotraustes, Sphaeroceras, Eurystomiceras)*, and partly by young (wholly chambered) specimens of larger species *(Phylloceras, Lytoceras, Spiroceras)*.

Besides the ammonites the gastropods, bivalves and echinoderm-spines are abundant in the fauna. Further collections can make a detailed study on the whole fauna and the paleoecological conditions possible.

Közöskút-ravine

The Közöskút-ravine is a glen which runs SW about 2.5 km from the village Hárskút, bordering westerly the Borosthánhajag-hill.

The first to record the exposed Jurassic rocks of this locality was N o s z k y jun. (1943). He dealt with the Lower Jurassic sequence, and mentioned the presence of Middle Jurassic rocks. Later, in his 1:25.000 geological map of the Northern Bakony (1957) he recorded, besides the Liassic and Upper Jurassic, Dogger "Massive limestones" too. In his rewiew on the Jurassic rocks of Hungary (1961) also N o s z k y mentioned the Közöskút-ravine as one of the localities of the Aalenian-Bajocian manganese-nodulous, Cephalopod-bearing rocks and figured the outlined profile of this section.

In the Excursion Guide for the Mediterranean Jurassic Colloquium (F ü l ö p et al. 1969) a detailed profile demonstrated the locality, and the description presented the succession and the lithology. K o n d a

(1970) also treated this locality, and called the attention to the importance of this discontinuous sequence.

Recently a layer by layer collection work was made, which resulted a relatively rich material.

Succession

In the Közöskút-ravine, within the sequence exposed in the creek bed, the Upper Toarcian uppermost bed (No. 12) of the discontinuous Lower Jurassic is disconformably overlain by the Bajocian beds. The thickness of the 11 Middle Jurassic beds is 133 cm. The overlying rock of the red, nodular, ammonitic limestone is the Bathonian-Callovian radiolarite, but the boundary of the two different rock-type is unexposed in the section. On the other hand, by the oral communication of N o s z k y jun. it is expected that the section will yield limestone beds beneath the radiolarite with younger Bajocian, or Lower Bathonian faunas.

Fauna and zonation

In the Bajocian ammonite fauna of Közöskút-ravine, similarly as in the other Jurassic faunas from the Bakony Mountains, characteristic is the predominance of the phylloceratids and lytoceratids. Here these forms represent a 60% from the 271 Bajocian specimens. The additional faunal elements are subordinate, only a single *Inoceramus* sp. (Bed No. 10), a single nautilid (Bed. 11) and some belemnite fragments occur.

On the basis of the study of the stratigraphically diagnostic Ammonitina, two Bajocian zones can be recognized within the section (Fig. 3). The Bed. No. 11, i.e. the lowermost Bajocian layer yielded an extremely poor fauna, but the single *Emileia* sp. specimen certainly suggest the presence of the Otoites sauzei Zone.

The other beds (Nos. 10 – 1) seem to range into the Stephanoceras humphriesianum Zone, on the basis of the several species of the abundant *Stephanoceras* and *Normannites* genera. The threefold subdivision of the zone is untraceable here. The occurence of the *Teloceras* in the upper beds (Nos. 5 – 1) suggests the Teloceras blagdeni Subzone. The lower boundary of the subzone can be drawn between the Beds Nos. 6 and 5, because the large *Dorsetensia* sp. specimen yielded from the Bed No. 6 represents the middle Humphriesianum Zone. The subzonal arrangements of the lower beds are uncertain.

Kisnyerges-ravine

The Jurassic rocks of the Kisnyerges-ravine situated in the SE part of the Hajag Mountain-group (Northern Bakony) were firstly recorded by N o s z k y jun. (1953). Later on his geological map (1957) he figured Middle Dogger limestones in this area.

K o n d a (1970) gave a detailed description on the steeply dipping Liassic, Middle and Upper Jurassic rocks. From the red ammonitic limestones, overlying the Liassic rocks, he mentioned (in the preliminary determination of B. G é c z y) a *Stephanoceras* sp. specimen.

In the years 1970—71 a detailed layer by layer collection work was carried out by the Geological Survey of Hungary, and this work resulted in a relatively rich fauna.

Succession

In the steeply dipping sequence of the Kisnyerges-ravine the oldest rock is the Lower Liassic limestone of Dachsteinkalk-type. Upon its uneven surface disconformably lies the massive ammonitico rosso limestone. The lower 6 beds of 88 cm thickness form a discontinuous Upper Sinemurian and Pliensbachian sequence. It is disconformably overlain by the 173 cm thick Bajocian limestone, represented in the Beds Nos. 9—15. From the Bajocian zones the Otoites sauzei and the Stephanoceras humphriesianum were undoubtedly, and the Strenoceras subfurcatum Zone was uncertainly proved. The interest of this markedly discontinuous sequence is that it lacks the radiolarite, i.e. the Bajocian is followed by Kimmeridgian, *Aspidoceras*-bearing limestones.

Fauna and zonation

The evaluation of the Bajocian fauna from the Kisnyerges-ravine is encumbered by the poor state of preservation and the low specimen number as well.

The beds collected from 3,4 m^2 average surface yielded 97 ammonite specimens altogether. The additional fauna is represented merely by a single brachiopod specimen (Bed No. 9) and some belemnite rostra.

It is proved on the basis of the ammonites, that the sequence shows hiatuses within the Bajocian too, since only portions of the certain zones are represented (Fig. 4).

The majority of the fauna is consisted of phylloceratids and lytoceratids. From the stratigrafically important Ammonitina the most common forms are the *Stephanoceras* species. On the basis of the *Emileia* sp. occured in the Bed No. 9 the lower three beds (Nos. 7—9) can be ranged into the Otoites sauzei Zone.

In addition to the *Stephanoceras* spp., the Bed No. 10 yielded a *Teloceras*, which shows the presence of the upper subzone of the Humphriesianum Zone. From the Bed No. 13 upwards appear the Bajocian perisphinctids, suggesting the Subfurcatum Zone. The precise determination of these poorly preserved *Leptosphinctes*-allies is impossible, hence to drow the upper boundary of the Humphriesianum Zone is uncertain.

Conclusions

The most complete Bajocian sequence of the sections studied from the Northern Bakony is of the Lókút-hill locality. The extremely rich ammonite fauna giving the base for the zonal and subzonal subdivisioning is of international interest, in the points of view of paleogeography, evolution and stratigraphy.

The other, markedly discontinuous sections can be correlated with the previously studied Bajocian profiles of Gyenespuszta (Galácz 1970) and Csernye (Géczy 1967a,b), (Fig. 5.).

In the Bajocian sections of the Bakony Mountains the greatest areal distribution is shown by the Humphriesianum Zone, while the Lower and Upper Bajocian zones are frequently unrepresented.

The Mediterranean type ammonite faunas can be correlated with those of NW Europe; however the further studies are hopeful, in the point of view of the Mediterranean Bajocian stratigraphy.

REFERENCES

Arkell, W. J. (1956): Jurassic geology of the world. Oliver and Boyd, Edinburgh. pp. 1–806.

Fülöp, J. (1971): Les formations jurassiques de la Hongrie. Coll. Jurassique Medit. MÁFI Évk., LIV., 2. pp. 31–62.

Fülöp, J. et al. (1969): Excursion géologique dans le montagnes centrale de Transdanubie, Mecsek et de Villány. Coll. Jurassique Medit. pp. 1–63.

Galácz, A. (1970): Biostratigraphic investigation of the Middle Jurassic of Gyenespuszta, Northern Bakony, Transdanubian Central Mountains, Hongary. Ann. Univ. Sci. Budapest., Sec. Geol. t. XIII. (1969). pp. 109–128.

Galácz, A. (1972): Trilobiticeras (Ammonoidea, Otoitidae) from the Bajocian (Middle Jurassic) of the Bakony Mountains. Ann. Univ. Sci. Budapest., Sec. Geol., t. XV. (1971). pp. 41–45.

Géczy, B. (1967a): Ammonoides jurassiques de Csernye, Montagne Bakony, Hongrie. – Part II. (excl. Hammatoceratidae). Geol. Hung., Ser. Palaeont., fasc. 35. pp. 1–413.

Géczy, B. (1967b): Biozones and chronozones in the Jurassic of Csernye, Bakony Mts, Hungary. (In Hungarian, with English abstract). Földt. Közl., 97., 2. pp. 167–176.

Géczy, B. (1969): [The biostratigraphical evaluation of the Liassic profile of Közöskút-Ravine (Bakony Mts.)]. (In Hungarian) Manuscript, MÁFI Adattár.

Géczy, B. (1971): (Lower Jurassic ammonites from the Kisnyerges-Ravine). (In Hungarian). Manuscript, MÁFI Adattár.

Imlay, R. W. (1973): Middle Jurassic (Bajocian) ammonites from Eastern Oregon. Geol. Soc. Prof. Pap., 756. pp. 1–100.

Konda, J. (1970): Litologische und Fazies-Untersuchung der Jura-Ablagerungen des Bakony-Gebirges. Földt. Int. Évk., L. 2. pp. 1–260.

Noszky, J., jun. (1943): Bericht über geologische Untersuchungen im Innengebiet des nördlichen Bakonygebirges. Földt. Int. Évi Jel. (1939–40). I. pp. 253–261.

Noszky, J., jun. (1953): La levé géologique des terrains jurassique des environs de Szentgál, Herend, Márkó, Városlőd. (In Hungarian, with French and Russian abstract). Földt. Int. Évi Jel. (1941–42.) Last vol. pp. 3–6.

Noszky, J., jun. (1957): Geologische Karte des Nordteiles des Bakony-Gebirges im Masstab 1:25 000. Földt. Int. Évk., XLVI., 3. (1950–54).

Noszky, J., jun. (1961): Formation jurassiques de la Hongrie. Földt. Int. Évk., XLIX., 2. (1969). pp. 481–501.

Paul, K. M. (1862): Übersicht der rätischen, Lias- und Jura-Bildungen im Bakonyer Gebirge. Jb. k.–k. geol. Reichsanst. XII., 2. pp. 226–229.

Pavia, G. (1972): Ammoniti del Bajociano superiore di Digne (Francia SE, dip. Basses-Alpes). Bol. Soc. Paleont. Ital., 10., 2. (1971). pp. 75–142.

P a v i a, G. – S t u r a n i, C. (1968): Étude biostratigraphique du Bajocien des Chaines Subalpines aux environs de Digne (Basses Alpes). (Note préliminaire). Boll. Soc. Geol. Ital. 87. pp. 305 – 316.

R o t h, K. (1934): Daten aus dem nördlichen Bakony-Gebirge zur jungmesozoischen Entwicklungsgeschichte der "Ungarischen Zwischenmasse". Mat. Naturwiss. Anz. Ung. Akad. Wiss. LII. pp. 205 – 252.

S c h a f a r z i k, F. (1890): Daten zur Geologie des Bakony. Földt. Közl., XX., 1 – 3. pp. 57 – 60.

T a e g e r, H. (1912): (Contribution to the building and geological picture of the Bakony). (In Hungarian) Földt. Int. Évi Jel. (1910). pp. 61 – 68.

T a e g e r, H. (1912b): (New data to the geology of the Bakony). (In Hungarian) Földt. Int. Évi Jel. (1911) pp. 61 – 66.

V a d á s z, E. (1960): (The Geology of Hungary) (In Hungarian) 2nd. ed. Akadémia, Budapest. pp. 1 – 646.

W e n d t, J. (1971): Genese und Fauna submariner sedimentärer Spaltenfüllungen im mediterranen Jura. Palaeontographica Bd. 136., Abt. A. 1 – 6. pp. 122 – 192.

PLATE TECTONICS AND PALEOBIOGEOGRAPHY

by

B. GÉCZY

Department of Paleontology, Eötvös University, Budapest
Received: 1 March, 1974

РЕЗЮМЕ

Одинаково неправильно и слишком подчеркивать, и оставлять без внимания палеобиогеографическое значение результатов тектоники плит. Палеонтология частично представляет собой науку о пространстве, но в то же время жизнь и развитие общества в определенных размерах независимы от физических условий. Тектоническое движение плит со своей пространственностью оказывает определенное влияние на район, диверсию и эволюцию, но не управляет им.

Из-за пористости фсссильного материала мы не в состоянии определить действительный *район*. Однако реконструкция тектонических движений плит помогает определить *возможный* район, облегчает интерпретацию распространения организмов, объясняет сходство фауны удаленных друг от друга территорий (дрифтирование), а также различия в фауне близких территорий (коллизия). поскольку распространение объясняется не только физическими причинами, то реконструкция древних районов происходит не по границам тектонических плит, а по распространению фоссилий. Обратная реконструкция сегодняшних залежей с учетом движения плит является важной задачей палеонтологии.

Число таксонов или пропорция между таксонами и единицами, которое отражает собой диверсию, в первую очередь зависит от постоянства или колебания физических условий. Диверсия и проявляющиеся в ней изменения может быть объяснена в первую очередь тектоническими движениями плит. Поскольку среди физических условий климат является наиболее существенным, то одностороннее изменение диверсии, проявляющееся в течение долгого промежутка времени на данной территории, может быть объяснено продольными движениями плит.

Зволюционная роль движений тектонических плит в изменениях района (географическое изолирование) и в изменениях диверсии (например, вымирание) проявляется косвенным путем. Медленные тектонические процессы заслуживают особого внимания. Прерывы в цепи эволюции наиболее просто объяснить последотательным уничтожением самой океанской плиты в случае океанских организмов.

Малый, но обладающий богатым прошлым район Венгерского Бассейна из-за своей богатой и хорошо сохранившейся фауны является очень пригодным для исследования тектонических и пелеобиогеографических изменений.

Introduction

The question arises: is it reasonable the paleontological approach to the goals of plate tectonics? In the case of the continental drift theory the balance is positive for the paleontology. For W e g e n e r in 1911 the decisive motive for the definitive elaboration of the drift theory were the paleontological similarities between Brazil and Africa (c. f. W e g e -

ner 1922). As of Hungary, Nopcsa (1934) interpreted the agreements between the European and North American Paleozoic tetrapod faunas by the connection and the subsequent separation of these continents (c. f. Milnur et Panchen 1973). In those days, however, when the drifting of the continents seemed to be unacceptable on the basis of the geophysical knowledge of that time, paleontology could not but choose to interpret the evident faunal and floral agreements indirectly, by continental bridges, dispersal routes of chance, etc. The life-work of Simpson (1953, etc.) and the paleobiographical atlas of Termier (1952) essentially based on "fixist" principles. Recently Wesson (1972) – quoting Meyerhoff – concluded stable continents from the ancient floras and faunas. Thus it is hard to state, that the fossil record proves *unequivocally* the theory of continental drift.

The situation, however, changed when the plate tectonics and thus the continental drift became a *fact* based on qualitative ground. The global nature of the plate tectonics involves the reevaluation of the former results of the earth sciences, and especially does found the paleogeographical reconstriuctions upon new grounds (Dickinson 1972). The dynamic approach, which emphasizes the movements of the oceanic and continental crustal parts, in contradiction to the static views based on the permanence of oceans and continents, is a step similar to that resulted in the paleontology by Darwin's evolution theory, as opposed to the former fixist view. It seems to be justified the designation of Maxwell (1970), who called the geology of the last half century as the „Wegener Era".

The question is: how to apply the results of plate tectonics to the evaluation of the biospheric history? The organisms live not only in time, but in space too, therefore *paleontology is a spatial science* in part. One of the basic goals of paleontology is to throw light on the paleobiogeographical situations. The plate tectonic movements affect the geographical distribution of the organisms, the variousness of the living world and the evolution as well. Consequently, it is reasonable to consider the relation of the plate tectonics and the paleobiogeography in the points of view of area, diversity and evolution.

Area

The plate tectonic movements biogeographically fistly determine the outermost distributional limits of the marine and land organisms, and rearrange subsequently the original areas of distribution.

According to the first formulation of Hess (1962) „The ocean basins are impermanent features, and the continents are permanent...". The contrasting of the simaic ocean with the sialic continent here is of geophysical, though the ocean–land contrast is more conspicuous from the point of view of geology and biogeography. The principle of permanent continents do not exclude the possibilities of occasional transgressions and regressions. These sea-level changes, however, are directly or

indirectly in connection with plate tectonic movements. The arising mid-oceanic ridges expel the water masses of the ocean basins, resulting in transgressions on the continents. On the other hand, the emergence and disintegration (or rifting) of the continents bring regressions about (H a l l a m 1969, B r o o k f i e l d 1969). Since in the course of the movements continents may join (e.g. Precambrian and Permo-Triassic Pangea), or disintegrate, these movements influence the proportion of the continents, as well as of the related shelf regions so essential for the marine organisms (V a l e n t i n e 1971).

Thus understandable the recent richness of studies dealing with and evaluating generally the areal distribution of an animal or plant group of a given geological interval, in the light of plate tectonic movements (M i d d l e m i s s et R a w s o n 1971, H a l l a m 1973, T a r l i n g et R u n c o r n 1973).

The biogeographical evaluation of the plate tectonic movements may bear a twofold hazard: i.e. either the overemphasize, or the neglect of the physical conditions. The global dynamism of the plate tectonic movements embraces a so attractive richness of possibilities, that one could easily lean to the opinion: the plate tectonic movements not only have influence on, but lastly do determine the distribution of the organic life. Nevertheless, the recent observations do not support this supposition.

The animal and plant establishment and distribution can be promoted or restricted by *biological* conditions. The following factors should be take into consideration:

- The weight, size, buoyancy and life-span of the spores, pollens, grains and larvae, the vagility of the adult animals, etc;
- The swimming or flying capacity of the transporting plants (driftwood, floating island) and animals (insects, birds), respectively;
- The tolerance and adaptability of the organism getting into new environment, including the interrelation between the aborigines and the invaders (overpopulation, competition, etc.).

A wide range of biologic factors, such as use of new materials (cuticule, calcareous test), appearance of new organs (e.g vascular tissue, coeloma, cordial and feather- and pilary system resulting in poikilothermy), and overpopulation resulted from the intensity of reproduction may start invasion, alike as the plate tectonic movements which enlarge the favourable physical conditions for the distribution.

Distribution, accordingly, is not merely a physical-ecological problem, but also of genetics and history, meaning the temporal results of the dynamic interrelation of the external and internal factors. It is understandable in this way, that while the vegetation maps do, the floral maps and especially the faunal geographic units do not conform to the climatic boundaries. The recent continental faunal provinces can be defined most by the faunas themselves (H e w e r 1971). Thus, in the biographic separation rather the identity and difference of the *faunas* are the decisive

factors, and not the hypothetical geographic boundaries between them. It could be unjustified to assume, even in the case of plants so sensitive to the environment, that the limits of distribution of a given species is directly determined by the external factors (W a l t e r 1970). In other words: an organism do not live everywhere the physical conditions enable, and hence the possibility of the limitation is more unfavourable (S y l v e s t e r – B r a d l e y 1971). For example the short larval state of the brachiopods unables to pass from a shelf region into an other, crossing the ocean. Thus on the basis of the brachiopod faunal differences of different shelf regions one can conclude the former existence of an ocean between these regions, but the width of this „barrier" cannot be estimated on plaeobiogeographic bases.

Now it is understandable from the above mentioned facts, why the biogeography of today concerns mainly problems such as the qualitatively approachable question of the balance of immigrant and extinct species on a given area, and not the drawing of the province boundaries (S i m b e r l o f f 1972). Because of the eventuality of the fossil record, the area of the fossil species is uncertain in all cases. This is why the principal task of the paleobiogeography is the precise draw of the boundaries of floral and faunal provinces. It is realizable the recognition and characterization of the distinct provinces even in the lack of the whole fauna, but on the basis of the fossilized groups. The most proper way in the compilation of paleobiogeographical maps is to model the construction of facies maps.

In the point of view of paleobiogeographic evaluation very important is the role playing the plate tectonic movements by the *subsequent* disintegration of formerly contiguous areas, or closing of originally distant areas. In the geographical distribution of the certain genera the handbooks usually confine to indication of continents (Europe, North America, etc.). These indications show the recent region of localities, but do not concern the original area of the taxa. Considering plate tectonics, Europe, as well as the other continents developed through collisions of continental crust-parts. The narrow orogenic belts (Caledonic, Hercynic, Alpine belts) crossing Europe are the remnants of opened and subsequently closed oceans. The fossils which have been collected from Europe were inhabitants of the shelf regions of originally different oceans (Protatlantic, Theic, Rheic, Pleionic Oceans, c.f. M c K e r r o w 1972). Going backward in time, the subsequent effects should be more considered. In relatively small spots of the European map, e.g. in Scotland or in W Norway different Paleozoic paleogeographic units closed to each other (W i l s o n 1966, N i c h o l s o n 1971, G a r s o n et P l a n t 1973). The Mesozoic faunas of the geographically similarly small Pannonian basin originally belonged to two shelf regions, which were separated by an ocean (Tethys), and subsequently, through lateral movements followed the complex collision and subduction, came close to each other (G é c z y 1973). Consequently, Hungary cannot be regarded as a paleobiogeographical unit in the Mesozoic.

One of the usual attributes of the paleontological monographs was the tabulated or mapped recording of the areal distribution of the certain species. The "*rearrangement*" of the localities from these apparent areas, as well as the reconstruction of the actual areas applying the plate tectonic results are the perspective new task of paleontology.

Diversity

The paleobiogeographical reconstruction and the separation of faunal provinces are essencially based upon two antinomies:

– on the similarity and dissimilarity of the taxa, i.e. a qualitiative,

– on the diverseness and sameness, i.e. a quantitative evaluation.

The similarity and the dissimilarity can be measured with the proportion of the endemic forms of the compared areas, while the diversity is expressible with the number of the taxa of the different areas or with the taxon/specimen number ratio (density).

The diversity reflects the effect of the physical environment on the biosphere. Since physical environment is affected by the global plate tectonic mevements, the change in the diversity is a general phenomenon. The geonomic importance of the diversity is enlarged by its quantitative expressibility. It is why the significance of diversity in paleogeographical reconstruction is underlined by several authors (Fischer 1961, Valentine 1968, 1969, 1970, 1971, Valentine et Moores 1972, Hallam 1972, 1973, Raup 1972, Kauffman 1973, Stehli 1973, etc.).

High diversity, i.e. the great taxon number related to specimen-number suggests environmental consistency and stability. The stability of the energy sources support permanent food-supply and manifold, complete depletion. Hence the multiple food-chain may develop. Under the stable conditions there is possibility for manifold adaptation. The population adapted to the several, permanently small given environments and food, replenish the limited and different ecological niches. In seas the organisms can occupy the whole inhabitable area – besides the borrowing inbenthonic organisms the bottom-dweller, epibenthonic elements are also important. Corresponding with the favourable conditions and their specialization, endemic forms are abundant too. On the other hand, the low diversity is caused by the change or instability of the environmental conditions. The fluctuation in the energy quantity leads to alternation in the food-supply: with temporally sharp increasing then rapidly decreasing plankton production with related quickly declining, wide, but monotonous populations. The depletion is imperfect and the food-chain is incomplete. The large amount of organic detritus is more favourable for the infauna than for the epifauna. The stress of the changing conditions is sufferable for a few group of organisms, but these have a great areal distribution. Consequently the endemic forms are subordinated, while the ubiquitous elements are common (Valentine et Moores 1972).

The most important physical factor affecting the biospheric diversity is the *climate.*

Especially substantial is the regularity in the light, heat and precipitation distribution. Accordingly, the highest density can be recognized in equatorial regions, on lands and seas as well. Going polarward from the Equator the density decreases gradually (latitudinal change in diversity). In deep-sea regions characterized by uniform conditions, the diversity is also relatively high (M e n z i e s et al. 1973). Similarly as the extreme temperature fluctuations, other factors (such as changes in salinity, tidal or oscillatory variations) also reduce the diversity. These latter factors naturally are unrelated to the latitude.

The uniform or extreme character of the climate depends on the size, elevation and position relative to the pole of the continents. On the separated or partly sea-covered continents, especially on those situated near the Equator the climate is uniform. Here the effect of the planetary wind-system is weaker, the velocity of the sea currents is reduced and the salt-content of the waters is more stable (G o r d o n 1973). The water of the polar oceans is warmed up by tropical water masses. On the other hand, closing of continents leads to extreme climate, resulting in warm summers, cold winters and strong monsoonal influence. When continents are in elevated position, i.e. during the times of great regressions, this extremity increases. The continental effect culminates when a continent is in polar position. In this time the mean annual temperature decreases and the temperate climatic belt becomes narrower.

Plate tectonic movements evidently influence the size, elevation and position relative to the pole of the continents. Even in a case of a presumed uniform global climatic system a plate movement in polar or equatorial direction would result in climatic changes on the plate, because this movement necessarily cross climatic belts. The prolonged unidirectional diversity change visible on a given area ("in section") can be due partly to latitudinal plate movement. On the orther hand, longitudinal movements which are parallel to the Equator theoretically have no effect on the diversity. These considerations mainly refers to the terrestrial parts of the continental plates. In the seas the problem is more complicated by the heat-transport caused by currents. The diversity-maximum of the recent reef-building corals do not fit to the Equator, but is situated slightly north, where the sea-waters are warmest as a result of the currents (S t e h l i and W e l l s 1971).

Northwestern Hungary belonged in the s.l. tropical belt in Mesozoic times. The ammonites of the Bakony Mountains' profiles had a higher diversity, e.g. in the Davoei Zone (Carixian Substage, Lower Jurassic) the diversity derived from the ratio of specimen and species numbers (6.679 and 70, respectively) attained the value 11 (G é c z y 1974). It is reasonable to study further the ammonite diversity on this region, which was relatively unchanged through long geological intervals (Jurassic – Lower Cretaceous). The expected stability of the high

diversity presumably can be due to the fact that the main movement direction of the continents ("stable" Europe, "stable" Africa) bordered the Tethyan ocean in the Mesozoic, was from the Lower Jurassic to the Upper Cretaceous (during 117 m.y.) subparallel to the Equator, i.e. was more or less longitudinal in direction (D e w e y et al. 1973). The longitudinal changes supposed for the oceanic plate of the Tethys are the results of the opening and closing of the Tethys itself.

Evolution

The area and diversity are the results of historical processes. The physical factors affecting two of them, indirectly affect the organic evolution too. Because of the transmissive appearance of the relationships here, the study on the correspondences between plate tectonic movements and evolution is most complicated. The internal, genetic factors of the evolution are reasonably out of the scope of this paper.

The base of the evolution is the speciation, which is preconditioned by the *genetic isolation*. Without isolation there is no evolution recently. The plate tectonic movements through bringing barriers about, may promote the isolation directly. In the case of plates moving away, the barriers are the results of the rifting, drifting and the arising of the mid-oceanic ridges. On the margins of the convergent plates mountain chains (cordillera), or island arcs may form, separating the populations. The associated climatic changes e.g. development of desert zones, may also result in separation. Good examples of separations and developments of new evolution centres are in the Upper Cretaceous the formation of independent bivalve faunal provinces on the divergent shelf regions of the opened Atlantic (K a u f f m a n 1973), or in the Tertiary the peculiar development of the primitive marsupial faunas of Australia (K u r t é n 1969).

The plate tectonic and evolutionary processes are characterized by *slowness*. It is not for nothing that the recognition of these processes is so difficult. The biology accepted the concept of evolution after a long struggle. The continental drift theory became factual when the instrumentation of the geophysics and the organized marine research proved it. The slow plate tectonic movements are answered by the organic world with similarly slow processes. The recent Red Sea is regarded by the plate tectonists as a forming ocean. On the other hand, this barrier is too narrow for the present as to be a biogeographical boundary floristically or faunistically. The boundary of the "East African" and Mediterranean faunal provinces crosses the Red Sea. In the Mesozoic a similar case existed in connection with the opening of the Atlantic. The rift, indicating the formation of the ocean, started in the Jurassic, or possibly in some places as early as in the Triassic. But the unit of the North and South Atlantic – on the basis of the identity of the ammonite faunas – occured in the Turonian (L a r s o n and L a d d 1973). Consequently, even at the lowest estimate, the separation of

Africa and South America required a 40 m.y. duration. In related plates this process may be accelerated. This is the case in joining oceanic and continental plates, i.e. in mountain building of cordillera-type. According to Oberhauser (1973) the East Alpine Upper Cretaceous nappes formed in geologically very short interval (1–2 zones, or a substage). Despite of the extremely significant paleogeographic changes, the faunas of the successive transgressions were changed slightly. On the other hand, when the faunas of two continents, having been separated during long geological periods, attain different evolutionary level, the collision may result significant changes in the compositin of the biosphere. The classical example of such a process is in the Upper Pliocene North American carnivorous faunas, which caused the complete extinction of the peculiar South American mammal faunas.

The geographical separation is only *one* of the possibilities of the speciation. This is why the relationship of the plate tectonic and the evolutionary processes is severally debatable. Namely, the separation leading to evolution can be due in many cases to ecological or physiological causes. The ecological changes are frequently reflected in the sedimentation conditions, hence from the lithofacies variation one can conclude to the changes in the environment. On the other hand, many times very significant evolutionary changes are represented in the fossil record (e.g. the extinction of the dinosaurs or the large Tertiary mammals) without any changes in the lithofacies. The factors, which encumber the paleogeographical and evolutionary researches (the eventuality of fossilization and sedimentation and the eventuality of the preservation of fossils and sedimentary rocks) are necessarily in the historical nature of the subject. In this point of view remarkable is the work of Raup (1972). He studied the diversity of the marine invertebrates, and treated the possible errors deriving from the geological application of the diversity. Plate-tectonically oriented paleontologists explained the most remarkable break in diversity at the Perm/Triassic boundary (extinction of the 50% of the families) by the formation of the Pangea, which has been necessarily accompanied with the narrowing of the densely inhabitated shelf regions and the expansion of the variable unstable conditions (continental climate). In the case of the invertebrates it is remarkable the fact, that at the Perm/Triassic boundary a great regression took place, resulting in the documentation, i.e. in the sediment-quantity expressed in km^3, a striking decrease. In this case, consequently, it is also possible, that the plate tectonic movements (the emergence of the continents) caused changes not in the evolution, but in the documentation too, which seems to be a break in the evolution. In the organisms inhabitating oceanic areas the *subsequent* destruction of the plate may cause similarly *apparent* breaks in the faunal development (Géczy 1973).

According to the quantitative studies of Flessa et Imbrie (1973) the major plate tectonic events were "answered" by the marine and terrestrial organisms with diversity changes. The opening of the

western Tethys could be an exception, which did not lead to consequences in the diversity neither in the marine, nor in the terrestrial organisms. On the basis of the ammonites, this is a more complicated problem. In the Lower Jurassic, during the opening of the Tethys, the northern and southern marginal parts were separated, and on the southern margin the pelagic character became gradually dominant. This spatial separation was followed by the differentiation of the ammonite faunas (G é c z y 1973), which reflected on the southern, unvariable (oceanic) areas in higher diversity in the first place, and in greater proportion of the paleoendemic and neoendemic forms in the second. V a l e n t i n e (1969) suggested the necessity of the detailed analysis of the Mesozoic diversification circumstances. It is expected that the studies enlarged to different ages and taxa (brachiopods, gastropods, bivalves), together with the application of the plate tectonics, will lead to useful informations for the evolution of these groups.

Conclusions

It is equally wrong to neglect or to overemphasize the paleobiogeographic importance of plate tectonic results. Paleontology partly is a spatial science; but the organic life and the evolution are independent to some extent of the physical conditions. With their spatial nature the plate tectonic movements do influence, but do not direct unequivocally the area, diversity and evolution of the organisms.

Because of the incompleteness of the fossil record, the factual area cannot be recognized. On the other hand the plate tectonic reconstructions help to outline the *possible* area, facilitate to interpret the distribution of the organisms, and advance to understand the faunal similarity of distant regions (drifting) and the faunal differences of adjacent regions (collision). Since, however, the physical factors are not exclusive in the distribution, the reconstruction of the former areas is based not on the plate tectonic boundaires, but on the distribution of fossils. On the other hand, the „rearrangement" of the recent localities, considering the subsequent plate tectonic movements, is an important task of the paleontology.

The diversity, reflecting in the number of taxa or in the ratio of taxon and specimen numbers, depends firstly on the permanence or fluctuation of the physical conditions. The diversity, as well as its change, can be due firstly to the plate tectonic movements. Since the one of the most important physical factors is the climate, prolonged, unidirectional change in diversity traced on a certain area can also be due to the longitudinal motion of the plate.

The evolutionary importance of the plate tectonic movements appears transmissively in the areal variations (geographical separation) and in the diversity changes (e.g. extinction). Most remarkable are the slow plate tectonic movements. The most plausible explanation for the missing links of the evolution of the oceanic organisms is the subsequent destruction of the oceanic plates themselves.

The small, but geo-historically highly complicated Hungarian basin, with its rich and well preserved faunas is very suitable to study plate tectonic and paleobiogegraphic changes.

Acknowledgements

The writer is deeply indebted to Prof. L. S t e g e n a and Prof E. S z á d e c z k y-K a r d o s s, Dr. F. H o r v á t h and Dr. A. V ö r ö s for their help and discussions.

REFERENCES

Brookfield, M. E. (1970): Eustatic changes of sea-level and orogeny in the Jurassic. Tectonophysics 9, 347–363.

Dewey, J. F., Pitman, W. C., Ryan, W. B. F. and Bonnin, J. (1973): Plate tectonics and the evolution of the Alpine system. Geol. Soc. Amer. Bull. 84. 3137–3180.

Dickinson, W. R. (1972): Evidence for plate tectonic regimes in the rock record. Amer. Journ. Sci. 272, 551–576.

Flessa, K. W. and Imbrie, J. (1973): Evolutionary pulsations: evidence from Phanerozoic diversity patterns. in Tarling op. cit. 247–285.

Fischer, A. G. (1961): Latitudinal variations in organic diversity. Amer. Sci 49, 50–74.

Garson, M. S. and Plant, J. (1973): Alpine type episofic rocks and odic mountain building in the Scottish Highlands. Nature, 242, 34–37.

Géczy, B. (1973): The origin of the Jurassic faunal provinces and the Mediterranean plate tectonics. Ann. Univ. Sci. Budapest Sect. Geol. 16, 99–114.

Géczy, B. (1973): Lemeztektonika és paleogeográfia a kelet-mediterrán mezozoós térségben. Magy. Tud. Akad. X. oszt. Közl. 6, Budapest, 219–225.

Géczy, B. (1974): Les Ammonites du Carixien de la Montagne Bakony. Akad. Kiadó, Budapest (in press).

Gordon, W. A.)1973): Marine life and ocean surface currents in the Cretaceous. Journ. Geol. 81, 269–284.

Hallam, A. (1969): Tectonism and eustasy in the Jurassic. Earth. Sci. Rev. 5, 45–68.

Hallam, A. (1972): Diversity and density characteristics of Pliensbachian-Toarcian molluscan and brachiopod faunas of the North-Atlantic margins. Lethaia 5, 384–412.

Hallam, A. (1973) edit.: Atlas of Palaeobiogeography. Elsevier Sci. Publ. Amsterdam 1–531.

Hess, H. H. (1962): History of ocean basins. in: Petrologis Studies. Vol. Honor A. F. Buddington, Geol. Soc. Amer. 599–620.

Hewer, H. R. (1971): Modern zoogeographical regions. in Middlemiss op. cit. 19–30.

Kauffman, E. G. (1973): Cretaceous Bivalvia. in Hallam op. cit. 353–384.

Kurtén, B. (1969): Continental drift and evolution. Amer. Sci. 220, 54–64.

Larson, R. L. and Ladd, J. W. (1973): Evidence for opening at the South Atlantic in the Early Cretaceous. Nature, 246, 209–212.

Maxwell, J. C. (1970): The Mediterranean ophiolites and continental drift. in: Johnson Smith B. edit: The megatectonics of continents and oceans. New Brunswick, (167–193).

Mc Kerrow, W. S. and Ziegler, A. M. (1972): Paleozoic oceans. Nature, 240, 92–94.

Menzies, R. J., George, R. Y. and Rowe, G. T. (1973): Abyssal environment and ecology of the world oceans. Wiley Edit. New York, 1–488.

Middlemiss, F. A. and Rawson, P. F. (1973): Faunal provinces in space and time. Geol. Journ. Spec. Issue 4, Liverpool, 1–210.

Milner, A. R. and Panchen, A. L. (1973): Geographical variation in the tetrapod faunas of the Upper Carboniferous and Lower Permian. in: Tarling op. cit. 353–368.

Nopcsa, F. (1934): The influence of geological and chronological factors on the distribution of non-marine reptiles and Stegocephalia. Quart. J. Geol. Soc. London, 90, 76–140.

Nicholson, R. (1971): Faunal provinces and ancient continents in the Scandinavian Caledonies. Geol. Soc. Amer. Bull. 82, 2349–2356.

Oberhauser, R. (1973): Stratigraphisch-Paläontologische Hinweise zum Ablauf tektonische Ereignisse in den Ostalpen während der Kreidezeit. Geol. Rundschau 62, 96–106.

Raup, D. M. (1971): Taxonomic diversity during the Phanerozoic. Science, 177, 1065 – 1071.
Russel, L. S. (1973): Geological evidence on the extinction of some large terrestrial Vertebrates. Canad. Jour. Earth Sci. 10, 140 – 145.
Simberloff, D. (1972): Models in Biogeography. in Schopf, T. J. M.: Models in paleobiology. Freeman edit. San Francisco. (160 – 191).
Simpson, G. G. (1953): Evolution and geography. Oregon Stat. Syst. High. Educ. Eugene.
Stehli, F. G. (1973): Permian brachiopods. in: Hallam, 1973 op. cit. 1943 – 150.
Stehli, F. G. and Wells, J. W. (1971): Diversity and age patterns in hermatypic corals. Syst. Zool. 20, 115 – 126.
Sylvester-Bradley, P. C. (1971): Dynamic factors in animal paleogeography. in: Middlemiss op. cit. 1 – 16.
Tarling, D. H. and Runcorn, S. K. (1973): Implications of continental drift to the Earth Sciences. Vol. I. Acad. Press, London, 1 – 622.
Termier, H. and Termier, G. (1952): Histoire géologique de la biosphére. Masson edit. Paris, 1 – 721.
Valentine, J. W. (1968): Climatic regulation of species diversification and extinction. Geol. Soc. Amer. Bull. 79, 273 – 276.
Valentine, J. W. (1969): Patterns of taxonomic and ecological structure of the shelf benthos during Phanerozoic time. Palaeontology, 12, 684 – 709.
Valentine, J. W. (1970): How many marine invertebrate fossil species? Journ. Paleont. 44, 410 – 415.
Valentine, J. W. (1971): Plate tectonics and shallow marine diversity and endemism: actualistic model. Syst. Zool. 20, 253 – 264.
Valentine, J. W. and Moores, E. M. (1972): Global tectonics and the fossil record. Journ. Geol. 80, 167 – 184.
Walter H. and Straka, H. (1970): Arealkunde. Ulmer Verl. Stuttgart, 1 – 478.
Wegener, A. (1912): Die Entstehung der Kontinente. Geol. Runschau. 3. 276 – 292.
Wegener, A. (1922): Die Entstehung der Kontinente und Ozeanes. Vieweg Verl. Braunschweig, 1 – 144.
Wesson, P. S. (1972): Objections to continental drift and plate tectonics. Journ. Geol. 80, 185 – 197.
Wilson, J. T. (1966): Die the Atlantic close and then re-open? Nature, 211, 676 – 681.

THE MICROFAUNA OF THE CARBONIFEROUS LIMESTONE AT SZABADBATTYÁN (TRANSDANUBIA, HUNGARY)

PART II.

by

M. MONOSTORI

Department of Paleontology, Eötvös University, Budapest

Received: 1 October, 1972

Introduction

The writer, on the authority of the Geological Survey of Hungary studied the microfauna of the Carboniferous limestone of Szabadbattyán in 1971. This present paper contains the second part of the paleontological descriptions and the stratigraphical and faciological evaluation of the fauna.

Descriptions (Continuation)

Family ENDOTHYRIDAE BRADY 1884
Genus *Endothyra* PHILLIPS 1846

Endothyra cf. *bradyi* MIKHAILOV 1939

Pl. I., Figs. 1 – 2.

Description: Diameter: 0.45 – 0.60 mm
Number of whorls: 2.5
Number of chambers in the last whorl: 7 to 8.

The coiling have a planispiral tendency – apart from the initial chambers. The whorls rise gradually. The chambers are slightly convex, the sutures are pronounced only in some places. The septa are relatively weakly developed, with occasional proversity or convexity. The secondary deposit forms more or less developed knobs, with thin connecting wall-cover. The wall is dark and fine-grained.

Remarks: The specimen figured on Pl. I. Fig. 1. agrees well with the var. *alta* of CONIL and LYS 1964, Fig. 474.

For lack of sufficient comparative material it cannot be decided whether the *Endothyra bowmani* and *E. bradyi* species are synonyms. The forms figured here undoubtedly resemble the *E. bowmani* PHILLIPS specimen figured on Pl. V. Fig. 4. of BRADY (1876), the *E. bowmani* PHILLIPS in BROWN emend. BRADY specimen of MAMET (1970. Pl, VI, fig. 3.) and the specimen figured by LOEBLICH and TAPPAN (1964) as neotype. On the other hand, these differ completely from the neotype figured by ZELLER (1963).

Occurence at Szabadbattyán: Borehole Szabadbattyán – 9, from 285.1 m, Borehole Szabadbattyán – 10, from 339.3 m, and from the samples of the exploration shaft.

Endothyra cf. *omphalota* RAUSER – CHERNOUSSOVA et REITLINGER 1936

Pl. II., Fig. 3.

Diameter: 0.67 mm

Remarks: Only one section, without the possibility of more precise determination.

Occurence at Szabadbattyán: Borehole Szabadbattyán – 9, from 302.7 m.

Endothyra cf. *prisca* RAUSER-CHERNOUSSOVA et REITLINGER 1936

Pl. II., Fig. 4.

Description: Diameter: 0.37 mm
Number of whorls: 3.5
Number of chambers of the last whorl: 9.

The coiling is nearly regular, the chambers are convex, with pronounced sutures on the last whorl. The septa are slightly convex. Secondary deposit cannot be visible. The wall is relatively thin, dark and fine-grained.

Remarks: The single suitably oriented section shows a strong resemblance to the var. *undata* of CONIL and LYS (1964). It also resembles the *Endostaffella parva* (MOELLER), figured by ROZOVSKAJA (1963, Pl. XI., Fig. 12).

Occurence at Szabadbattyán: From the single sample of the Borehole Szabadbattyán – 6.

Endothyra cf. *similis* RAUSER-CHERNOUSSOVA et REITLINGER 1936

Pl. I., Figs. 3 – 7., Pl. II., Figs. 1 – 2.

Description: Diameter: 0.33 – 0.64 mm
Number of whorls: 3
Number of chambers in the last whorl: 6 to 9.

The coiling is asymmetrical, the included angle of the last and the penultimate whorls is nearly 90°. The last whorl rises quickly. The sutures are usually weak, but some pronounced sutures can occasionally occur between the last chambers. The septa are straight, rarely slightly convex, they are perpendicular to the spire, or curve in the direction of the coiling. The secondary deposits appear as distinct tubercules and inner wall-covering, but sometimes – owing to the poor preservation – these are hardly visible. The wall is fine-grained, granular, dark.

Remarks: The specimen figured here on Pl. I. Fig. 3. and Figs. 5–7. shows a good resemblance to that figured by CONIL and LYS (1964, Figs. 733–736) as var. *elegia* MALAKHOVA, but the specimen figured on Pl. I. Fig. 4. is close to the var. *crustata* designated in their work.

The originals of the Pl. II., Figs. 1–2. show the specific characters of this species, but the dimensions are greater than those given for this form so far. Because of the limited specimen-number it is impossible to decide whether there is wide variability, or subspecific-specific difference in the case of these forms.

Occurence at Szabatbattyán: Borehole Szabadbattyán–9, from 285.1, 302.7 and 306.8 m, Borehole Szabadbattyán–10, from samples between 338.5 340.1 m depth, and from samples of the exploration shaft.

Family OZAWAINELLIDAE THOMPSON et FOSTER 1937
Genus *Eostaffella* RAUSER-CHERNOUSSOVA 1948

Eostaffella cf. *ikensis* VISSARIONOVA 1948

Pl. IV., Figs. 5–7.

Description: Diameter: 0.7–0.82 mm
Width: 0.35–0.37 mm
Number of whorls: 4.

Compressed, lenticular form, with flat, or slightly depressed umbilicus. The inner whorls are rounded, the two outer whorls are narrowly rounded, sharp, or occasionally keeled. The last whorl increases more strongly. The last half whorl appears occasionally to be more rounded. Because of the poor preservation the character of the secondary deposit is hardly visible, but seems to be of variable strength. The wall is undifferentiated.

Remarks: The studied specimens appear to be slightly flattened in comparison to those assigned into this species in the literature, and the measurements are also greater. Special feature is the pronounced roundness of the last half whorl.

Occurence at Szabadbattyán: Borehole Szabadbattyán–10, from 342.6 m depth, and from samples from the exploration shaft.

Eostaffella cf. *parastruvei* RAUSER-CHERNOUSSOVA 1948

Pl. IV., Fig. 1.

Description: Diameter: 0.43 mm
Width: 0.215 mm
Number of whorls: 4.

It is a compressed, lenticular form, with slightly depressed umbilicus. The outer half whorl is narrowly rounded, sharp. The plane of coiling of the first whorl is different. The secondary deposits are hardly visible, and seem to be variable. The wall is dark, undifferentiated.

Remarks: The visible features of the available specimen are well comparable with those of the specimens figured by CONIL and LYS (1964).

Occurence at Szabadbattyán: Borehole Szabadbattyán – 10, between 338.5 – 340.1 m depth.

Eostaffella cf. *prisca settella* GANELINA 1951

Pl. IV., Figs. 3 – 4.

Description: Diameter: 0.20 – 0.24 mm
Width: 0.11 – 0.135 mm
Number of whorls: 3.

It is a lenticular form, with narrowly rounded edges. Because of the bad state of preservation the secondary deposits are hardly visible, but seem to be rather weak and irregular.

Remarks: On the basis of the visible features this form can be assigned into this subspecies.

Occurence at Szabadbattyán: Borehole Szabadbattyán – 9, from 309.1 m, and from samples of the exploration shaft.

Eostaffella cf. *vasta* ROZOVSKAJA 1963

Pl. III., Fig. 5.

Description: Diameter: 0.60 mm
Width: 0.25 mm
Number of whorls: 4.5.

It is a strongly compressed form, with narrowly rounded, sharpening edge. The secondary deposit is somewhat variable. The wall is dark and undifferentiated.

Remarks: The majority of the available specimens is fragmented and the sectional orientation of the single entire specimen is unconvenient. The character of the coiling, the shape and the width/diameter ratio as well, resemble to those of this species. The measurements are as the upper limits of the species.

Occurence at Szabadbattyán: Borehole Szabadbattyán – 10, samples between 338.5 – 340.1 m depth.

Eostaffella sp.

Pl. III., Fig. 6.

Description: Diameter: 0.65 mm
Width: 0.34 mm
Number of whorls: 3.5.

It is a compressed, lenticular form, with shallow umbilicus. The last 1.5 whorl is narrowly rounded. The secondary deposits developed unevenly and are hardly visible. The wall is dark, undifferentiated

Remarks: The figured form resembles the species *E. mosquensis* VISSARIONOVA, but its measurements are greater than the maximal dimensions mentioned in the literature so far.

Occurence at Szabadbattyán: From samples of the exploration shaft.

Eostaffella? sp.

Pl. IV., Fig. 2.

Description: Diameter: 0.35 mm
Width: 0.23 mm

The edges are rather narrowly rounded, with strong secondary deposits.

Remarks: A closer determination – owing to the poor preservation – is impossible, but the form resembles also the *Eoparastaffella* forms described by VDOVENKO (1964), therefore the generic state is uncertain.

Occurence at Szabadbattyán: Borehole Szabadbattyán – 10, from samples between 338.2 – 339.8 m depth.

Genus *Mediocris* ROZOVSKAJA 1961

Mediocris mediocris (VISSARIONOVA 1948)

Pl. II., Figs. 5 – 7.

1948. Eostaffella mediocris sp. nov. – VISSARIONOVA pp. 222 – 223., Pl. XIV., Figs. 7 – 9.
1954. Eostaffella mediocris VISSARIONOVA var. mediocris VISSARIONOVA – GROZDILOVA and LEBEDEVA, p. 120., Pl., Figs. 9 – 10.
1959. Eostaffella mediocris VISSARIONOVA – DURKINA, p. 193., Pl. XIX., Fig. 17.; Pl. XX., Figs. 1 – 3.
1960. Eostaffella mediocris VISSARIONOVA – GROZDILOVA and LEBEDEVA p. 109., Pl. XIII., Fig. 13.
1962. Mediocris mediocris (VISSARIONOVA) – BOGUSH and JUFEREV, P. 158., Pl. VI., Fig. 5.
1963. Mediocris mediocris (VISSARIONOVA) – ROZOVSKAJA, pp. 103 – 104., Pl. XVII., Figs. 26 – 33.
1964. Eostaffella mediocris VISSARIONOVA – CONIL and PIRLET, Pl. III., Fig. 42.

1964. Mediocris mediocris (VISSARIONOVA) – CONIL and LYS, p. 239., Pl. XL., Fig. 843., Pl. XLI., Figs. 844–846.

1965. Mediocris mediocris (VISSARIONOVA) – POJARKOV, pp. 96–98., Pl., Figs. 8–10.

1966. Mediocris mediocris (VISSARIONOVA) – BOGUSH and JUFEREV, pp. 154–155., Pl. X., Figs. 12–13.

1967. Mediocris mediocris (VISSARIONOVA) – PELHATE-PERON, p. 54., Pl. IV., Fig. 58.

Description: Diameter: 0.43 mm
Width: 0.21 mm
Number of whorls: 3.

It is a compressed, lenticular form, with broad'y rounded edges. Owing to the strongly increasing last half whorl, the periphery is slightly divergent. The whorls are planispiral. The secondary deposits form pronounced lateral infillings. The umbilical part is slightly depressed. The diameter of the proloculus is 0.035 mm. The wall-thickness on the last whorl is 0.01 mm. The wall is dark, fine-grained.

Remarks: The given measurements refer to the figured entire specimen.

Geographical distribution: Belgium, Germany, France, USSR.

Age: Viséan – Namurian.

Occurence at Szabadbattyán: Borehole Szabadbattyán – 9, from 296.3 m, Borehole Szabadbattyán – 10, from samples between 338.5 – 340.1 m depth, and from samples of the exploration shaft.

Mediocris cupellaeformis (GANELINA 1951)

Pl. II., Fig. 7.

1951 *Eostaffella mediocris* VISSARIONOVA var. *cupellaeformis* n. var. – GANELINA, pp. 196–197., Pl. II., Figs. 16–18.

1963. *Mediocris ovalis cupellaeformis* (GANELINA) – ROZOVSKAJA, pp. 105–106., Pl. XIX., Figs. 5–7.

1965. *Mediocris cupellaeformis* (GANELINA) – POJARKOV, p. 95., Pl., Figs. 5–6.

Description: Diameter: 0.23 mm
Width: 0.14 mm
Number of whorls: 3.

The cross-section is oval, slightly inflated at the umbilical part, the edge is narrowly rounded. The spire is involute, tightly coiled, planispiral. The secondary lateral deposit is well developed. The diameter of the proloculus is 0.035 mm. The wall is dark, fine-grained.

Geographical distribution: USSR.

Age: Middle to Upper Viséan (Tulaian – Venevian horizons)

Occurence at Szabadbattyán: Borehole Szabadbattyán–9, from 285.1 m.

Mediocris sp. 1.

Pl. II., Fig. 8.

Description: Diameter: 0.34 mm
Width: 0.13 mm
Number of whorls: 4.

It is a strongly compressed form, with rounded edges and nearly parallel sides. The coiling plane of the initial whorls is somewhat unstable. The secondary deposit is a developed lateral infilling. The wall-thickness at the last whorl is 0.010 mm. The wall is dark, fine-grained.

Remarks: The width/diameter ratio of the available specimens resembles to that of the species *M. breviscula* (GANELINA), but on the basis of the number of whorls and the size it compares to the *M. mediocris*.

Occurence at Szabadbattyán: Borehole Szabadbattyán–10, from samples between 335.9–338.2 m depth.

Mediocris sp. 2.

In the material there are rather poorly preserved *Mediocris* sections of 0.17–0.20 mm diameter. The number of whorls is 2 to 3. These seem to be allies of the species *Mediocris breviscula* (GANELINA).

Genus *Pseudoendothyra* MIKHAILOV 1939

Pseudoendothyra cf. *struvii supressa* (SCHLYKOVA 1951)

Pl. III., Figs. 1–2.

Description: Diameter: 0.73–0.78 mm
Width: 0.30–0.32 mm
Number of whorls: 4.

It is a strongly compressed form, with a rather depressed umbilicus. The outer 1.5 whorl is narrowly rounded. Because of the poor preservation, the secondary deposits cannot be studied sufficiently, but the presence of slight chomatas is presumable. The diafanotheca is developed.

Remarks: All of the visible features of the studied specimens indicate this subspecies, the measurements are near to the upper limits mentioned in the literature.

Occurence at Szabadbattyán: Borehole Szabadbattyán–9, from 285.1 m depth.

Pseudoendothyra sp.

Pl. III., Figs. 3–4.

Two badly preserved, strongly fragmented form, which are related to the *Pseudoendothyra struvii* (MOELLER) group.

Occurence at Szabadbattyán: Borehole Szabadbattyán–9, from 285.1 m depth.

Stratigraphical evaluation

1. The poor preservation, as well as the low specimen number of the fauna encumbers the stratigraphical interpretation. The data of the recent evaluation of the Carboniferous Foraminifera of Szabadbattyán (SIDÓ 1971), which suggest an agreement with the Upper Carboniferous of the Bükk Mountains, are not supported with the figured specimens. The *Plectofusulina* sp. figured on Pl. III., Fig. 2. in that work is not a well developed fusulinid, but presumably an *Eostaffella* section, which is undeterminable by the reason of unorientation. Similarly an unoriented section of an *Endothyra* is the *Codonofusiella* sp., figured on Pl. III., Fig. 3. (On the other hand it is unlikely the occurence of this Permian guide-fossil *Codonofusiella* in the Carboniferous!) The *Ozawainella* cf. *angulata* COLANI of Pl. III., Fig. 4. is presumably a form from the *Eostaffella ikensis* group. This latter is also an unconveniently oriented section, which unables closer determination.

The Szabadbattyán fauna is indisputably of Carboniferous. The available fauna furnishes a basis for preclusion the presence of the stages younger than Namurian: i.e. in the Foraminifera fauna the developed fusulinids are completely absent, which common in the Moskovian-Uralian limestones of the Bükk Mountains of similar facies (for detailed studies see ROZOVSKAJA 1963).

On the basis of the faunal composition, older rocks than Viséan can also not be proved. Consequently the studied sequence should be placed into the Viséan – Namurian stages.

2. With the stratigraphical arrangement the following difficulties arise:

A. The Foraminifera faunas studied from the European Namurian so far, are poor and less characteristic. Some basis for the separation of the Viséan and Namurian by foraminifers are the studies of MAMET, CHOUBERT and HOTTINGER in Marocco (1966). The most important, however, are the quantitative data, and the material of Szabadbattyán of small specimen number cannot be evaluated in this way. In this material forms of the characteristic Namurian *Asteroarchaediscus baschkiricus* group, and the genus *Loeblichia* are not represented.

B. The overlying rocks of the Viséan yield more richer Foraminifera fauna in the USSR, but the correlation of these strata with the W European Namurian is hitherto much debated question.

The recent studies on the ammonite faunas (RHUZENZEV and BOGOSLAVSKAYA 1971) made the parallelization of the W European Namurian and the corresponding sequences of the USSR possible. In these studies they used instead of the Baschkirian, suggested as an overlapping stage between the Namurian and Moscovian, the more precisely definiable Kayalian stage. Other workers (IVANOVA and ROZOVSKAJA 1970) correlate with the W European Namurian the strata between the Viséan and Baschkirian.

A third group of authors (POPOVA, EINOR, ALEXANDER, REITLINGER 1970, EINOR 1970) continues to debate the usefulness of the Namurian. The source of the controversies is the asynchronous rate of evolution of the different animal and plant groups. OSIPOVA, HECKER and BELSKAYA (1971) pointed out, that at the base of the Namurian just a few new element appears. In the time of significant evolutionary changes in several macrofaunal groups, the Foraminifera show a reduced evolution.

In the case the of Szabadbattyán fauna the controversies regarding the upper boundary of the Namurian are of insignificant. In all of the Soviet works mentioned above the upper boundary of the Viséan (i.e. the Viséan/Nanurian boundary) coincides with the base of the Serpuhov Superhorizon. In the parallelization of the Viséan – Namurian boundary of the USSR and W Europe the only problematic element is that RUZHENZEV and BOGOSLAVSKAYA (1971) regards the uppermost Viséan ($V3c^s$) strata of Belgium to be of lowermost Namurian.

The *Bradyina* sp., which is an ally of the *Bradyina cribostomata* RAUSER et REITLINGER is the single form previously unknown in the Viséan. All of the forms of the *Bradyina rotula* (EICHWALD) group in the USSR, as well as in Belgium and France are known from the Upper Viséan. The *Mediocris cupellaeformis* (GANELINA) is unknown from post-Viséan strata. In spite of the difficulties of the determination, it is recognizable, that the Szabadbattyán foraminifers show relation to species which appear within the Viséan in the USSR and in the Dinantian stratotype as well (CONIL, LIPINA and REITLINGER 1970). The differences can be due to facial causes (e.g. the genus *Mediocris* appears within the Middle Viséan in Belgium). These above mentioned arguments all suggest, that the Carboniferous limestone of Szabadbattyán is a sequence of not older than Middle Viséan and not younger than Lower Namurian in age. The Foraminifera fauna as a whole shows a closest resemblance to the Upper Viséan associations.

Because of the scarcity of the fauna a further subdivisioning of the Carboniferous sequence in boreholes is unrealizable, and the parallelization of the two section is difficult too. Some differences appear in the faunas of the two boreholes: e.g. the representatives of the genus *Bradyina* occur repeatedly in Borehole Szabadbattyán – 10, but are completely absent from the Borehole – 9 (Fig. 1.1 – 2). These disagree-

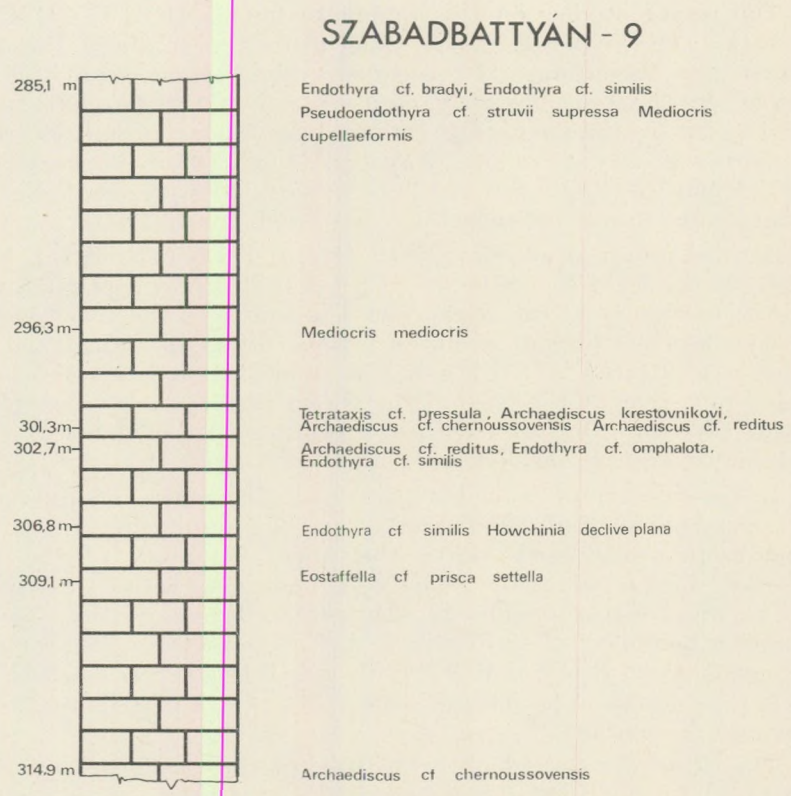

Fig. 1. Occurence of certain Foraminifera in Borehole Szabadbattyán – 9.

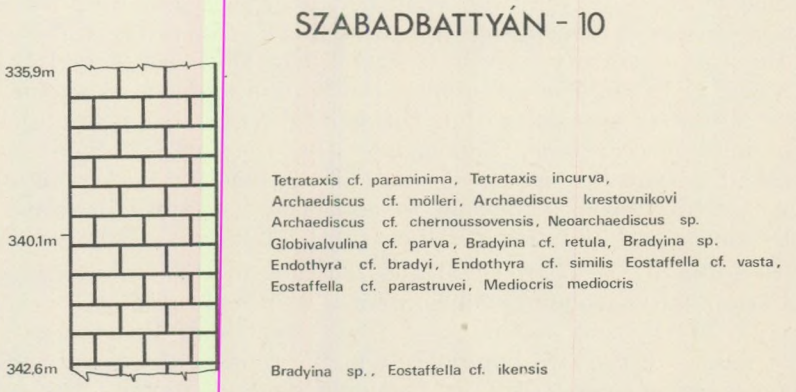

Fig. 2. Occurence of certain Foraminifera in Borehole Szabadbattyán – 10.

ments also can be due to facial differences. [The considerable temporal and areal facies-variablity is shown also by the fact, that the faunal spectrum and the foraminifer-content of the certain beds within the two boreholes are of remarkably different (Figs. 1.3 – 4).]

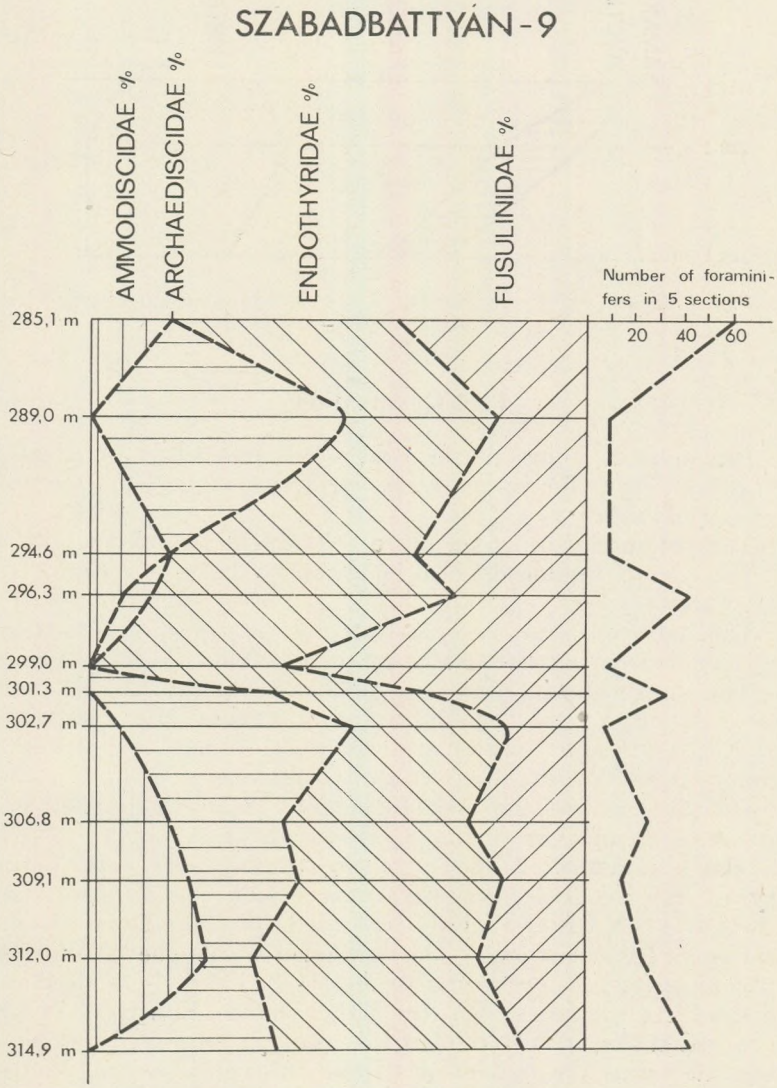

Fig. 3. Quantitative distribution of the Foraminifera in Borehole Szabadbattyán – 9.

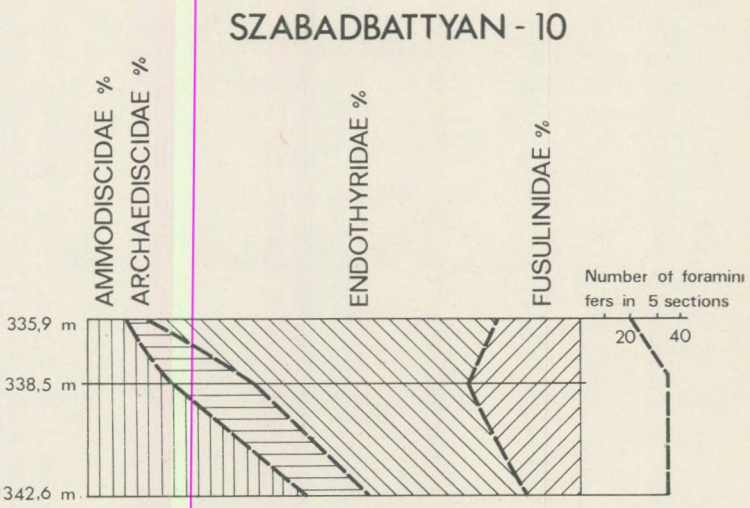

Fig. 4. Quantitative distribution of the Foraminifera in Borehole Szabadbattyán – 10.

Facies evaluation

1. Brachiopods, echinoderms, and corals frequently occur all along in the Carboniferous limestone sequence. These suggest marine environment of normal salinity.

2. The common blue-green algae *(Girvanella)* show shallow water.

3. The coarser organo-detrital beds can be due to occasionally more agitated water.

4. The main biogenic elements are not the foraminifers; this limestone rather can be regarded as brachiopodal-crinoidal limestone.

5. The study of the relative abundance, as well as the change of the specimen number of the four most important Foraminifera group suggest a considerable spatial and temporal variability of the biotic conditions within this shallow-water environment.

6. On the basis of the poor foraminifer fauna a detailed ecologic reconstruction cannot be outlined. However, according to MAMET (1968), the abundance of the primitive fusulinids is common in the vicinity of the biogenic accumulations ("bioherms"). From similar place KALASNIKOV (1967) recorded the abundance of attached foraminifers (Tuberitinidae). The abundance of the „*Calcisphaera*" (=*Pachysphaerina*) – according to MAMET (1970) – is characteristic in the back-reef lagunes. On the other hand KALASNIKOV (1967) regarded the primitive fusulinids as eurybionts, and he considered their abundance as the indication of the unfavourable life conditions.

Conclusively, the Carboniferous limestone of Szabadbattyán deposited in shallow marine water of normal salinity, partially in form of

biogenic accumulation. The life conditions, which changed significantly in space and time within this shallow-water environment were unfavourable for the Foraminifera.

Conclusions

In the point of view of stratigraphy the study of the foraminifer fauna of Szabadbattyán permitted to reinforce the Viséan age of this limestone, which age was previously suggested by FÖLDVÁRI (1952), on the basis of corals and brachiopods. The importance of the Viséan Foraminifera fauna of Szabadbattyán is the fact that the knowledge, as well as the localities of connecting foraminifer faunas between Eastern and Western Europe are very limited.

Besides of stratigraphical conclusions the fauna enabled some facies evaluations. It is suggested a normal marine, shallow-water environment, with repeated local changes in the life conditions and with resulted various faunal composition.

REFERENCES

Brady, H. B. (1876): A monograph of Carboniferous and Permian foraminifera (the genus Fusulina excepted). (Palaeontographical Society, pp. 1 – 166. Pl. I – XII.)

Conil R., Lys M. (1964): Matériaux pour l'étude micropaléontologique du Dinantien de la Belgique et de la France. (Mém. de l'Inst. Geol. de L'Univ. de Louvain, t. XXIII, pp. 1 – 292, Pl. I – XLII.)

Conil R. and Pirlet H. (1963): Sur quelques Foraminiferes caractéristiques du Viséen supérieur de la Belgique (Bassins de Namur et de Dinant). (Bull. Soc. belge de Géol., de Paléontol. et d'Hydrol., 1964. t. LXXII pp. 183 – 197, Pl. I – III.

Loeblich A. R. and Tappan H. (1964): Protista 2. Treatise on Invertebrate Paleontology (Lawrence, Univ. Kansas Press).

Mamet B. (1968): Sur les macrofacies calcaires du Viséen de la Montagne – Noire (France). (Revue d.Micropal., 11, No. 3. pp. 121 – 136, Pl. 1 – 5.)

Mamet B. L. (1970): Carbonate microfacies of the Windsor Group (Carboniferous), Nova Scotia and New Brunswick. (Geol. Surv. of Canada, Paper 70 – 71, pp. 1 – 82, pl. I – XIX).

Mamet B., Choubert G. and Hottinger L. (1966): Notes sur le Carbonifere du jebel Ouarkziz. Etude de passage du Viséen au Namurien d'apres les Foraminiferes. (Notes et Mém. Serv. géol. Maroc., No. 198, pp. 7 – 21. Pl. 1 – 4.)

Pelhate-Peron A. (1967): Micropaléontologie des calcaires dinantiens du bassin de Laval. (Bull. Soc. Geol. et Min. de Bretagne. pp. 27 – 76, Pl. I – VI.)

Rozovszkaja Sz. E. (1963): Bükkhegységi Fusulinidák. (Geol. Hung. Ser. Pal. 28. pp. 1 – 38, t. I – II.)

Sidó M. (1971): Adatok a hazai paleozóikum mikropaleontológiájához. (M. Áll. Földt. Int. Évi Jel. az 1969. évről, pp. 703 – 705, t. I – VI.)

Zeller D. E. N. (1963): Endothyra bowmani Brown, 1834. Designation of Neotype. (J. Paleont., 37., pp. 502 – 503.)

Богуш О. И., Юферев О. В. (Bogush O. J., Juferev O. V.): (1962) Фораминиферы и стратиграфия каменноугольных отложений Каратау и Таласского Алатау. (Изд. АН СССР, pp. 1 – 222, t. I – IX

Богуш О. И., Юферев О. В. (Bogush O. J., Juferev O. V.): (1966) Фораминиферы карбона и перми Верхоянья.
(Наука, pp. 1—96, т I – XIV.)

PLATE I.

Fig. 1 – 2. Endothyra cf. *bradyi* Mikhailov. From sample of the exploration shaft. X 100

Fig. 3 – 7. Endothyra cf. *similis* Rauser-Chernoussova et Reitlinger.

Fig. 3 – 4. Borehole Szabadbattyán-9., 306,8 m. X 100

Fig. 5 – 6. From sample of the exploration shaft. X 100

Fig. 7. Borehole Szabadbattyán-9., 285,1 m. X 100

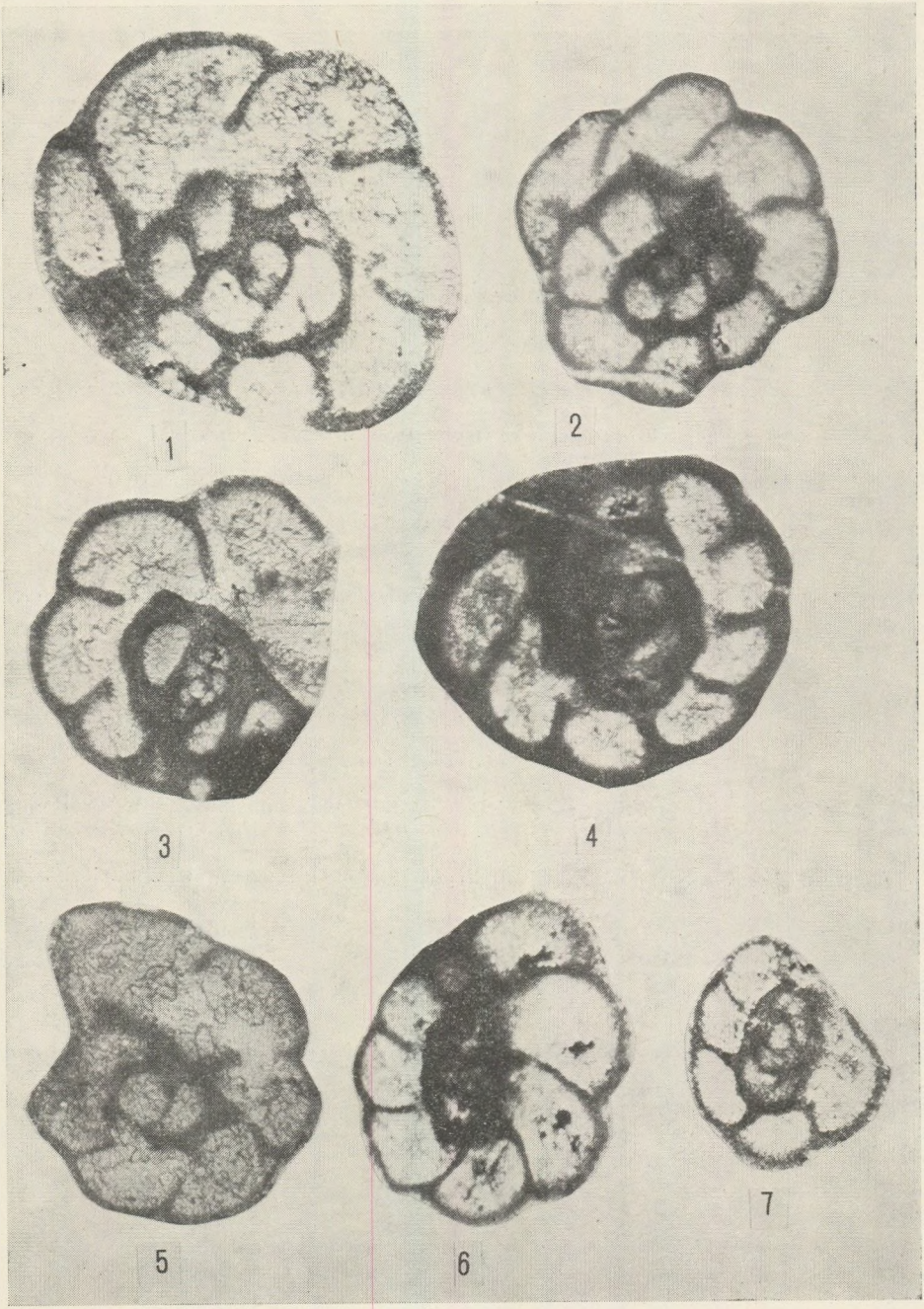
1
2
3
4
5
6
7

PLATE II.

Fig. 1–2. Endothyra cf. *similis* Rauser-Chernoussova et Reitlinger

Fig. 1. From sample of the exploration shaft. X 100

Fig. 2. Borehole Szabadbattyán-10., between 338,5 – 340,1 m. X 100

Fig. 3. Endothyra cf. *omphalota* Rauser-Chernoussova et Reitlinger. Borehole Szabadbattyán-9., 302,7 m. X 100

Fig. 4. Endothyra cf. *prisca* Rauser-Chernoussova et Reitlinger. From sample of the exploration shaft. X 100

Fig. 5–6. Mediocris mediocris (Vissarionova)

Fig. 5. Borehole Szabadbattyán-9., 296,3 m. X 100

Fig. 6. Borehole Szabadbattyán-10., between 338,5 – 340,1 m. X 100

Fig. 7. Mediocris cupellaeformis (Ganelina). Borehole Szabadbattyán-9., 285,1 m. X 100

Fig. 8. Mediocris sp. Borehole Szabadbattyán-10., between 335,9 – 338,2 m. X 100

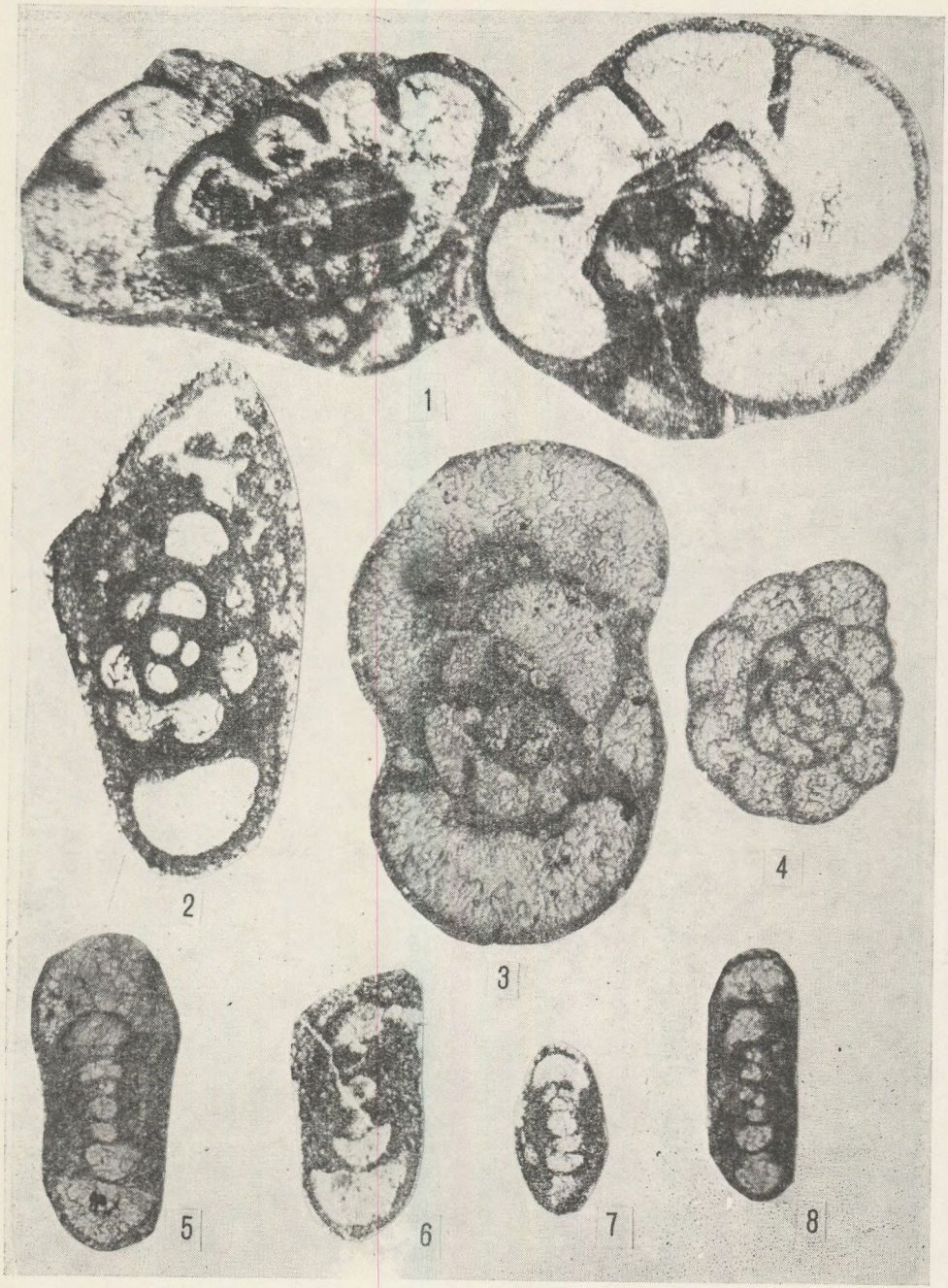
1
2
3
4
5
6
7
8

PLATE III.

Fig. 1 – 2. Pseudoendothyra cf. *struvii supressa* (S c h l i k h o v a). Borehole Szabadbattyán-9., 285,1 m. X 100

Fig. 3 – 4. Pseudoendothyra sp. Borehole Szabadbattyán-9., 285,1 m. X 100

Fig. 5. Eostaffella cf. *vasta* R o s o v s k a j a. Borehole Szabadbattyán-10., between 338,5 – 340,1 m. X 100

Fig. 6. Eostaffella sp. From sample of the exploration shaft. X 100

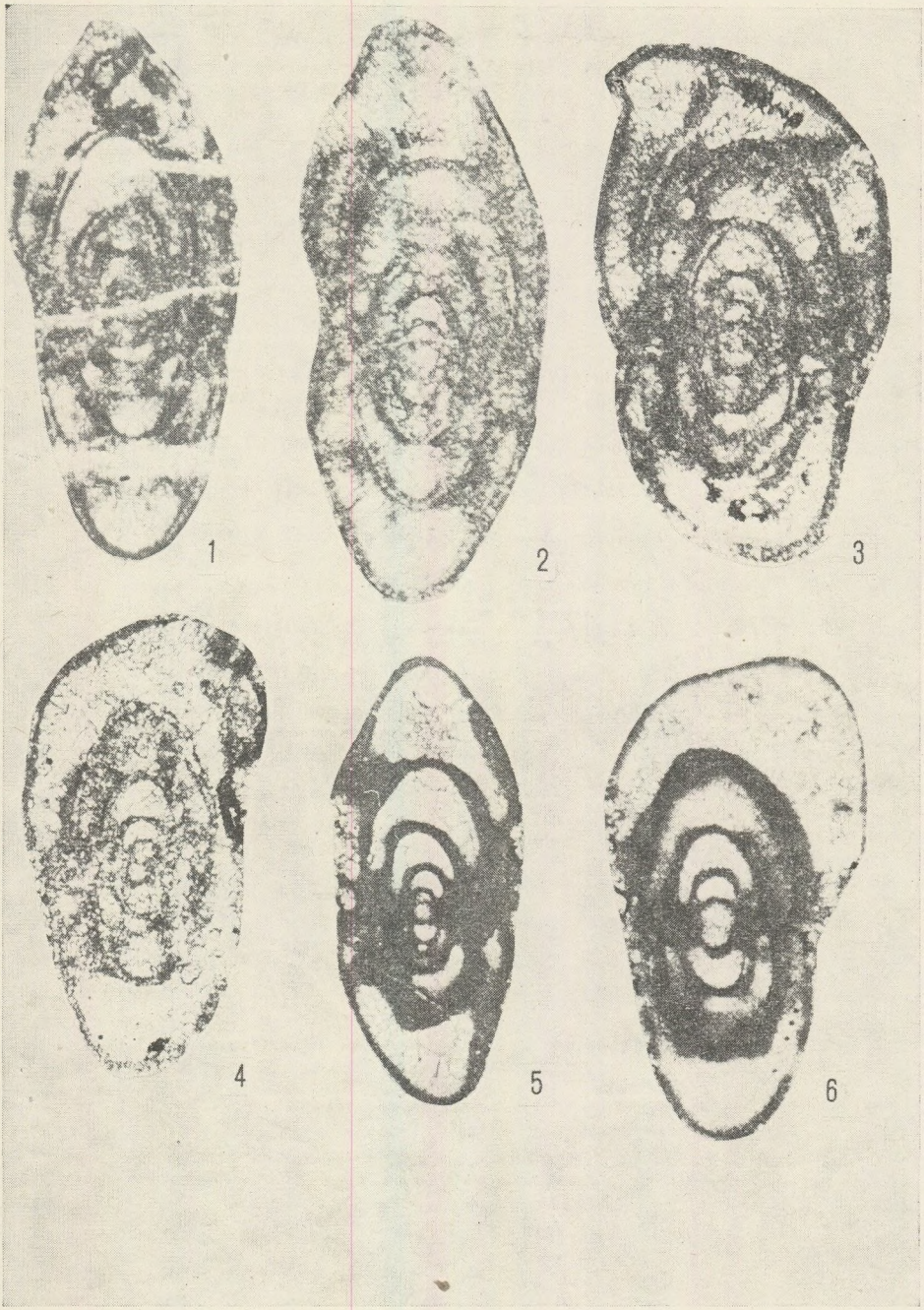
1
2
3
4
5
6

PLATE IV.

Fig. 1. Eostaffella cf. *parastruvei* Rauser-Chernoussova et Reitlinger
Borehole Szabadbattyán-10., between 338,5 – 340,1 m. X 100

Fig. 2. Eostaffella? sp. Borehole Szabadbattyán-10., between 338,2 – 339,8 m. X 100

Fig. 3 – 4. Eostaffella cf. *prisca settella* Ganelina

Fig. 3. From sample of the exploration shaft. X 100

Fig. 4. Borehole Szabadbattyán-9., 309,1 m. X 100

Fig. 5 – 7. Eostaffella cf. *ikensis* (Vissarionova)

Fig. 5. Borehole Szabadbattyán-10., 342,6 m X 400

Fig. 6 – 7. From sample of the exploration shaft. X 100

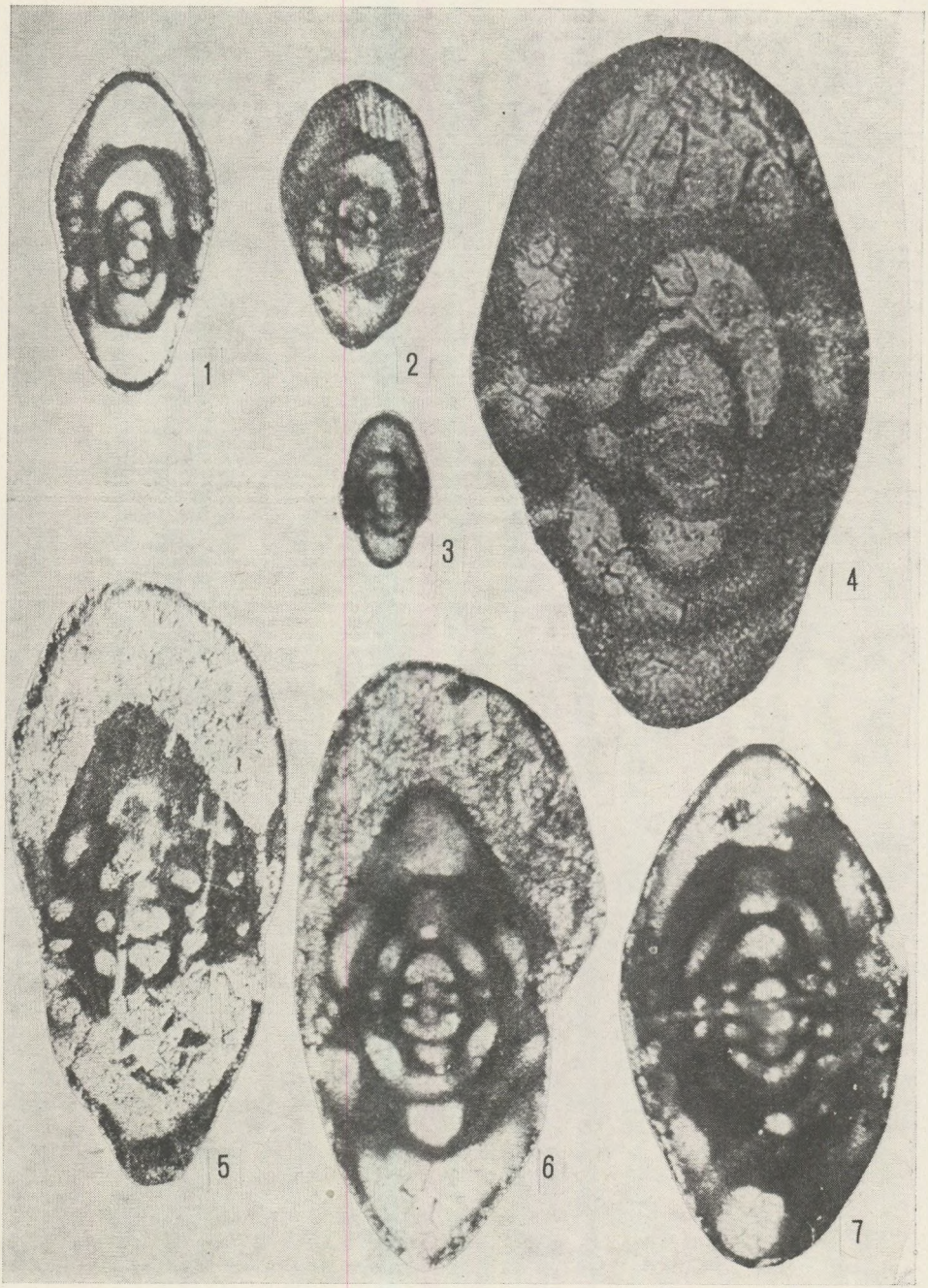
1
2
3
4
5
6
7

Вдовенко М. В. (Vdovenko M. V.) (1964): Эволюция ряда Eoparastaffella – – Pseudoendothyra. (Материалы к фауне верхнго палеозоя Донбасса. II., Тр. ИГН АНУССР, Сер. страт. и пал., Вып. 48, pp. 16 – 3, t. I – II)

Виссарионова А. Я. (Vissarionova A. Ja.) (1948): Примитивные фузулиниды из нижнего карбона Европейской части СССР. (Тр. ИГН АН СССР, Вып. 62, Геол. сер. № 19, pp. 216 – 226, t. XIII – XIV)

Ганелина Р. А. (Ganelina R. A.) (1951): Эоштаффеллы и миллереллы визейского и намюрского ярусов нижнего карбона западного крыла Подмосковной котловины. (Тр. ВНИГРИ, нов. сер. Вып. 56, pp. 179 – 207, t. I – III)

Гроздилова Л. П., Лебедева Н. С. (Grozdilova L. P., Lebedeva N. S.) (1954): Фораминиферы нижнего Карбона и башкирского яруса среднего карбона Колво-Вишерского края, (Микрофауна СССР VIII, Гостоптехиздат, pp. 4 – 203, t. I – XV)

Гроздилова Л. П., Лебедева Н. С. (Grozdilova L. P., Lebedeva N. S.) (1960): Фораминиферы каменноугальных отложений западного склона Урала и Тимана. (Тр. ВНИГРИ, Вып. 150, pp. 1 – 188, t. I – XXXIII)

Дуркина А. В. (Durkina A. V. (1959): Фораминиферы нижнекаменноугольных отложений Тамано – Печорской провинции. (Микрофауна СССР X, Гостоптехиздат, pp. 132 – 335, t. I – XXVII)

Иванова Е. А., Розовская С. Е. (Ivanova E. A., Rozovskaja S. E.) (1970): О подразделении каменноугольной системы на отделы. (Проблемы стратиграфии карбона, Наука, pp. 17 – 27)

Калашников Н. В. (Kalasnikov N. V.) (1967): Экология фауны и биономическое районирование каменноугольного моря Северного Урала. (Наука, pp. 1 – 54, t. I – VI)

Кониль Р., Липина О. А., Рейтлингер Э. А. (Conil R., Lipina O. A. Reitlinger E. A.) (1970): Фораминиферовые комплексы и корреляция динанта Бельгии и СССР. (Вопросы микропалеонтологии 13, Наука, pp. 128 – 139)

Михайлов В. К. (Mikhailov V. K.) (1939): К характеристике родов каменноугольных фораминифер. (Ленингр. геол. упр., сб. 3)

Осипова А. И., Геккер Р. Ф., Бельская Т. Н. (Osipova A. J., Hecker R. F., Belskaya T. N. (1971): Закономерности распространения и смены фауны в поздневизейском и ранненамюрском эпиконтинентальных морях Русской платформы. (Тр. Пал. инст. АН СССР, Т. 130, pp. 279 – 293)

Попова З. Г., Эйнор О. Л., Александров В. А., Рейтлингер Э. А. (Popova Z. G., Einor O. L., Alexandrov V. A., Reitlinger E. A.) (1970): К проблеме намюрского яруса по новым данным классического разреза р. Шартым. (Проблемы стратиграфии карбона, Наука, pp. 123 – 132)

Поярков Б. В. (Pojarkov B. V.) (1965): Систематика и филогения рода Mediocris Rozovskaja, 1961. (Вопр. микропал., 9, pp. 89 – 110 + t.)

Раузер. Черноусова Д. М., Беляев Г. М., Рейтлингер Е. А (Rauser – Chernoussova D. M., Beljaev G. M., Reitlinger E. A.) (1936): Верхнепалеозойские фораминиферы Печорского края. (Труды Полярн. комис. АН СССР, Вып. 28)

Раузер – Черноусова Д. М. (Rauser – Chernoussova D. M.) (1948): Материалы к фауне фораминифер каменноугольных отложений Центрального Казахстана. (Тр. ИГН АНСССР, Вып. 66, Геол. сер. № 21)

Розовская С. Е. (Rozovskaja Sz. E.) (1963): Древнейшие представители фузулинид и их предки, (Тр. Пал. инст. АН СССР, Т. 97, pp. 1 – 118, t. I – XXII)

Руженцев В. Е., Богословская М. Ф. (Ruzhencev V. E., Bogoslovskaya M. Ф.) (1971): Намюрский этап в эволюции аммоноидей. Ранненамюрские аммоноидеи. (Тр. Пал. инст. АН СССР, Т. 133)

Шлыкова Т. И. (Schlykova T. J.) (1951): Фораминиферы визейского и намюрского ярусов нижнего карбона западного крыла Подмосковной котловины. (Тр. ВНИГРИ, Вып. 56, pp. 109 – 176, t. I – VI.)

Эйнор О. Л. (Einor O. L.) (1970): Сернуховский ярус и его положение в каменноугольной системе. (Проблемы стратиграфии карбона, Наука, pp. 107 – 122)

CONTENTS

A kiadásért felelős: az Eötvös Loránd Tudományegyetem rektora — A kézirat nyomdába érkezett: 1975. július — Megjelent: 1976. június — Terjedelem: 19,75 (A/5) ív — Példányszám: 850 — Készült monó szedéssel, íves magasnyomással az MSZ 5601—59 és az MSZ 5602—55 szabvány szerint.
75.1000. Állami Nyomda, Budapest